AN OSTEOHISTOLOGIC ANALYSIS OF GROWTH IN ORNITHOPODA

by
Catherine E. Sartin

A thesis submitted to Johns Hopkins University in conformity with the requirements for the degree of Master of Science

Baltimore, Maryland

August, 2017

Abstract

In Iguanodontian dinosaurs, histologic ontogentic series of two basal taxa (*Dysalotosaurus lettowvorbecki* and *Tenontosaurus tilletti*) and one derived taxon (*Maiasaura peeblesorum*) are known. Two of the ontogenetic series of taxa sectioned for this study (*Eolambia caroljonesa* and *Iguanacolossus forti*) are phylogenetically situated between these basal and derived taxa. The third ontogenetic series of taxa sectioned for this study (*Hypacrosaurus stebingeri*) is a derived taxon, similar to *Maiasaura*; however, *Hypacrosaurus* is a lambeosaurine, while *Maiasaura* is a hadrosaurine.

This sample provides a good opportunity to begin to understand how small, basal members of the iguanodontian clade evolved into enormous derived members. By comparing the histology of humeri with that of femora and tibiae in each series, we can begin to understand how bipediality in basal members of the clade evolved into the facultative bipediality of derived members.

Eolambia exhibits growth similar to *Dysalotosaurus* and *Tenontosaurus*. Bone growth is relatively slow (i.e., well organized tissue, small vascular canals), although the youngest specimens do preserve areas of knitted texture which is indicative of rapid growth. The first annual growth marks (AGMs) appear in small sized individuals; secondary osteons begin appearing in mid-sized individuals and increase in number with increasing age. *Iguanacolossus* and *Hypacrosaurus* exhibit growth more similar to *Maiasaura*. Bone growth is relatively fast (i.e., poorly organized tissue, large vascular canals) until specimens reach mid-size. The first AGMs appear in mid-sized individuals, and secondary osteons begin appearing soon thereafter and increase in number with increasing age.

In all taxa under consideration in this study, growth is similar between forelimb and hind limb elements throughout the respective ontogenetic series. This indicates that even as juveniles, these taxa were likely facultative bipeds.

Advisors: David B. Weishampel, Christopher Ruff

Acknowledgements

It is with immense gratitude that I acknowledge the support of the American Association of Anatomists for awarding me the Visiting Scholar Grant, and the Mid-American Paleontological Society for awarding me the Outstanding Student Research Grant. I am also indebted to numerous collegaues for making specimens and supplies available to me, including and in no particular order: Joe Sertich, James Hagadorn, Jack Horner, Pete Makovicky, Ken Carpenter, Rod Scheetz, Randy Irmis, Jim Kirkland, and Rich Cifelli. Lastly, I would like to thank my readers and advisors – Andrew Farke, Kristi Curry Rogers, Dave Norman, Chris Ruff, and Dave Weishampel – who slogged through this work out of the goodness of their own hearts.

Table of Contents

1. Introduction

Studies of the organismal biology of extant and extinct organisms are similar in that they both seek to understand how organisms live and interact with their environments in an evolutionary context. Part of this understanding comes from the study of ontogeny -- how individuals grow and develop. However, such ontogenetic studies can be extremely challenging in paleobiology, because of the fossilized remains of terrestrial organisms are frequently based upon small sample sizes and there can be difficulty in identifying multiple remains as members of different age groups of a single taxon, or deciding whether they belong to different taxa. Despite these difficulties, it is nevertheless important to study ontogeny in extinct taxa. For instance, extinct taxa provide the means to explore morphological and phylogenetic spaces that no longer exist. One such morphologic space is gigantism of terrestrial taxa (often defined as a taxa whose average weight exceeds one metric ton); these giants are sometimes referred to as "megafauna" (Price & Piper, 2009). In the Cretaceous, for instance, there were numerous gigantic, reptilian terrestrial taxa among the dinosaurs and pterosaurs (e.g. Titanosauria, Iguanodontia, Ceratopsidae, and Azhdarchidae). During the Plio-Pleistocene, there were also many gigantic, mammalian terrestrial taxa (e.g. *Indricotherium, Andrewsarchus, Elasmotherium, Diprotodon, Glyptodon, and Megatherium*). Among extant land-dwelling taxa, few taxa approach the size of the gigantic taxa from these previous geologic time periods. Furthermore, all of the extant giants are mammals (e.g. elephants). By studying ontogeny only among extant taxa, we would have a very poor grasp of body size changes in all megataxa. Examining ontogeny in extinct taxa also makes it possible to examine evolutionary processes in

deep time; it provides the means to examine these processes as they were occurring, as opposed to post-hoc reconstructions of extinct taxa.

Ornithopods are particularly well-suited for investigating the evolution of body size and life history traits (Figs. 1.1 and 1.2). Ornithopods are members of Dinosauria; more specifically, they are a part of Ornithischia (Norman, 2004; Butler et al., 2008). Unlike many clades in Ornithischia (e.g. Stegosauria, Ankylosauria), which are usually found as isolated specimens, ornithopods are often found in monodominant bone beds (Varricchio & Horner, 1993). These bonebeds are referred to as "monodominant" because the overwhelming majority of the material in the bonebed belongs to a single taxon; however, there may be isolated elements and/or fragmentary material of other taxa present in the bonebed as well. Therefore, for some taxa, we have large sample sizes that reflect either samples from a single population or a minimally time-averaged population. Because of this taphonomic situation some taxa, such as *Maiasaura* (a hadrosaurid ornithopod) have served as model organisms for examining both behavior (e.g. herding and parental care) and ontogeny (Horner et al., 2000; Horner et al., 2001; Horner & Weishampel, 1988).

The basal members of the ornithopod clade, which first appear in the Middle Jurassic (Fig. 1.3), are small-bodied (1-2m long), herbivorous, and obligate bipeds (Butler et al., 2008). The young are suspected to have exhibited precocial development (Horner & Weishampel, 1988), implying that they would have needed very little or no parental care. They include taxa such as *Orodromeus makelai* (Scheetz, 1999) and *Hypsilophodon foxii* (Galton, 1983). The clade persists until the Cretaceous-Paleogene extinction event. The most derived members of the clade, Late Cretaceous

hadrosaurids, are large-bodied (8-14m long), herbivorous, facultative bipeds. There is evidence that in some taxa their young exhibited altricial development, and consequently need extended parental care (Horner & Weishampel, 1988). Hadrosaurids include taxa such as *Maiasaura peeblesorum* and *Hypacrosaurus stebingeri*, and it has been suggested that many hadrosaurs lived in herds, which would likely have had to migrate seasonally to avoid depleting local resources (Horner et al., 2004). Lambeosaurine hadrosaurids, are notable for their varied hollow cranial crests. As the crests grow rapidly around the time that sexual maturity would likely have been attained (Dodson, 1975; Evans, 2010; Farke et al., 2013), it is reasonable to suggest that they may have, at least in part, functioned as display structures to attract mates (Hopson, 1975; Weishampel, 1981).

This study will examine growth and development within this diverse and interesting clade – Ornithopoda -- in two ways: the first examines how we reconstruct the growth history of a taxon within this clade; the second examines growth and development of across a range of ornithopod taxa in an attempt to extract evolutionary trends with respect to body size within the context of phylogeny.

Before it is possible to reconstruct the growth history of a taxon within a clade, we must disambiguate growth and development of individuals within a taxon from the evolutionary changes between taxa. We can consider, for example, the case of *Glishades ericksoni.* This taxon was erected on the basis of partial paired premaxillae from the Two Medicine Formation (late Campanian, Montana) and classified as a non-hadrosaurid hadrosauroid (Figs. 1.1 and 1.2) (Prieto-Márquez, 2010). Prieto-Márquez (2010) had assumed that the material was adult, making its less derived characters a

result of its basal phylogenetic position. *Glishades* represented the first occurrence of a non-hadrosaurid hadrosauroid from the late Campanian of North America. This in turn had potential ecological implications. It could be taken to imply that for a prolonged period of time, non-hadrosaurid hadrosauroids and hadrosaurids co-existed in the same geographic area, utilizing the same or similar resources. Or it could also be taken to imply a biotic exchange with Asia at this time.

As part of a study of juvenile hadrosaurid material, the specimen was re-examined by Campione et al. (2013) in order to consider the possibility that the material may be juvenile. This meant that its less derived characters could be the result of ontogeny, not phylogeny. Their analysis, based on morphologic comparison to known juvenile hadrosaurid specimens, demonstrated that this was the case; the material was a juvenile saurolophine and *Glishades ericksoni* became a *nomen dubium*.

The case of *Glishades ericksoni* is not isolated; several examples are known from material that had previously been taken to be adult, only later to be determined to be sub-adult or juvenile. Nor is this problem only found within this particular clade or when the material under examination is of such limited quantity. For example, Scannella & Horner (2010) re-examined *Triceratops* and *Torosaurus* frill material and determined that *Triceratops* is a juvenile form of *Torosaurus*. Since being described by Bakker & Williams (1988), researchers (e.g. Brusatte et al., 2016; Currie et al., 2003) have re-examined *Tyrannosaurus* and *Nanotyrannus* material, in attempts to demonstrate whether *Nanotyrannus* is a juvenile *Tyrannosaurus*. These researchers found that the *Nanotyrannus* material is consistent with it being an ontogenetic stage of *Tyrannosaurus* based on limb proportions (Currie et al., 2003) and dental groove

morphology (Brusatte et al., 2016). Both Schott et al. (2011) and Horner & Goodwin (2009) have attempted to distinguish between ontogeny and phylogeny with respect to Pachycephalosauridae. Schott et al (2011) determined that *Ornatotholus browni* as a juvenile *Stegoceras*, while Horner & Goodwin (2009) proposed that *Dracorex hogwartsia*, *Stygimoloch spinifer* and *Pachycephalosaurus wyomingensis* are the same taxon at different ontogenetic stages. It should be noted; however, that some of the studies mentioned above have caused deep divides between researchers, and are far from being either generally accepted or dismissed.

The second way in which the present study will examine the growth and development of Ornithopoda, is to compare the growth histories of specific ornithopod taxa in search of evolutionary trends with respect to body size within phylogentic lineages. Such trends can provide important insights into the processes that underlie ecological and evolutionary relationships. With respect to Ornithopoda, as mentioned above, both migration and parental care have received considerable attention (e.g. Horner & Weishampel, 1988; Horner et al., 2000; and Horner et al., 2001). Seasonality of resources can make it advantageous for a given taxon to undertake seasonal migration. This is common among extant taxa – for instance, ruby throated hummingbirds migrate from central and southern United States to Mexico (Zenzal & Moore, 2016), and caribou migrate from the interior of Alaska to more coastal regions (Nicholson et al., 2016). In order to participate in migratory events, the young must have reached a size such that they can keep up with the group. This is depedent upon the interval of time between birth and the onset of migration, as well as by their growth rate during this interval (for example, see Bety et al., 2003; Tucker, 2000).

Before describing in more detail how this study will examine the growth and development of Ornithopoda, let us first turn our attention to describing Ornithopoda as a whole.

1.1 Systematics

Ornithopoda is one of the major clades of Dinosauria (see Figs. 1.1 & 1.2; an evaluation of Baron et al. 2017 is beyond the scope and relevance of this study). Members of this clade were herbivorous, (facultative) bipeds, many of which are thought to have lived in large herds (*Shantungosaurus,* Hone et al., 2014*; Amurosaurus,* Lauters et al., 2008*; Edmontosaurus,* Evans et al., 2015). The first appearance of the ornithopod clade is in the Middle Jurassic (169 Ma) of Asia; it persists up until the Cretaceous- Paleogene extinction event (66 Ma) and is cosmopolitan (Norman, 2004).

Ornithopoda can be further divided into three smaller groups – basal ornithopods, (non- hadrosaurid) iguanodontians, and hadrosaurids. Current systematics of each of the major ornithopod groups – basal ornithopods (Boyd et al., 2015; Brown et al., 2013; Ősi et al., 2012; Fig. 1.3), iguanodontians (Boyd et al., 2015; McDonald, 2012; Norman, 2015; Fig. 1.4), and hadrosaurids (Evans et al., 2007; Horner et al., 2004; Prieto-Márquez, 2010; Fig. 1.5) - will be used as the basic means of compartmentalizing the clade throughout this study.

The phylogenies have been divided in this manner because no modern, detailed, comprehensive phylogenetic analyses of the clade as a whole exist. There are several modern analyses of Ornithischia (Boyd, 2015; Butler et al., 2008); however, these lack sufficient resolution with respect to the groups included in this

study. Although the results of the present study are not meant as contributions to the topologies of the cladograms mentioned above, the data will be available for inclusion and testing of these cladistic analyses at a future date.

It should be noted that I have used the word 'groups' here, instead of clades because the first two are paraphyletic. When using the term 'basal ornithopods' (Fig. 1.3), I am referring to those ornithopods that occur after the origin of the clade and before the origin of iguanodontians. When I use the term 'iguanodontians' (Fig. 1.4), I refer to those ornithopods included in Iguanodontia, but not in Hadrosauridae. The name for this group is 'non-hadrosaurid iguanodontians'; however, this name is cumbersome, so for the remainder of the study I will use the term 'iguanodontians' for this group, with the understanding that it be read as 'non-hadrosaurid iguanodontians'. Despite the paraphyletic nature of the first two groups, all three of these groups have a long history with respect to dinosaur studies.

Iguanodon, discovered in 1822 by Gideon Mantell (or possibly his wife, Mary Ann, depending on which account you take to be veridical) in Sussex, England (Dean, 1999; Sues, 1997). Along with *Megalosaurus* and *Hylaeosaurus*, *Iguanodon* was one of the taxa included in Sir Richard Owen's original description of Dinosauria in 1842. Of note, *Iguanodon* was among the taxa represented by Benjamin Waterhouse Hawking for the Great Exhibition of 1854 (McCarthy & Gilbert, 1994). When the models were installed in a newly-built park at Sydenham Hill following the exhibition, Hawkins held a (now famous) New Year's Eve banquet inside one of the *Iguanodon* molds in celebration; Sir Richard Owens was reportedly at the head of the table, which was surrounded by plaques honoring such notable figures as William Buckland,

George Cuvier, and Gideon Mantell.

Hypsilophodon was discovered on the Isle of Wight a few years after *Iguanodon*, in 1849, and sold to Mantell; both Mantell (1849) and Owen (1855) described the material as belonging to a young *Iguanodon*. It was not until 1869, when Thomas Henry Huxley provided an extensive description of that material (Huxley 1869, 1870), that it became clear that the material belonged to a different taxon, one more basal than *Iguanodon*, and was given the name *Hypsilophodon foxii*.

About a decade after the discovery of *Hypsilophodon*, the first hadrosaur remains were discovered. This time the discovery took place in North America, but like *Iguanodon*, the initial discovery was of teeth. Joseph Leidy (1855) was the first to examine them, erecting a new (now invalid) genus *Trachodon*. In 1858 Leidy discovered a more complete specimen and named it *Hadrosaurus foulkii*. Interestingly, this specimen became the first mounted, publicly displayed dinosaur skeleton in the world. It was assembled and mounted by Benjamin Waterhouse Hawkins in 1868 at the Philadelphia Academy of Sciences (Philadelphia, Pennsylvania) (Norman, 2000; Brinkman, 2010).

The earliest members of the ornithopod clade (Fig. 1.3), which is here not taken to include Heterodontosauridae (Becerra et al., 2016; Butler et al., 2010; Norman et al., 2011), appear in the Middle Jurassic (169 Ma) and persist up to the Cretaceous-Paleogene extinction 66 Ma. They are small-bodied (1--2m in length), bipedal, herbivores. Proportions of the hindlimbs suggest that many taxa were cursorial (Norman, 2004).

The group may have had an Asian origin (*Yandusaurus hongheensis,* Barrett et

al., 2005), dispersing to North America during the Late Jurassic (*Othnielia rex,* Galton, 1983). Two dispersal events occurred from North America in the Early Cretaceous, one to Europe (*Hypsilophodon foxii,* Huxley, 1870)) and the other to South America (*Gasparinisaura,* Coria & Salgado, 1996)). By the end of the Cretaceous, they are also found on Antarctica (*Trinisaura santamartaensis*. Hooker et al., 1991) and Australia ("hypsilophodontids", Rich et al., 1989). Previously histologically sectioned material, examined in this study, includes *Orodromeus makelai* (Horner & Weishampel, 1988; Horner et al., 2009), from the Two Medicine Formation of Montana (Campanian, 75 Ma). This is a small (2.5m length), dedicated biped. Advanced development of hatchlings led Horner & Weishampel (1998) to conclude that the young were likely to have been precocial.

Iguanodontians (Fig. 1.4) appeared in the Late Jurassic (157 Ma) and persisted up to the Cretaceous-Paleogene extinction event (66 Ma). They are medium to large-bodied (5-15m in length), facultative bipeds. Many members of this group are notable for having a thumb spike.

The group originates in the Middle Callovian (165 Ma) of England (*Callovosaurus leedsi*, Ruiz-Omeñaca et al., 2007). By the middle of the Kimmeridgian (155 Ma), they are known from North America (*Camptosaurus dispar,* Gilmore, 1909; *Dryosaurus altus,* Marsh, 1894) and Africa (*Dysalotosaurus lettowvorbecki,* Virchow, 1919). Given the basal position of *Tenontosaurus*, a substantial ghost lineage is implied in North America (Norman, 2004; Werning, 2012). Throughout the Early Cretaceous, iguanodontians diversified on all three continents (North America, Europe and Africa); however, by the Late Cretaceous, they are only found in Europe (*Telmatosaurus*

transsylvanicus, Weishampel et al., 1993; *Tethyshadros insularis,* Dalla Vecchia, 2009; *Zalmoxes robustus,* Nopsca, 1900; *Zalmoxes shqiperorum*, Weishampel et al., 2003).

Included among iguanodontians in the present study are *Tenontosaurus tilletti* (Ch. 5), *Iguanacolossus fortis* (Ch. 3 and 5), *Dysalotosaurus lettowvorbecki* (Ch. 5) and *Eolambia caroljonesa* (Ch. 4 and 5). *Tenontosaurus tillettii* is a stem iguanodontian from the mid- Cretaceous Cloverly Formation (115 Ma) of Montana and Wyoming, and from the Antlers Formation of Oklahoma (Ostrom, 1970). *Tenontosaurus* was between 6.5 and 8m in length, and likely a facultative biped. *Dryosaurus altus* is a dryosaurid from Late Jurassic Morrison Formation (156 Ma) of Utah. *Dryosaurus* is between 2.4 and 4.3m in length and likely an obligate biped. *Camptosaurus dispar* is an ankylopollexian from the Late Jurassic Morrison Formation (165 Ma) of Utah (Marsh, 1879). *Camptosaurus* was approximately 8m in length and facultative biped. *Iguanacolossus fortis* is a styracosternan from the Cenomanian Yellow Cat Member (124 Ma) of the Cedar Mountain Formation of Utah (McDonald et al., 2012). *Iguanacolossus* was approximately 9m in length and a facultative biped. *Eolambia caroljonesa* is a basal hadrosauroid from the Cenomanian Mussentuchit Member (97 Ma) of the Cedar Mountain Formation of Utah (McDonald, 2012). *Eolambia* was approximately 9m in length and a facultative biped.

The last group under consideration is Hadrosauridae (Fig. 1.5). Although their origins remain uncertain, it may have been as early as the Cenomanian (95 Ma), based on *Protohadros* (Head, 1996), and they persisted to the Cretaceous-Paleogene extinction event (66 Ma). They are (generally) large-bodied, herbivorous, facultative

bipeds.

It is likely that the hadrosaurids originated in North America in the Early Cretaceous (Horner et al., 2004; Prieto-Marquez, 2010). By the Late Cretaceous, hadrosaurids are found in North America (Cifelli et al., 1997), South America (Valieri et al., 2010), Europe (Weishampel et al., 1990), Asia (Xing et al., 2014) and Antarctica (Case et al., 2000). It is thought that dispersal from North America occurred after the split between hadrosaurines and lambeosaurines (Case et al., 2000; Prieto-Marquez, 2010). Within Hadrosaurinea, there was a posited dispersal event to Asia in the Early Maastrichtian (*Saurolophus angustirostris*, Case et al., 2000) and another to South America no later than the late Campanian (*"Kritosaurus"*australis, Case et al., 2000). Within Lambeosaurinea, a dispersal event to Asia has been suggested to have occurred no later than the Campanian (*Tsintaosaurus spinorhinus*, Weishampel et al., 1990).

Included in the present study are *Maiasaura peeblesorum* (Ch. 4 & 5) and *Hypacrosaurus stebingeri* (Ch. 5). *Maiasaura peeblesorum* is a hadrosaurine from the Campanian Two Medicine Formation (77 Ma) of Montana (Horner & Makela, 1979). *M. peeblesorum* was approximately 9m in length and a facultative biped. Lack of development in the appendicular elements of hatchlings, particularly with respect to condyles, led Horner & Weishampel (1988) to conclude that hatchlings followed an altricial developmental pathway. *Hypacrosaurus stebingeri* is a lambeosaurine from the Campanian Two Medicine Formation (Horner et al. 1994) and the Maastrichtian St. Mary River Formation of Montana (Sartin et al. in prep.). *H stebingeri* was approximately 9m in length and a facultative biped. The narial crest progressively

becomes proportionally larger throughout ontogeny; when maturity is reached the crest closely resembles that seen in *H. altispinatus* and *Corythosaurus casuarius* and in its semi-circular profile, but differs with repect to its internal construction (Evans, 2007; Evans, 2010).

1.2 Outline

1.2.1. General Considerations

To study the growth and development of individuals of any species, it is ideal to have multiple specimens, from a single population, at a broad range of ontogenetic stages. One way to obtain many specimens of the same taxon is to use material from bonebeds. In some cases, a bonebed is created by a catastrophic event; in these cases it is reasonable to assume that all individuals are of the same taxon and part of a single, biologic population (Rogers et al., 2010). Choosing a sample from a single, biologic population helps to mitigate variations in growth due to non-taxonomic factors (e.g. environmental). In many other cases, however, bonebeds are created over tens, or even hundreds of years (Rogers et al., 2007). Elements can be concentrated in an area through biogenic (e.g. nesting horizons, feeding sites) or physical (e.g. floodplain, ox-bow lakes) factors (Rogers et al., 2007). In cases such as these, it is not possible to assign all individuals of a given taxon to a single, biologic population. However, given the relatively short time over which these concentrations accumulate, it is reasonable to assume that all the specimens shared similar non-taxonomic factors.

It is also essential that all the specimens in the sample be from the same taxon. With respect to a given clade or group (e.g. hadrosaurid, iguanodontid), bonebeds are

often monodominant. Monodominant is different than monospecific; the former implies that one taxon dominates the fauna present, while that latter implies that there is only one taxon present in the fauna. That bonebeds may be monodominant is particularly helpful because the material in bonebeds is often disarticulated and unassociated. However, while bonebeds are often monodominant, it is rare for a bonebed to be completely monospecific, even within a given clade (Brinkman et al., 2007; pers. comm. J. Sertich, M. Getty). Morphologic characters can often help determine which elements belong to a given taxon. However, one must be careful when using morphologic characters associated with display structures. Recently, researchers have begun to question whether specimens that are generally considered to be separate taxa (often with different cranial display anatomy) simply represent different ontogenetic stages and/or different sexes of the same species (for examples, see Horner & Goodwin, 2009; Schott et al., 2011 [pachycephalosaurs]; Dodson, 1976; Horner & Goodwin, 2006; Scannella & Horner, 2010 [ceratopsians]). These studies have employed histology to determine the age of specimens, as well as to determine whether a given specimen was still growing at time of death.

With respect to herbivorous taxa, bonebeds are often dominated by juveniles and subadults (Brinkman et al., 2007; Forster, 1990; Varricchio & Horner, 1993; pers. comm. J. Sertich, M. Getty). Varricchio & Horner (1993) suggested that this might indicate that juveniles of these taxa tended to live in cohorts, apart from the adults, but they did not test this hypothesis. Determining whether or not this is true for a given bonebed is important for taxonomic identification of the material but this can be especially difficult because adult traits of basal taxa are commonly juvenile traits in

more derived taxa due to heterochronic changes within evolutionary lineages (e.g. Guenther, 2007; Guenther, 2009 [Hadrosauridae]; Chinnery, 2001 [Ceratopsidae]). Several examples of material have previously been assessed as adult, then later determined to be sub-adult or juvenile (for examples, see Schott et al. 2011 and Horner & Goodwin 2009 [pachycephalosaurs]; Scannella & Horner 2010, and Horner & Goodwin 2006 [ceratopsians]; Campione et al., 2013 [hadrosaurs]).

Histology can inform about the age and growth rate of each specimen, and whether the individual has reached skeletal maturity in ways that gross morphology alone is often unable to do. This information can be obtained by counting the number of annual growth marks (AGM), measuring the spacing of the AGMs and determining whether or not an outer circumferential layer (EFS) is present. One common type of AGM is Lines of Arrested Growth (LAGs), although LAGs are not the only type of AGM. AGMs will be discussed in greater detail in the following section ("2.6 Annuli and Growth Cycles"; Fig. 1.6).

However, for reasons yet to be determined, AGMs are not always present. In cases where they are absent, it is still possible to determine the age class (e.g. juvenile, subadult) and relative growth rate of the specimen by analyzing the vascularity and secondary remodeling of the cortex (both measures of vascularization and secondary remodeling are discussed in greater detail in Section 2, "Analysis of Slides"). When bone grows rapidly, it is more highly vascularized and vascular canals are predominately radially oriented; when bone is undergoing slower growth, it is less vascularized and longitudinally orientated of vascular canals predominate (Botha & Chinsamy, 2001; Chinsamy, 1997; Horner et al., 2000; Hübner, 2012; Klein & Sander,

2008; Ray et al., 2004). Rapid growth in the skeletal system is an indication that the specimen is a hatchling or juvenile, and that it has not yet reached sub-adulthood (Castanet et al., 2000; Chinsamy, 1997; Horner et al., 2000; Huttenlocker et al., 2013; Klein & Sander, 2008).

Bone secondary remodeling, also known as the development of a secondary Haversian system, is the result of osteoclasts resorbing bone, followed by osteoblasts depositing bone. Secondary osteons can be differentiated from primary osteons by the outer layer of cement and the appearance of a Maltese-cross pattern when viewed under crossed-Nicols prisms (Ricqlès, 1976; Huttenlocker et al., 2013). This process starts in juveniles and continues past the point of skeletal maturity (Botha & Chinsamy, 2001; Currey, 2003; McFarlin et al., 2008; Rayfield, 2007; Sander, 2006). Remodeled bone is weaker than primary fibro-lamellar bone, so it may at first seem disadvantageous (Currey, 2003); however, under closer inspection possible advantages present themselves.

Haversian systems occur under two conditions. The first is when an element is placed under significant mechanical stress by a muscle or group of muscles. Under this condition, the remodeling is localized to the area deep to the muscle attachment. In growing bone, these attachments grow and migrate as well. It has been suggested that this remodeling may provide mechanical advantage by replacing disorganized bone characteristic of fast growth with well-positioned secondary osteons (Currey, 2003). Additionally, the stress placed on these areas of bone may make them more susceptible to fatigue damage, such as micro-cracking. While Haversian bone is mechanically weaker than fibro-lamellar bone, it does inhibit crack propagation (Aguirre et al., 2006;

Currey, 2003; Hedgecock et al., 2007; Mori & Burr, 1993; van Oers et al., 2008).

The second condition under which Haversian systems develop is age. Remodeling can happen at different rates in different elements in the same individual (Horner et al., 1999; Mitchell & Sander, 2014; Sander & Tückmantel, 2003; pers. obs.). As with areas of muscle attachment discussed above, it has been suggested that this is a response to micro-cracks. However, remodeling during the aging process occurs more or less consistently throughout the cortex, beginning with the most interior portions and moving towards the surface; it is unlikely that micro-cracks occur with such regularity in every element, and accordingly, is unlikely the sole explanation for the occurrence of secondary remodeling. It has also been suggested that after bone cells die, they may become hypermineralized and therefore more brittle; removing such bone and replacing it with Haversian bone would be mechanically advantageous (Currey, 2003). Combining information from histology, AGMs, and measures of vascularity with that gained through gross morphology can facilitate taxonomic identification of the material.

The last requirement, after assuring that all specimens are from the same population and taxon, is that the sample includes all age stages. If a given bonebed contains only juveniles and subadults, it may still be possible to find and include adult material from the same taxon within the same general stratigraphic horizon and geographic area as the bonebed material. Including such adult material does introduce a number of assumptions into any study and should be considered thoughtfully. It is, nonetheless, important to try to include adult material in these cases.

1.2.2 Study Organization

The present study is concerned with examining the growth and development of three different ornithopod taxa. Cross-sectional and longitudinal data are essential for studies of growth and development in fossil taxa (Lee et al., 2013). Cross- sectional data give us a view of multiple specimens at a specific time; longitudinal data give us a view of the same specimen at many different times. Cross-sectional data are important for minimizing the effects of variation between individuals of the same group. Longitudinal data are important for minimizing the effects of variation within individuals of the same group and uncovering changes over lifetimes. Linear measurements and geometrical morphometrics have the advantage of being non-consumptive, and yield important information about gross morphology and allometry (Lee et al., 2013). However, these methods can only provide cross-sectional, as opposed to longitudinal, data in fossil taxa. Histologic analysis, which examines the microstructures of bone, on the other hand, provides longitudinal data for a specimen. Given a sufficient sample size, it is also possible to obtain cross-sectional data from histologic studies (Chinsamy-Turan, 2005).

Section 2 describes in detail the techniques used in making and analyzing histologic thin-sections. The techniques used to make the thin-sections are standard in the field; they are described in detail so that other researchers may replicate them. This section also details the methods used to analyze these slides. This includes both qualitative methods (e.g. tissue descriptions) and analytic methods (e.g. calculation of Percent Vascular Density).

Section 3 describes in detail the histology of the ontogenetic series of three

ornithopod taxa. The first ontogenetic series examined in the present study consists of iguanodontian material from the Doelling's Bowl bonebed, in the lower Yellow Cat Member of the Cedar Mountain Formation of western Utah. With respect to ornithopod material, the bonebed is monodominant and contains individual skeletal elements from a broad range of sizes. The material is morphologically very similar to the only known iguanodontian, *Iguanacolossus forti*, from the same stratigraphic horizon and similar geographic area (the two sites are separated by 50 km) as the Doelling's Bowl iguanodontian. However, the Doelling's Bowl material is significantly smaller than the only known specimen of *I. forti.*

Histologic analysis was conducted on individual elements of varying size from Doelling's Bowl, as well as on a partial limb shaft from the hologtype of *I. fortis.* Very few annual growth marks (AGMs) were found in the Doelling's Bowl material, whereas the *I. fortis* element was completely secondarily remodeled with no visible AGMs (as might be expected in large individuals). This prevents a comparison of growth rate using AGMs. Instead, age stage and growth rate of the Doelling's Bowl material were primarily determined by analysis of vascular patterns, osteon size and development.

The second ontogenetic series examined consists of iguanodontian material from the *Eolambia*/Cifelli #2 Quarry in the Mussentuchit Member of the Cedar Mountain Formation of eastern Utah. As with the material from the Doelling's Bowl bonebed, this sample contains individual skeletal elements of a broad size range. The largest individuals in this sample have been referred to adult *Eolambia*, but significantly larger material from other quarries has also been assigned to this taxon.

Histologic analysis was conducted on individual elements of varying size from *Eolambia*/Cifelli #2 Quarry, as well as on a partial femur of *E. caroljonesa* from the FMNH Quarry. Analysis of annual growth marks (AGMs) was used to determine the age stage and growth rate of all specimens in the study. Additional measures, such as vascular pattern, osteon size and density, were also used to inform the analysis with respect to both age stage and growth rate.

Whether the appearance of the first AGM is a reliable indicator that the specimen no more than one year old, and that the absence of an AGM is a reliable indicator that the specimen was under one year of age, was addressed. Sections of tibiae, femora, and humeri of varying sizes from the *Eolambia*/Cifelli #2 Quarry were made. The decision to include three different elements was made in response to the discrepancy in LAGs Horner et al. (1999) found in different elements from the same skeleton and that Horner et al. (2000) found in different elements from the same size-class. This study found that all elements of subadult size possessed AGMs, as Woodward et al. (2015) had found in *M. peeblesorum*. However, the largest specimen sampled (large femur from the FMNH Quarry) contained fewer AGMs than smaller specimens in the sample. This is not what one would expect if there are no missing AGMs, as one would expect the larger specimen to be older than the smaller specimens. The validity of retrocalculations in this specimen was then examined.

The third ontogenetic series consists of the lambeosaurine material from the BFD Quarry in the St. Mary River Formation of Montana. As in the case of the material from Doelling's Bowl and Eolambia/Cifelli #2, this sample also contains individual elements of a broad size range. The individuals in this sample have been

identified as *Hypacrosaurus stebingeri. Hypacrosaurus stebingeri* (although similar to *M. peeblesorum,* (Woodward et al., 2015)), does not show LAGs until it reaches what is generally considered to be subadult in size and the largest specimens show relatively few LAGs (max = 8). (Horner et al. 1999; pers. obs.)

Unlike the material in the previously described ontogenetic series, the adult size of *Hypacrosaurus* is known and the identification of the material as *Hypacrosaurus* is not in question. As with *Eolambia,* whether the appearance of the first AGM is a reliable indicator that the specimen no more than one year old was addressed, as was whether the absence of an AGM is a reliable indicator that the specimen was under one year of age.

Sections of tibiae, femora, humeri, and ulnae of varying sizes from the BFD Quarry were made. As with *Eolambia*, the decision to include four different elements was made in response to the discrepancy in LAGs Horner et al. (1999) found in different elements from the holotype of *Hypacrosaurus stebingeri*. The present study found that all elements of subadult size, and only elements of this size, possess AGMs; this is similar to what as Woodward et al. (2015) found in *M. peeblesorum*.

Figures

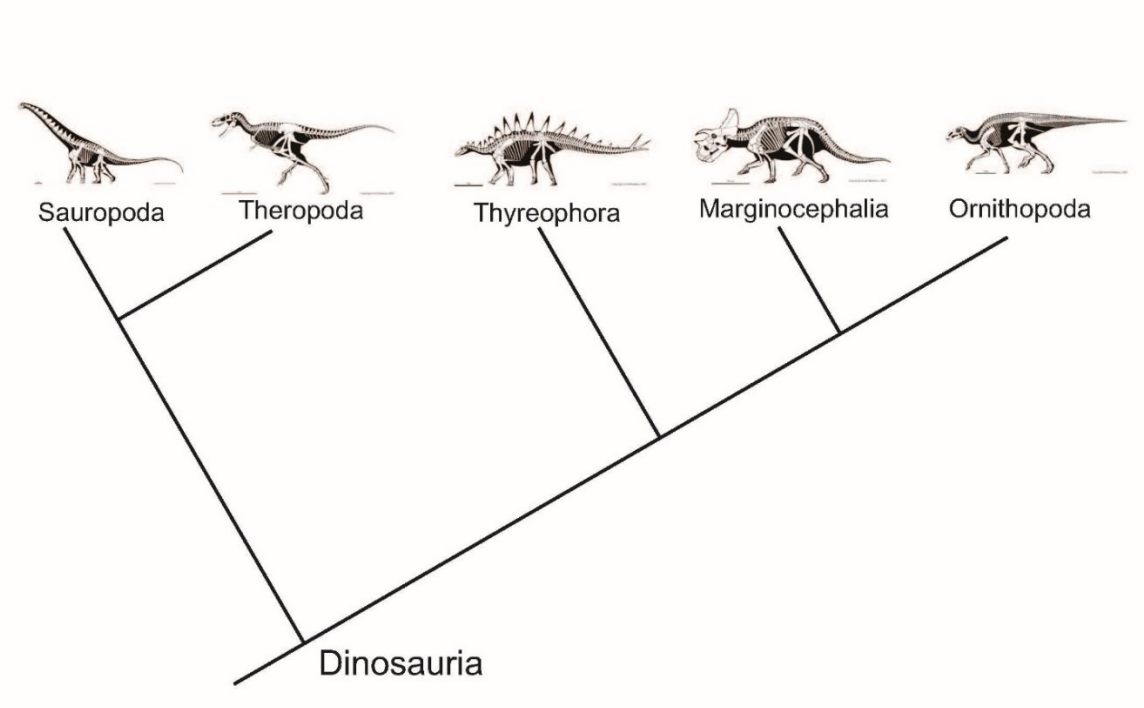

FIGURE 1.1 Cladogram of Dinosauria. (Images used with permission of Scott Hartman)

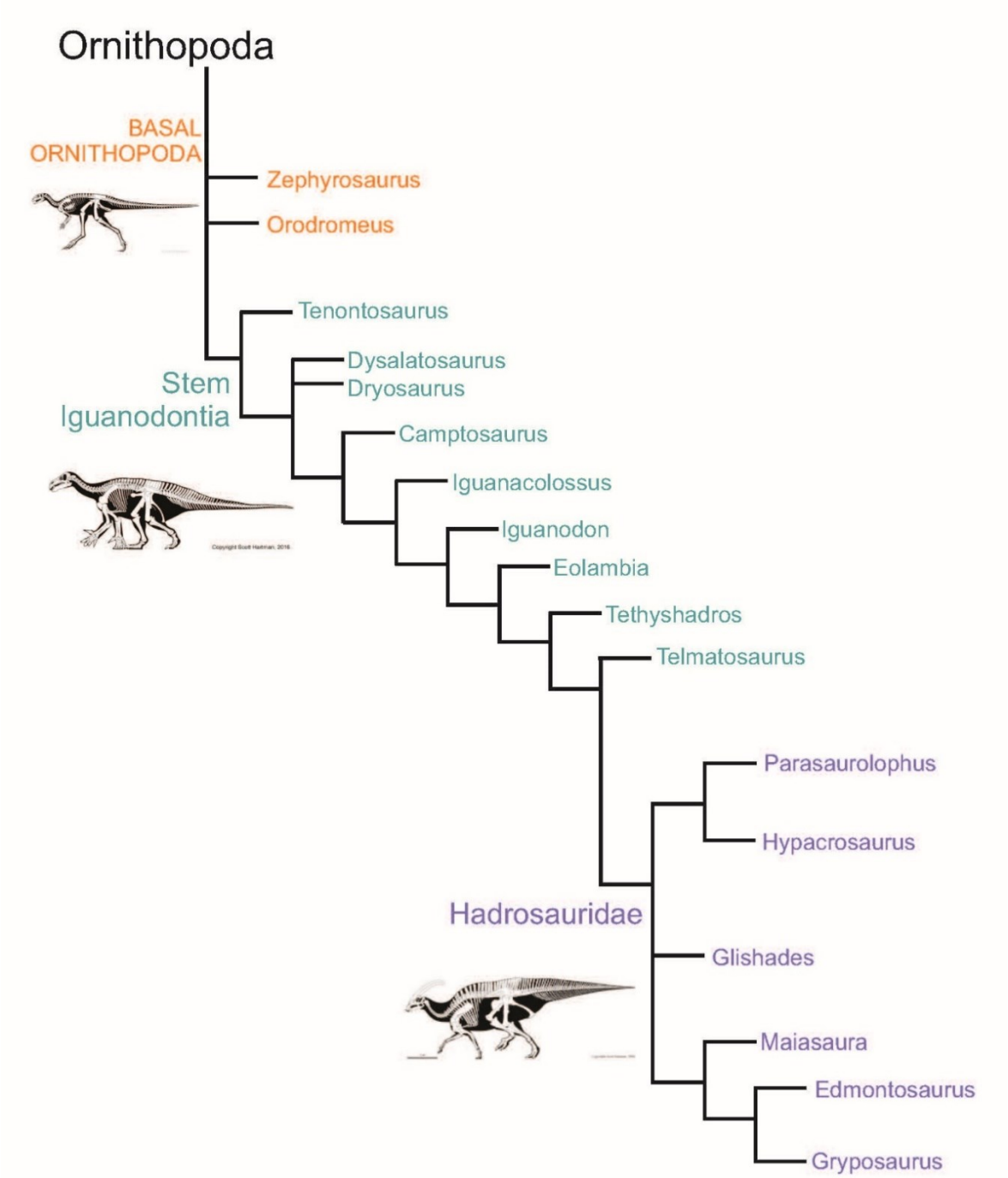

FIGURE 1.2 Cladogram of Ornithopoda (after MacDonald 2012, Prieto-Marquez 2010; images used with permission of Scott Hartman)

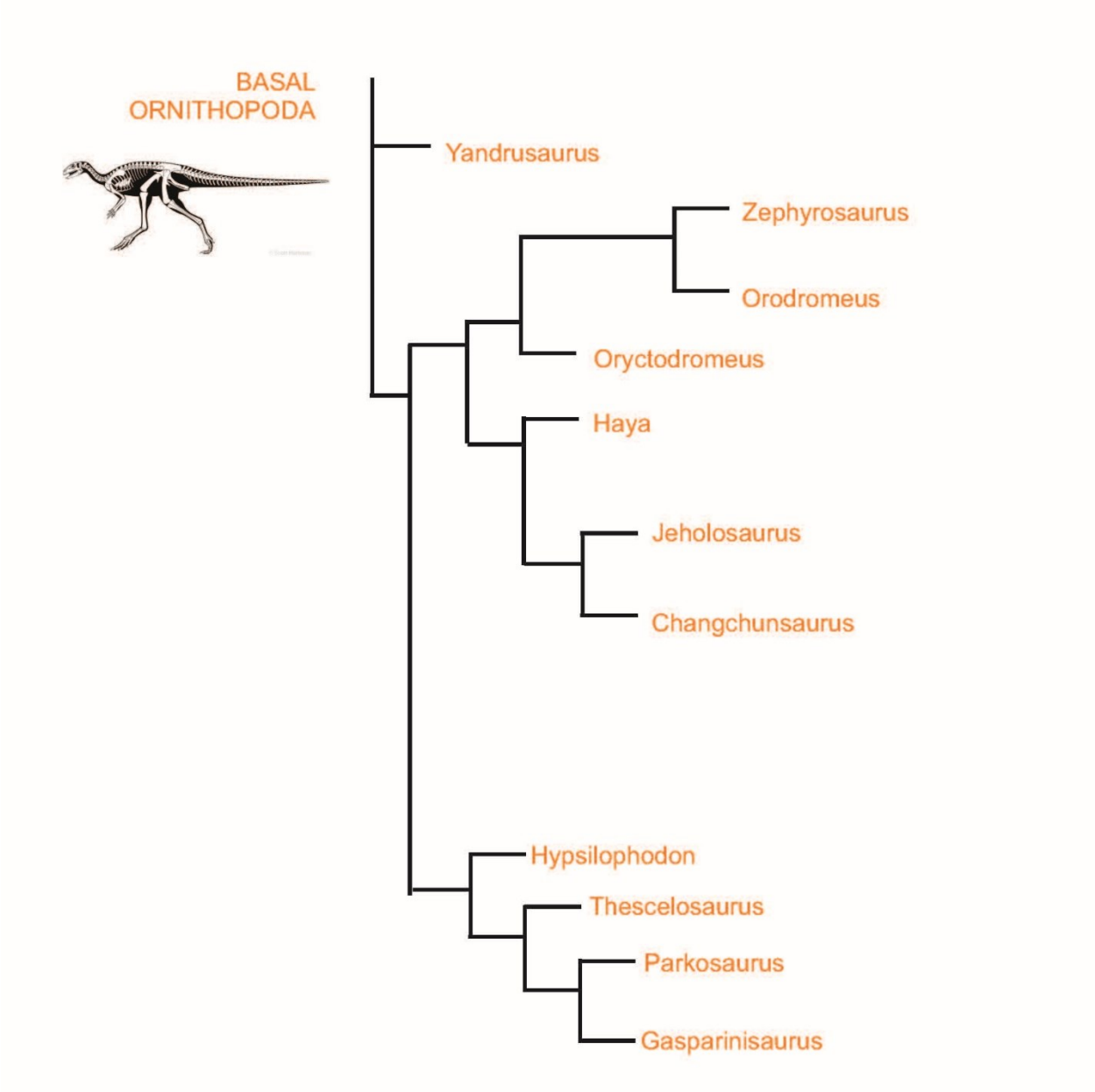

FIGURE 1.3 Cladogram of Basal Ornithopoda (after Brown 2013, Osi 2012; images used with permission of Scott Hartman)

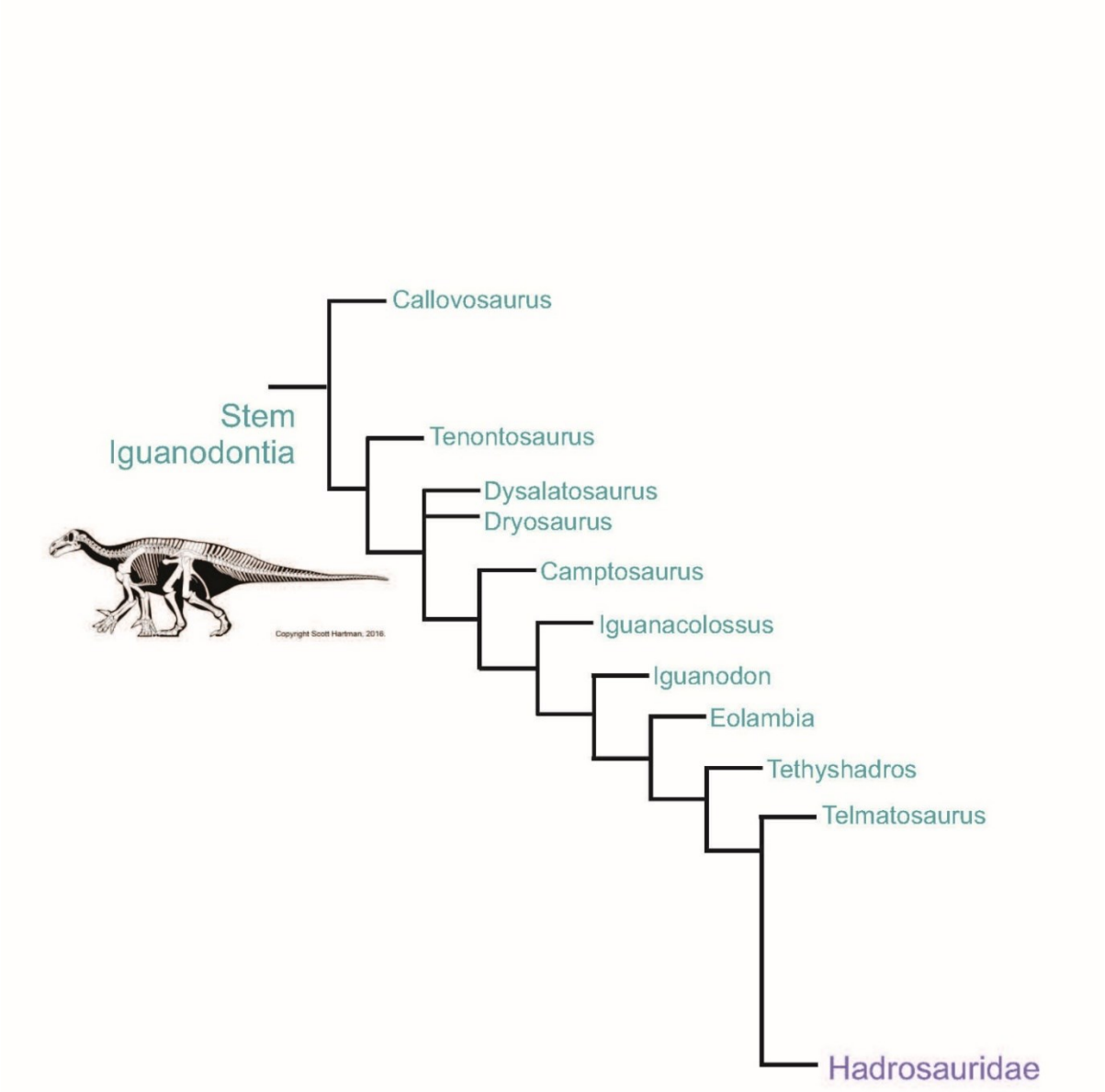

FIGURE 1.4 Cladogram of Iguanodontia (after MacDonald 2012, Norman 2015; images used with permission of Scott Hartman)

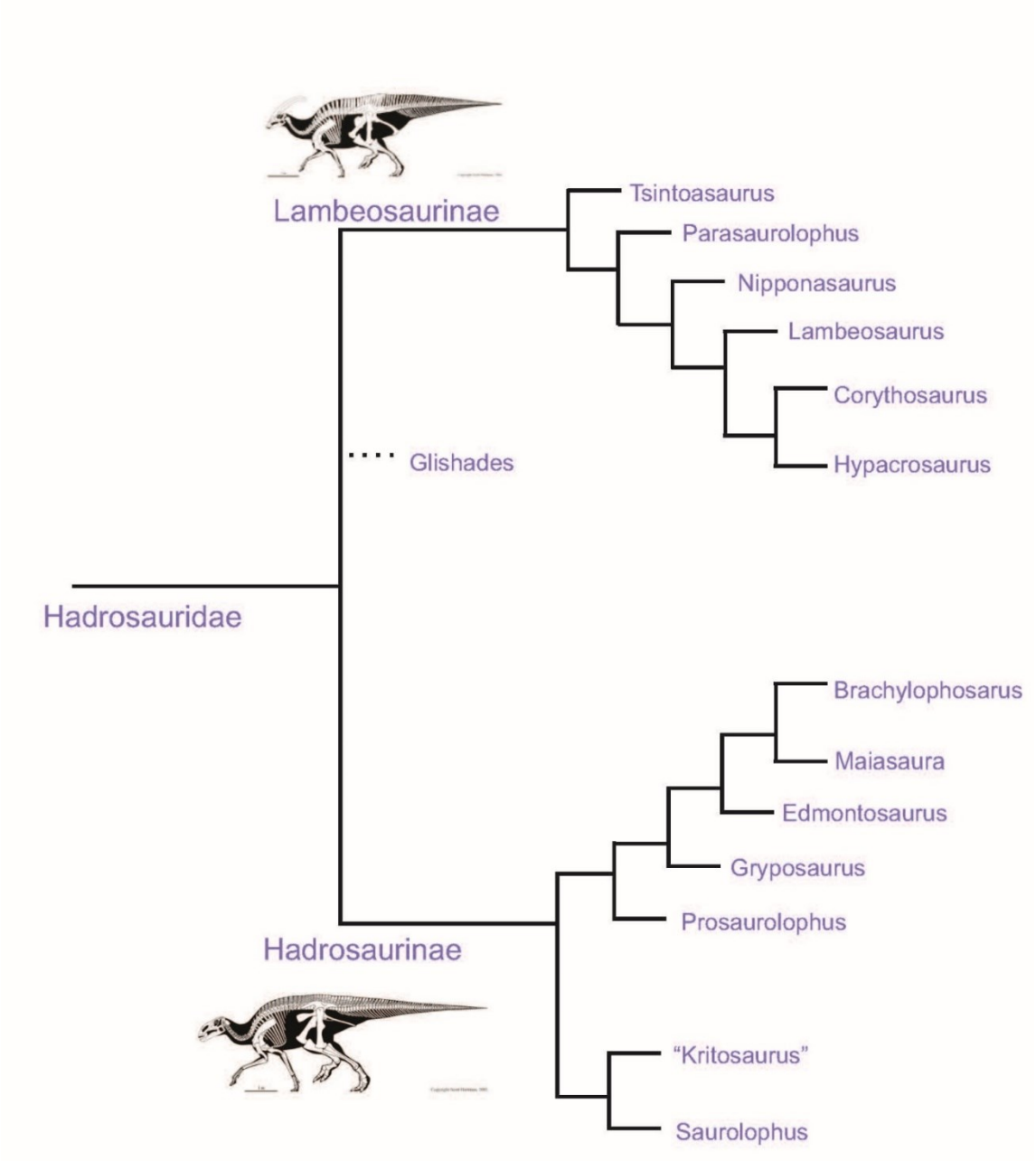

FIGURE 1.5 Cladogram of Hadrosauridae (after Evans et al 2007, Horner 2004; images used with permission of Scott Hartman)

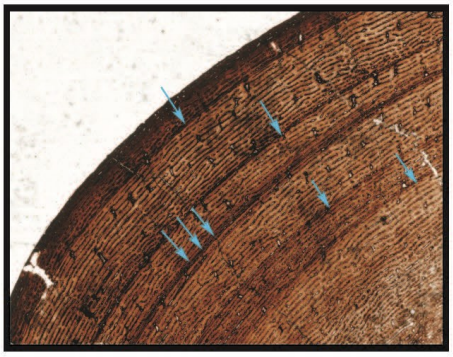

(A) Lines of Arrested Growth.

Lines of Arrested Growth (LAGs) appear as thin, semi-transparent to opaque bands with clear edges that represent the complete cessation of growth. Blue arrows mark the LAGs.

(B) Annuli

Annuli appear as narrow bands of parallel-fibered or lamellar bone that represents a period of slow growth, following a period of rapid growth. The large arrow marks the annuli; the smaller arrow marks the narrow band of lamellar bone within the annuli.

*FIGURE 1.6 Annual Growth Marks (AGMs). The present study uses both **(A)** Lines of Arrested Growth and **(B)** Annuli to assess the age of specimens.*

2: Materials and Methods

This study utilizes material previously un-sectioned and undescribed (see Table 2.1). For each taxon examined in this study, multiple specimens of each limb element (e.g. humerus, ulna, femur, and tibia) and age class were sectioned and measured.

2.1 Age Class Estimation

It is often difficult to estimate age class (e.g., hatchling, juvenile, subadult, adult) prior to histologic examination. Bone surface texture has been suggested (Callison & Helen, Helen, 1984; Tumarkin-Deratizian, 2003; Tumarkin-Deratzian et al., 2006; Tumarkin-Deratzian et al., 2007), although has not been successful when used on *Alligator* (Tumarkin-Deratzian et al., 2007). In light of these mixed results, and diagenetic changes that often occur during fossilization, bone surface texture was not used to assess age class. In Dinosauria, as well as Reptilia more generally, age assessments are often based on suture closure in the skull and vertebrae. This is problematic for the current study as many of the specimens that were used for this study do not have associated skulls and/or vertebrae (Brochu, 1996; Irmis, 2007; Maisano, 2002). In the absence of associated material, the only reasonable alternative is to choose specimens based on size alone. Once each element was histologically sectioned, it was assigned age classes following Horner et al. (1999 and 2000; see 'Analysis of Slides' below for more details).

2.2 Linear Measurements

Least Circumference.

It is standard procedure to section an element at the least circumference of the diaphysis. The least circumference often occurs at or around midshaft, but may occur more proximally or distally. This is especially true of the humerus and femor, where the deltopectoral crest and fourth trochanter, repectively, can occur at or around midshaft. Given this, it is possible to determine least circumference for all specimens – whether from the gross specimen or from the slide. When possible, both the gross specimen and the slide were measured. A cloth tape measure was used to measure the gross specimen (Fig. 2.1). To measure a specimen on a slide, the image of the slide (including a scale) was imported into Adobe Photoshop CC 2014 for measurement.

Maximum Length.

Methods and landmarks are taken from von den Dreisch (1976). For each element, two anatomical landmarks were established and the measurement taken between these (Fig. 2.1). This is important because it standardizes the measurements, although it is sometimes the case that absolute maximum length of the element is not taken. These measurements were taken using Mitutoya digital calipers (< 150 mm, to the nearest 0.1 mm) and dial calipers (>150 mm, to the nearest 1 mm). The following is a list of anatomical landmarks used:

- Humerus – proximal apex superior to the head; distal apex of medial condyle
- Ulna – proximal apex of olecranon process; distal apex of medial condyle
- Femur – proximal apex of greater trochanter; distal apex of medial condyle

- Tibia[1] – apex of proximal condylar surface (not including the cnemial crest); distal apex of ascending process for the fibula

Not all measurements were possible, particularly if the anatomic landmarks are not preserved or because the diaphysis is not preserved after sectioning. In the case of the latter, if values for the specimen were available (e.g., in the literature, personal communication) these were used.

2.3 Slide Preparation

Thin-sections were made following standard techniques (see Chinsamy-Turan, 2005; Padian & Lamm, 2013; Werning, 2012). The details are given below to ensure that they are clear and reproducible by future investigators. Additionally, photographs and sketches were made of the specimens at various stages of this process.

Molding and Casting.

Some institutions (e.g. UMNH) require that all specimens be molded and cast prior to sectioning regardless of element size. In these cases, the entire element was molded and cast prior to sectioning. For the largest elements (for example, UMNH VP 25139, UMNH VP 25146), layers of water-based liquid latex (#74 Latex Molding Compound, A-R Products) were used to create the mold and a mother mold was created using plaster and fiberglass cloth. The elements were then cast

[1] In general, avian models are sufficient. However, the tibiae of ornithopods are unlike those of birds and mammals. The points used for this element follow von den Dresich (1976), but are entirely of my own choosing.

using urethane casting resin (Smooth Cast 300; Smooth-On, Inc.). For smaller elements (UMNH VP 25144, UMNH VP 25140), pourable, platinum cure, silicon rubber (Dragon Skin 20 Silicon Rubber, Smooth-On, Inc.) was used to create the mold and a mother mold was created using plaster. Sulfur-free clay was used throughout this process to create molds and dams for the pourable silicon rubber and plaster. The elements were the cast using urethane casting resin (Smooth Cast 300; Smooth-On, Inc.).

For institutions that did not require casts of whole elements, whether a cast of the whole element or only the section ('plug') was made was determined by element size. In the case of elements shorter than approximately 20 cm, molds of the entire element were made prior to sectioning; elements longer than 20 cm were not molded prior to sectioning. Molds of these small elements were made using a two-part, platinum cure, silicone rubber (Silputty, Douglas & Sturgess). Paper labels, containing the institution code and specimen number, were covered in contact paper and embedded in the top half of each mold. The molds were cast using a resin impregnated plaster (Resin Rock, Whip Mix). Yellow labels were painted on the casts and specimen numbers were written on these with permanent markers.

Molds and casts of all sections were made prior to embedding. Molds were made using a two part, platinum cure, silicone rubber (Silputty, Douglas & Sturgess). Paper labels, containing the institution code and specimen number, were covered in contact paper and embedded in the top half of each mold. The molds were cast using a resin impregnated plaster (Resin Rock, Whip Mix). Yellow labels were painted on the casts and specimen numbers were written on these with permanent markers. Molds and

casts are reposited at the same institution as the specimen from which they were obtained.

Selection and Extraction of Section ('plug').

Transverse sections of each element were taken at the point of least circumference (Fig. 2.1), which helps to ensure that sections are taken from the same place relative to features that change during ontogeny (i.e., trochanters, condyles). In femora, this point consistently occurred immediately distal to the forth trochanter; in tibia, approximately 2/3 the length of the shaft; in humeri, the least circumference is found immediately distal to the deltopectoral crest. In the case of femora and humeri, it was always possible to visualize the forth trochanter and deltopectoral crest, respectively. In the case of tibiae, it was sometimes the case that only the shaft was present; in these cases, the section was taken at the point of least circumference along what was present of the shaft.

Prior to extraction, a line of white dots was painted (acrylic paint) around the least circumference. Sections were extracted such that the plug extended 2-3 cm to either side of this line. Sections with diameters equal to or less than 4 cm were extracted using a diamond blade precision saw (Acutech); sections with diameters greater than 4 cm were extracted using a diamond blade on a standard tile saw. In all cases, if glue lines or natural breaks were present where cuts were to be made, these lines or breaks were utilized instead; cyanoacrylate glues were dissolved with acetone, and epoxies were heated with a heat gun.

After extraction, a series of marks were painted on each plug. The plug was aligned with the remaining specimen, so that the orientation could more easily be

assessed. This was done to ensure that anatomical positions could still be determined after embedding, and subsequently translated to the finished slides. The code used is as follows:

- Yellow Dot – Medial
- Green Dot – Lateral
- Orange Dot – Cranial
- Blue Dot – Caudal
- Red Dot – Distal
- White Square – Proximal (the specimen number was written on this in permanent marker)

The first four were painted on both sides of the white dotted line; the latter two were painted on the cut or broken ends.

Embedding

Specimens were embedded in polyester resin (Silmar 41 Clear; Illstreet Composites, Inc.). Containers were chosen to allow at least 2 cm of space between the specimen and side of the container. Prior to pouring, containers were sprayed with a silicon mold release agent (Universal Mold Release; Smooth-On, Inc.). A base of approximately 1 cm was poured and allowed to cure in the fume hood. The specimen was then placed on this base; sometimes a small amount of cyanoacrylate glue was used to keep the specimen from moving during the embedding process. A layer of resin, no greater than 100 g, and embedding no more than half of the specimen was poured and vacuumed. This layer was allowed to cure (typically 24-48 hours) before pouring successive layers.

Successive layers were added in this manner until the specimen was fully embedded, with 1-2 cm of resin covering the topmost surface. Embedded specimens were then released from their molds and excess resin trimmed away with a tile saw.

Mounting and Grinding

The embedded specimens were then cut in half along the dotted white line using either a diamond blade precision saw (Acutech) or a diamond blade on a standard tile saw. If the cut surface of the specimen had significant porosity, the surface was covered with a layer of resin, epoxy or cyanoacrylate glue (depending on the size of the pores), vacuumed and allowed to cure.

The cut surfaces were then ground on a lapidary wheel with 90, 300, and 600 grit silicon carbide paper, in that order. Next, the surface was hand ground on a glass plate with 600 silicon carbide grit. Following this, specimens were then allowed to dry for at least 24 hours.

Specimens were then adhered to a frosted glass slide with epoxy (2 Ton Epoxy, Devcon), clamped and allowed to cure for 48 hours. After difficulties with many specimens "peeling up" from the glass slides, a set of plastic slides was made as well. The 3 mm thick plastic slides were hand frosted with 600 silicon carbide grit prior to mounting. Specimens were mounted using cyanoacrylate glue and allowed to cure for 2 hours.

Specimens were then cut into approximately 0.10 cm thick sections[2] with a precision saw (Hilquist). Slides were then ground to desired optical contrast, not a

[2] This thickness only reports the thickness of the specimen, and not the slide to which it is attached.

preset thickness, with a 600 grit upright grinder (Hilquist). Slides were again ground to desired optical contrast, not a preset thickness, by hand with 600 grit silicon carbine. Once the desired optical contrast was achieved, slides were polished by hand with 1000 grit silicon carbide to remove any visible scratches.

Slides were labeled with the specimen number, project number and anatomic positions noted with a permanent marker (glass: Lumocolor Fine Tip Permanent Marker, Staedtler; plastic: Fine Tip Permanent Marker, Sharpie) and archived at the specimen's home institution.

2.4 Slide Imaging

Slides were imaged using a petrographic microscope (Buehler; Nikon) under both plane polarized light and crossed Nicols at 4x magnification. The microscope is equipped with a digital camera, allowing images to be taken easily. Imaging equipment at six different institutions was used for this study. Images taken at MOR and ROM were taken with a microscope that has a mechanized stage. These images were stitched together by the Nikon software as the images were taken; once complete, the composite was saved in both .tiff and .jpeg format. Images taken at FMNH, University of Maryland, and University of Utah were taken with a microscope that lacks a mechanized stage. Individual images were taken manually and stitched together by PTGui; both the individual images and the composite were saved in .jpeg format.

Composite images were imported into Adobe Photoshop CC 2014 for further processing. In all cases this included color and tone adjustments. In the case of images stitched by PTGui, this also included cropping the image, then formatting the background to a solid color similar to that of the exposed blank slide. All images

included below were take in plain polarized light.

Unprocessed and processed digital images will be made available to researchers through Morphobank (morphobank.org), as originally done by Werning, 2012.

2.5 Analysis of Slides

Axis Measurements

The major and minor axes of the cross-section and medullary cavity are measured both in Adobe Photoshop CC 2014, as well as by hand with a metric ruler. The major axis was determined; then the minor axis, perpendicular to the major axis, was determined (Fig. 2.2). The major and minor axis of the medullary cavity was also determined in this manner.

Average Cortical Thickness

For each specimen, the cortical thickness is taken at the "thinnest", "fattest" and most common thickness in Adobe Photoshop CC 2014, as well as by hand with a metric ruler. These measurements are then averaged to calculate average cortical thickness (Fig. 2.2). Only areas that preserved the full cortical thickness were selected for measurement.

Age Class Determination

As mentioned above, determination of hitstological age class was made following Horner et al. (1999 and 2000). A brief description of how each stage is assessed is as follows:

- **Hatchlings**[3] – largely undifferentiated bone matrix surrounding vascular canals;

  medullary cavity is not present or just beginning to develop.

- **Juveniles** – well-formed primary osteons; annuli or lines of arrested growth (LAGs) may or may not be present; Haversian systems have formed; well-developed, but largely hollow, marrow cavity.

- **Subadults** – thick, dense cortical bone; annuli or LAGs present; marrow cavity is filled in with trabeculae; a faint External Fundamental Sytem (EFS) may be beginning to develop.

- **Adults** – distinguished from subadults primarily on the basis of a well-developed External Fundamental System (EFS). It is important to note that 'adult' refers to skeletal, not reproductive, maturity. It is likely that skeletally immature subadults were reproductively mature (Lee & Werning, 2008)

Analysis of Vascularity

Percent Vascular Density (PVD).

The PVD is the percent of analyzed area occupied by vascular canals (Cubo et al., 2005). When bone is grows rapidly, it is more highly vascularized than when it is undergoing slower growth. Rapid growth in the skeletal system is an indication that the specimen is a hatchling or juvenile, and that it has not yet reached sub- adulthood

[3] The terms 'hatchlings' and 'nestlings' are used interchangeably in the literature. I have chosen to use the term
'hatchling'. It should also be noted that Horner et al. (2000) describe two hatchling and juvenile stages. As in other studies by these researchers (Horner et al. 1999), I have combined the two hatchling stages into one age class and the two juvenile stages into another.

(Castanet et al., 2000; Chinsamy, 1997; Horner et al., 2000; Huttenlocker et al., 2013; Klein & Sander, 2008).

To calculate Percent Vascular Density, the following equation was used:

PVD = (Total Area of Specimen) / (Total Vascular Area)

A standard area for an element was chosen to ensure that commensurate areas were analyzed for all elements. The areas selected for analysis were then extracted from the images using the crop tool in Adobe Photoshop CC 2014; all subsequent analyses were conducted in this program. The scale was set to 1 pixel = 1 pixel; as PVD is a measure of percent, this scale is sufficient.

The total area of the slide was determined by selecting Image > Properties to find the height and width of the image in pixels. To easily exclude background, cracks, mineral inclusions, etc., the pencil tool was used to cover these areas with a contrasting color (e.g. blue).This was done so that these areas could easily be excluded. To determine the Total Area of the Specimen, the area of contrasting color was subtracted from the total area of the slide. This was done by using Select > Color Range, with Fuzziness set to 150 (this value was selected based on visual inspection).

To determine the Total Vascular Area, first the color of the vascular canals was observed. Then this value was selected by using Select > Color Range. For most slides, as Fuzziness of 150 was used in order to include all the vascular areas. On occasion, when a slide was particularly light, this value was increased; when such adjustments were made, the adjustment has been noted. Magic Eraser was then used to remove these

areas. The background was then set to a contrasting color (e.g. bright green) and the RGB value of that color noted. Next, the replaced area was selected by using Select > Color Range (using the noted RGB to make the selection), then measured using Image > Analysis > Record Measurements. There are sometimes small dark areas unrelated to vascularity that were also replaced during this procedure. When this is the case, the size of these areas was determined, then excluded from the sample in Excel using the formula: SUMIF(range, size condition).

Finally, to calculate PVD, the value for Total Vascular Area was divided by Total Area Measured.

Obliquity Index (OI)

The Obliquity Index is a measure to the vascular orientation (Cubo et al., 2005; De Boef & Larsson, 2007). More specifically, the ratio of the area of canals that are oriented longitudinally to the total area of all canals; the more canals that are oriented longitudinally, the higher the value of the index. When bone grows rapidly, vascular canals are predominately radially oriented; when bone is undergoing slower growth, longitudinal orientation predominates (Botha & Chinsamy, 2001; Chinsamy, 1997; Horner et al., 2000; Hübner, 2012; Klein & Sander, 2008; Ray et al., 2004). As mentioned above, rapid growth is an indication that the specimen has not yet reached sub-adult size.

To calculate Obliquity Index, the following equation was used:

OI = (Total Area of Longitudinal Canals) / (Total Vascular Area)

The Total Vascular Area was determined above, as part of the PVD calculation. To determine the Total Area of Longitudinal Canals, all non-longitudinal canals were marked out using the Pencil Tool in Adobe Photoshop in a contrasting color. The area of the remaining canals was then measured using Select > Color Range, with Fuzziness = 150 (unless otherwise noted). In cases where most of the canals are non-longitudinal, the longitudinal canals were marked out, then the remaining area was analyzed and its area determined. This area was then subtracted from the Total Vascular Area, in order to determine the Total Area of Longitudinal Canals.

Haversian Remodeling Index (HRI)

Third, the Haversian Remodeling Index was calculated (Cubo et al., 2005). This measure indicates how much of the cortex has been secondarily remodeled; the higher the index, the greater percentage of the cortex that has been secondarily remodeled. Secondary remodeling, also known as the development of a Haversian system, occurs as an individual ages or when an element is placed under significant mechanical stress by a muscle or group of muscles. In the case of the former, the remodeling occurs consistently around the cortex, beginning first with the endosteal margin, then moving towards the periosteal surface. In the case of the latter, the remodeling is limited to the area of the muscle attachment. Under both conditions, the remodeling process starts in juveniles and continues past the point of skeletal maturity (Botha & Chinsamy, 2001; Currey, 2003; McFarlin et al., 2008; Rayfield, 2007; Sander, 2006). To ensure that the Haversian Remodeling Index is a function of age, and not mechanical stress induced by

muscular attachments, care was taken to select areas of bone that are not adjacent to muscle attachments and that show the generalized pattern of remodeling beginning along the endosteal margin and moving towards the periosteal margin.

In each case, it was impossible to measure all the vascular canals in any specimen in the sample due to the extensive fracturing. Instead, a section(s) of each specimen in a standardized location(s) was measured; in the case of multiple sections, the average all sections measured was applied to the specimen as a whole.

2.6 Annuli and Growth Cycles

The primary purpose of histologic analysis of the slides is to determine age of the individual. This can be done by counting the annual growth marks[4] (Fig. 1.6). For all elements, the circumference of the each AGM present was measured (Fig. 2.3). The cortical thickness and distance between AGMs was also calculated by averaging the thickness along the major and minor axes of each (Werning, 2012). AGMs was identified using two criteria generally accepted in the literature (see Chinsamy-Turan, 2005; Huttenlocker et al., 2013; Werning, 2012). First, to identify LAGs, the semi-translucent to opaque band is visible at multiple levels of magnification, has few or no cells, and little to no vascularity. Second, for all LAGs and annuli, the band continues around the entire circumference of the section.

The presence of an external fundamental system (EFS) is important for determining that the element is skeletally mature. This structure is formed by the

[4] In the case that LAGs are suspected to be missing, retrocalculations will be made to determine if this is the case, and if so, how many LAGs are missing (For more detailed information about these calculations, see 'Growth Rate and Growth Curve' below). In the case that not LAGs are present, growth cycles will be counted.

outermost periosteal layers. This subperiosteal tissue consists of parallel, longitudinally-arranged collagen fibers, and is almost entirely avascular (although it may contain a few secondary osteons). It is formed when annuli are laid down with no growth in between the individual annuli. As is the case with identifying individual annuli, this structure must be visible at different magnifications and be continuous around the circumference of the specimen.

While AGMs can provide an age estimate for the individual, this is not the same as an age class. Age class is important for a number of reasons. First, it provides a way of determining whether the entire range of growth has been examined. For instance, it can be used to determine whether the largest specimens in a sample represent skeletally mature adults. Second, when missing annuli are suspected, it can be used to assess the reasonableness of any retrocalculations. For instance, if retrocalculations on a juvenile indicated 40 missing LAGs, further investigation would be warranted.

The age of a specimen is usually determined by counting the number of annual growth marks (AGM, see Fig. 1.6). These growth marks take three distinct forms in long bones[5] – lines of arrested growth (LAGs), annuli, and polish lines (Ricqlès, 1980; Hübner, 2012; Huttenlocker et al., 2013; Lee et al., 2013; Sander et al., 2011). In thin-section, LAGs appear as thin, semi-transparent to opaque bands with clear edges that represent the complete cessation of growth (Huttenlocker et al., 2013) (see Fig 1.6A), whereas annuli appear as narrow bands of parallel-fibered or lamellar bone that represents a period of slow growth (e.g. Huttenlocker et al., 2013) (see Fig. 1.6B). Polish lines, on

[5] Teeth also record growth marks, known as lines of von Ebner (Erickson, 1996). These marks are usually daily, not annual, and are beyond the scope of the present study.

the other hand, are not usually prominent in thin-section, but they can easily be identified under reflected light when the core (or even transverse section) is polished to a mirror finish (Sander et al., 2011). Polish lines are usually examined when thin sections are not available; accordingly, these will not be used in the present study. How each structure presents itself histologically will be discussed in more detail below, but first let us turn our attention to their formation.

AGMs have been found in a wide variety of modern vertebrate clades – fishes (Ashiley, 1975; Hibiya et al., 1982), amphibians (frog: Guarino et al., 1998; newt: Halliday & Verrell, 1988; salamander: Measey & Wilkinson, 1998), reptiles (alligator: Woodward, Horner et al., 2011; Nile monitor: de Buffrénil & Castanet, 2000), turtles (Goshe et al., 2009; Wilson et al., 2003), birds (moas: Turvey et al., 2005; kiwis: Bourdon et al., 2009), and mammals (*Microcebus*: Castanet et al., 2004; ruminants: Köhler et al., 2012; xenarthrans: Straehl et al., 2013). These groups include taxa from many different environments (e.g. tropic, temperate), as well as from both exothermic and endothermic physiologies. The one feature that all these taxa have in common is that they take more than one year to reach skeletal maturity (Woodward et al., 2013). AGMs are also found in a wide variety of fossil vertebrate clades – non-avian dinosaurs (for example, sauropods, Sander, 2000); non-avian theropods (Bybee et al., 2006); stegosaurs (Hayashi et al., 2009); ceratopsians (Erickson & Tumanova, 2000); ornithopods (Hübner, 2012); Mesozoic birds (Chinsamy & Elzanowski, 2001); therapsids (Ray et al., 2004); and ungulates (Sander, 2006).

That AGMs are annual marks is supported by evidence in extant taxa. For example, Castanet et al. (2004) experimentally manipulated the photoperiodicity of

Microcebus such that the animals experienced 365 periods of light and dark every 280 days under constant, controlled environmental conditions. The result was that the animals laid down LAGs every 280 days. This suggests that LAGs are laid down annually. Furthermore, although the annual timing may be correlated with environmental cues (e.g. seasonal scarcity of resources, breeding cycles), it is not caused by these cues. Marangoni et al. (2009) ran a similar experiment with subtropical anurans with and produced similar findings. Buffrenil & Castanet (2000) injected bone-marking dye into wild Nile monitors. The monitors were then recaptured after a year and sacrificed; the formation of one LAG after the marking dye was visible in the specimens. Additionally, several studies have successfully correlated the numbers of annuli preserved in specimens of known ages (Hutton, 1986; Klein et al., 2009; Peabody, 1961; Snover & Hohn, 2004; Woodward et al., 2011).

While it is the case that the literature supports the view that AGMs are annual marks, the physiological and/or cellular processes that cause them to form are not known (Huttenlocker et al., 2013). Köhler et al. (2012) surveyed 115 extant ruminants; this sample included specimens from across the globe, as well as across many different biomes and found that in each taxon, the timing of growth marks corresponded to the annual unfavorable season for that taxon. During this time, animals also decrease their body temperature and metabolic rates, and bone- growth-mediating plasma insulin-like growth factor-1 levels; however, it is still unclear how this causes the formation of AGMs.

As mentioned above, AGMs take three distinct forms – LAGs, annuli and polish lines (Fig. 1.6). LAGs are perhaps the most commonly cited AGMs (for example, see

Erickson, 2005; Horner et al., 1999; Horner et al., 2000; Horner & Goodwin, 2009; Huttenlocker et al., 2013; Werning, 2012). In thin-section, they appear as thin, semi-transparent to opaque bands with clear edges that indicate the complete cessation of growth (Huttenlocker et al., 2013). These bands can be traced around the circumference of the cross-sections; they form around cells in the compacta, and never cut through them. The bands are acellular; in modern bone they are strongly basophilic (i.e., stain strongly with basic dyes, such as haematoxylin), indicating a high protein content (Castanet, 1994).

Annuli are not noted as often as LAGs, but as histologic studies become more common this is changing (for examples, see Botha & Chinsamy, 2001; Chinsamy, 1990; Ricqlès et al., 2008; Erickson & Tumanova, 2000; Hübner, 2012; Woodward et al., 2011). In thin-section, an annulus appears as a narrow band of parallel-fibered or lamellar bone that represents a period of slow growth (e.g. Huttenlocker et al 2013). Annuli are followed by a zone indicative of an elevated rate of growth, creating what some have labeled a "growth cycle" (Hübner, 2012). As with LAGs, annuli can be traced completely around the circumference of the section. In some taxa, younger individuals form annuli and not LAGs, although older individuals of these same taxa do lay down LAGs (e.g. Horner et al., 2009; Hübner, 2012; and Werning, 2012). These growth cycles match well with age predictions based on retrocalculations performed on older individuals (that do have LAGs) and the diameter of the element.

In subadult and adult sauropods, age has not always been determined by counting LAGs or annuli (Sander, 2000). Assessing LAGs and annuli reliably requires that one can visualize the entire cross-section of the diaphysis. Making transverse thin-

sections of these sizes poses practical problems; cores are generally made instead. A core of bone is similar to a geologic core; in both cases, a cylinder of material is removed with a hollow drill bit. In some cases thin-sections are made of these cores and potential LAGs and/or annuli are identified. In other cases, the core is polished, allowing polish lines to be identified (Klein & Sander, 2008; Klein & Sander, 2007; Sander, 2000; Sander & Tückmantel, 2003). These lines are not artifacts of the process of polishing, despite what the name might suggest; rather, they are concentric lines in the specimen that are better visualized once the specimen has been polished. These lines do not appear prominently in thin-sections, as LAGs and annuli do; instead, they can easily be identified under reflected light when the core (or even transverse section) is polished to a mirror finish (Sander et al., 2011).

Identifying AGMs is a necessary first step in estimating the age of a given specimen, but it is not always sufficient. In large specimens, especially those that have reached skeletal maturity, early AGMs may have been resorbed by the medullary cavity and/or obscured by secondary remodeling. In these specimens the margins of the cavity show signs of resorption and/or there is extensive secondary remodeling. To account for this loss, retrocalculations can be made to recover the number of missing AGMs and to help estimate their diameters. One way to do this, is to determine which LAGs overlap between specimens in an ontogenetic series (see Fig 2.4). It should be noted that different elements in the same individual often have different numbers of AGMs (Castanet et al., 2000; Horner et al., 1999; Werning, 2012), due to different rates of remodeling, expansion of the medullary cavity, and so on. When performing retrocalculations, it is important that if multiple specimens are used; they all must be

the same skeletal element of the same taxon. Using an ontogenetic series, instead of a single adult specimen, helps to strengthen the reliability of any necessary retrocalculations (Horner et al., 1999).

It is not necessarily the case that if a specimen has reached skeletal maturity, it will have resorbed AGMs or that they will be obscured by secondary remodeling (Woodward et al., 2013; Woodward et al., 2015). Determining whether there are missing AGMs is important for constructing a growth curve for the taxon. For example, consider a skeletally mature individual of a given size. This first LAG visible in the thin-section from this individual appears halfway through the cortex. This could be explained by accelerated growth rate during the first year, with a slowing of growth in subsequent years may result in no missing AGMs. However, it could also be explained by gradual growth during the first years of life if no AGMs were laid down, or if they had been resorbed, as might happen during expansion of the medullary cavity (Woodward et al., 2013).

Determining whether there are missing AGMs is essential before attempting to describe the growth of a taxon. However, this may not be as simple as it seems *prima facie*. Consider the case of *Maiasaura peeblesorum*. Horner et al. (2000) sectioned over 50 different elements, including vertebrae, ribs, limb girdles and long bones of *M. peeblesorum*; however, their study largely concerns six femora that span the known body size range of the species. They found that the smallest femora (< 50 cm in length) do not have AGMs, while the largest femora (>58 cm in length) showed signs of potentially missing AGMs. They considered both possibilities, that there are and are not missing AGMs, but did not reach a conclusion in favor of one over the other. In support of there

being no missing AGMs, they cited a number of studies on growth rates in extant birds. These studies, which will be discussed at greater length in Section 3, suggest that extant birds experience rates of growth commensurate with a *Maiasaura* femur reaching 50 cm in length during the first year of life. In support of missing AGMs, they examined LAG counts from elements of *M. peeblesorum* other than the femora. While none of the material in this study came from associated skeletons, it is possible to associate elements based on the size of individual from which they come, (although they may all come from different individuals of that size). When they looked at AGMs in elements in what was estimated to be the same size category as the femur with 3 LAGs (approx. 68 cm in length), they found that the rib contained 9 and the tibia 5. The difference in LAG counts suggests etiher that there are missing AGMs in at least both the tibia and femur, or that there is a substantial amount of intraspecific variation with respect to body size and age.

Woodward et al. (2015) examined 50 tibiae of *M. peeblesorum*; the specimens included the known size range for the taxon and came from the same stratigraphic level (even the same site in some instances) as those examined by Horner et al (2000). Woodward et al. (2015) found no signs of missing AGMs in any of their specimens, no evidence of resorption along the margin of the medullary canal, and no extensive secondary remodeling. As with the previous example (Horner et al., 2000), they did not find any AGMs in specimens smaller than ~50 cm in length. Based on this lack of AMGs, they concluded that there are no missing AGMs and, accordingly, estimate these individuals to be under 1 year of age. Woodward et al. (2015) did not discuss LAG counts from elements other than the tibiae and did not address the discrepancy pointed out by Horner et al. (2000).

2.7 Tissue Description

As is standard, a complete tissue description of the specimens is also included. This description provides additional information about growth trends, complementing the information provided by the growth curves. A description of the mineral and fiber organization is given following the classification of Francillion-Vieillot, et al. (1990). This classification system was chosen because it is comprehensive and used by most of the previously published studies considered here. Orientation of collagen fibers throughout the slide will be diagnosed using crossed Nicols as follows:

- **Lamellar Bone** – collagen fibers form a plywood-like pattern. This results in an alternating light and dark pattern under crossed Nicols.
- **Parallel Fibered Bone** – collagen fibers are closely packed and parallel to one another. They are highly anisotropic (i.e., fibers go in and out of extinction together as the stage is rotated). This type of tissue is sometimes referred to as 'pseudolamellar'.
- **Woven Fibered Bone** – collagen fibers are highly disorganized. They are relatively isotropic (i.e., remain extinct as the stage is rotated).

It should be noted that more than one type of fiber organization may be, and often is, present in a single slide. These orientations are useful in determining how quickly (or slowly) the bone was growing at the time of their deposition. For instance, woven fiber bone indicates that the bone was growing very rapidly, whereas lamellar bone indicates a much slower rate of growth. Vascular orientation and arrangement, as well as osteonal orientation, arrangement and development is also indicative of the rate

of both growth; radial orientation of canals is indicative of fast growth, while longitudinal orientation is indicative of slow growth.

As noted by Chinsamy (2005), most dinosaur bone is fibrolamellar. In this type of bone, primary osteons are embedded in woven bone matrix. When the vascular canals are organized in a radial manner, this type of bone can be called 'reticular fibrolamellar bone'; when the vascular canals are organized in a longitudinal manner, this type of bone can be called 'plexiform fibrolamellar bone'. Most of the tissues described in this study are of these two types.

Other notable features, such as calcified cartilage, and presence and direction of Sharpey's fibers, are documented when present. Calcified cartilage indicates that the individual is perinatal; it can also indicate whether or not the element was capable of bearing weight. Sharpey's fibers are indicative of muscle attachments.

2.8 Comparison of Growth Rates

The samples in this study are composed primarily of juveniles and subadults, as diagnosed by both size of the element and histologic characteristics. As discussed above, the lack of adult material available for sectioning means that growth curves were not constructed for any of the samples in this study. However, a number of measurements were taken from the samples in this study. For example, for each AGM, the major and minor axis were measured, as well as the circumference. From these data, it is possible to estimate the element length for each AGM. Using these data, it is possible to compare the relative sizes (e.g. percent of adult size) of different taxa at the same age.

Figures

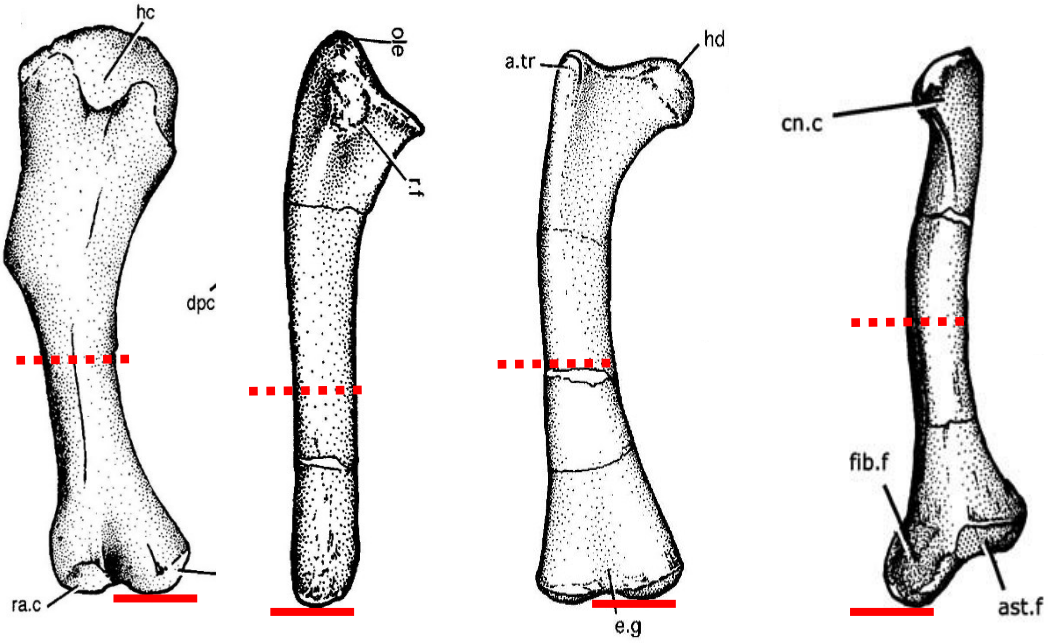

FIGURE 2.1 Linear Measurements. The solid lines indicate the locations used for maximum length. The dashed lines indicate the most common location of the least circumference for each element. (after Weishampel et al. 2003)

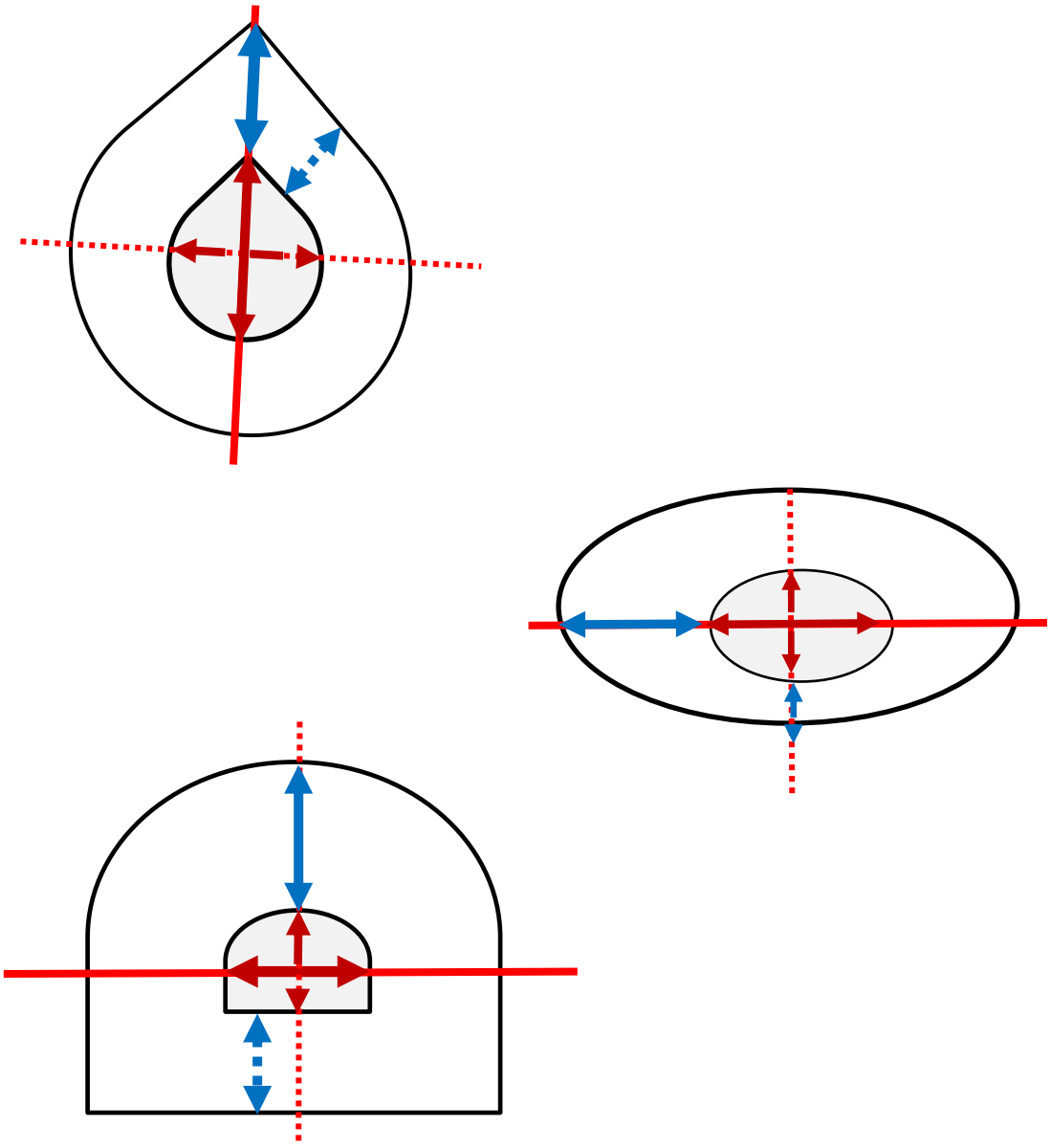

FIGURE 2.2 Cross-Sectional Measurements. The most common cross-sectional shapes are shown.The solid line shows the major axis; this axis was determined first. The dashed line shows the minor axis; this is perpendicular to the major axis. The solid red arrow shows the major axis of the medullary cavity; the red dashed line shows the minor axis of the medullary cavity. The "fattest" thickness (solid blue arrow) and "thinnest" thickness (dashed blue arrow) of the cortex was measured, then averaged.

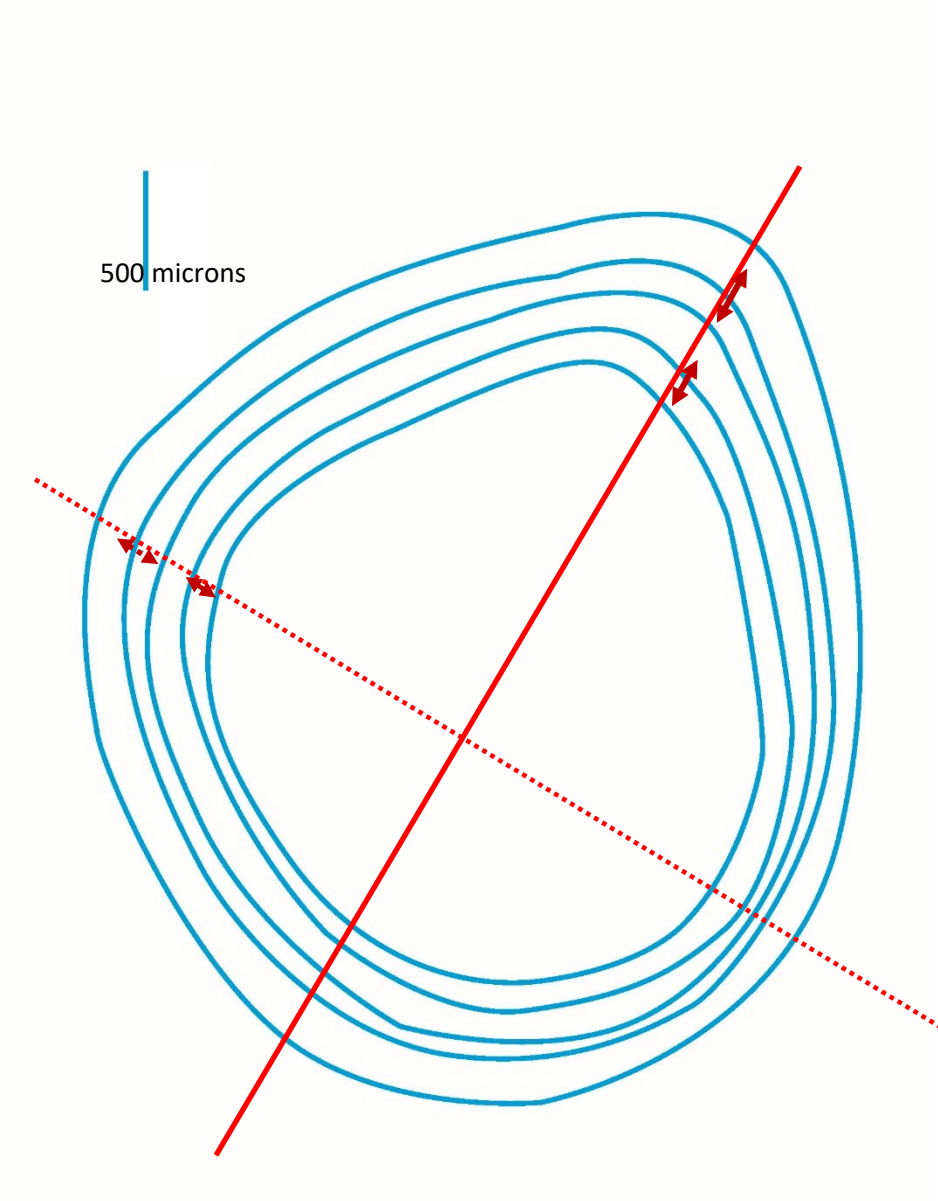

FIGURE 2.3 Measurements of Annual Growth Marks (AGMs) The concentric blue lines mark the LAGs, while the straight line marks the scale. The solid red line marks the major axis; the double-headed arrows along the major axis mark where cortical thickness between LAGs was measured. The dashed red line marks the minor axis; the double-headed arrows along the minor axis mark where cortical thickness between LAGs was measured. The measurements along the major and minor axis for each interval were then averaged.

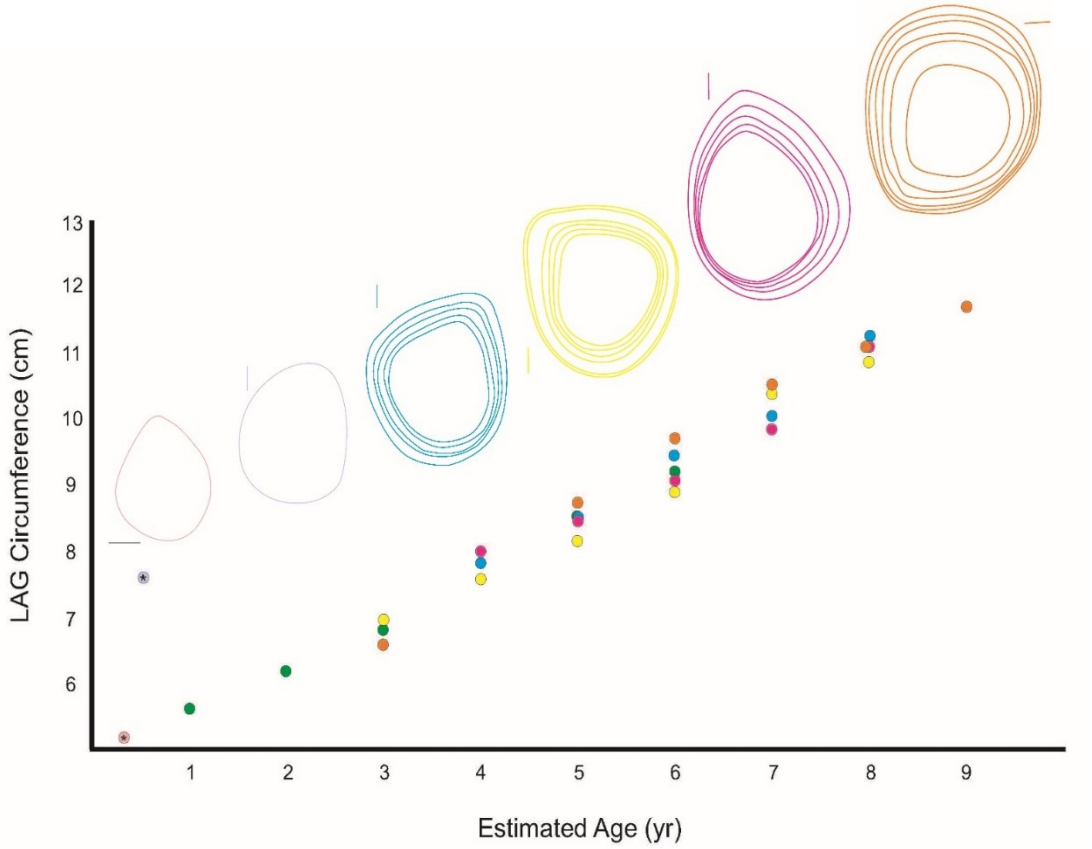

FIGURE 2.4 Retrocalculations by Superimposition of Individuals. Sequence of LAGs in an ontogenetic series of tibiae are graphically overlapped to form a composite growth record. Data was adapted from Eolambia specimens in this study; the dimensions of the LAGs has been adjusted to better display the method.

Tables

Taxa	Specimen Number	Study Code*	Element	Age Assessment	Length (cm)	Least Circumference (cm)
Doelling's Bowl Iguanodontian	UMNH VP 25142	H1	Humerus	Juvenile	15.7	5.5
Doelling's Bowl Iguanodontian	UMNH VP 25138	H2	Humerus	Juvenile	16.9	6.0
Doelling's Bowl Iguanodontian	UMNH VP 25137	H3	Humerus	Juvenile	26.4	8.5
Doelling's Bowl Iguanodontian	UMNH-VP 25139	H4	Humerus	Subadult	30.6	11.2
Doelling's Bowl Iguanodontian	UMNH VP 25146	H5	Humerus	Subadult	----	15.9
Doelling's Bowl Iguanodontian	UMNH VP 25143	F1	Femur	Juvenile	26.2	10.8
Doelling's Bowl Iguanodontian	UMNH VP 25145	F2	Femur	Juvenile	33.1	12.5
Doelling's Bowl Iguanodontian	UMNH VP 25135	F3	Femur	Subadult	48.3	20.0
Doelling's Bowl Iguanodontian	UMNH VP 25141	F4	Femur	Subadult	63.9	28.0
Doelling's Bowl Iguanodontian	UMNH VP 25144	T1	Tibia	Juvenile	31.9	10.6
Doelling's Bowl Iguanodontian	UMNH VP 25140	T2	Tibia	Juvenile	42.3	16.0
Doelling's Bowl Iguanodontian	UMNH VP 25136	T3	Tibia	Subadult	48.0	17.0
Iguanacolossus forti	UMNH VP 20205	U1	????	Adult	----	13.5
Eolambia caroljonesa	CEUM 35641	H1	Humerus	Juvenile	>8.03	4.8
Eolambia caroljonesa	CEUM 35369	H2	Humerus	Juvenile	>16.0	6.3
Eolambia caroljonesa	CEUM 35621	H3	Humerus	Subadult	>16.0	6.5
Eolambia caroljonesa	CEUM 35719	H4	Humerus	Subadult	>12.3	7.0
Eolambia caroljonesa	CEUM 35743	H5	Humerus	Subadult	>17.0	8.1
Eolambia caroljonesa	CEUM 35662	H6	Humerus	Subadult	>13.1	8.7
Eolambia caroljonesa	CEUM 35357	H7	Humerus	Subadult	>17.9	12.1
Eolambia caroljonesa	OMNH 62250	H8	Humerus	Subadult	23.5	9.2
Eolambia caroljonesa	FMNH 3848	F0	Femur	Hatchling	----	4.0
Eolambia caroljonesa	CEUM 13317	F1	Femur	Juvenile	>12.0	8.2
Eolambia caroljonesa	CEUM 34399	F2	Femur	Juvenile	>22.1	10.6
Eolambia caroljonesa	CEUM 35444	F3	Femur	Juvenile	>31.8	5.1
Eolambia caroljonesa	CEUM 14503	F4	Femur	Juvenile	>30.9	16.8
Eolambia caroljonesa	OMNH 62194	F5	Femur	Juvenile	----	16.0
Eolambia caroljonesa	FMNH UT130825-3	F6	Femur	Subadult	---	24.0
Eolambia caroljonesa	CEUM 34276	T0	Tibia	Hatchling	25.9	8.8
Eolambia caroljonesa	CEUM 13306	T1	Tibia	Juvenile	>15.6	8.4
Eolambia caroljonesa	CEUM 35386	T2	Tibia	Subadult	>21.6	9.2
Eolambia caroljonesa	CEUM 52874	T3	Tibia	Subadult	>18.5	11.1
Eolambia caroljonesa	CEUM 35704	T4	Tibia	Subadult	>19.4	11.2
Eolambia caroljonesa	CEUM 74590	T5	Tibia	Subadult	>22.0	11.8
Eolambia caroljonesa	CEUM 35491	T6	Tibia	Subadult	>19.3	11.8
Eolambia caroljonesa	CEUM 14582	T7	Tibia	Subadult	>30.1	13.5
Eolambia caroljonesa	OMNH 62213	T8	Tibia	Subadult	>28.3	11.2
Hypacrosaurus stebingeri	MOR 609-89-82	H1	Humerus	Juvenile	26.4	9.7
Hypacrosaurus stebingeri	MOR 609-89-3	H2	Humerus	Juvenile	22.6	11.8
Hypacrosaurus stebingeri	MOR 609-89-15	H3	Humerus	Subadult	52.5	25.0
Hypacrosaurus stebingeri	MOR 609-89-191	U1	Ulna	Hatchling	23.4	6.5
Hypacrosaurus stebingeri	MOR 609-89-41	U2	Ulna	Adult	65.4	15.0
Hypacrosaurus stebingeri	MOR 609-89-111	U3	Ulna	Adult	----	15.0
Hypacrosaurus stebingeri	MOR 609-89-18	F1	Femur	Juvenile	35.6	14.5
Hypacrosaurus stebingeri	MOR 609-89-173	F2	Femur	Juvenile	40.6	14.5
Hypacrosaurus stebingeri	MOR 609-89-43	F3	Femur	Subadult	102.0	37.0
Hypacrosaurus stebingeri	MOR 609-638-13	T1	Tibia	Juvenile	34.6	14.5
Hypacrosaurus stebingeri	MOR 609-89-195	T2	Tibia	Juvenile	35.6	13.5
Hypacrosaurus stebingeri	MOR 609-89-145	T3	Tibia	Juvenile	37.1	14.5
Hypacrosaurus stebingeri	MOR 609-89-18	T4	Tibia	Subadult	75.0	28.0

TABLE 2.1 The above table lists all of the elements sectioned as a part of this study. The age class assessment, length and least circumference for each element sectioned are provided.

3: Results

3.1 Doelling's Bowl Iguanodontian

The first ontogenetic series examined was iguanodontian material from the Doelling's Bowl bonebed. While this portion of the study focuses on a specific case, the principles used to identify the material, thereby providing an adult end member to the ontogenetic series, are broadly applicable.

When new material is discovered, one must determine whether that material belongs to an existing taxon or is a new taxon entirely. One potential complication is that taxa are generally, and preferably, diagnosed on the basis of adult, skeletally mature material. Sometimes what had previously been taken to be *adult* material is discovered to be sub-adult or juvenile (for examples, see Horner & Goodwin, 2009; Schott et al., 2011 [pachycephalosaurs]; Horner & Goodwin, 2006; Scannella & Horner, 2010 [ceratopsians]; Campione et al., 2013 [hadrosaurs]). In these instances, the *adult* form is known in the literature and the taxon becomes a junior synonym. Histology of a specimen can inform us about the age, growth rate, and whether it has reached skeletal maturity in ways that gross morphology alone is often unable to do. Combining this information with gross morphology can help us best determine taxonomic identification of new material.

The Doelling's Bowl bonebed (Fig. 3.1.1) is a multi-taxon bonebed in the lower Yellow Cat Member of the Cedar Mountain Formation of western Utah. This site is named for the Utah geologist Helmut Doelling, whose maps of the Arches region led to the eventual discovery of the site by Jim Kirkland (Utah State Paleontologist, Utah

Geologic Survey) in 1990. The bonebed covers more than 25 acres and contains unassociated elements of many different taxa, including the type specimen of *Yurgovuchia doellingi* (Theropoda: Dromaeosauridae), an unidentified polacanthine ankylosaur, an unidentified sauropod, as well as teeth from numerous dinosaur taxa and crocodilians (Senter et al., 2012).

Despite its overall diversity, the Doelling's Bowl bone bed is dominated by iguanodontian dinosaur elements, both cranial and postcranial. Based on morphological similarities, these elements all appear to be from individuals of a single taxon at different ontogenetic stages. Among the largest elements, in particular the vertebrae, sutural closure suggests that these individuals had reached skeletal maturity. These neurocentral sutures are synchondroses, not sutures in the strictest sense of the term. However, as has been noted (for example, see Brochu, 1996; Horner et al., 2000; Irmis, 2007), using neurocentral suture closure to assess skeletal maturity in arhcosaurs is potentially problematic. For this reason, sutural closure is not taken as definitive evidence of skeletal maturity.

The only exception to the relatively uniform morphology in the iguanodontian sample is found in the ilia. Of the six ilia that have been discovered at the site, all but one share the same morphology. The dominant morphology is a simple blade-like morph (Fig. 3.1.2 C) and ranges from ~20 cm total length to ~ 60 cm total length. The singular morph is complex by comparison (Fig. 3.1.2 A&B) and ~ 47 cm in length.

The complex morph has what appears to be a supracetabular shelf and highly arched, laterally compressed cranial process; the simple morph lacks a supracetabular shelf and has a straight cranial process. The complex morph, however, has been

crushed and distorted to a greater degree than the other specimens; it is possible that the features it exhibits are artifacts of its preservation and not its original form. If original, the derived morphology of the complex morph's ilia suggests that the other post- cranial elements would likewise show derived characters as well, such as an increasingly closed extensor canal and more distally placed fourth trochanter of the femur. None of the postcranial elements (that have been fully prepped) in the assemblage show any evidence of such derived characters. All of the postcranial elements show the more basal characters that are consistent with the more basal morphology of the simple morph. This supports that observation that the complex morph's features are the result of taphonomy, and not biology.

One taxon of iguanodontian dinosaur, *Iguanacolossus fortis*, is known from an equivalent stratigraphic horizon within the Cedar Mountain Formation (McDonald et al., 2010). The type locality for *I. fortis*, known as Don's Ridge, is roughly 50 km away from the Doelling's Bowl site (pers. comm. Don DeBlieux; Fig. 3.1.3). *Iguanacolossus* is known from a single associated skeleton that includes both cranial and postcranial material. When the two different ilia morphologies from Doelling's Bowl are compared to *Iguanacolossus*, the simpler, blade morph is assignable to *Iguanacolossus*. When the other overlapping elements from the Doelling's Bowl iguanodontian and *Iguanacolossus* are compared, they are morphologically similar, even indistinguishable. This includes diagnostic elements, such as the pubis (pers. comm., Andrew McDonald); however, other diagnostic elements, such as the squamosal and axis, are not represented in the Doelling's Bowl material.

Given the morphologic similarity and the equivalent stratigraphic horizons for

the samples, it is reasonable to tentatively assign the Doelling's Bowl material (with the exception of the complex ilium) to *Iguanacolossus.* However, the elements at Doelling's Bowl are from individuals with a drastically different body size compared to that of the type of *Iguanacolossus*. Given this, if the largest individuals from Doelling's Bowl are indeed skeletally mature, it is difficult to assign them to *Iguanacolossus* without evidence of something (e.g. sexual dimorphism, evolutionary variation, environmental variation, etc.) to explain this great difference in size.

I examine the histology of the Doelling's Bowl iguanodontian to determine whether the largest specimens had reached skeletal maturity and, if not, whether its growth trajectory is compatible with it reaching the size attained by *Iguanacolossus*. I also examine the histology of *Iguanacolossus* to examine whether it had reached skeletal maturity and to compare its growth with that of the Doelling's Bowl iguanodontian.

Geologic Setting

Both Doelling's Bowl and Don's Ridge are located in the lower unit of the Yellow Cat Member of the Cretaceous Cedar Mountain Formation in western Utah (Figs. 3.1.1 & 3.1.3). This unit is bounded along its lower border by the smectitic mudstone of the Upper Jurassic Brushy Basin Member of the Morrison Formation, and along its upper border by a caprock layer of chert that separates the lower and upper units of the Yellow Cat Member. Hendrix et al. (2015) used U-Pb analysis of populations of 300 zircon grains from paleosols by laser ablation-inductively coupled mass spectrometry (LA-ICP-MS) to determine maximal depositional ages for the Yellow Cat Member. Their U-Pb

zircon data place the maximal depositional age of the paleosol at the base of the Yellow Cat Member at 139.7 ±2.2 Ma (Valanginian); the paleosol from the Upper Yellow Cat Member shows a maximal depositional age of 137.2±2.0 Ma (Hauterivian).

The lithology of Doelling's Bowl is characterized by mottled paleosols with matrix- supported chert pebbles. The presence of iron-rich, "hydromorphic gley soils" led Senter et al. (2012) to suggest that this was a wet, boggy environment. Elements of the same individual are often found articulated or in close association, and the long axis of elements show little to noevidence of being aligned along a preferred axis of orientation (Fig. 3.1.1). This supports the lithologic evidence of a low energy depositional environment.

Don's Ridge contains a single, isolated associated skeleton - that of the holotype (and only published specimen) of *Iguanacolossus*. The site extends over roughly 35 square meters in western Utah (Fig. 3.1.3). The lithology of Don's Ridge is characterized by a pale greenish grey to olive gray, sandy mudstone with widely scattered, floating chert pebbles (0.5-1.0 cm) and abundant purple mottled root traces. All elements of the individual were found in close association and the long axes of those elements show little to no evidence of being aligned along a preferred axis of orientation (Fig. 3.1.3). The skeleton appears to have been scavenged and trampled *in situ*. The amount of plastic deformation suggests that the sediment and elements were water logged for a significant period of time. The lithologic and taphonomic evidence supports a depositional environment of a stacked crevasse splay on a flood plain (Senter et al. 2012).

Materials

Limb elements from the Doelling's Bowl iguanodontian were selected based on their completeness and state of preservation. Only elements that could be clearly identified and that had mostly intact shafts (on gross examination) were used; I use the term 'gross examination' here because under histologic examination, it is obvious that the outermost portion of the cortext is missing. Care was taken in selecting elements to ensure that all sizes present in the bonebed were represented. Four femora, three tibiae, and five humeri were included in the sample (Table 3.1.1). For location of the section extracted and methods used to extract it, please refer to "Selection and Extraction of Section ('plug)" in Section 2.

The only nearly complete limb element from the type of *Iguanacolossus*, as mentioned above, is a fibula. However, because fibulae show extensive remodeling prior to skeletal maturity (Horner et al., 1999; pers. obs.), it was not selected for histologic examination. The only other limb material available from Don's Ridge is the shaft of a long bone that does not preserve either articular end (Fig. 3.1.4). The specimen is part of a single, insolated skeleton; no other vertebrate taxa were found at this site, so it is reasonable to conclude that it does belong to *Iguanacolossus.* The lack of 'twisting' indicates that it is not a tibia, and its cross-sectional shape demonstrates that it is not a fibula or radius. Beyond this, however, it is not possible to conclusively identify the element. Despite being unable to conclusively identify this element, it can reasonably be concluded that it will preserve a record of growth. Accordingly it was sectioned for this study.

Osteohistologic Analyses of Doelling's Bowl and *Iguanacolossus* Specimens

As part of the histologic description, the minor and major axes of both the outer cortex and medullary cavity, as well as the average cortical thickness were calculated using methods detailed under "Analysis of Slides" in Section 2 (Table 3.1.2). It should be noted that measurements were not always possible due to significant crushing and distortion of certain specimens.

Assessment of age category was made based on histologic features (Table 3.1.1). In addition to this, three measurements of vascularity were taken from each slide (Table 3.1.3). Percent Vascular Density (PVD), Obliquity Index (OI), and Haversian Remodeling Index (HRI) were calculated; a detailed description of these calculations can be found under "Analysis of Slides" in Section 2.

In each case, it was impossible to measure all the vascular canals in any specimen in the sample due to the extensive fracturing. Instead, multiple sections of each specimen in standardized locations were measured and the average applied to the specimen as a whole. In addition to measurements of vascularity, Annual Growth Marks (AGMs; see 'Objectives" for more information about AGMs) were identified; when present, the circumference of each AGM was measured and AGMs present in each specimen were counted.

For each section, both a full view and close-up image are included (see Figs. 3.1.5-3.1.17); the images of these sections will also be made available on MorphoBank.

Doelling's Bowl Specimens

Humeri

Juvenile

Specimens Examined: UMNH VP 25142 (H1), UMNH VP 25138 (H2),
UMNH VP 25137 (H3)
(Figs. 3.1.5-3.1.7)

The cross-section and medullary cavity UMNH VP 25142 (H1) are oval. The cross-sections of UMNH VP 25138 (H2) and UMNH VP 25137 (H3) are triangular; the medullary cavity of UMNH VP 25138 is roughly triangular, while that of H3 is more elliptical. In all three specimens, the medullary cavities show signs of crushing and distortion; these cavities are filled with sediment, isolated pieces of cortex, and an iron-bearing mineral. The original endosteal margins have been obscured by the distortion, as well as by mineral growth in the medullary cavity.

The distinction between inner and outer cortex of H1 is not readily apparent; this specimen closely resembles the inner cortex of the other two, H2 and H3. The cortex of H1 and inner cortex of H2 and H3 have similarly high Percent Vascularity Densities (PVD); both osteonal canals and primary osteons are present. The vascular canals are highly disorganized, as can be determined from their low Obliquity Index (OI). This portion of the cortex is composed of reticular fibrolamellar bone matrix. H1 and H2 show no signs of secondary remodeling; there are resorption cavities present at the endosteal margin of H3, as well as a few scattered secondary osteons, indicating the beginning of secondary remodeling.

The outer cortex of H2 and H3 is also highly vascularized, although it has a lower PVD than the specimen discussed above. This tissue is dominated by osteonal canals that are organized longitudinally, and have correspondingly high OI, with

primary osteons scattered throughout. This portion of the cortex is composed of plexiform fibrolamellar bone. In H2, there is a sharp distinction between inner and outer cortex demarcated by more open vascular canals in the latter.

No definitive LAGs or annuli are visible in any of these sections; no outer circumferential layer (OCL) is present in any of these specimens.

Subadult

Specimens Examined: UMNH VP 25139 (H4), UMNH VP 25146 (H5)
(Figs. 3.1.8-3.1.9)

The cross-section of UMNH VP 25139 (H4) is roughly elliptical, although extensive crushing obscures the original outline of the section, as well as completely obscuring the medullary cavity. The cross-section of UMNH VP 25146 (H5) is roughly reniform; the medullary cavity is elliptical and is filled with sediment and an iron-rich mineral.

The inner cortices of H4 and H5 are moderately to highly vascularized, with values of PVD similar to the inner cortices of the specimens discussed above. Like the inner cortices of the specimens discussed above, the osteonal canals and primary osteons are highly disorganized, have correspondingly low OI, and are composed of reticular fibrolamellar bone (Chinsamy, 1997; Huttenlocker et al., 2013). Similar to what is seen in H3 above, the inner cortexes of H4 and H5 show signs of both resorption along the endosteal margin and development of secondary Haversian Systems. The secondary osteons are more numerous in H4 and H5 than in H3, although their Haversian Remodeling Indexes (HRI) remain low overall. In H5, the secondary osteons for a band between the inner and outer cortex; within the band, the secondary

osteons dominate, but are not present outside of this band.

The outer cortices of H4 and H5 are moderately vascularized and have a similar PVD to the specimens discussed above. However, the outer cortices of H4 and H5 is up to twice as thick as that of H2 and H3. The outer cortices of H4 and H5 are dominated by osteonal canals that are organized longitudinally, with many areas that exhibit radial anastomoses and primary osteons scattered throughout (Chinsamy, 1997; Huttenlocker et al., 2013); this is a much more regular pattern than seen in H2 or H3, and the OI is correspondingly higher. This portion of the cortex is composed of plexiform fibrolamellar bone. The presence of iron rich minerals in this portion of the cortex can be mistaken for osteons; care was taken to visualize slides under crossed Nichols to confirm the identity of supposed osteons. No definitive LAGs or annuli are visible in any of these sections; no outer circumferential layer is present in any of these specimens.

Along the medial edge of H5 is an area of highly disorganized tissue, which could be described as reticular fibro-lamellar bone, with a PVD and OI more similar the values of the inner cortex. Primary and secondary osteons are present in this region as well. The appearance of this area is similar to that described by Hübner (2012) as the 'posteriolateral plug' of the femur of *Dysalotosaurus*. Hübner (2012) proposed that this may be due to muscle attachments in the overlying periosteum, and the stress produced by those muscles in the underlying tissues. Sharpey's fibers are generally found in the periosteum and the bone immediately deep to the periosteum. In the case of the H5, the periosteum is not preserved, nor is the outermost layer of bone. Given this, it is not possible to

determine whether Sharpey's fibers are present in this location. However, it is immediately distal to the attachment sites for m. pectoralis major and m. deltoideus; while these muscles attach in close proximity to each other, the attachment site of m. deltoideus is slightly more distal and closer to the site. Given this location, it is possible that the stress from this muscle produced the proxies for 'strain' observed in the fabric of the bone.

Femora

Juvenile

Specimens Examined: UMNH VP 25143 (F1), UMNH VP 25145 (F2)
(fig. 3.1.10-3.1.11)

The cross-section of UMNH VP 25143 (F1) is a rounded triangle; the cross-section of UMNH VP 25145 (F2) is a rounded crescent. The medullary cavities of both specimens are elliptical in cross-section and infilled with calcite and an iron bearing mineral. The division between the medullary cavity and the endosteal margin of F1 is distinct around most of the border. The medullary cavity of F2 shows signs that it has been crushed and distorted; the original endosteal margin has been obscured by this distortion.

The inner cortex of both F1 and F2 is highly vascularized, with a PVD similar to that seen in other juvenile specimens in this study. Both osteonal canals and primary osteons are present and highly disorganized throughout, with a correspondingly low OI. This portion of the cortex is composed of reticular fibrolamellar bone matrix. Resorption cavities are present at the endosteal margin, indicating the onset of secondary remodeling; no secondary osteons are present in F1, very few are present in

F2.

The outer cortex of both specimens is also moderately-to-highly vascularized with a PVD similar to the outer cortices of other subadults and juveniles in this study. It is dominated by simple canals that show alternating areas of longitudinally organized canals (plexiform and lamellar fibrolamellar bone) and areas with little organization (reticular fibrolamellar bone). The OI of the organized areas is high, while the OI for the disorganized areas is more similar to that of the inner cortex of each specimen. These areas are superficially similar to patterns that have been described as annuli (Chinsamy-Turan, 2005; Hübner, 2012; Woodward et al., 2013). In F1, the outer 1/3 of the cortex is highly vascularized, grading into the less vascularized inner 2/3 of the cortex; however, no LAG or clear demarcation is present between these zones. In F2, the outer cortex can be divided into thirds, where the middle third is less vascular and those on either side of it are highly vascularized; however, there are no LAGs or clear demarcations between these zones. For this reason, these zones are not considered annuli. No evidence of secondary remodeling in the outer cortex, except in area discussed below. No LAGs or annuli are visible in either section; no outer circumferential layer is present in either specimen.

Along the posterior lateral edge of both F1 and F2, an area of highly disorganized tissue is found, with a PVD and OI more similar to the values of the inner cortex. Primary and secondary osteons are present in this region as well. The appearance of this area is similar to that described by Hübner (2012) as the 'posterolateral plug' of the femur of *Dysalotosaurus* (mentioned above). In the both elements (F1 and F2), neither the periosteum, nor the outermost layer of bone is

preserved. Given this lack of preservation, it is not possible to determine whether Sharpey's fibers are present at this location. Both specimens have experienced some degree of crushing. It is possible that in both cases, this area lies in approximately the same position of the posterolateral plug of Hübner's *Dysalotosaurus* specimens. In this case, it is likely that m. caudofemoralis is responsible for the strain in the bone.

Subadult

Specimens Examined: UMNH VP 25135 (F3), UMNH VP 25141 (F4)
(Figs. 3.1.12-3.1.13)

The cross-section of both specimens is roughly elliptical (UMNH VP 25135, F3; UMNH VP 25141, F4). Both specimens are highly distorted around the entire margin; extensive crushing makes determining an average cortical thickness and dimensions of the medullary cavity impossible in both cases. In places, this cavity was exposed during the fossilization process; it is filled with sediment, iron bearing minerals and bone fragments.

The inner cortex of F4 is highly vascularized, with a PVD similar to that seen in the inner cortex of juveniles in this study; osteonal canals and primary osteons are present and highly disorganized, with a correspondingly low OI. The inner cortex of F5 is moderately vascularized, with a PVD similar to the inner cortex of other subadults in this study; osteonal canals are present and moderately organized. In both specimens, this portion of the cortex is composed of reticular to plexiform fibrolamellar bone matrix. The endosteal margin has experienced substantial crushing, making is difficult to determine if resorption has occurred. Little to no evidence of secondary remodeling is found in F3; there are scattered secondary osteons in this portion of the cortex of F4.

The outer cortex of both F3 and F4 is moderately vascularized, like that of the juvenile femora above, except this portion of the cortex is over twice as thick as that found in the juvenile specimens. In F3, the outer cortex is dominated by simple canals that show alternating areas of longitudinally organized canals (plexiform fibrolamellar bone) and areas with little organization (reticular fibrolamellar bone). The OI of the organized areas is high, while the OI for the disorganized areas is more similar to that of the inner cortex of each specimen. Extensive fracturing of the cortex makes it impossible to trace these areas around the full circumference; however, no clear LAG or demarcation is found between the zones. In F4, the outer cortex is dominated by plexiform and laminar fibrolamellar bone with no signs of secondary remodeling.
It is possible to trace one annulus around the circumference of the section, towards the periosteal margin of the section. No outer circumferential layer is present in either specimen.

Crushing and distortion prevents assessing whether there is an area of highly disorganized cortex along the lateral edge of F3, as exists in F1 and F2; an area of highly disorganized cortex is found along the lateral edge of F4, as in F1 and F2. As in the two femora above, neither the periosteum nor is the outermost layer of bone is preserved. Given this absence, it is not possible to determine whether Sharpey's fibers are present in this location.

Tibiae

Juvenile

Specimens Examined: UMNH VP 25144 (T1)
(Fig. 3.1.14)

The specimen is roughly elliptical in cross-section. Extensive crushing obscures the

original outline of the section, as well as the borders of medullary cavity. Some indications of the original endosteal margins of this cavity remain and show no signs of resorption. The cavity is filled in by cortical bone that has been dislocated from its original position, calcite and an iron-rich mineral.

The inner cortex is highly vascularized, with a PVD similar to that seen in the inner cortices of the juvenile specimens discussed above. Both osteonal canals and primary osteons are present and highly disorganized, with a correspondingly low OI. This portion of the cortex is composed of reticular fibrolamellar bone. There is no evidence of resorption or formation of secondary osteons. The outer cortex is moderately vascularized; it is dominated by circularly oriented osteonal canals and is composed of plexiform fibrolamellar bone. A posterior-medially localized area of alternating bands of longitudinal organization and bands with little organization is present; in this area, two such pairs of bands are present. However, these bands cannot be traced around the cortex and cannot, therefore, be considered annuli. The iron rich mineral that is present in the medullary cavity is distributed throughout this portion of the cortex, although its presence is sufficiently sparse that it does not obscure the overall features present. The presence of iron rich minerals in this portion of the cortex can be mistaken for osteons, care was taken to visual slides under crossed polarized light to confirm the identity of supposed osteons. Evidence of resorption canals can be found internally, but no secondary osteons are present.

An area of bone is visible extending from the inner to the outer cortex, which is highly disorganized along the craniolateral margin. It has a PVD and OI that is similar to those of the inner cortices of juvenile and subadult specimens in this study.

This is similar to areas of disorganization, within an otherwise organized outer cortex, that has been discussed above.

No LAGs or annuli are visible; no outer circumferential layer is present in the section.

Subadult

Specimen Examined: UMNH VP 25136 (T2), UMNH VP 25140 (T3)
` (Figs.. 3.1.15-3.1.16)

The cross-section of both UMNH VP 25136 (T2) and UMNH VP 25140 (T3) are both elliptical. With respect to T2, extensive crushing obscures the original outline of the section, as well as the borders of medullary cavity; with respect to T3, the caudal margin is crushed in towards the medullary cavity, obscuring the original outline of the section. Extensive fracturing in both specimens makes it impossible to obtain the average cortical thickness. In both specimens, the medullary cavity is filled with sediment and an iron-rich mineral, although more of the cavity is preserved in T3 than in T2. In both specimens, existing endosteal margin is wavy and fragmented, and appears to be the result of erosion of the endosteal bone during fossilization. This erosion has destroyed most, of the primary bone tissue of the inner cortex.

The remaining outer cortex is moderately vascularized, with a PVD similar to that of the outer cortex of other subadult specimens in this study; this portion of the cortex is dominated by osteon canals that are organized longitudinally and anastomose radially, and which have a correspondingly high OI; primary osteons arepresent throughout. The outer cortex is composed of laminar-to-plexiform fibrolamellar bone.

The outer cortex of T3 is extensively fractured. There are two bands that on first inspection appear to be LAGs. The fracturing prevents visualizing them around the

cortex. However, on higher magnification (x100) and under crossed polarized light, it is apparent that these reflect a combination of mineral staining and localized changes in vascular canal orientation, and no LAGs. No outer circumferential layer is present.

Iguanacolossus fortis specimen

UMNH VP 20205 (Fig. 3.1.17, U1)

This specimen (Fig. 3.1.4) is the shaft of long bone that does not preserve either articular end (Table 3.1.1). As mentioned above, the lack of 'twisting' indicates that it is not a tibia, and its cross-sectional shape demonstrates that it is not a fibula or radius. The circumference of the element indicates that it is not a rib. Beyond this, however, it is not possible to conclusively identify the element. Although the material cannot be identified as to element, it still has value in assessing the minimum age of Iguanacolossus.

The specimen is roughly elliptical in cross section. There is no evidence of a medullary cavity; the cortex that is present shows evidence of crushing around the margins, but the interior seems mostly intact. The lack of a medullary cavity indicates that it is likely not part of a limb element; given the overall shape of the element and the lack of a medullary cavity, it is more likely part of a metatarsal or metacarpal.

The element shows extensive secondary remodeling; there is almost no primary bone tissue present. This specimen has the highest HRI of any specimen in the sample. It is not possible to draw any conclusions about the texture of the primary bone from the little that is present in the section.

No LAGs or annuli are visible; no outer circumferential layer is present in the section.

Discussion

Identification of Doelling's Bowl Material

The material sectioned from the Doelling's Bowl iguanodontian is consistent with and indeed seems to represent an ontogenetic series. The smallest elements, those diagnosed as juvenile, are characterized by structures associated with fast growth. This includes a cortex that has no LAGs or annuli, and where secondary remodeling is limited to resorption, with no or few secondary osteons. The cortex is either dominated by reticular fibrolamellar bone, or shows localized alternating bands of plexiform and reticular fibrolamellar bone.

The largest elements of the Doelling's Bowl iguanodontian (Fig. 3.1.13 F4, 3.1.16 T3, 3.1.9 H5) are identified as subadult. All three elements have features indicating that the animal(s) was still growing at the time of its death. Growth is slower than that of the juvenile specimens; however, there are no signs of approaching a cessation of growth. The outer cortex is moderately vascularized, dominated by plexiform and laminar fibrolamellar bone. In one of the specimens (F4, UMNH VP 25141), it is possible to visualize a single annulus. One would expect these features to be more numerous and closely spaced if growth was slowing or had ceased. None of the specimens show an outer circumferential layer, which one would expect if the individual had reached skeletal maturity. There are few, and in some cases no, secondary osteons; the only robust evidence of secondary remodeling is resorption along the endosteal margin.

To estimate the asymptotic size of an adult of this taxon, it can be compared to

known growth series of closely related taxa. In this case, the most closely related taxa with known growth series are *Tenontosaurus tilletti* and *Maiasaura peeblesorum* (Fig. 1.2). Histologic analysis has been conducted on both of these taxa, so it is possible to compare both the size and the microstructure of the elements.

1. *Tenontosaurus tillettii* is a basal iguanodontian from the mid-Cretaceous Cloverly Formation (115 Ma) of Montana, Wyoming and the Antlers Formation of Oklahoma (Ostrom,1970). *Tenontosaurus* was between 6.5 and 8m in length, making it large-bodied given its basal phylogenetic position and is considered to have been a facultative biped. An adult femur has a length of 70 cm; an adult tibia has a length of 68 cm (FMNH PR 2261, Werning 2012). Ontogenetic series of both femora and tibiae were included in Werning (2012).
2. *Maiasaura peeblesorum* is a hadrosaurine from the Campanian Two Medicine Formation (77 Ma) of Montana (Horner & Makela 1979), was approximately 7 to 9 m in length, andwas inferred to be a facultative biped (Horner et al., 2000; Werning, 2012; Woodward et al., 2015). An adult femur has a length of 102 cm (MOR 005A), and an adult tibia has a length of 98 cm (MOR 005; Horner et al., 2000; Woodward et al., 2015). While an adult femur was sampled as part of Horner et al. (2000), the ontogenetic series (Woodward et al., 2015) is based exclusively on tibiae.

Although both adult sizes and histology are available for both femora and tibiae, only the tibiae are included in both of the known ontogenies (Table 3.1.4). When the length of the tibiae and femora of isolated specimens of closely related taxa (*Hypacrosaurus,*

Horner et al., 1999; *Maiasaura,* Horner et al., 2000; *Tenontosaurus,* pers. comm. Rich Cifelli) are compared, the elements are approximately equal in length (the greatest difference being 4 cm). The large femur in this study (F4, UMNH VP 25141) is the only specimen to have a LAG. This specimen is 63.9 cm in length; given the comparisons mentioned above, the tibia of this animal would likely be between 63.9 and 59.9 cm in length. This is larger than the largest tibia in this sample (T3, UMNH VP 25136), which has no LAGs; it is 48 cm in length and has a least circumference of 16.6 cm.

The Doelling's Bowl tibia (T3) has a least circumference of approximately 16.6 cm and a total length of 48 cm. Werning (2012) describe a tibia of *Tenontosaurus* that is approximately 16.5 cm in circumference (OMNH 16563; as measured with Adobe Photoshop CC from Morphobank image M75918). This specimen has between six and nine LAGs of decreasing width, some of which might be double LAGs, making it difficult to get an exact count. Additionally, expansion of the medullary cavity has likely obliterated LAGs, also making it difficult to obtain an exact count. No outer circumferential layer is present, leading Werning (2012) to diagnose this specimen as late subadult.

The tibia that corresponds to the largest femur in this study (F4) would be between 59.9 and 63.9 cm in length. This is similar to the size of the largest tibia sectioned by Werning (2012) (FMNH PR 2261). This specimen has at least eight narrowly spaced LAGs. As with the specimen discussed above, expansion of the medullary cavity has likely obliterated LAGs, making it difficult to obtain an exact count. No outer circumferential layer is present. However, extensive secondary remodeling, tissue indicting slow growth, and the narrow spacing of the LAGs led

Werning (2012) to diagnose this specimen as an adult.

Woodward et al. (2015) included four tibiae of *Maiasaura* of comparable size to T3. All four specimens have circumferences of 16.6-16.8 cm and lengths of 47.2-48.1 cm (MOR 005 T25-28). None of these specimens have LAGs or annuli. The first specimens of *Maiasaura* to have LAGs have two LAGs each. These three tibia have circumferences of 21.3-21.4 cm and lengths of 56-69 cm (MOR 005 T30-32). The cortices of these specimens transition from more reticular fibrolamellar bone endosteally to more plexiform fibrolamellar bone towards the periosteal margin. There are no indications that the medullary cavity has expanded, and/or that annuli or LAGs have been obliterated by secondary remodeling.

As mentioned above, the tibia that corresponds to the largest femur in this study (F4) would be between 59.9 and 63.9 cm in length. Woodward et al. (2015) included two tibiae of *Maiasaura* of comparable size (MOR 005 T31, T32). These specimens have circumferences of 21.4 and 21.4 cm, and lengths of 63.0 and 69.0 cm respectively. Woodward et al. (2015) estimated the corresponding femoral lengths to be 65.2 and 71.5 cm respectively. Both of these specimens have two LAGs. The LAGs are widely spaced, occurring more towards the middle of the cortex than the periosteal margin. Immediately following the second LAG, vascular canals are initially reticular, then transitions to laminar or plexiform fibrolamellar bone. This is true not only of these specimens, but also of the larger specimens in the study. This indicates that there was a period of rapid growth following deposition of the second LAG, before returning to a slower rate growth.

Horner et al (2000) sectioned a *Maiasaura* femur that is 68 cm in length (MOR

005 SA). This is close in size to that of the largest femur in the present study (F4), which is 63.9 cm in length. This specimen has two LAGs; these are widely spaced and occur in outermost third of the cortex. There is no indications that expansion of the medullary cavity obliterated LAGs. The cortex is laminar to plexiform fibrolamellar bone. Horner et al (2000) diagnosed this specimen as a subadult on the basis of the growth marks, lack of an outer circumferential layer (authors use the term "external fundamental system") and cortical texture. The largest femur in Horner et al (2000) by comparison, is 100 cm in length; this specimen has an outer circumferential layer (authors use the term "external fundamental system"), extensive secondary remodeling throughout the cortex and 5 narrowly spaced LAGs.

Overall, the histology of the Doelling's Bowl taxon is more similar to comparably sized specimens of *Maiasaura* than *Tenontosaurus.* Given this similarity, it is reasonable to conclude that the Doelling's Bowl taxon probably attained a skeletally mature size similar to that of *Maiasaura peeblesorum,* with a tibia of approximately 90 cm in length, and an overall body length of approximately 7 to 9 m (Woodward et al., 2015). Woodward et al. (2015) found that tibiae of this length have ten LAGs. However, three of these LAGs occur within the outer circumferential layer (although the authors use the term "external fundamental system"). Taking this into consideration, along with data from younger specimens in the sample, Woodward et al. (2015) estimate that skeletal maturity is achieved around 8 years of age. It is important to note here that they take the first LAG (or annuli) to signify the end of the first year of life. Accordingly, specimens that lack LAGs (or annulus) were taken to have not yet reached their first birthday.

This size estimation is commensurate with that of 9m in length for the holotype of *Iguanacolossus fortis* (McDonald 2010). The material sectioned for the specimen sampled here is almost entirely secondarily remodeled, which indicates that the specimen is skeletally mature. As mentioned above, the material sectioned from *Iguanacolossus* is likely part of a metacarpal or metatarsal. Smaller elements (e.g. metacarpals, metatarsals) remodel at a faster rate than larger elements (e.g. femora, tibiae) (Horner et al., 1999; Padian et al., 2013). However, even for smaller elements, such extensive remodeling (e.g. no primary bone tissue, secondary osteons forming over older secondary osteons), sometimes referred to as a "dense Haversian system", only occurs late in ontogeny (Chinsamy-Turan, 2005; Huttenlocker et al., 2013). For these reasons, as well as the morphologic analysis conducted by A. McDonald (pers. comm.), it is reasonable to assign the Doelling's Bowl material to *Iguanacolossus*.

The only nearly complete limb material known from the *Iguanacolossus* holotype is a fibula, which is missing the distal, articular end and measures over 65 cm in length. It is reasonable to expect, given their anatomic relationship, that the length of the fibula will be similar to the length of the tibia in a given individual. Accordingly, we would expect the tibia of this specimen to be 65 cm long when excluding the distal, articular end at a similar level to that of the fibula. A conservative estimate, given the anatomical landmarks present on the preserved fibula, would be 70-75 cm in length for the corresponding tibia. Woodward et al (2015) found adult *Maiasaura peeblesorum* tibiae to vary in length between 75 and 88 cm. While the two size ranges overlap, this indicates that *Maiasaura* was a slighter larger adult that *Iguanacolossus*. This supports the histologic data that indicates that the Doelling's Bowl material, here attributed to

Iguanacolossus, started laying down lags at a slightly smaller body size than *Maiasaura*.

Conclusion

The Doelling's Bowl material and *Iguanacolossus* are both found at the same stratigraphic level and broad geographic area. The gross morphology of the two is also very similar; although it should be noted that the Doelling's Bowl material does not include cranial elements. However, the Doelling's Bowl material is substantially smaller in size than the type specimen of *Iguanacolossus*. Based on histologic analysis, the Doelling's Bowl material is juvenile to subadult. The rapid growth observed in these specimens, with no signs of slowing, is consistent with these specimens reaching an adult size similar to that of *Iguanacolossus*. Given the weight of the morphologic and histologic evidence, I conclude that the Doelling's Bowl material is *Iguanacolossus*. This histologic technique provides a means of assessing the identity and ontogenetic age of relatively poorly preserved specimens when the assemblage lacks definitive diagnostic characters. This is the first time that this approach has been successfully used.

Figures

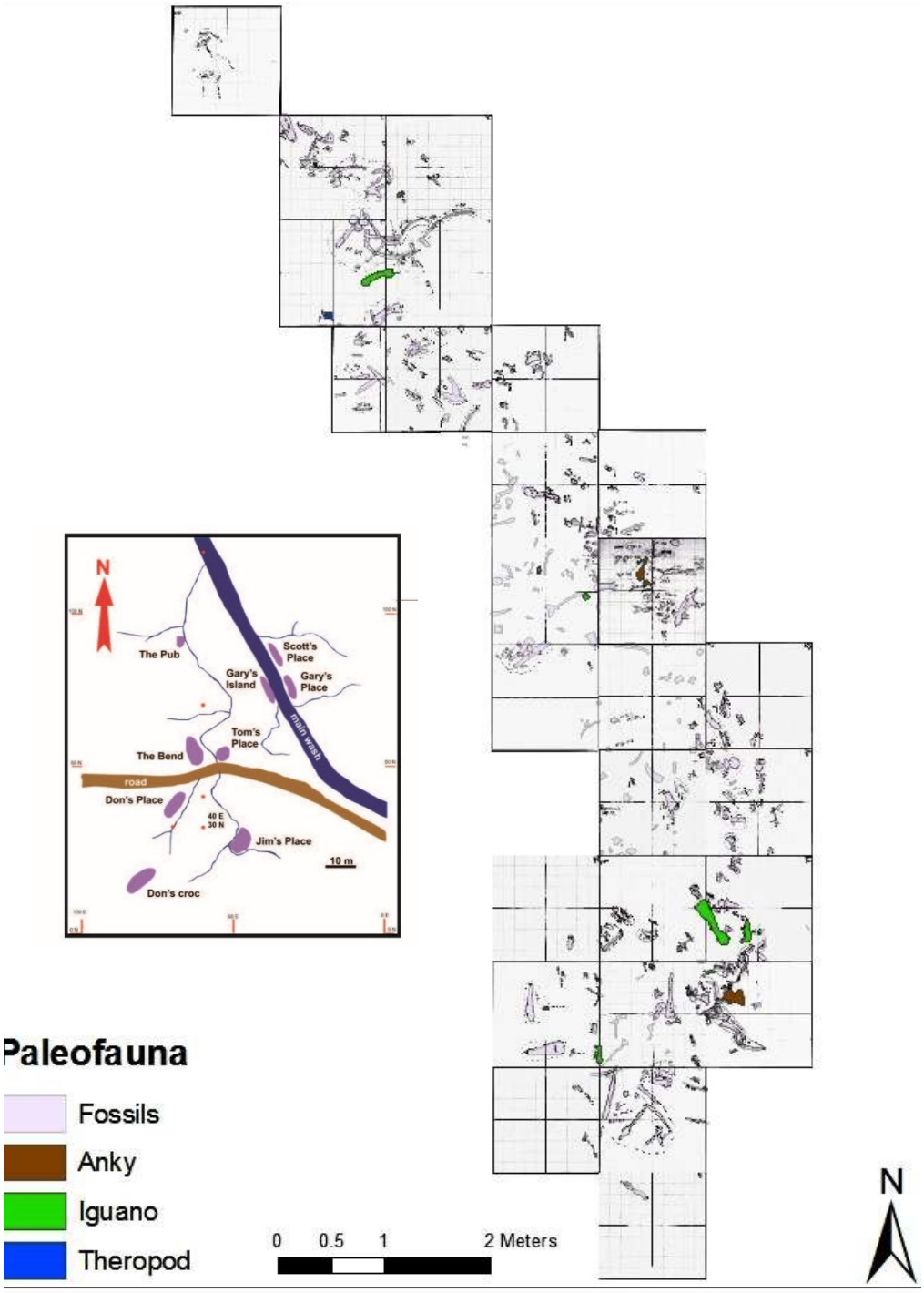

FIGURE 3.1.1 Inset shows the locations of the different Doelling's Bowl Quarry (courtesy of Jim Kirkland). The large map is a quarry map of the Jim's Place site in Doelling's Bowl (modied from Toth, unpublished thesis, University of Utah, 2012).

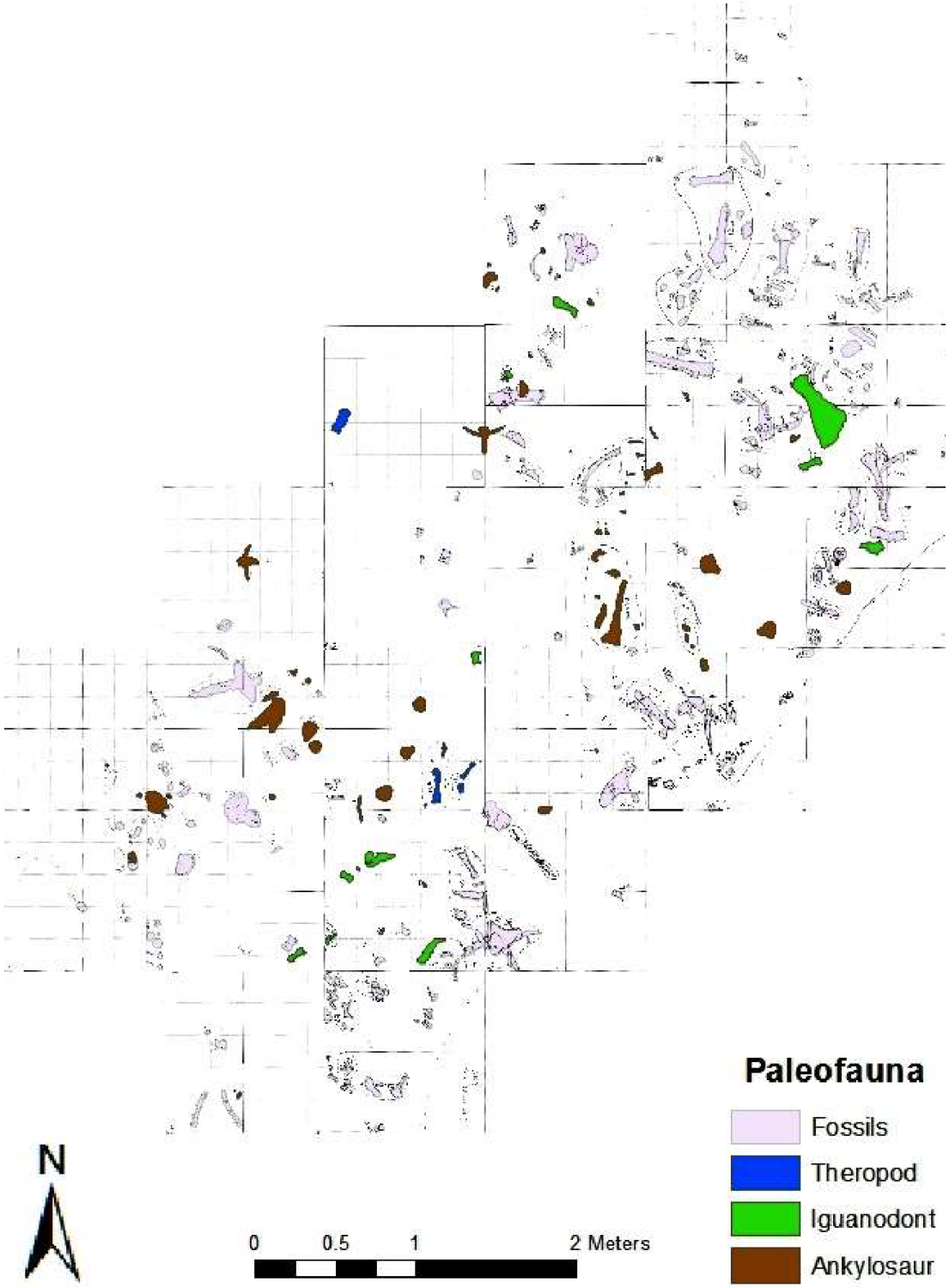

FIGURE 3.1.1 (con't) Quarry map of Don's Place (see Fig. 3.1.1. for location of Don's Place within Doelling's Bowl; modified from Toth, unpublished thesis, University of Utah, 2012).

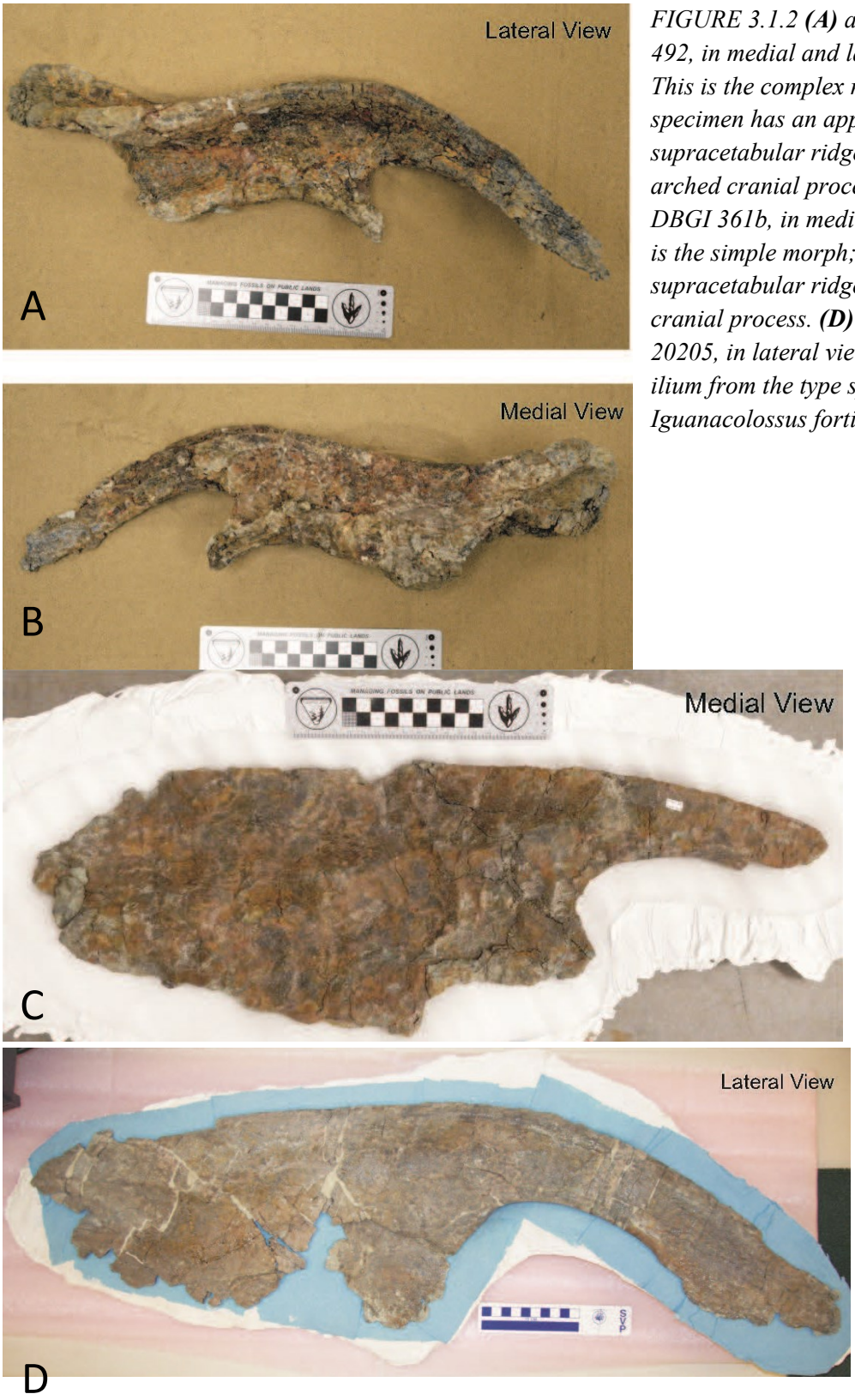

FIGURE 3.1.2 ***(A)*** *and* ***(B)*** *DBJP 492, in medial and lateral view. This is the complex morph; the specimen has an apparent supracetabular ridge and highly arched cranial process.* ***(C)*** *DBGI 361b, in medial view. This is the simple morph; it lacks a supracetabular ridge and arched cranial process.* ***(D)*** *UMNH VP 20205, in lateral view. This is the ilium from the type specimen of Iguanacolossus forti.*

FIGURE 3.1.3 (A) Quarry map of type locality of I. fortis at Don's Ridge. (B) Stratigraphy of Don's Ridge. Inset map shows location of site. Courtsey of Jim Kirkland and Don DeBlieux.

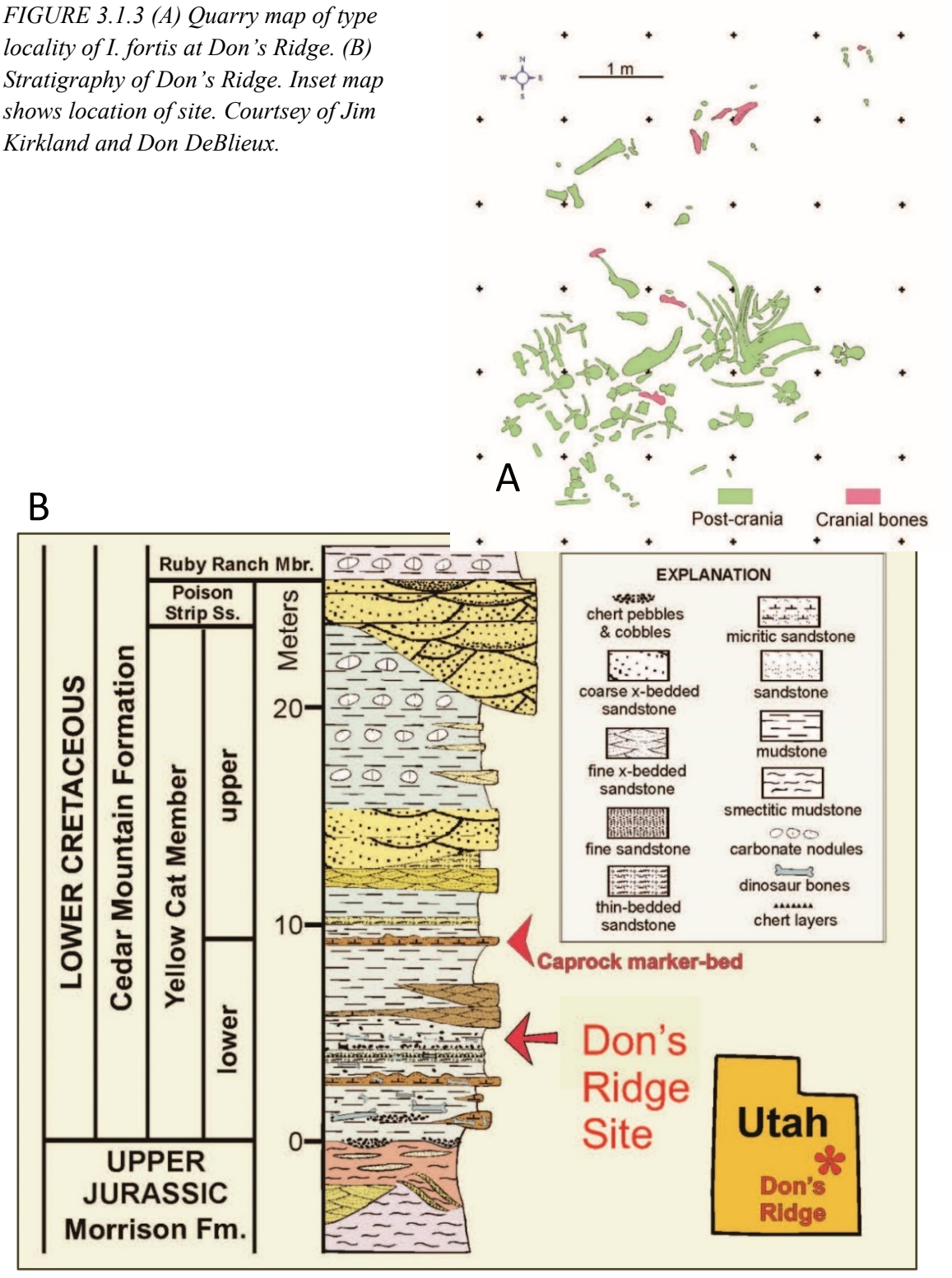

FIGURE 3.1.4 UMNH VP 20205, Iguanacolossus forti specimen sectioned for this study.

FIGURE 3.1.5 UMNH VP 25142, H1

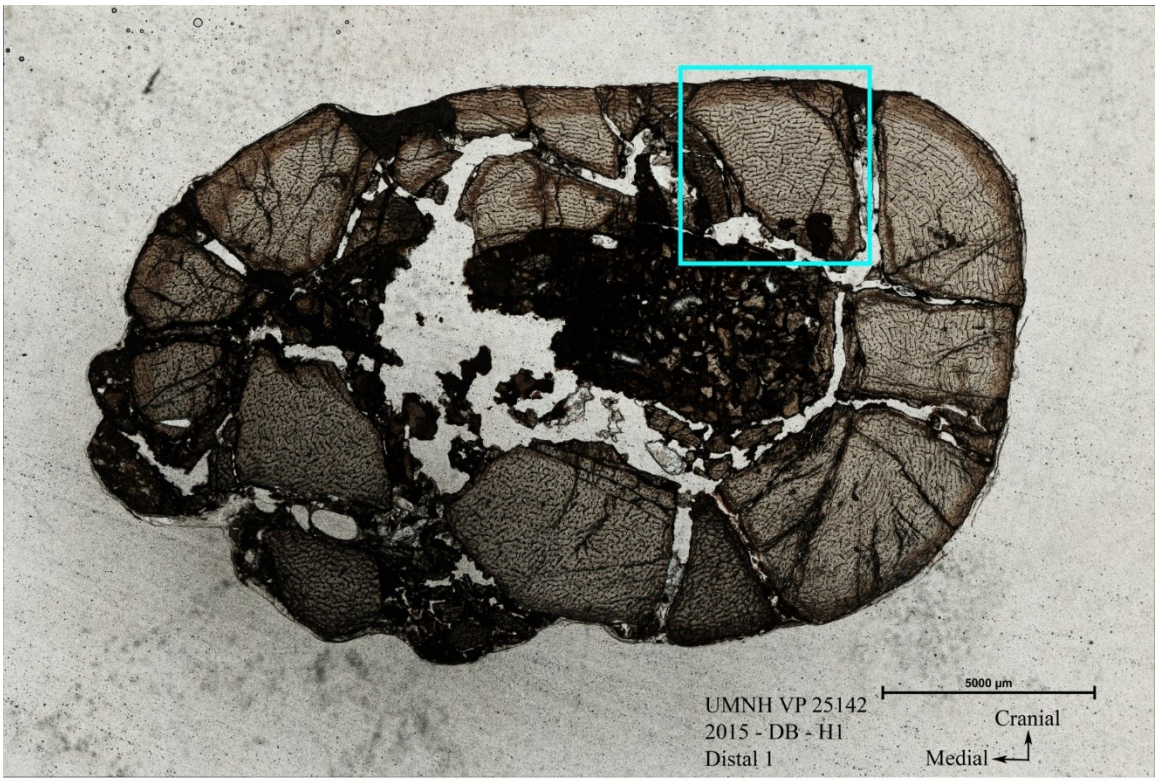

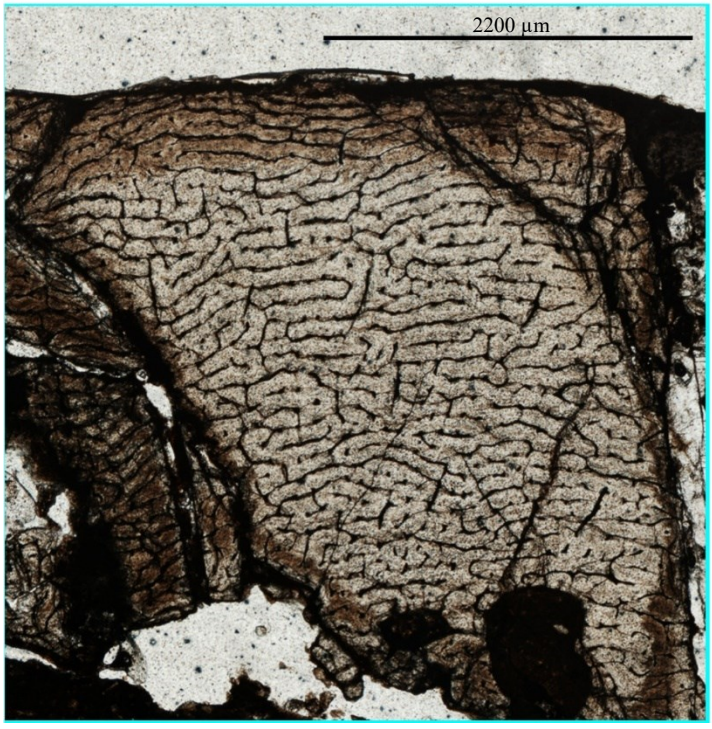

Above: Image of cross-section. Blue box shows location of close up image.

Left: Close-up image showing little organization throughout the cortex.

FIGURE 3.1.6 UMNH VP 25138, H2

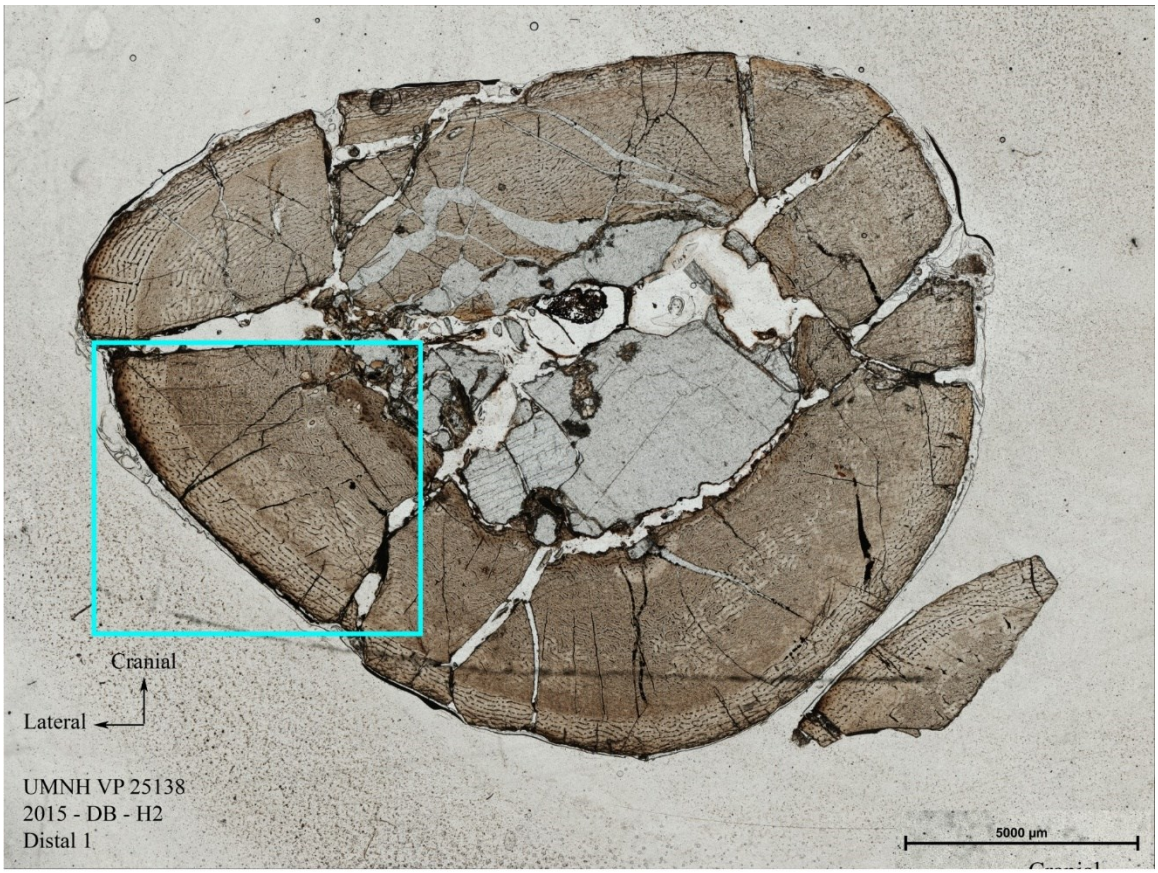

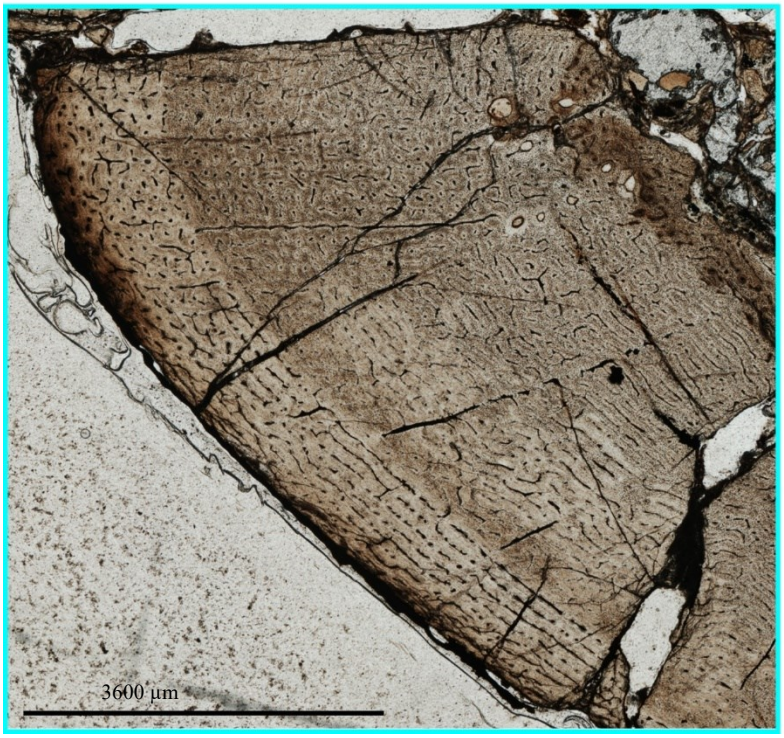

Above: Image of cross-section. Blue box shows location of close up image.

Left: Close-up image showing progressively more organization from the medullary cavity to the outer cortex.

FIGURE 3.1.7 UMNH VP 25137, H3

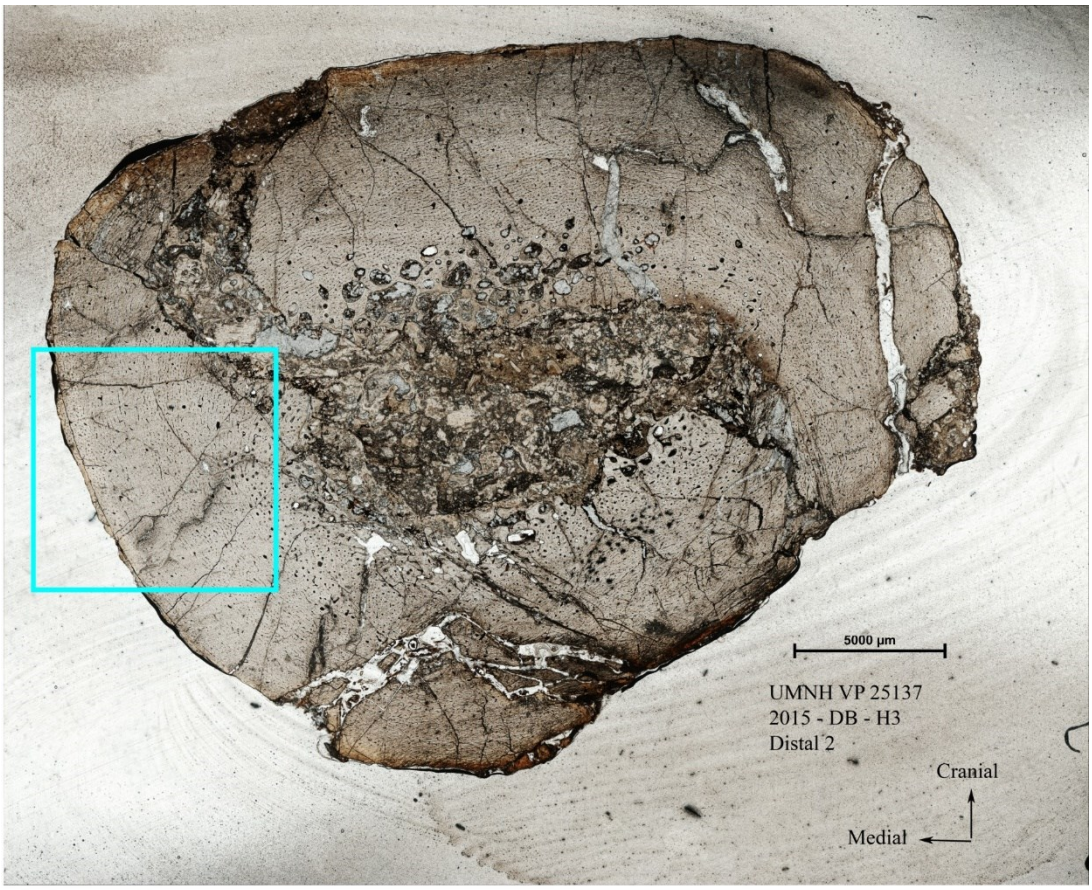

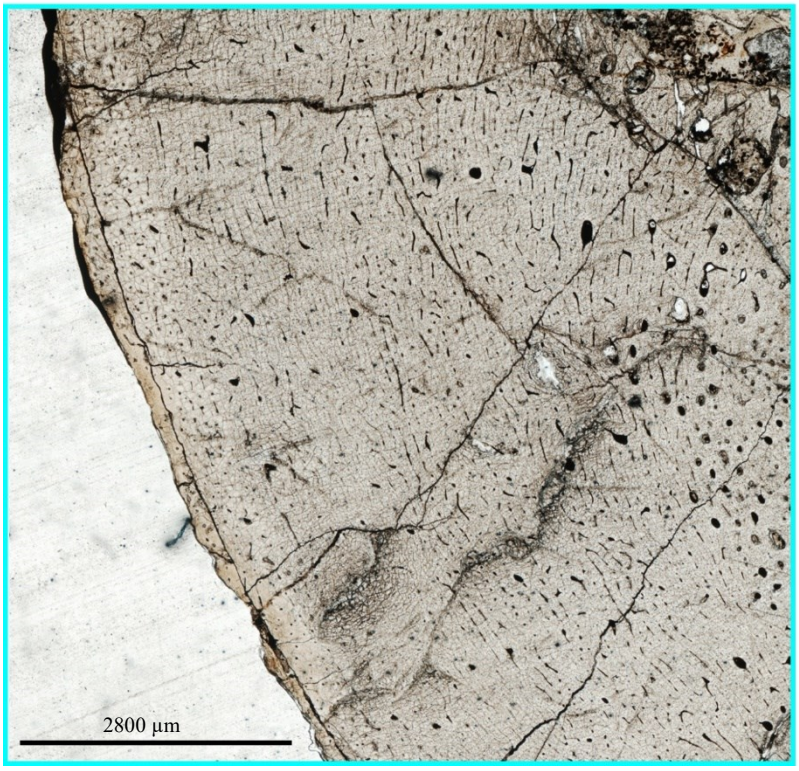

Above: Image of cross-section. Blue box shows location of close up image.

Left: Close-up image showing progressively more organization from the medullary cavity to the outer cortex.

FIGURE 3.1.8 UMNH VP 25139, H4

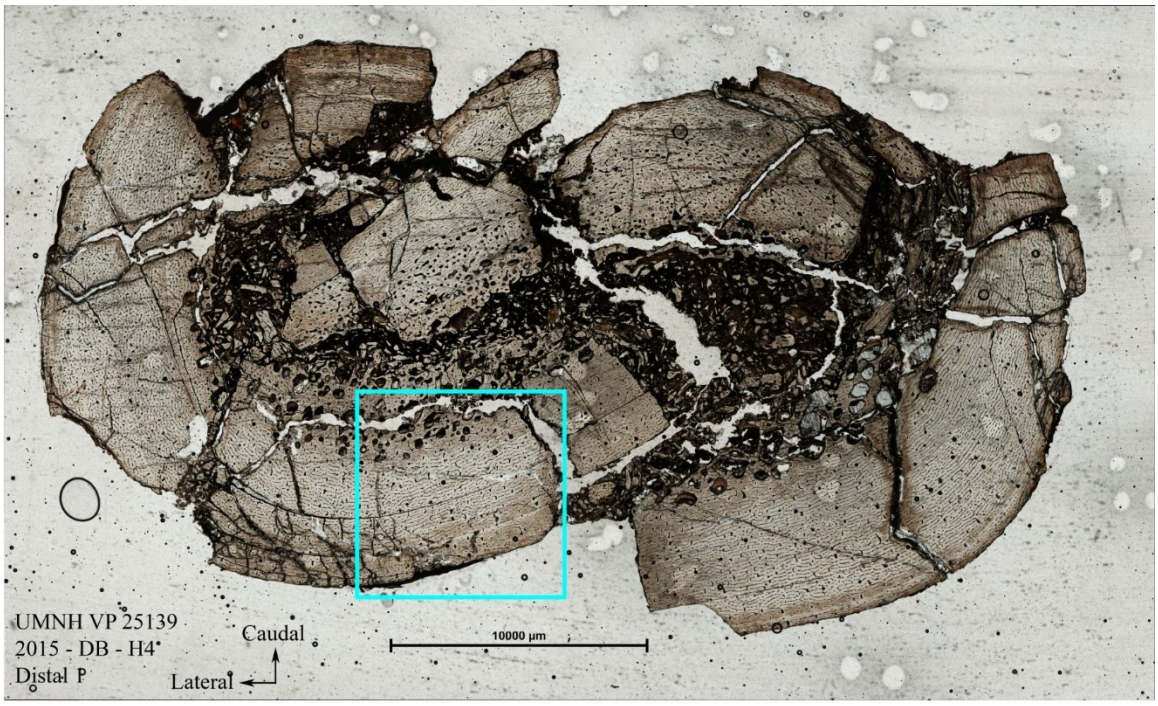

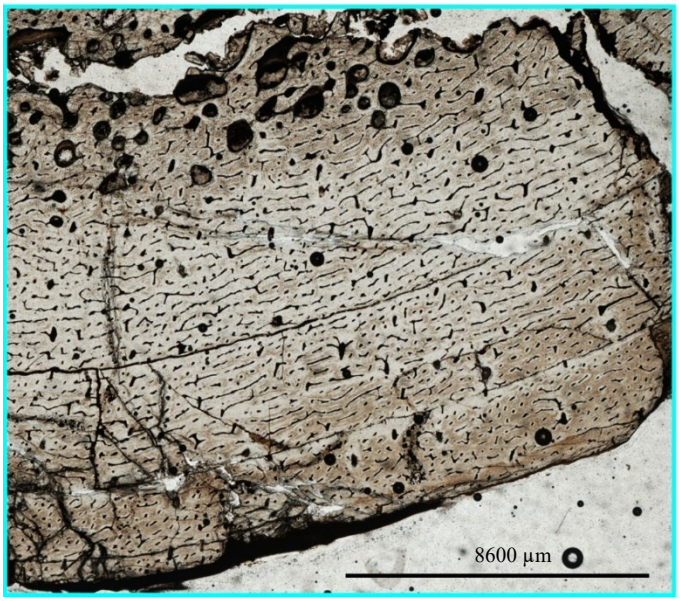

Above: Image of cross-section. Blue box shows location of close up image.

Left: Close-up image showing outer cortex with longitudinal canals radially anastomosing.

FIGURE 3.1.9 UMNH VP 25146, H5

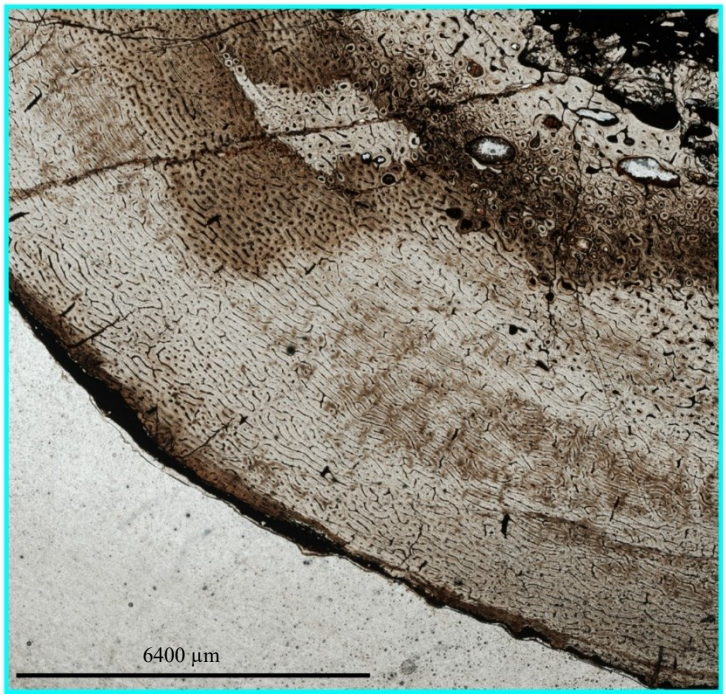

Above: Image of cross-section. Blue box shows location of close up image.

Left: Close-up image showing outer cortex with longitudinal canals radially anastomosing.

FIGURE 3.1.10 UMNH VP 25143, F1

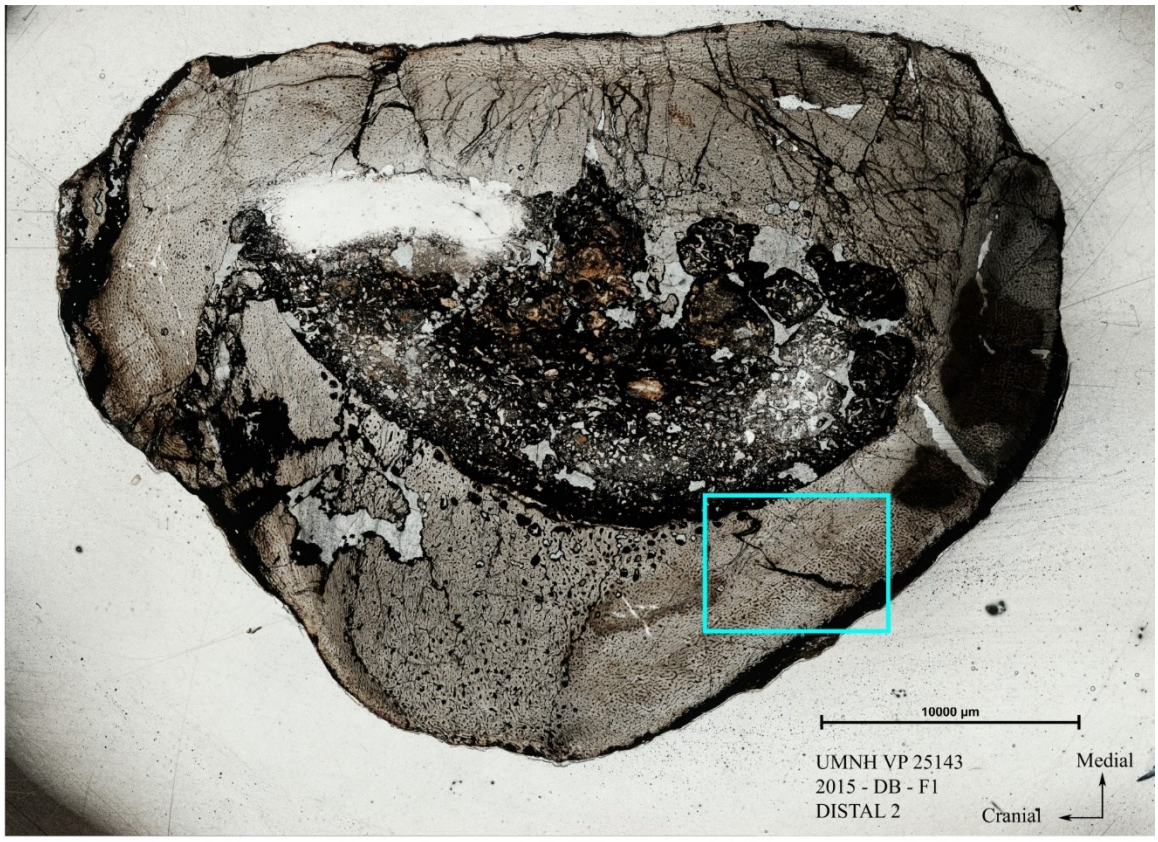

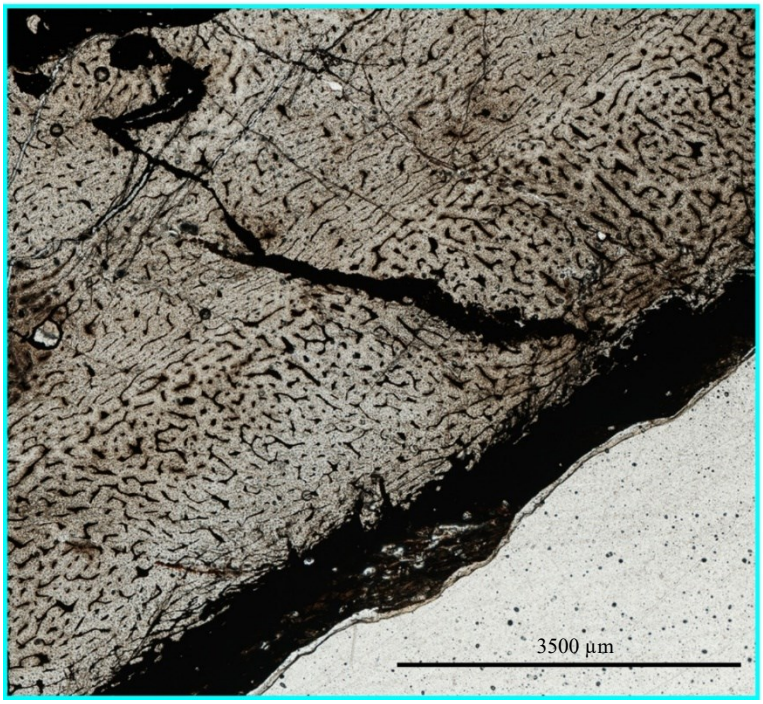

Above: Image of cross-section. Blue box shows location of close up image.

Left: Close-up image showing alternating areas of longitudinally oriented canals and areas with little organization.

FIGURE 3.1.11 UMNH VP 25145, F2

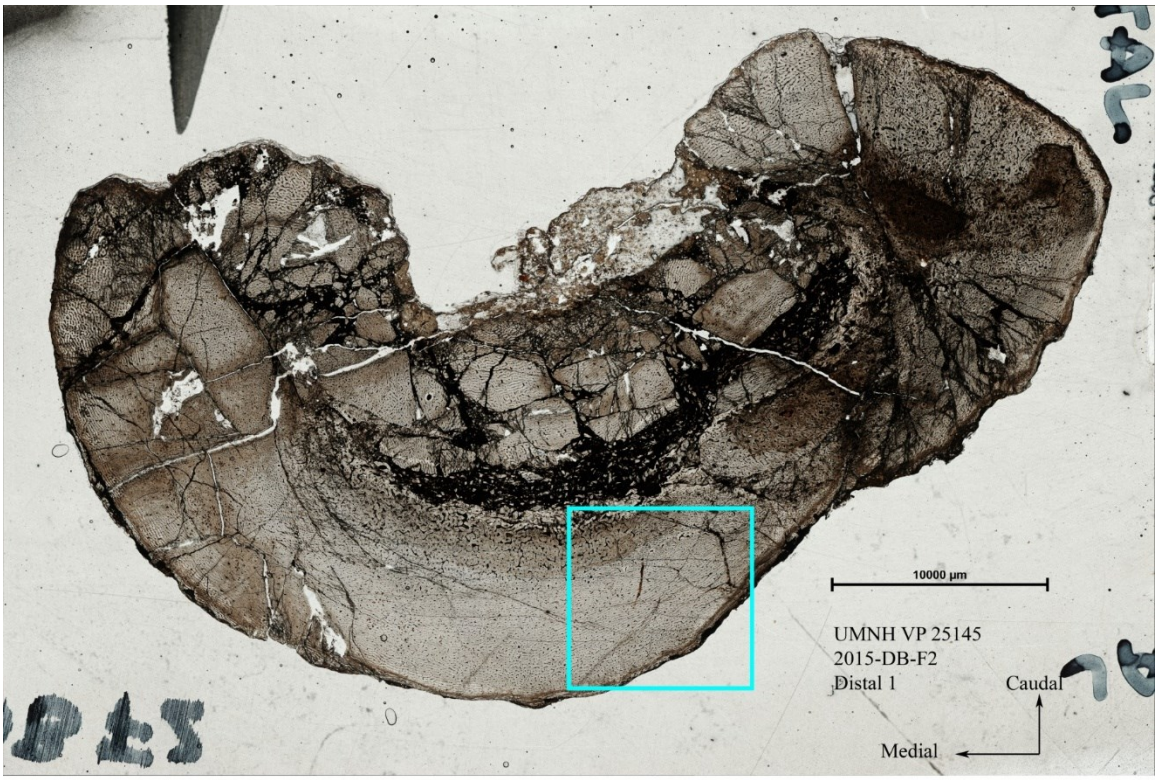

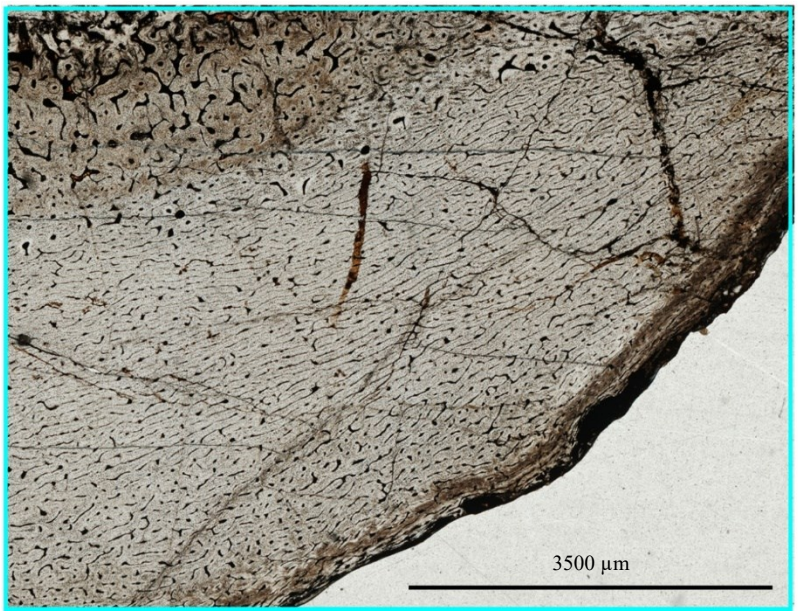

Above: Image of cross-section. Blue box shows location of close up image.

Left: Close-up image showing alternating areas of longitudinally oriented canals and areas with little organization.

FIGURE 3.1.12 UMNH VP 25135, F3

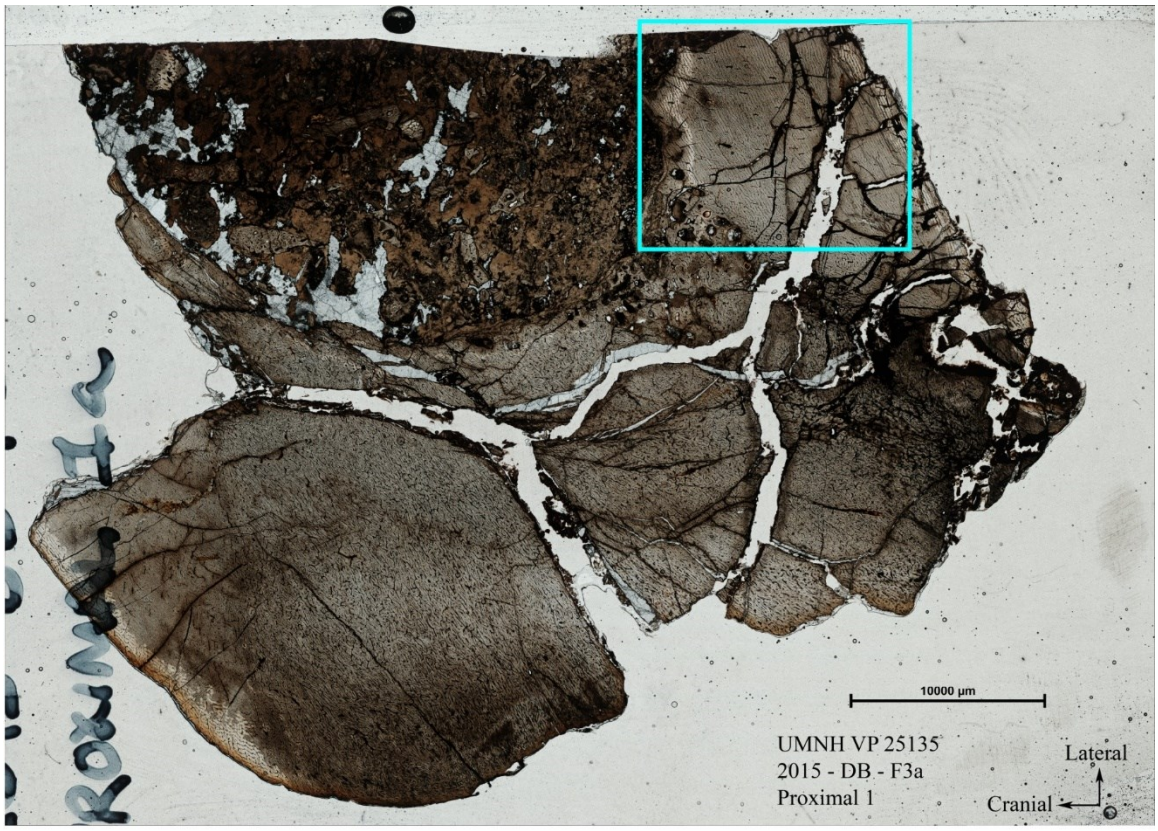

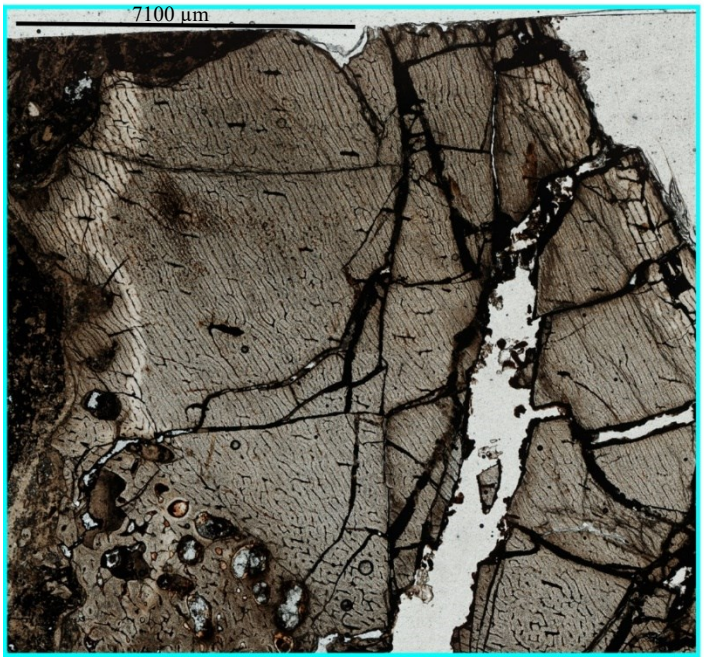

Above: Image of cross-section. Blue box shows location of close up image.

Left: Close-up image showing alternating areas of longitudinally oriented canals and areas with little organization.

FIGURE 3.1.13 UMNH VP 25135, F4

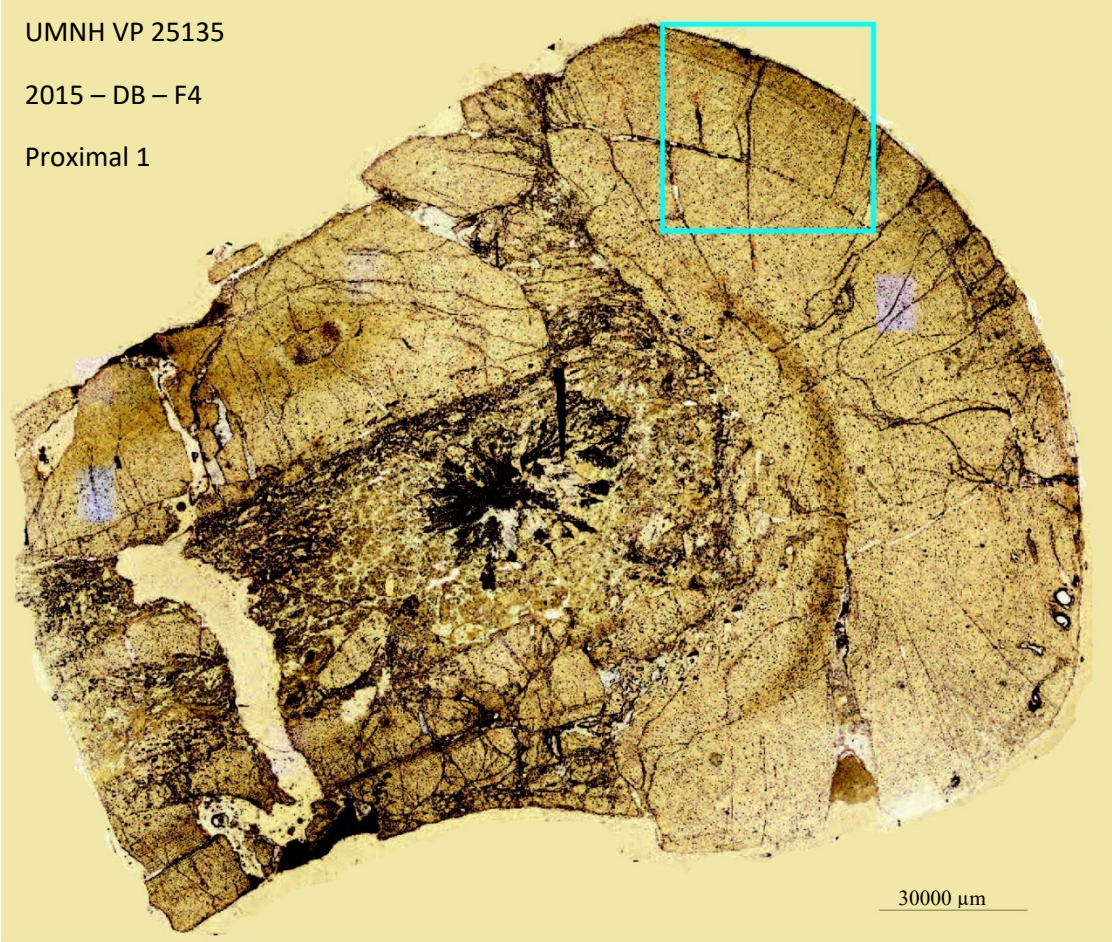

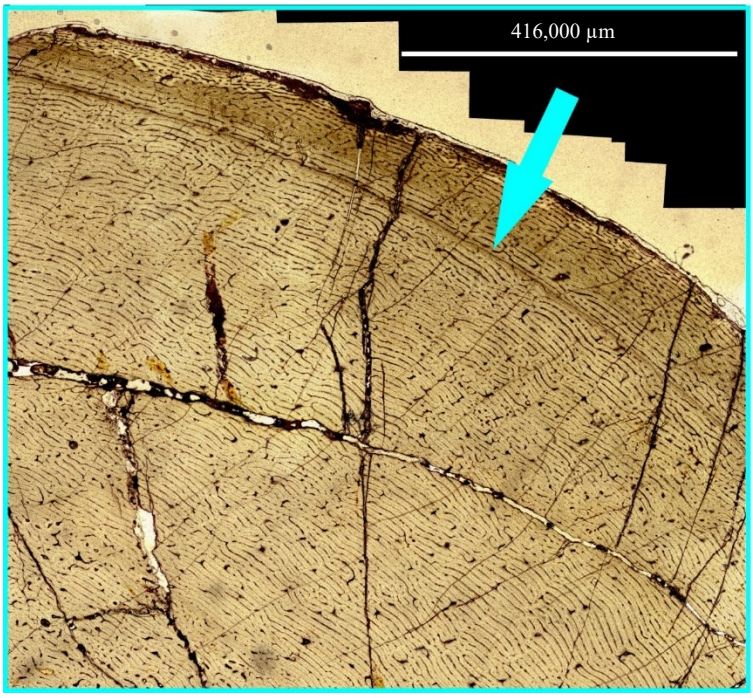

Above: Image of cross-section. Blue box shows location of close up image.

Left: Close-up image showing alternating areas of longitudinally oriented canals and LAG (marked with an arrow).

FIGURE 3.1.14 UMNH VP 25114

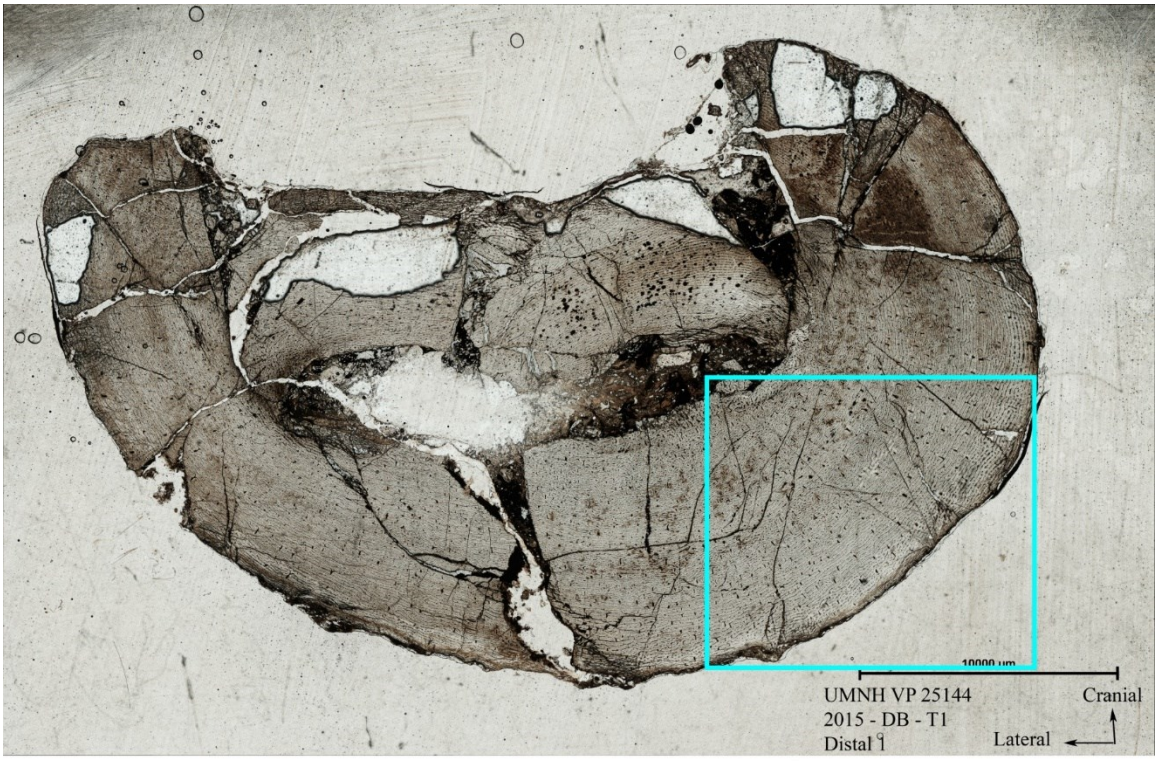

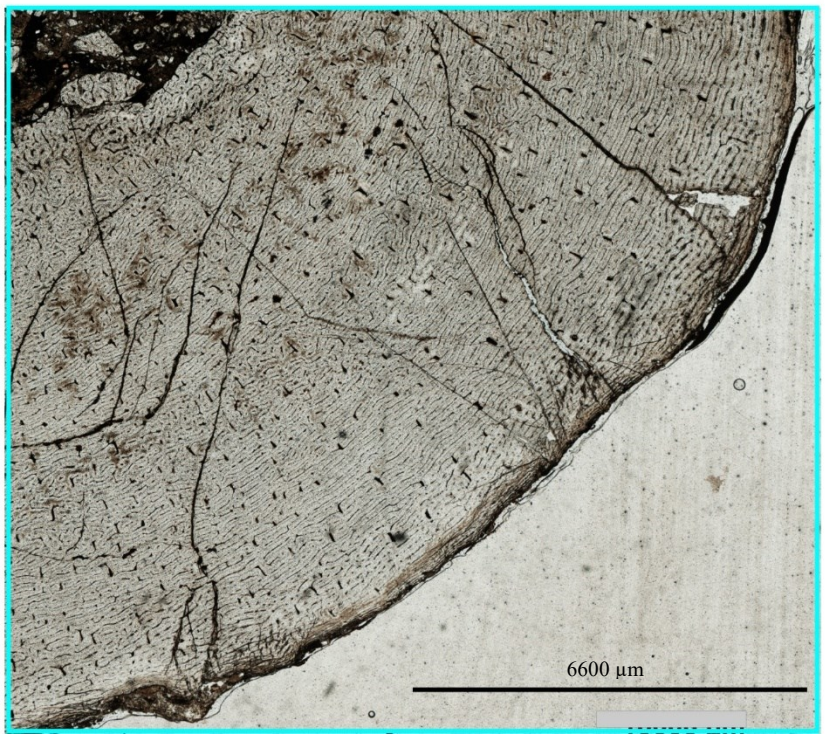

Above: Image of cross-section. Blue box shows location of close up image.

Left: Close-up image showing alternating bands of longitudinally oriented canals and bands with very little organization.

FIGURE 3.1.15 UMNH VP 25140, T2

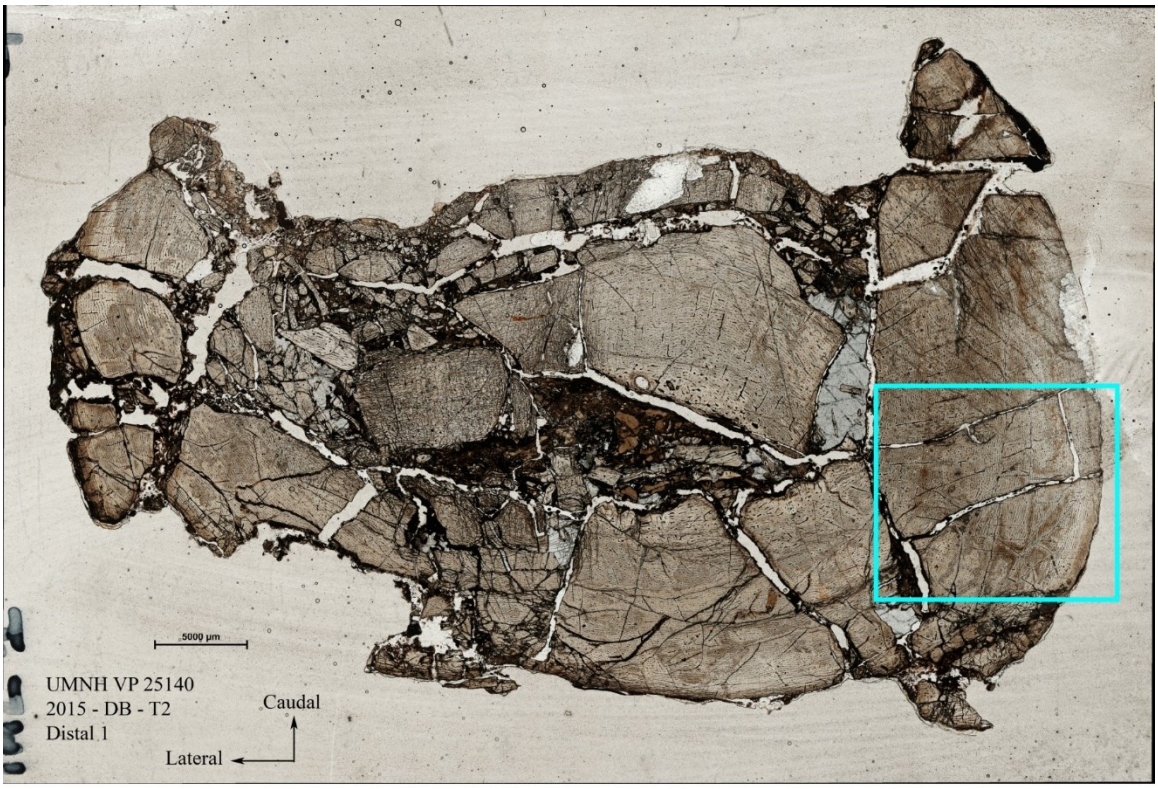

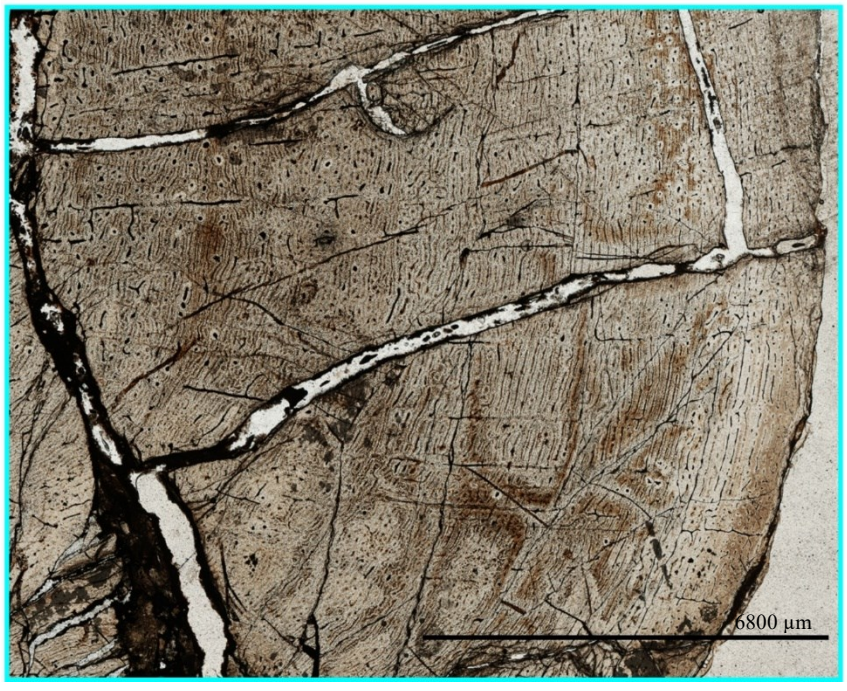

Above: Image of cross-section. Blue box shows location of close up image.

Left: Close-up image showing alternating bands of longitudinally oriented canals and bands with very little organization.

FIGURE 3.1.16 UMNH VP 25136, T3

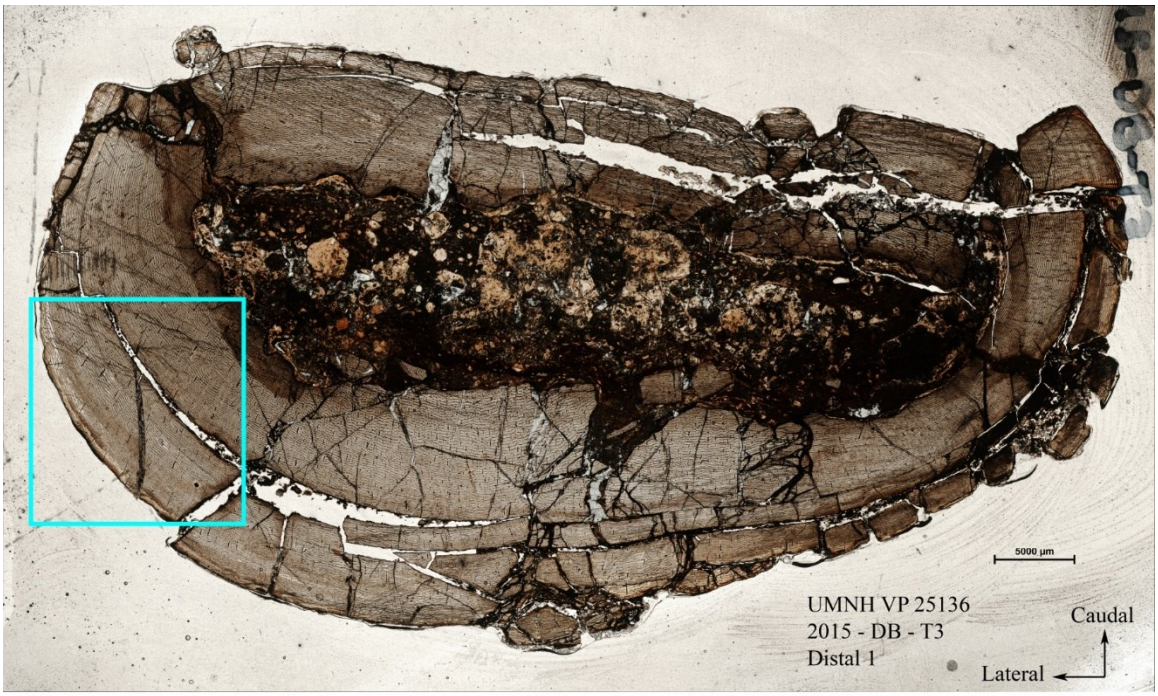

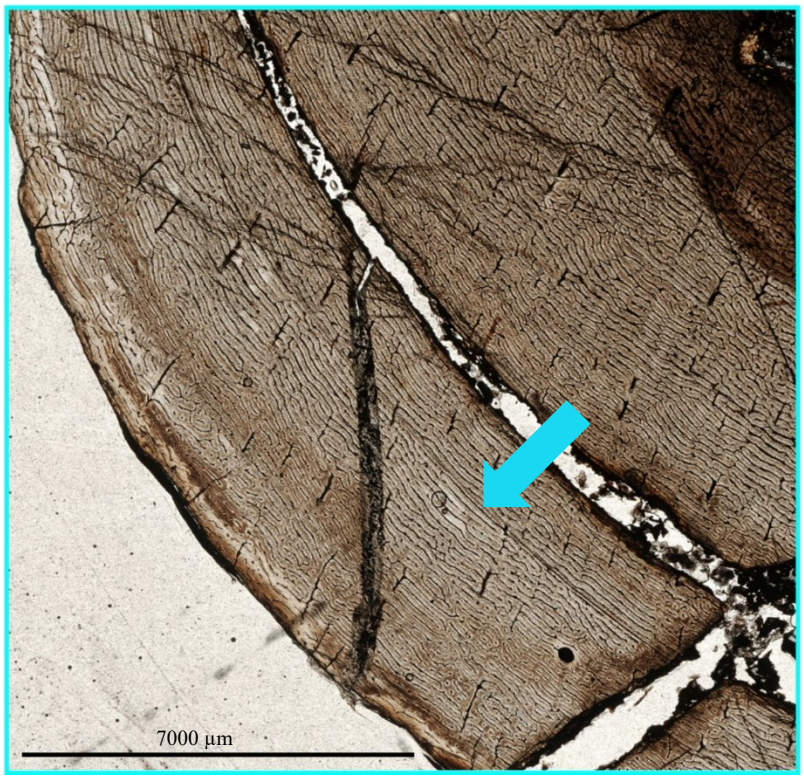

Above: Image of cross-section. Blue box shows location of close up image.

Left: Close-up image showing alternating bands of longitudinally oriented canals and a LAG (marked by arrow).

FIGURE 3.1.17 UMNH VP 20205, U1

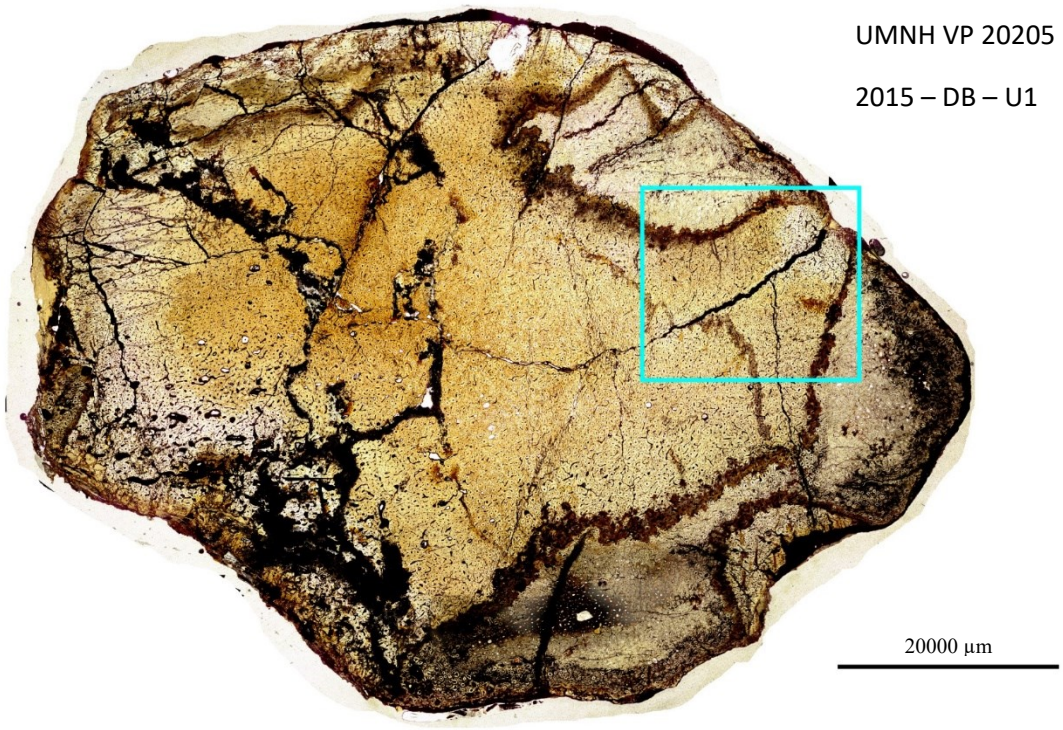

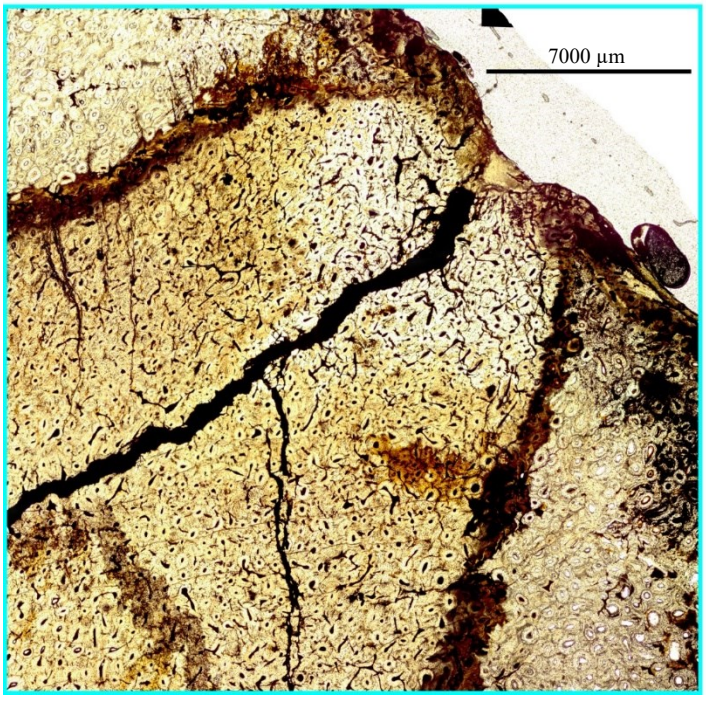

Above: Image of cross-section. Blue box shows location of close up image.

Left: Close-up image showing extensive secondary remodelling.

Tables

TABLE 3.1.1.Specimen List

Specimen Number	Study Code	Age Assessment	Element	Length (cm)	Least Circumference (cm)
UMNH VP 25143	F1	Juvenile	Femur	26.2	10.8
UMNH VP 25145	F2	Juvenile	Femur	33.1	12.5
UMNH VP 25135	F3	Subadult	Femur	48.3	20.0
UMNH VP 25141	F4	Subadult	Femur	63.9	28.0
UMNH VP 25144	T1	Juvenile	Tibia	31.9	10.6
UMNH VP 25140	T2	Juvenile	Tibia	42.3	16.0
UMNH VP 25136	T3	Subadult	Tibia	48.0	17.0
UMNH VP 25142	H1	Juvenile	Humerus	15.7	5.5
UMNH VP 25138	H2	Juvenile	Humerus	16.9	6.0
UMNH VP 25137	H3	Juvenile	Humerus	26.4	8.5
UMNH VP 25139	H4	Subadult	Humerus	30.6	11.2
UMNH VP 25146	H5	Subadult	Humerus	----	15.9
UMNH VP	U1	Adult	????	???	13.5

TABLE 3.1.2 Cross-Section Measurements. The table below shows the minimum and maximum measurement of the cortex and medullary cavity for each specimen, as well as the average cortical thickness.

		Cortex			Medullary Cavity		
Specimen Number	**Study Code**	Min.	Max.	Avg. Thickness	Min.	Max.	**Quarry Name**
UMNH VP 25143	F1	28	38	6	7	26	Doelling's Bowl (Jim's Place)
UMNH VP 25145	F2	19	49	10	10	26	Doelling's Bowl (Don's Place)
UMNH VP 25135	F3	40	60	---	--	--	Doelling's Bowl (Don's Place)
UMNH VP 25141	F4	60	115	---	--	--	Doelling's Bowl (Jim's Place)
UMNH VP 25144	T1	19	36	8	4	20	Doelling's Bowl (Gary's Island)
UMNH VP 25140	T2	27	55	---	--	--	Doelling's Bowl (Gary's Island)
UMNH VP 25136	T3	33	67	---	11	42	Doelling's Bowl (Gary's Island)
UMNH VP 25142	H1	12	20	4	5	11	Doelling's Bowl (The Pub)
UMNH VP 25138	H2	15	20	4	4	9	Doelling's Bowl (Gary's Island)
UMNH VP 25137	H3	24	29	7	7	10	Doelling's Bowl (Gary's Island)
UMNH VP 25139	H4	21	39	---	--	--	Doelling's Bowl (Jim's Place)
UMNH VP 25146	H5	28	59	8	6	22	Doelling's Bowl (Don's Place)

TABLE 3.1.3 Quantitative Histology. The table below shows the PVD, OI and HRI values calculated for each specimen in the study. When the distinction between inner and outer cortex could be made, these regions were measured separately.

Specimen	AGMS	Percent Vascular Density	Obliquity Index	Haversian Remodelling Index
H1 Outer Cortex	0	23%	46%	---
H1 Inner Cortex	0	23%	5%	---
H2 Outer Cortex	0	15%	64%	---
H2 Inner Cortex	0	24%	5%	---
H3 Outer Cortex	0	12%	58%	---
H3 Inner Cortex	0	21%	5%	---
H4 Outer Cortex	0	12%	51%	---
H4 Inner Cortex	0	19%	12%	< 5%
H5 Outer Cortex	0	13%	83%	---
H5 Inner Cortex	0	19%	88%	***
F1 Outer Cortex	0	15%	22%	---
F1 Inner Cortex	0	26%	5%	---
F2 Outer Cortex	0	18%	22%	---
F2 Inner Cortex	0	19%	3%	< 5%
F3 Outer Cortex	0	11%	86%	---
F3 Inner Cortex	0	25%	5%	---
F4 Outer Cortex	1	13%	92%	---
F4 Inner Cortex	0	12%	85%	< 5%
T1 Outer Cortex	0	15%	92%	---
T1 Inner Cortex	0	27%	14%	---
T2 Outer Cortex	0	13%	68%	---
T2 Inner Cortex	0	---	---	---
T3 Outer Cortex	0	13%	86%	---
T3 Inner Cortex	0	---	---	---

Table 3.1.4 Comparative Sizes. The table above shows the total lengths of the femora and tibiae of adult specimens of adult size (with the exception of the Doelling's Bowl Material) of various ornithopods. Measurements were taken directly from the specimens (Eolambia caroljonesa, Hypacrosaurus BFD, Tenontosaurus tillettii, Doelling's Bowl Materia) and from the literature (Maiasaura peeblesorum, Horner et al. 2000; Iguanacolossus forti, MacDonald 2012; Hypacrosaurus stebingeri, Horner et al. 1999).

	Femur Specimen	Length (cm)	Tibia Specimen	Length (cm)	
Tenontosarus tillitei	FMNH PR 2261	70	FMNH PR 2261	68	Associated
Doelling's Bowl Material*	UMNH VP 25141	64	UMNH VP 25136	48	Not Associated
Iguanacolossus forti	---	-----	UMNH VP 20205	>65**	----
Eolambia Caroljonesa	CEUM 8786	80	---	----	----
Hypacrosaurus stebingeri	MOR 549	102	MOR 549	98	Associated
Hypacrosarus sp. (BFD material)	MOR 609-89-43	102	MOR 609-89-18	75	Not Associated
Maiasaura peeblesorum	MOR 005A	100	MOR 005	98	Associated

* All other specimens are assessed to be adult; this is assessed subadult

** based on fibula length

TABLE 3.1.5 Size at First LAG. The above table shows the circumference of the first LAG for three

	Humerus Specimen	Least Circ. (cm)	Femur Specimen	Least Circ. (cm)	Tibia Specimen	Least Circ. (cm)
Tenontosarus tilleti	OMNH 8137	8	OMNH 34787	7.7	OMNH 2926	11
Iguanacolossus forti	--- ---	----	---	---	UMNH VP (F4)	17.2
Eolambia Caroljonesa	CEUM 357 (H5)	8.1	CEUM 343 (F3)	10.6	CEUM 528 (T2)	11

3.2 Eolambia

Eolambia caroljonesa was a comparativey large-bodied iguanodontian ornithopod (Fig. 1.3). I will first examine an ontogenetic series of this taxon, from a single site. The growth of these specimens is reconstructed as far as possible and discussed. I will then examine a section of a larger specimen of *Eolambia* from a second site. This specimen shows the same number of AGMs as much smaller specimens of the same taxon sectioned for this study. I examine whether or not retrocalculation of AGMs is appropriate in this isolated specimen.

Eolambia caroljonesa was discovered in 1993 by Carol and Ramal Jones while they were prospecting the northwest San Rafael Swell near Castle Dale, Utah. They brought the material to Don Burge at the College of Eastern Utah Prehistoric Museum in Price, Utah. The museum excavated the site, naming it the Carol Jones Quarry (later named the *Eolambia*/Cifelli #1 Quarry, EC1), and found a partial skeleton with a disarticulated skull. This material was initially determined to belong to an adult on the basis of gross morphology and suture closure; it was designatd the holotype of *Eolambia caroljonesa* (Kirkland et al. 1998). Around the same time, the Sam Noble Museum of Natural History (Norman, Oklahoma) collected fossil vertebrates in the southwest San Rafael Swell. This site, *Eolambia*/Cifelli #2 Quarry (EC2), has abundant, disarticulated material of *Eolambia*. The material was initially determined to belong to subadult as well as adult individuals on the basis of gross morphology and sutural closures (R. Cifelli, pers. comm.) and is commensurate in size with material from EC1. The majority of the material included in the current study is from EC2 (see Table 3.2.1). Screenwashing by the Sam Noble Museum also revealed that teeth similar to those

associated with *Eolambia* occur at all microsites in the Mussentuchit Member of the Cedar Mountain Formation.

Kirkland (1998) originally diagnosed *Eolambia* as a basal lambeosaurine, as indicated by its name "dawn lambeosaur." Kirkland considered the material from the EC1 to be adult and designated it as the holotype; he also considered the largest specimens from the EC2 quarry to be adult and included them among the designated paratypes. Head (2001) re-examined the material diagnosed by Kirkland, as well as additional material from the EC2 quarry. On the basis of this examination, Head (2001) found *Eolambia* to be a basal hadrosauroid, outside Hadrosauridae (see Figure 1.2). Head (2001) also found the material from the EC2 Quarry to be subadult and juvenile by comparison with the holotype. The position of *Eolambia* as basal hadrosauroid has been upheld by numerous phylogenetic analyses using different character-taxon matrices (for example, see McDonald 2012 and Prieto-Marquez 2010).

Multiple elements of various sizes from the *Eolambia*/Cifelli #2 Quarry (EC2 Quarry) were sectioned for this study (Table 3.2.1). This includes some of the largest specimens, which were considered to be adult by Kirkland (1998) and subadult by Head (2001) and McDonald (2012). , While only postcranial elements are included in this study, the diagnosis was based on both cranial and postcranial elements. On gross observation of broken diaphyses from the largest specimens at the site, upwards of 12 apparent annual growth marks (AGMs) are visible. Moreover, these lines of arrested growth (LAGs) become increasingly narrowly spaced towards the periosteal margin, indicating that the individuals were beginning to slow their growth and were close to reaching skeletal maturity.

As mentioned above, the majority of the characters used to diagnose the EC2 Quarry material are cranial; very few are from the postcranium, and fewer still are from the elements sectioned in this study. Head's (2001) analysis includes 27 characters; only three of these characters are postcranial (two femoral and one pelvic). McDonald (2012) included 134 characters in his analysis; only 36 of these characters are postcranial characters (9 femoral, 27 axial skeleton). Prieto-Marquez (2010) included 286 characters in his analysis; only 82 of these characters are postcranial (12 hindlimb characters; including 2 femoral, 1 tibial and 1 fibular characters).

This focus on cranial characteristics can make the identification of postcranial elements problematic. For instance, a femur was found approximately 100 meters southwest of the ECI Quarry, but was referred to the holotype material (McDonald 2012) given its morphology, as well as its proximity to the EC1 Quarry and its stratigraphic level. It is complete, and measures over 80 cm long and 37 cm in circumference (at the point of least circumference). The size difference between the material from EC2 and the isolated femur is striking. The largest femur from the EC2 quarry is incomplete and measures only 48 cm long and 17.5 cm in circumference (at the point of least circumference). The largest complete femur from the site is 41 cm long and 16 cm in circumference. If the largest individuals from EC2 are indeed skeletally mature, it would be difficult to assign them to the same taxon as the isolated femur from EC1 without evidence of something to explain this great difference in size (e.g. sexual dimorphism, evolutionary variation, etc.).

Although this specimen is not available for sectioning, the Field Museum (FMNH) has discovered several sites in the Mussentuchit Member of the Cedar

Mountain Formation of eastern Utah with isolated, partial postcranial skeletons, similar in size to the large femur discussed in the previous paragraph. These elements have also been diagnosed as *Eolambia* based on both their gross morphology and stratigraphic level. Fortunately, one of these femora was made available for sectioning and is included in this study. That femur (Table 3.2.1) is more than twice the size of the largest material at the EC2 Quarry. If the material from the EC2 Quarry is truly close to skeletal maturity, it would follow that the material from the FMNH Quarry is likely not the same taxon.

As with the previous section, it is necessary to determine whether the material from the two sites belongs to the same taxon, or if one site represents a previously unknown taxon. The gross morphology of the specimens from the two sites is consistent with them being the same taxon; however, the FMNH Quarry specimen lacks cranial elements. If the FMNH Quarry specimen is a new taxon, it would be phylogenetically related to *Eolambia*. The characters they share in common are characters all derived ornithopods share in common (pers. comm. Pete Makovicky, pers. obs.), such as the morphology of the fourth trochanter. Despite there being numerous fossil sites, some of which have yielded substantial material, there are no other ornithopods known from the Mussentuchit Member of the Cedar Mountain Formation (for example, see (Kirkland, 1998; Carpenter et al, 1999; Cifelli et al, 1999.

Geologic Setting

Eolambia caroljonesa is known exclusively from the Mussentuchit Member of the Cedar Mountain Formation (Albian-Cenomanian boundary, 98.39 $\pm$ 0.07 Ma) of eastern

Utah. This formation consists of cycles of upwardly fining muddy sandstone to mudstone layers. These strata have been interpreted by Garrison et al (2007) to represent either a poorly drained floodplain or a lacustrine floodplain environment that experienced seasonally wet and dry periods.

Both Stokes (1944, 1952) and Young (1960) considered this formation to be largely devoid of fossils, particularly with respect to large vertebrates such as dinosaurs. The first evidence of dinosaurs in this formation, a highly eroded hadrosaur femur, was reported by Galton and Jensen (1979). More recently, abundant vertebrate fossil material has been recovered from the Mussentuchit Member (Kirkland et al, 1997, 1999; Carpenter et al, 1999; Cifelli et al, 1999). In addition to *Eolambia*, the vertebrate fauna now includes shamosaurine ankylosaurs, neoceratopsians, therizinosauroids, and gobiconodontid mammals. The relationship between the holotype material from the EC1 quarry and the isolated femur near EC1 is unclear. They are both at the same stratigraphic level. The lithology does not give any evidence to support or refute the hypothesis that the femur was transported from the holotype material; however, the difference in size would suggest that the isolated femur is from a different individual.

The accumulation of disarticulated remains at the EC2 Quarry has been interpreted by Garrison et al (2007) to have been caused by winnowing due to wave-action. In particular, the sedimentological evidence and orientation of fossils suggests that they were initially deposited as a fluvial lag, and later reworked by the waves of a transgressing lacustrine shoreline. The geology of the isolated remains discovered by FMNH has not been analyzed; however, the sediments are generally similar to those at

both the EC1 and EC2 quarries.

Materials and Methods

Only incomplete specimens from the EC2 Quarry were considered for sectioning because of curatorial restrictions. In turn, only those elements with clear morphological landmarks were selected, to ensure that sections would be taken from the same location across specimens. Given these conditions, five femora, nine tibiae and eight humeri were selected for this study (Table 3.2.1). The large femur from the FMNH Quarry was also sectioned for this study. For location of the section extracted and methods used to extract it, please refer to "Selection and Extraction of Section ('plug')" in Section 2. All complete femora, tibiae and humeri from the EC2 Quarry were measured (Table 3.2.2). While these elements were not sectioned, these measurements do provide an estimation of total lengths of the incomplete specimens that were sectioned (Fig. 3.2.1, Table 3.2.2). Slides were made and imaged according to standard practices as described in Section 2.

Osteohistology of *Eolambia caroljonesa* from Eolambia/Cifelli #2 Site

As part of the histologic description, the minor and major axes of both the outer cortex and medullary cavity, as well as the average cortical thickness were calculated using methods detailed under "Analysis of Slides" in Section 2 (Table 3.2.3). It should be noted that measurements were **not always possible** due to significant crushing and distortion of certain specimens.

Assessment of age category was made based on histologic features (Table

3.2.4). In addition to this, three measurements of vascularity were taken from each slide. A brief description of each measure is given below; a detailed description can be found under "Analysis of Slides" in Section 2. Percent Vascular Density (PVD), Obliquity Index (OI), and Haversian Remodeling Index (HRI) were calculated; a detailed description of these calculations can be found under "Analysis of Slides" in Section 2.

In addition to measurements of vascularity, Annual Growth Marks (AGMs) were identified; when present, the circumference of each AGM was measured and AGMs present in each specimen were counted (Table 3.2.5)

For each section, both a full view and close-up image are included (see Figs. 3.2.2-3.2.24); the images of these sections will also be made available on MorphoBank.

Humerus

Juvenile

Specimens examined: CEUM 35641 (H1), CEUM 35369 (H2)
(Figs. 3.2.2, 3.2.3)

The cross-sectional shapes of all specimens (H1, H2) is a rounded trapezoid, with medullary cavities between rounded trapezoid and oval. The endosteal margin of H1 is preserved and shows little to no signs of resorption; the endosteal margin of H2 has largely been obliterated by crystal growth in the medullary cavity. The inner cortex and outer cortex of H1 cannot be distinguished; the cortex is highly vascularized, with highly disorganized osteonal canals and primary osteons present. The inner cortices of H2 is similar; it is highly vascularized, with both disorganized osteon canals and primary osteons. In all specimens, this portion of the cortex is composed of reticular

fibrolamellar bone matrix. The cortex of H1 and inner cortex of H2 have a high PVD and low OI, similar to the inner cortices of juvenile specimens in this study.

The outer cortices are also highly vascularized; they are dominated by osteon canals that are oriented longitudinally. This portion of the cortex is composed of plexiform fibrolamellar bone matrix. This portion of the cortex also has a high PVD, although somewhat lower than the inner cortex. The OI, however, is much higher because the canals are almost exclusively longitudinal.

There are no annuli visible; no outer circumferential layer is visible.

Subadult

Specimens Examined: CEUM 35621 (H3), CEUM 35719 (H4), CEUM 35743 (H5), CEUM 35662 (H6), CEUM 35357 (H7), OMNH 62250 (H8) (Figs. 3.2.4-3.2.8)

The cross-section in all the specimens (H3-H8) is a rounded triangle or trapezoid, with medullary cavities that are of similar shape (H3-H7) to roughly elliptical (H8). Much of the endosteal margin is intact and shows signs of resorption. However, in all specimens, some portion of the endosteal margin and inner cortex has been obliterated by calcite crystal growth.

The innermost cortex, where visible, is increasingly dominated by secondary osteons. In smaller specimens (H3-H6), the secondary Haversian system is primarily restricted to the caudal margin; in larger specimens (H7-H8), the secondary Haversian system is present around the entire circumference. Accordingly, the HRI of these specimens varies greatly around the circumference; the HRI near the caudal margin is high, while near the cranial margin it is very low (H3-H6) to moderate (H7-H8). PVD and OI were calculated along the cranial margin, where secondary remodeling was, generally, low; the PVD of these regions is high and OI low, similar to the juvenile

specimens above. Where the cortex has not been completely secondarily remodeled, the bone is plexiform fibro-lamellar matrix.

The outer cortex of all the specimens is moderately vascularized; it is dominated by osteonal canals that are organized longitudinally. The cortex is composed of plexiform fibro- lamellar bone matrix. The PVD of these regions is low and OI high, similar to other subadult specimens of other taxa in this study. No specimen has an outer circumferential layer. However, several specimens do have annuli; these will be discussed individually below.

CEUM 35621 (H3) and CEUM 35719 (H4) both have one AGM visible. Starting from the medullary cavity outwards, the AGM occurs approximately one third of the way to the periosteal margin in both specimens. These AGMs are both LAGs. In H4, the LAG is accompanied by a bright band, deep to the LAG that follows the LAG around the entire circumference.

CEUM 35743 (H5) has five AGMs visible. Counting from the medullary cavity outwards, the first three AGMs are widely spaced. The first is an annulus, although it has been partially resorbed by the marrow cavity. The second is a LAG, and can be traced around the complete circumference of the specimen. The third is a LAG; it is widely spaces with respect to the second LAG, but moderately-to-closely spaced with respect to the fourth. The fourth and fifth are closely spaced and are LAGs. The fifth is a double LAGs throughout portions of the cortex, and is equidistance from the periosteal margin and fourth AGM.

CEUM 35662 (H6) this specimen has numerous pyrite inclusions; this made slide production problematic. As a result, no image is available for this specimen.

CEUM 35357 (H7) has five AGMs visible, but the endosteal margin is so heavily secondarily remodeled that it is impossible to determine if any AGMs were present. Counting from the medullary cavity, the first visible AGM is approximately halfway through the cortex, immediately superficial to the cessation of heavy secondary remodeling. The second AGM is a LAG and is moderately-to-widely-spaced from the first. The third AGM is narrowly spaced with respect to the second; it is LAG, sometimes appearing as a double LAG and sometimes as a single LAG. The fourth AGM is moderately to widely-spaced with respect to the third and is an annulus. The fifth AGM is a LAG; it is narrowly spaced with respect to the fourth and moderately spaced with respect to the endosteal margin.

OMNH 62250 (H8) has five visible AGMs. Counting from the medullary cavity outwards, the first three AGMs are widely spaced. The first AGM is an annulus and occurs approximately one third of the way through the cortex. The second AGM is also an annulus. Both the first and second AGM are locally destroyed in areas of high secondary remodeling, but can otherwise be traced around the circumference of the specimen. The third AGM is a double LAG in some portions of the cortex, and a single LAG in other portions. It is widely spaces with respect to the second AGM and moderately spaced with respect to the fourth. The fourth AGM is a LAG, and is the fifth. On first inspection, it may seem that these are forming a double LAG; however, on closer inspection, a single row of osteons is present between the two around the entire circumference of the specimen. The fifth AGM is moderately spaced with respect to the periosteal margin.

Femur

Hatchling

Specimens Examined: FMNH 3848 (F0)
(Fig. 3.2.9)

The cross-section of FMNH 3848 (F0) is roughly triangular, as is the cross-section of the medullary cavity. The margin of the medullary cavity is preserved and shows no signs of resorption. The cavity has been filled with trabecular bone tissue and calcite crystals. Although no hatchlings of hadrosauroids are described in the literature, the size of F0 is commensurate with that of hadrosaurid hatchlings (Horner & Currie, 1994; Horner, et al 2000).

The inner cortex is highly vascularized and dominated by primary osteons. This portion of the cortex is very darkly stained, but individual osteons can be visualized by increasing the intensity of the light passed through the specimen. The osteons are highly disorganized and completely fill the available space. Given the absence of canals and the problematic nature of the staining, neither PVD nor OI was calculated. The osteons were visualized under crossed polarized light with a rotating stage to verify that they are primary, not secondary, osteons.

The outer cortex is also highly vascularized; both osteon canals and primary osteons are present. Unlike the other hatchling specimen in this study (F0) in which the osteons dominate, in this specimen, canals and osteons are closer to equal in proportion. However, there is still a relatively low number of canals, so neither PVD nor OI was calculated. This portion of the cortex is composed of reticular to plexiform fibrolamellar bone matrix. As with other femora in this study, there is an area of reticular fibrolamellar bone matrix that appears highly disorganized, along the caudal to caudal

lateral margin of the element. Neither AGMs nor an outer circumferential layer are visible.

Juvenile

Specimens examined: CEUM 13317 (F1), CEUM 34399 (F2), CEUM 35444 (F3), CEUM 14503 (F4), OMNH 62194 (F5)
(Figs. 3.2.10-3.2.14)

The cross-section of all the specimens (F1-F5) are almost identical in shape, but defy easy explanation; in general, it is a right triangle and a half circle, such that the hypotenuse and diameter share a common junction. The cross-section of the medullary cavity is roughly circular in all specimens. In all specimens, the endosteal margin and much of the inner cortex has largely been obliterated by calcite and pyrite crystal growth. Where the margin is intact, it shows signs of resorption, with the larger specimens (F3-F5) showing the most significant signs of resorption.

The inner cortex of all specimens is highly vascularized; both osteon canals and primary osteons are present and highly disorganized. This portion of the cortex is composed of reticular fibrolamellar bone matrix. The specimens have a high PVD and low OI, similar to the inner cortices of juvenile specimens in this study. Secondary osteon formation has begun in all but one of the larger specimens (F2-F5), but does not extend beyond the inner cortex. Specimens were viewed under cross-polarized light to verify the identity of secondary osteons.

The outer cortex is highly vascularized; it is dominated by osteon canals that are oriented longitudinally. This portion of the cortex is composed of plexiform fibrolamellar bone matrix. This portion of the cortex also has a high PVD, although somewhat lower than the inner cortex. The OI, however, is much higher as the canals

are almost exclusively longitudinal. No specimen has an outer circumferential layer. However, several specimens (F3-F5) do have AGMs; these will be discussed individually below.

CEUM 35444 (F3) has five AGMs visible. Counting from the medullary cavity outwards, the first visible AGM appears in the inner cortex and has been obliterated in a few places by secondary remodeling. It appears that there may have been a LAG deep to this LAG, but the secondary remodeling has made its verification impossible. The second AGM is a LAG that is moderately spaced with respect to the first. At times is appears that this is a double LAG, it also appears in places that there are up to three AGMs between the first and second LAG; however, none of these marks can be traced around the circumference of the specimen, and so are not considered to be true AGMs. The third AGM is an annuli and is moderately to widely spaced with respect to the second; it sometimes appears as a double annuli, but only a single annulus can be traced all the way around the circumference of the specimens. The last two AGMs are two LAGs and a widely spaced with respect to the third AGM. These LAGs are very narrowly spaced and close to the periosteal margin. These are not a double LAG as there is at least one row of osteons between them all the way around the circumference of the specimen.

CEUM 14503 (F4) has two AGMs visible. There are some indications that AGMs have been resorbed by the medullary cavity; however, none of these marks can sufficiently be traced around the circumference of the specimen to make a determination as to their identities. The first AGM that can be traced around the circumference is a LAG and located close to the endosteal margin. The second AGM is

also LAG and occurs slightly more than halfway through the cortex to the periosteal margin. OMNH 62194 (F5) has one AGMs visible, a double LAG. As with specimens above, there are some indications that AGMs have been resorbed by the medullary cavity, but the marks cannot be adequately traced around the circumference of the specimen to make a determination as to their identities. There is also differential staining that may be mistaken for AGMs on gross inspection; however, close histologic analysis demonstrates that they are not AGMs.

As with the hatchling femora in this study, all of these specimens also show an area of disorganization along the posterior lateral margin. The disorganization extends completely through both the inner and outer cortex, from the endosteal to periosteal margin of the specimen. This portion of the cortex is composed of reticular fibrolamellar bone matrix. The osteonal canals in this region are markedly larger than in another area of the cortex. Secondary osteon formation is more prevalent in this region than throughout the cortex. Specimens were viewed under cross-polarized light to verify the identity of secondary osteons.

Tibia

Hatchling

Specimen Examined: CEUM 34276 (T0)
(Fig. 3.2.15)

The cross-section of CEUM 34276 (T0) is roughly lacrimiform, as is the cross-section of the medullary cavity. The margin of the medullary cavity is preserved and shows no signs of resorption. The cavity has been filled with trabecular bone tissue and calcite crystals. While there are no hatchlings of hadrosauroids in the literature, its size is

commensurate with that of hadrosaurid hatchlings (Horner & Currie, 1994; Horner, et al 2000). The inner cortex highly vascularized and dominated by primary osteons. At first glance, the osteons resemble the secondary osteons formed during remodeling. The osteons are highly disorganized and completely fill the available space. Given the absence of canals, neither PVD nor OI was calculated. The osteons were visualized under crossed polarized light with a rotating stage to verify that they are primary, not secondary, osteons.

The outer cortex is also highly vascularized; both osteon canals and primary osteons are present, although the osteons predominate. Given the relatively low numbers of canals, neither PVD nor OI was calculated. This portion of the cortex is composed of reticular fibrolamellar bone matrix. The osteons and canals appear to form longitudinal bands with annuli in between; however, when visualized under higher magnification and crossed polarized light, it is only mineral staining and not true annuli. There is no outer circumferential layer visible.

Juvenile

Specimens examined: CEUM 13306 (T1)
(Fig. 3.2.16)

The cross-section of CEUM 13306 (T1) is roughly circular, while that of its medullary cavity is roughly elliptical. Although the majority of the endosteal margin has been obscured by breakage and growth of crystals, there are no signs of resorption. The cavity is filled with calcite and pyrite crystals.

The inner cortex is highly vascularized; both osteonal canals and primary osteons are present and highly disorganized. This portion of the cortex is composed of

reticular fibrolamellar bone matrix. This specimen has a high PVD and low OI, similar to the inner cortices of other juvenile specimens in this study.

The outer cortex is also highly vascularized; it is dominated by osteonal canals that are organized longitudinally. This portion of the cortex is composed of plexiform fibrolamellar bone matrix. This portion of the cortex also has a high PVD, although somewhat lower than the inner cortex. The OI, however, is much higher as the canals are almost exclusively longitudinal.

There are no annuli visible; no outer circumferential layer is visible.

Subadult

Specimens examined: CEUM 35386 (T2), CEUM 52874 (T3), CEUM 35704 (T4), CEUM 74590 (T5), CEUM 35491 (T6), CEUM 14582 (T7), OMNH 62213 (T8)
(Figs. 3.2.17 – 3.2.23)

The cross-section in all the specimens (T2-T8) is approximately lacrimiform, with medullary cavities that are elliptical (T2, T3, T5, T6, T7) to roughly circular (T4, T8). In all but one specimen (T5), the endosteal margin and much of the inner cortex has largely been obliterated by calcite and pyrite crystal growth. Where the margin is intact, it shows signs of resorption.

The innermost cortex, where visible, is dominated by secondary osteons. The varying degrees of obliteration due to crystal growth make it impossible to accurately assess the HRI of these specimens. Superficial to the innermost cortex, but deep to the outer cortex, the bone becomes reticular to plexiform fibro-lamellar matrix. The PVD of these regions is high and OI moderate to high, similar to the inner cortex of other subadult specimens in this study.The outer cortices of all the specimens are moderately vascularized and are dominated by osteon canals that are oriented

longitudinally. The cortices are composed of plexiform fibro-lamellar bone matrix. The PVD of these regions is low and OI high, similar to other subadult specimens of other taxa in this study. No specimen has an outer circumferential layer. However, several specimens do have AGMs; these will be discussed individually below.

CEUM 35386 (T2) has five AGMs visible. Counting from the medullary cavity outwards, the first three AGMs are narrowly spaced. The first is a LAG, although it has been partially resorbed by the marrow cavity. The second is an annulus, and can be traced around the complete circumference of the specimen. The third is a double LAG, as is the fourth. These double LAGs are widely spaced; the span between the third and fourth is similar to that between the first and third. The fifth and final annuli is a LAG, and is close to the external margin of the bone.

CEUM 52874 (T3) has five visible AGMs. Counting from the medullary cavity outwards, the first AGM is an annulus and occurs approximately a third of the way through the cortex. The second is a LAG, it is narrowly spaced and accompanied by an annulus around the complete circumference of the specimen. The third annulus is a double, and at times a triple LAG. It is widely spaced; the distance between second and third annuli is approximately double the distance between the first and second. The fourth is narrowly spaced, single LAG. This is followed by the fifth and final LAG. The distance between the fifth and fourth annuli is similar to that between the second and third.

CEUM 35704 (T4) has 5 visible annuli. Counting from the medullary cavity outwards, the first AGM is a LAG and occurs approximately a third of the way through the cortex. The next AGM is also a LAG and is widely spaced from the first.

In between the two LAGs are two dark bands; these appear under low magnification to be annuli, but this is shown not to be the case under higher magnification. The next annulus is a LAG, and is widely spaced from the second. This is in turn followed by the fourth annulus, also a LAG, and is narrowly spaced from the third. It may appear to be a double LAG with the third at first glance, but on closer inspection, three rows of osteons can be seen between the two LAGs around the entire circumference of the specimen. The fifth and final annulus is a LAG very close to the periosteal margin. In places, this portion of the specimen has been lost during the grinding process, but can otherwise be traces around the entire circumference of the specimen.

CEUM 75490 (T5) has five annuli visible. Counting from the medullary cavity outwards, the first AGM is an LAG. The LAG appears at the border between more organized bone on the interior side and less organized bone to the exterior side; the less organized bone becomes more and more organized moving exteriorly, forming what has been called a growth cycle. The second AGM is a LAG and is widely spaced with respect to the first. The third AGM is also a LAG, but is very narrowly spaced with respect to the second; it is possible to visualize between two and three rows of osteons between the second and third AGM, verifying that they are distinct marks. The fourth AGM is a LAG and is moderately spaced with respect to the third. The fifth and final AGM is a LAG and is moderately spaced with respect to both the fourth and periosteal margin.

CEUM 35491 (T6) has two annuli visible. Counting from the medullary cavity outwards, the first AGM is a LAG that occurs about 2/3 the way through the cortex. The second LAG is moderately spaced with respect to the first and appears close to the

periosteal margin.

CEUM 14582 (T7) has five annuli visible. Counting from the medullary cavity outwards, the first two AGMs is are both LAGs. While they are very narrowly spaced, there are two rows of osteons between the LAGs. The second LAG appears at the border between more organized bone on the interior side and less organized bone to the exterior side; the less organized bone becomes more and more organized moving exteriorly, forming what has been called a growth cycle. The next AGM is a LAG and appears at the beginning of another growth cycle. This LAG is widely spaced with respect to the annulus. The fourth AGM is a LAG; it is widely spaced with respect the third AGM. The fifth and final AGM is LAG. It is widely spaced with respect to the fourth AGM, but close to the periosteal margin.

OMNH 62213 (T8) has five annuli visible. Counting from the medullary cavity outwards, the first AGM is a LAG and is marked by a bright band for the entire circumference of the specimen. The next AGM is also a LAG, this time marked by a dark band, which is the result of staining. The second is moderately spaced with respect to the first. The third annulus is a LAG and is widely spaced with respect to the second. This LAG often appears as a pair or triplet; however, only the middle band can be traced around the entire circumference of the specimen. The fourth annulus is a LAG and is narrowly spaced with respect to the third. The fifth and final annulus is a LAG; it is narrowly spaced with respect the fourth and close to the periosteal margin of the specimen.

Discussion

Skeletally mature *Eolambia* is completely unrepresented in the above sample. The

largest of the elements (H7, T7, F4) are all juvenile or subadult by the criteria of osteological histology. These elements all lack an outer circumferential layer, extensive secondary remodeling of the outer cortex and narrowly spaced annuli that are characteristic of skeletally mature individuals. Some of these specimens (H7, T7) do show signs of approaching skeletal maturity, such as the presence of secondary osteons in the outer cortex or a trend towards more narrowly spaced annuli. However, we should be careful in assessing closely spaced AGMs as a mark of skeletal maturity given the differential growth patterns, which will be more fully discussed later in this section (for example, see Petermann & Gauthier, 2017).

That there are no skeletally mature adults in the sample is surprising, given initial inspection of the material. On gross inspection, many of the larger specimens appeared to have up to 12 AGMs. It was only after close histologic analysis that this was demonstrated not to be the case. Many of what appeared to be AGMs, proved to be nothing more than differential staining; upon close inspection, these specimens had a maximum of five true AGMs. Despite its inherently consumptive nature, histologic analysis was shown to be the only way to properly assess AGMs.

As noted in the introduction, it is not uncommon to find bonebeds dominated by juvenile and subadult ornithopod material; at the same time, these bonebeds do not often include adult material (Varricchio & Horner, 1993). Given this taphonomic pattern, the early life of ornithopods is of special interest. Iguanodontians are not known to be sexually dimorphic (Mallon, 2017); medullary bone has been found in some specimens, although not in this sample (Hübner, 2012). Given this, it is possible that all of the specimens in bonebeds containing exclusively juvenile and subadult

material are male. Among large bodied, herbivorous extant taxa, a common social structure is a three part system: first, there is a female dominant herd (which sometimes include juveniles of both sexes, and sometimes only females); second, there are associated groups of territorial adult males; third, there are juvenile bachelor herds (Averbeck et al., 2010; Cox et al., 2007; Foster, 1966; Gibson & Guinness, 1980; Hass & Jenni, 1991; Smuts, 1975; Yoccoz & Mesnager, 1998). Given that these seem to be such a successful evolutionary strategy among modern taxa, there is reason to suppose that it might have been a similary successful strategy among extinct taxa. However, this hypothesis warrents further investigation.

In this sample, the tibia contains the best record of growth. This is similar to what has been found in other ornithopod taxa (Horner et al., 1999; Werning, 2012; Woodward et al., 2015). Using the circumference of each LAG (Table 3.2.1) and the linear regressions discussed earlier (Fig. 3.2.1), it is possible to estimate the size of the element at the time each LAG was deposited (Fig. 3.2.26). The elements not only increase in length with age, they also increase in girth. To examine this, we can look at the appositional growth rate (Fig. 3.2.25). While the bone is increasing in diameter, the rate at which new bone is being deposited decreases over time. The maximum cortex width was examined because its location is relativey unaffected by cortical drift and does not tend to shift over time. It was also chosen as this is a commonly cited measurement in the literature, as opposed to, for example, diameter of the cortex.

As we can see from the graphs (Figs. 3.2.25 & 3.2.26), most of the specimens increase their size by 30-50% during their first five years of life. However, if we are to assume that they would have reached the adult size of the holotype specimen and the

large femur found near the holotype, then after five years, the specimens have, on average, achieved 30% of their adult size. This is similar to the rate of growth Hubner (2012) found in *Dysalotosaurus*, which reached adult size around age 20 and; at five years of age had reached around 40% of their adult size. Hubner (2012) found the inflection point of the growth curve, which is generally taken to be the point at which sexual maturity is reached (as discussed above), to occur around 10 years of age. *Dysalotosaurus* can, therefore, be characterized as a slow growing taxon; one whose males might benefit by forming bachelor herds. Given the similarity between the growth of *Eolambia* and *Dysalotosaurus* it is also reasonable to draw the same conclusion for *Eolambia*.

It has been suggested that ornithopod locomotion depends on body size, not phylogeny; small-bodied individuals are primarily bipedal as adults, while larger-bodied individuals are facultative bipeds as adults. Under this hypothesis, locomotor mode is tied to body size of the individual, not its ontogenetic state. For example, a large-bodied taxon may be bipedal as juveniles, while they still have a small body size, and become facultative bipeds later in life, when they achieve large body size. If an individual was using both its fore- and hind limb for locomotion, then we would expect both elements to grow at the same rate during this time; if an individual, on the other hand, was only using its hind limb for locomotion, it is reasonable that the forelimb might grow at a different rate as it would be under different mechanical pressures. Because both fore- and hind limb elements were sampled, it is possible to test this hypothesis with respect to *Eolambia* (see Heinrich et al. 1993).

As discussed above, the tibia has the best record of growth. In the forelimb, the

humerus also shows a good record of growth. It is true that the former is part of the stylopodium, while the latter is part of the zygopodium. Despite this, both elements are weight-bearing when used during locomotion and should show similar patterns of growth if used in this manner.

As can be seen from the graphs (Fig. 3.2.25 & 3.2.26), the growth rate of the tibia is similar to the growth rate of the humerus. To test whether the difference between the slopes is statistically significant, the following formula was used (Paternoster et al., 1998):

$$Z = (\text{slope H} - \text{slope T}) / \text{sqrt}(\text{SE slope H}^2 + \text{SE slope T}^2)$$

where SE is the standard error of the slope (calculated in Excel using the LINEST command), H stands for Humeri, and T stands for Tibiae. When values from the appositional growth graphs (Fig. 3.2.25) are used:

$$Z = (8.416 - 8.318) / \text{sqrt}(2.53^2 + 1.70^2)$$

$$Z = 0.098 / \text{sqrt}(6.4 + 2.89)$$

$$Z = 0.098 / 3.05$$

$$Z = 0.032$$

And when values from the linear growth graphs (Fig. 3.2.26) are used:

$$Z = (18.533 - 20.691) / \text{sqrt}(5.81^2 + 4.22^2)$$

$$Z = -2.158 / \text{sqrt}(33.76 + 17.8)$$

$$Z = -2.158 / 7.18$$

$$Z = -0.300$$

The resulting values were then compared to those looked up in a Z table (Zar, 1996) with the following degrees of freedom:

$$(nH + nF) - 4 = \text{Degrees of Freedom}$$

$$(7 + 9) - 4 = 12$$

$$Z_{0.5(1),12} = 1.782$$

When we consider either appositional or linear growth, the Z value is less than $Z_{0.5(1),12}$, so we are unable to reject the null, that the growth rates are not statistically different.

These results suggest that the humerus was under the same mechanical constraints as the tibia during this stage of ontogeny, (i.e. that *Eolambia* was quadrupedal or facultative bipedal during this period of its life). As an adult, *Eolambia*, as an iguanodontian, was likely a facultative biped (Norman 2004).

Osteohistology of *E. caroljonesa* from the FMNH Quarry

While the large femur mentioned above was not available for sectioning, a large specimen of the same taxon, but from a different site (FMNH Quarry), was available. The adult specimen sectioned below is from the same taxon, the same geologic unit and geographic area as the population under study. The results of this histologic analysis, as well as the resulting growth curve, are discussed below.

Femur, FMNH UT130825-3

The cross-section of FMNH UT130825-3 (F6, Fig. 3.2.24) is approximately oval, with a medullary cavity that is approximately the same shape. The endosteal margin and much of the inner cortex have largely been obliterated by calcite and pyrite crystal growth. Where the margin is intact, it shows signs of resorption. There are also indications that the specimen has undergone post-depositional breakage; this has resulted in an offset at two places in the cortex, but has not obscured any of the

features.

The innermost cortex, where present, is dominated by secondary osteons. The remodeling is sufficiently extensive to obscure the original bone morphology; hence, neither PVD nor OI were calculated. The HRI of this region is quite high; similar to the HRI of posterior-lateral regions of the hatchling and juvenile femora discussed above. Specimens were viewed under cross-polarized light to verify the identity of secondary osteons.

The outer cortex is moderately vascularized; it is dominated by longitudinally-organized osteon canals. The cortex is composed of plexiform fibro-lamellar bone matrix. The PVD of these regions is low and OI high, similar to other subadult specimens of other taxa in this study. Secondary osteon appear in this portion of the cortex as well. While they are more numerous than in the specimens discussed above, they do not dominate the cortex and the HRI remains low.

As with the other femora, discussed above, this specimen also shows an area of disorganization along its posterior lateral margin. The disorganization extends completely through both the inner and outer cortex, from the endosteal to periosteal margin of the specimen. This portion of the cortex is composed of reticular fibrolamellar bone matrix. The osteonal canals in this region are markedly larger than in another area of the cortex.

This specimen has no outer circumferential layer; however, it does have two AGMs. The first AGM is a LAG that appears approximately one half to two thirds the way through the outer cortex. It is possible that this is not the first AGM, and that earlier AGMs have been obliterated by secondary remodeling. The second and last

AGM is a LAG and appears very close to the endosteal margin.

Discussion

The extent of secondary remodeling, as well as the slowing of growth as evidenced by the size and orientation of vascular canals, indicates that this specimen is subadult. After careful consideration, I conclude that FMNH UT130825-3 (F6) is *Eolambia,* based on the stratigraphy, gross morphology and histologic evidence.

This specimen shows only two AGMs, despite being significantly larger than other femora of this taxon that also show two AGMs. If retrocalculations are not appropriate, this would argue against F6 belonging to *Eolambia*. After careful consideration, discussed below, I conclude that retrocalculations are appropriate in this case, given the AGMs present in smaller specimens of the same taxon and evidence of resorption along the endosteal margin.

As mentioned in the introduction, F6 and the other femora in the study are from the Mussentuchit Member of the Cedar Mountain Formation of eastern Utah. The two sites are geographically close and have similar lithology. Although the Mussentuchit Member contains abundant vertebrate fossil material from numerous taxa, *Eolambia* is the only known ornithopod.

The gross morphology of the specimen supports the conclusion that F6 is *Eolambia*. F6 preserves the fourth trochanter and part of the shaft; however, it does not preserve either articular end. The fourth trochanter is prominent and oval in cross-section; its overall morphology is identical to the other specimens of *Eolambia*. Among non-avian dinosaurs, prominent fourth trochanters are only found in ornithopods, basal marginocephalians and theropods (Hailu & Dodson, 2004; Horner et al., 2004;

Maryanska, et al., 2004)). The shafts of theropod limbs can be readily distinguished from those of ornithischians by the relative thickness of the cortical bone and medullary cavity; in addition, theropods have hollow shafts, whereas iguanodontians and hadrosaurs have non-hollow shafts. F6 has a relatively thick layer of cortical bone and is not hollow. The trochanters of basal ceratopsians and pachycephalosaurs are both described as pendant; iguanodontians and hadrosaurs have a more triangular trochanter. The trochanter of F6 is not pendant, but is roughly triangular.

When the first LAG of F6 is compared in size with those of the other femora in this study (Table. 3.2.1), we can see that it is larger than the outermost AGMs of F4 and F5. It could be the case that this is simply an instance of intraspecific variation; i.e. some individuals grow quicker and reach larger body sizes than others. [For instance, sexual dimorphism has been documented in the extant phylogenetic bracket (birds: Owens & Hartley, 1998; Szekely et al., 2007; crocodilians: Cox et al., 2007)]. Difference in growth rate and adult body size has also been documented in relation to the seasonal timing or resources at time of conception and/or birth (voles: Yoccoz & Mesnager, 1998; ectotherms: Angilletta et al., 2004; birds: Lepage et al., 1998; squamates: Petermann & Gauthier, 2017).

Of all the studies above, Petermann & Gauthier (2017) found the greatest disparity in body size among individuals of the same age. However, they only found significant size disparities among individuals over the age of two; this is the age at which the taxon under study reaches sexual maturity. Petermann & Gauthier did not find a causal link between achievement of sexual maturity and differential growth, however, the strength of the correlation is suggestive. When we compare the size of the

first AGM in the largest femur (F6) to the first AGM in the smallest femur (F3), it is obvious that they are very different in circumference. The first AGM of F3 is 41% of the circumference of the first AGM of F6. While there is no direct way to test when sexual maturity is reached in non-avian dinosaurs, it is unlikely that it was reached before the end of the first year of life (Case, 1978; Erickson et al., 2007; Lee & Werning, 2008).

Given the resorption evident around the endosteal margin of F6, it is plausible that the earliest AGMs of F6 have been obliterated. The first LAG appears half-way through the outer cortex; if one or more LAG has been resorbed, it could be no closer than the border between the inner and outer cortex. This would mean that the LAGs were widely spaced, much more widely spaced than any of the LAGs in the other juvenile femora. This difference in growth rate is consistent with the differences observed by Petermann & Gauthier (2017), provided the early history of growth (the LAGs that were obliterated) of F6 is similar to the other femora in this study.

If we were to try to estimate the number of missing AGMs in this specimen (F6) we should start by looking at the smaller specimens sectioned. Among the smaller femora, F3 has the best record of growth preserved with 5 LAGs. The fifth and largest LAG in this specimen is 120 mm in circumference. This would easily fit within the first LAG of the F6, which is 194 mm in circumference. The endosteal margin of F6 is 110 mm; it is quite possible that a LAG near this margin would have been obliterated by secondary remodeling. It is reasonable to conclude, therefore, that up 5 LAGs could have been laid down and obliterated in F6. This would mean that the retrocalculated LAG count for F6 could be as great as 7 LAGs.

While many studies support the application of retrocalculations (for examples see: (Lee et al., 2013; Lee & O'Connor, 2013; Lee & Werning, 2008), there are two notable exceptions, both of which concern *Maiasaura*. The first is Horner et al. (2000), who found no evidence of resorbed AGMs in *Maiasaura* specimens from the Two Medicine Formation of Montana. In particular, they looked at six femora, varying in size from early nestling to adult. The first visible LAG occurs in an individual that is a late juvenile (femur = 50 cm; body length est. = 3.5 m). This begs the question as to whether such large size can be accomplished in a single year. In support of there being no missing AGMs, they cite a number of studies on growth rates in extant birds. Castanet et al. (1993) found that the highest rate of osteogenesis in mallard ducks between hatching and 169 days is 15 μm/day; Church et al (1964) found that between 3 and 14 weeks, White Leghorn and New Hampshire Barred Rock chickens increase the length of their humeri and femora by ~5 mm/week and tibiae by ~8mm/week (tibia); Latimer (1927) found that the long bones of chickens increase in size approximately 5 times over their hatchling size. Woodward et al. (2015) also found no signs of missing AGMs in their sample of 50 *Maiasaura* tibiae. Their sample consisted of tibia of varying sizes, including adult sized material.

This suggests that rapid growth could result in very large, year old animals. The closest living relatives to *Maiasaura* are crocodilians and birds. Among the extant birds, the ratites are the largest. Emus (*Dromaieus novaehollandiae*) are approximately 12 cm tall when they hatch, and reach 150-190 cm (adult size) in five to six months (Davies & Bamford, 2002). Cassowaries

(*Casuarius casuarius* and *Casuarius unappendiculatus*) have a similar size to emus at hatching and as adults; they take approximately nine months the reach adult size. (Davies & Bamford, 2002) As adults, the femora length varies between approximately 20-25 cm and the tibiotarsi between 35-38 cm (personal data from USNM and FLMNH; Fowler, 1991). In these taxa, the femora are significantly smaller than the tibiotarsi, where as in *Maiasaura*, the femur and tibia are more commensurate in size. While it is true that these modern birds are somewhat smaller at one year of age than *Maiasaura*, it is suggestive that *Maiasaura* could reach a similar size in their first year.

Maiasaura peeblesorum is similar to *Eolambia* both phylogenetically (i.e. both are derived ornithopods; *Maiasaura*: Hadrosaurine, *Eolambia*: Iguanodontian) and with respect to adult body size. It might be reasonable, then, to conclude that *Eolambia* could also reach a large body size in the first year. Recall that F6 has two LAGs; Woodward et al. (2015) found that specimens similar in size to F6 to have 1-2 AGMs.

However, Woodward et al. (2015) did not find AGMs in any of their smaller specimens; this includes specimens commensurate in size with F5 and F6. The lack of AGMs in these smaller specimens is consistent with not using retrocalculations in larger specimens for *Maiasauara*. The smaller specimens of *Eolambia* do contain AGMs. If we are to assume that retrocalculations are inappropriate in the larger specimen in this study, then the specimens from the two quarries in this study could not be from the same taxon. Given the weight of the morphologic and taphonomic evidence this seems improbable. Additionally, the evidence or resorption along the endosteal margin

suggests that the use of retrocalculations in larger specimens is reasonable.

Woodward et al. (2015) found that *Maiasaura* reached skeletal maturity around 15 years of age. Similar studies, which use retrocalculations, have found other large-bodied ornithopods reach skeletal maturity at 20-24 years of age (Hübner, 2012; Myhrvold, 2013). The large *Eolambia* femur from EC2 Quarry (which was unavailable for sectioning) is 374 mm in circumference and 809 mm in length. Woodward et al. found that femora of *Maiasaura* of commensurate size are between 4 and 15 years of age. F6 is 225 mm in circumference, but is incomplete and its length cannot accurately be determined. It is possible that this specimen would reach the size of the large femur from EO2 Quarry at around 15-24 years of age.

If we suppose that F6 is *Eolambia* and would likely reach a similar size to *Maiasaura*, it would have a very different pattern of growth than *Maiasaura*. *Eolambia* shows AGMs at a much smaller body size than *Maiasaura*, which indicates slower growth in its early years and much more accelerated growth as it approached skeletal maturity. This is counter to the growth curves of most previously described ornithopod taxa – which grow rapidly until point of inflection of the curve, then decelerate until skeletal maturity is reached. Logistic, Gompertz and von Bertalanffy (based on the Richards model, Tjørve & Tjørve, 2010) curves are commonly used to model growth of extant and extinct organisms (Fitzhugh, 1976; Lee et al., 2013; Rao, 1958; Tsoularis & Wallace, 2002). When growth follows a logistic curve, the inflection point occurs at 50% of asymptotic size; when growth follows a Gompertz curve, the inflection point occurs at 37% of asymptotic size; when growth follows a von Bertalanffy curve, the inflection point occurs at 29% of asymptotic size. If F1-6

and the Cifelli #2 large femora are all attributalble to *Eolambia*, then F6 would be roughly at the inflection point on a Gompertz or von Bertalanffy curve– where growth rate should start to decelerate. Lee et al., 2013 have demonstrated that Gompertz and von Bertalanffy curves are the best fit for all of the dinosaurian taxa they examined. If growth of *Eolambia* follows either a Gompertz or Bertalaniffy curve, and *Eolambia* reaches adult body size in 15 and 24 years, then sexual maturity would be reached at approximately 5 to 8 years of age. This is consistent with Petermann & Gauthier's (2017) finding of a strong correlation between differential growth and attainment of sexual maturity. This also fits with retrocalculations applied above to F6; the widely spaced LAGs in F6 could then be the result of differential growth after reaching sexual maturity.

Conclusion

The histologic analysis of the growth of specimens from the EC2 Quarry suggests that this is an assemblage of juveniles and subadults. The histologic analysis also suggests that *Eolambia* was a relatively slow-growing taxon, comparable to *Dysalotosaurus*. Among modern herbivores, juvenile males often form bachelor herds, as a means of protections again territorial, adult males. The assemblage from the EC2 Quarry is anatomically and histologically consistent with it having been a bachelor herd. Analysis of these specimens also suggests that *Eolambia* was quadrupedal or a facultatively bipedal during its early life; this is similar to the locomotion that has been suggested for the taxon as an adult.

By comparing the histology of smaller femora in this study with that of F6, I conclude that retrocalculations of AGMS are appropriate for this sample of this taxon.

Furthermore, I conclude that the wide spacing of LAGs in F6 represent differential growth following the attainment of sexual maturity.

The histologic analysis of growth, including the use of retrocalations of AGMs, suggest that F6 could be the same taxon as F0-F5: *Eolambia.* The geographic proximity of the sites and the fact that they have been recovered from the same stratigraphic horizon, supports the conclusion. The gross morphology of the specimen similarly supports this conclusion. On the basis of this evidence, I conclude that F6 is most parsimoniously assigned to *Eolambia*.

Figures

*FIGURE 3.2.1 Circumference vs Length of Various Elements. The graphs below show the least circumference and total length for the **(A)** Humeri, **(B)** Femora, and **(C)** Tibiae. Data used was from complete specimens from the EC2 Quarry, see Table 3.4.2.*

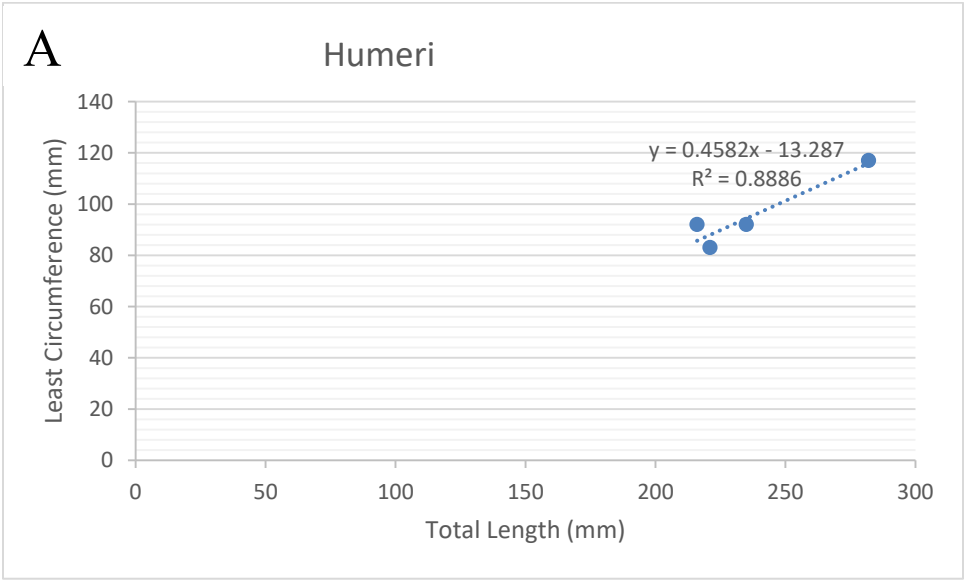

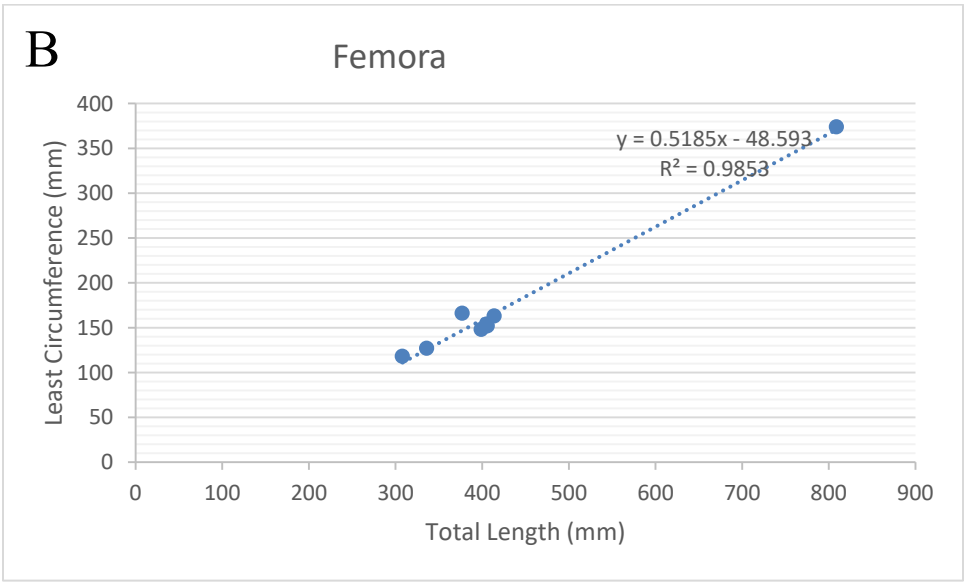

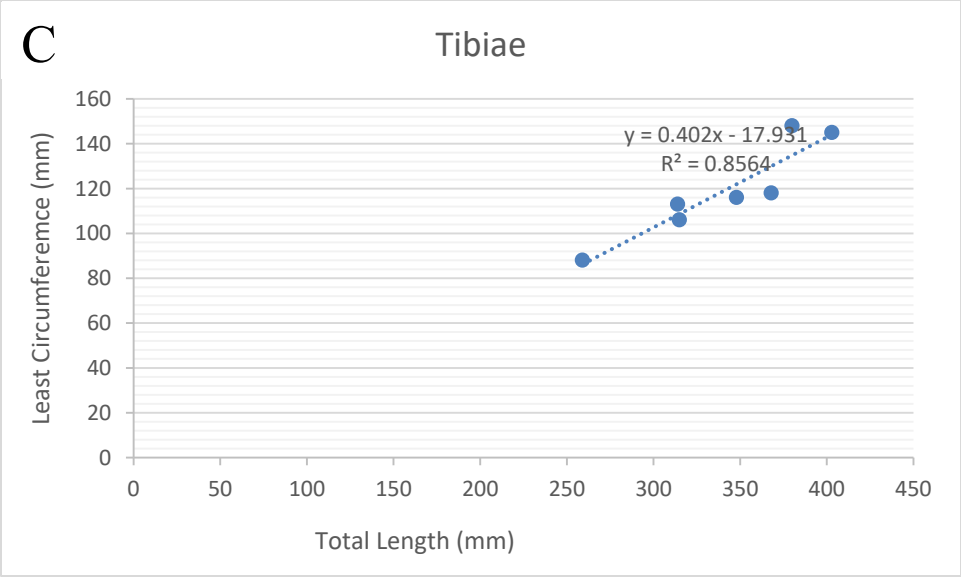
C
Tibiae
Least Circumferemce (mm)
Total Length (mm)
y = 0.402x - 17.931
R² = 0.8564
0
20
40
60
80
100
120
140
160
0
50
100
150
200
250
300
350
400
450

FIGURE 3.2.2 CEUM 35641, H1

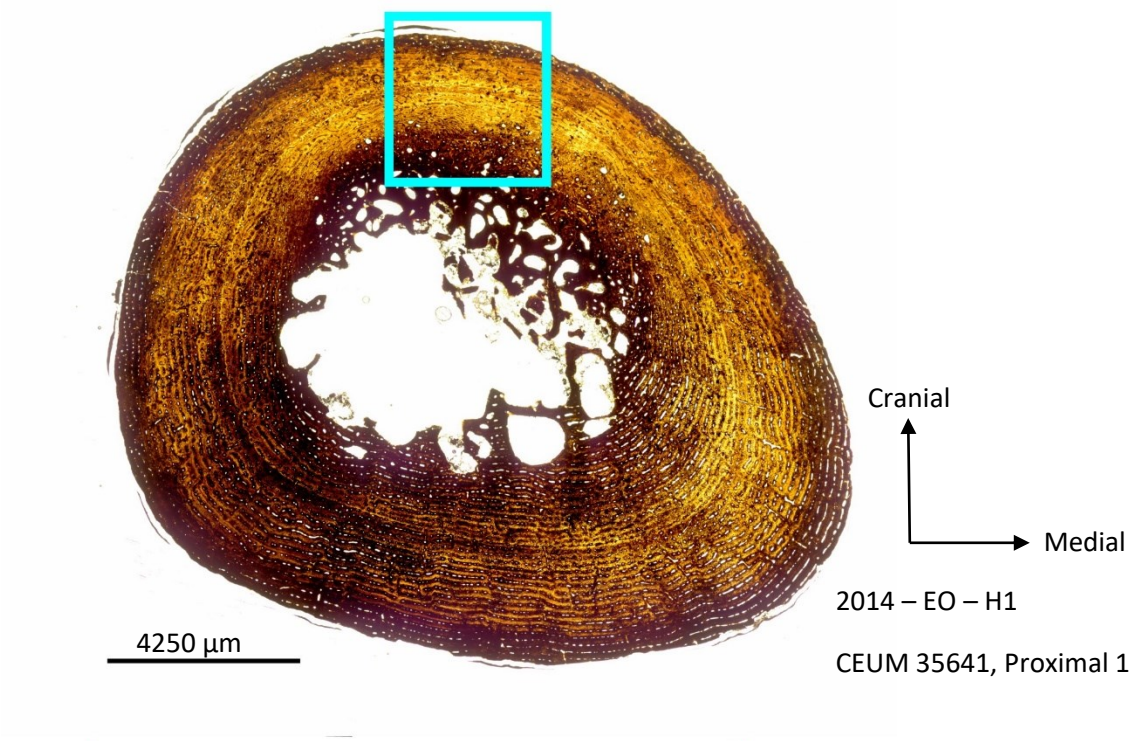

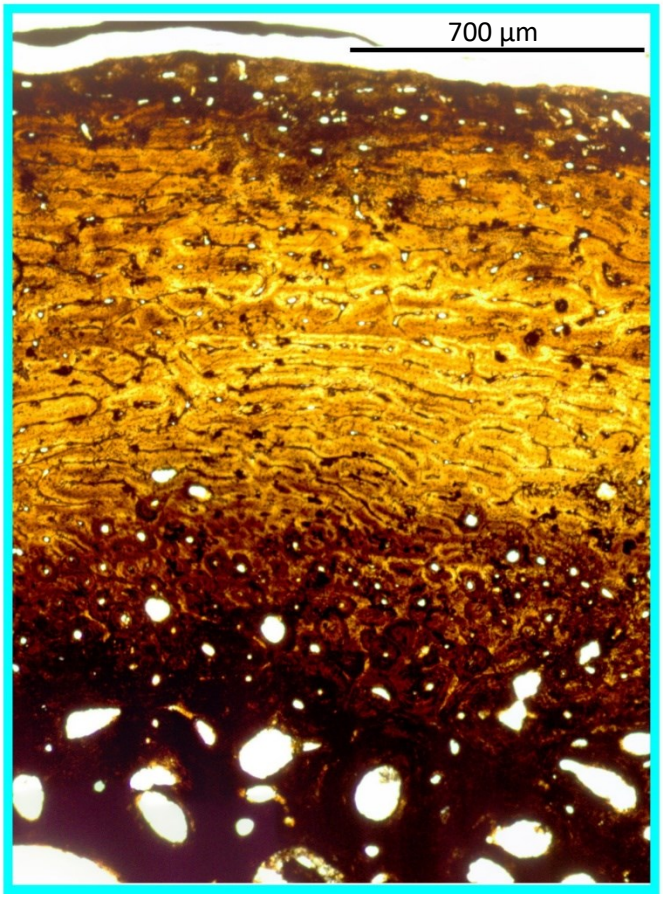

Above: Image of cross section. Blue box shows location of close up image.

Left: Close-up image showing highly disorganized cortex with no clear distinction between inner and outer corter.

FIGURE 3.2.3 CEUM 35369, H2

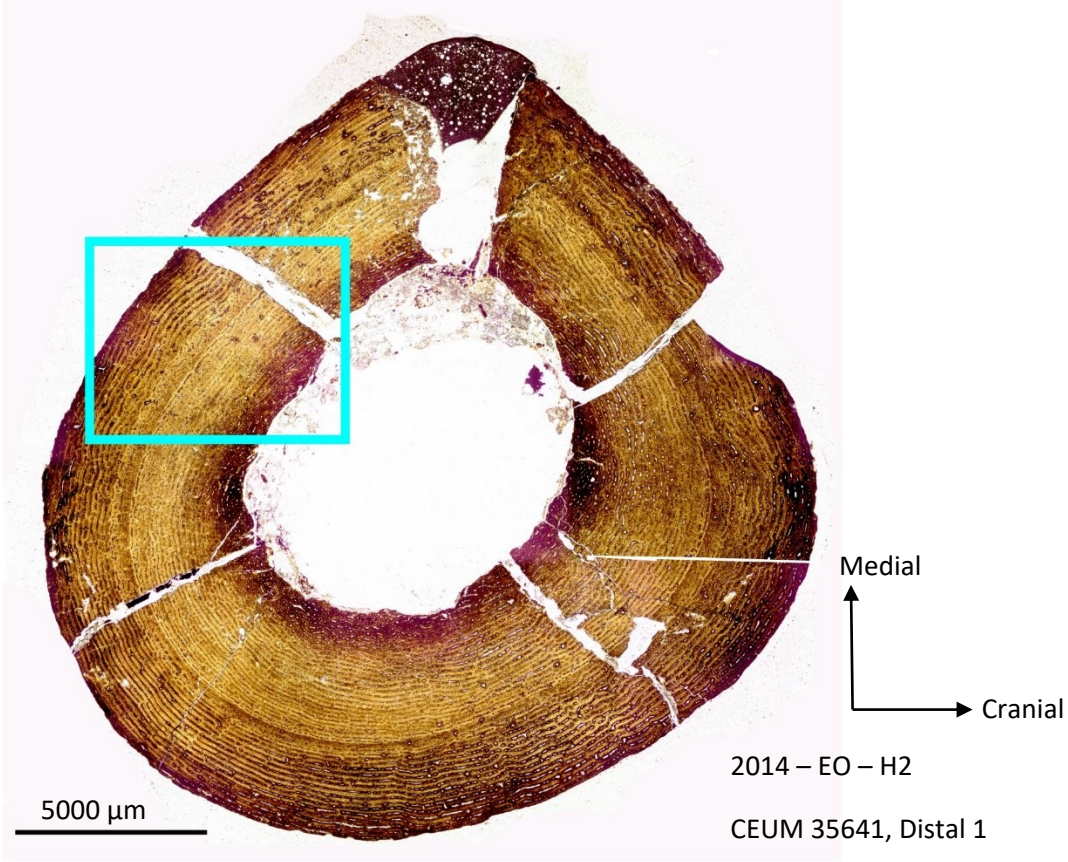

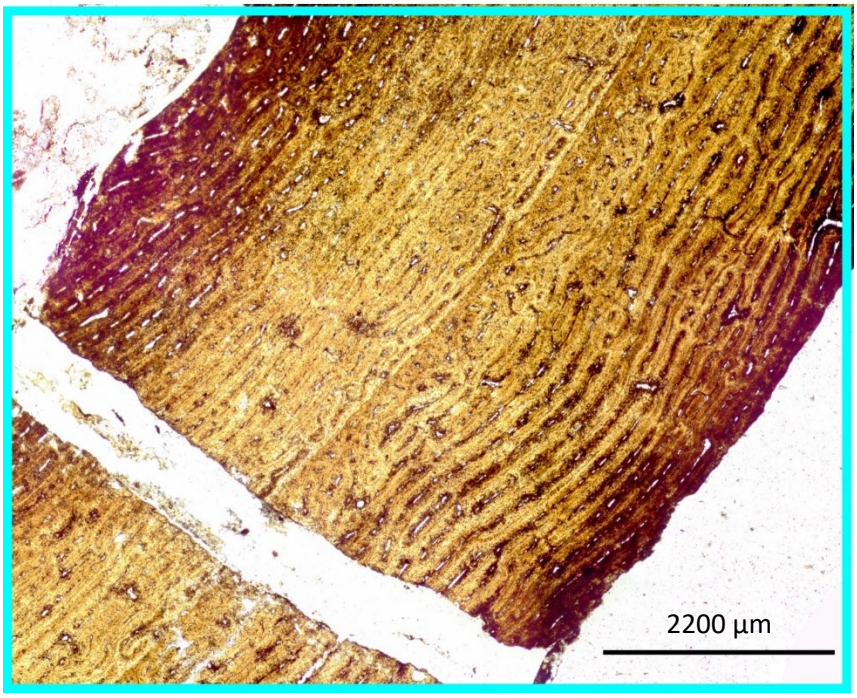

Above: Image of cross section. Blue box shows location of close up image.

Left: Close-up image progressively more organization from the medullary cavity to the outer corter.

FIGURE 3.2.4 CEUM 35621, H3

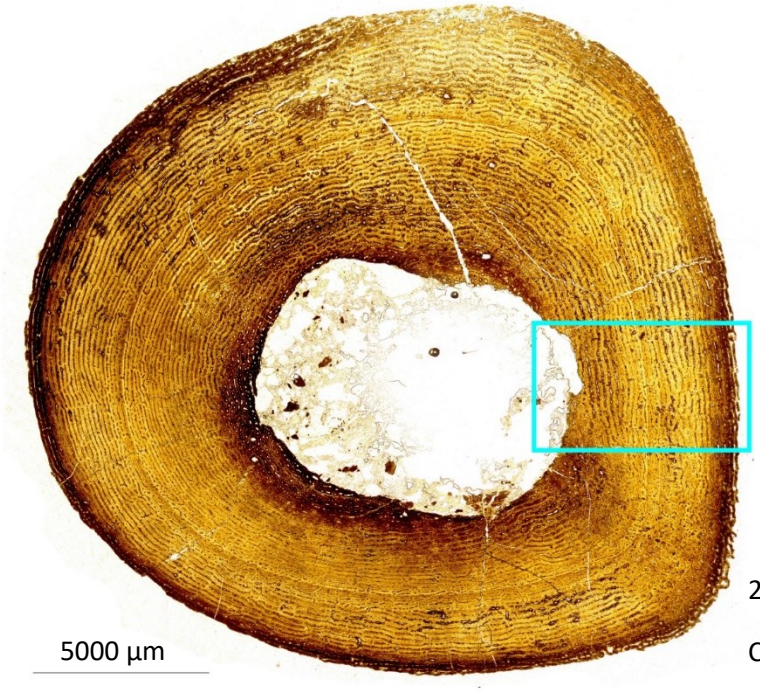

2014 – EO – H3

CEUM 35621, Distal 1

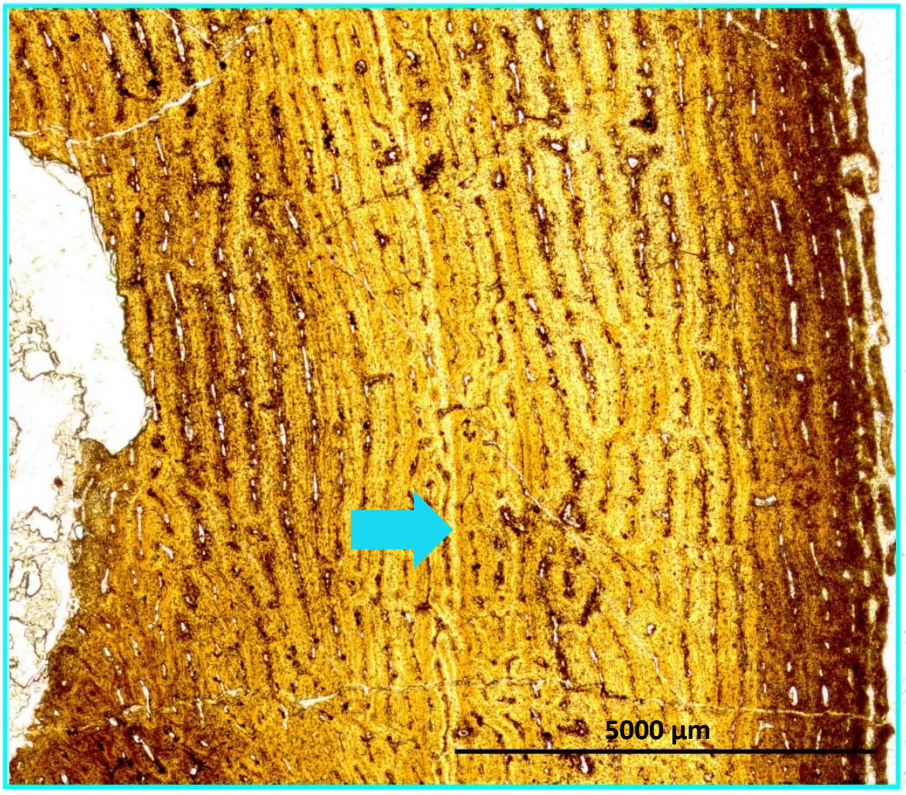

Above: Image of cross section. Blue box shows location of close up image.

Left: Close-up image; arrow shows location of LAG.

FIGURE 3.2.5 CEUM 35719, H4

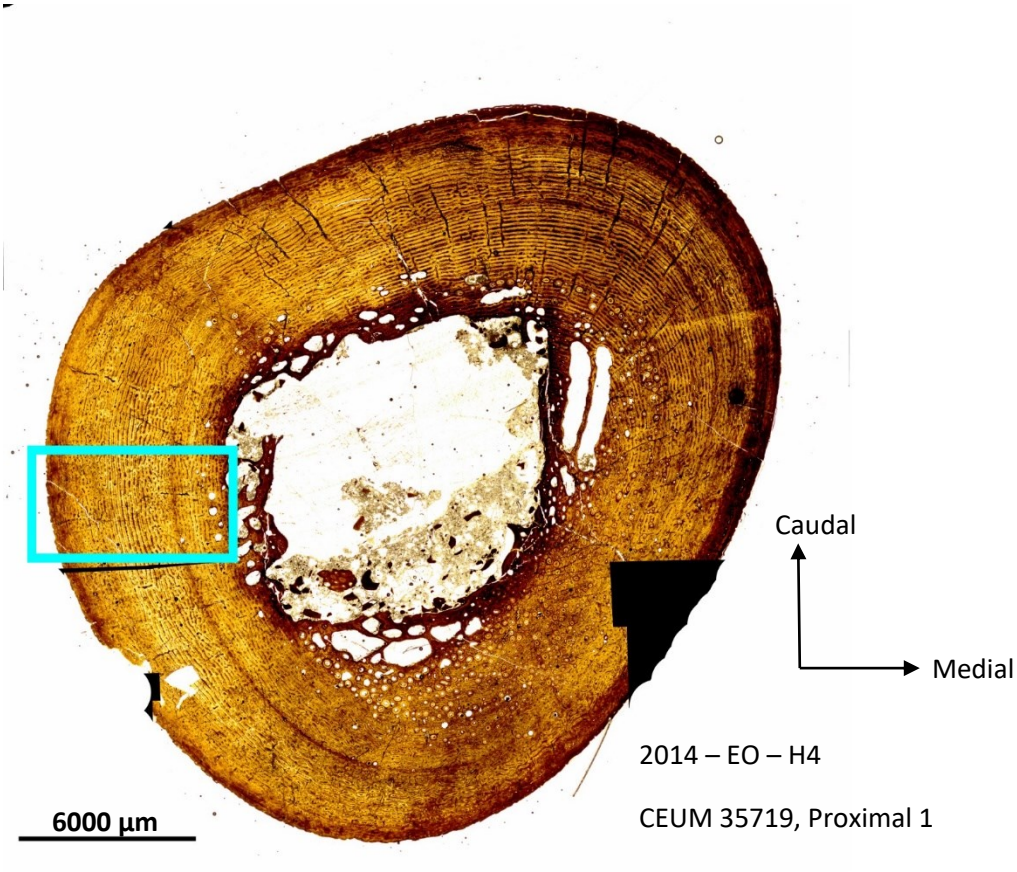

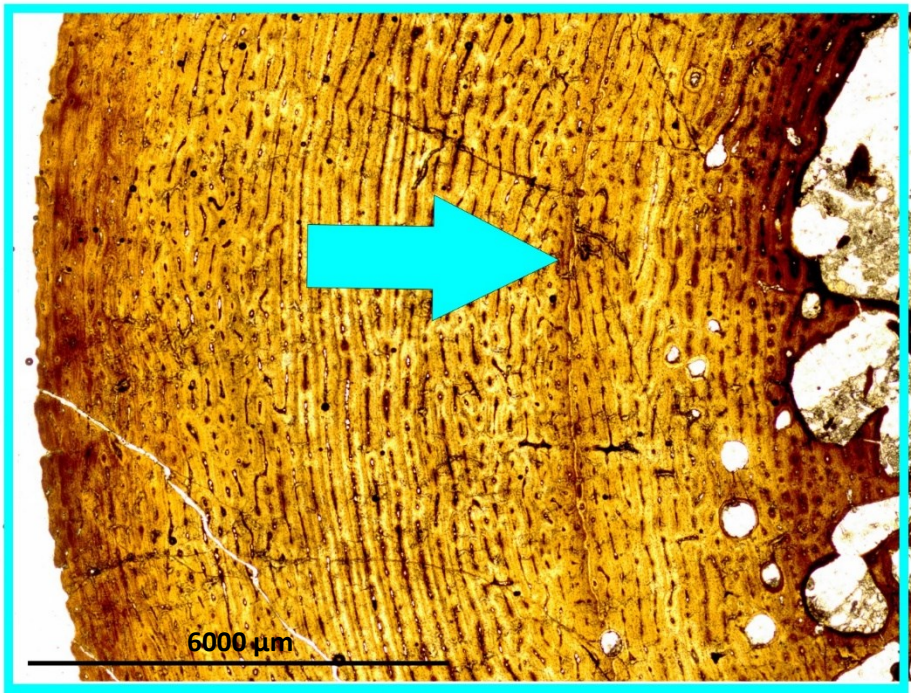

Above: Image of cross section. Blue box shows location of close up image.

Left: Close-up image; arrow shows location of LAG.

FIGURE 3.2.6 CEUM 35743, H5

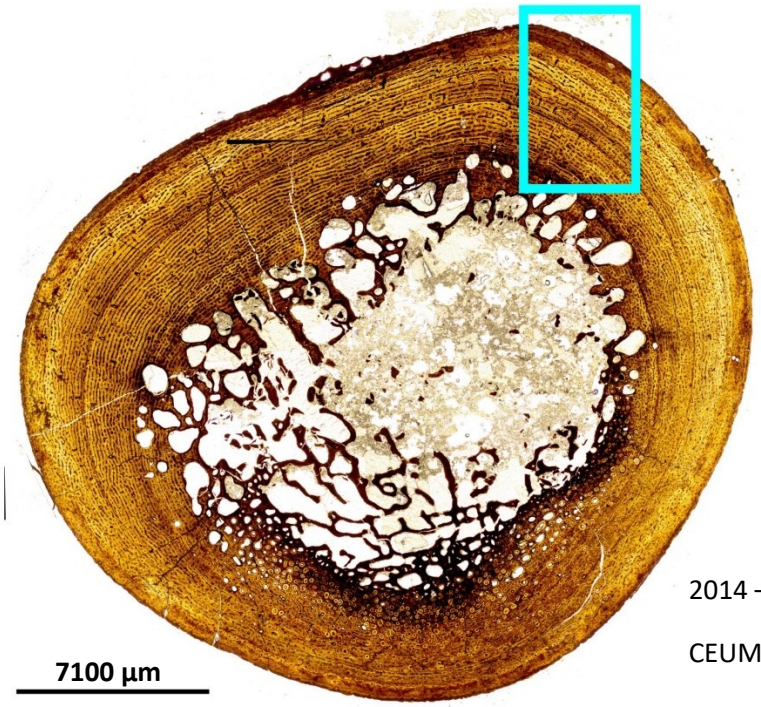

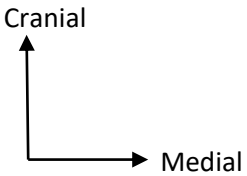

2014 – EO – H5

CEUM 35719, Distal 1

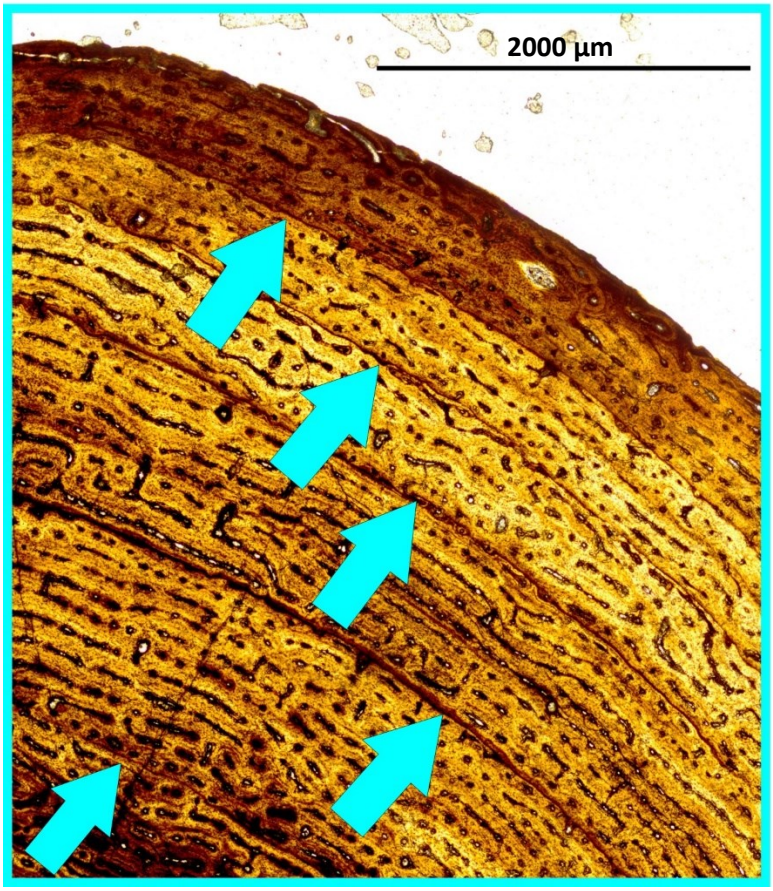

Above: Image of cross section. Blue box shows location of close up image.

Left: Close-up image; arrows show location of 5 LAGs.

FIGURE 3.2.7 CEUM 35357, H7

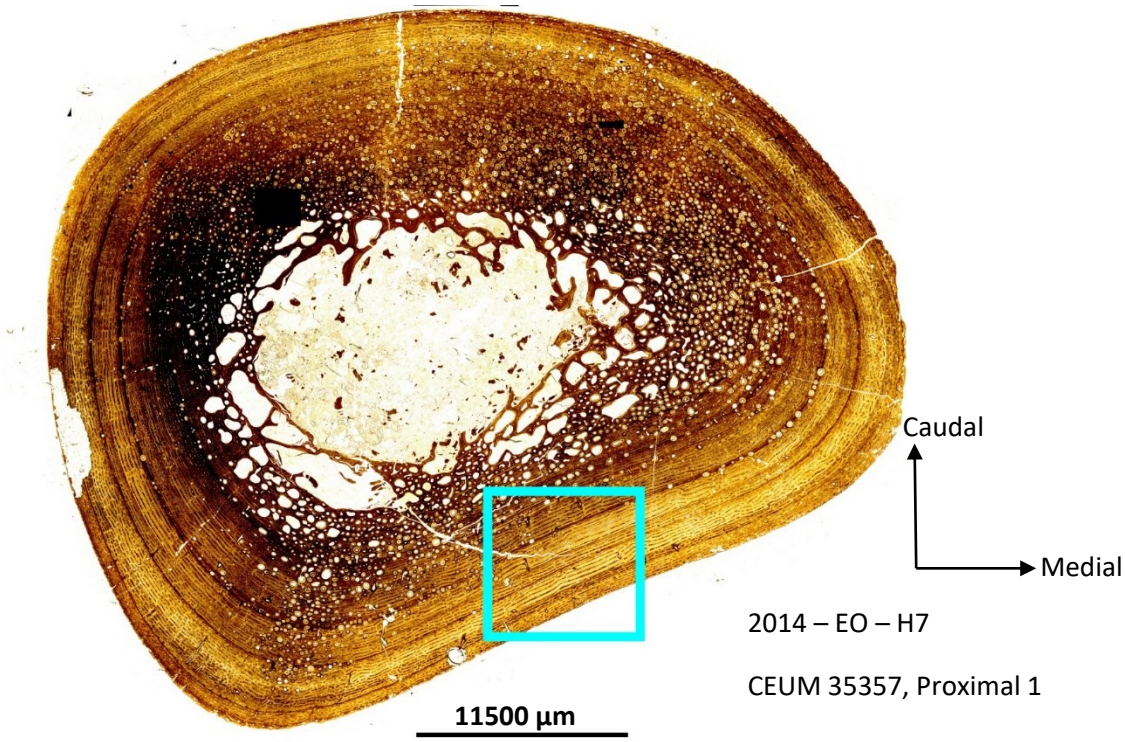

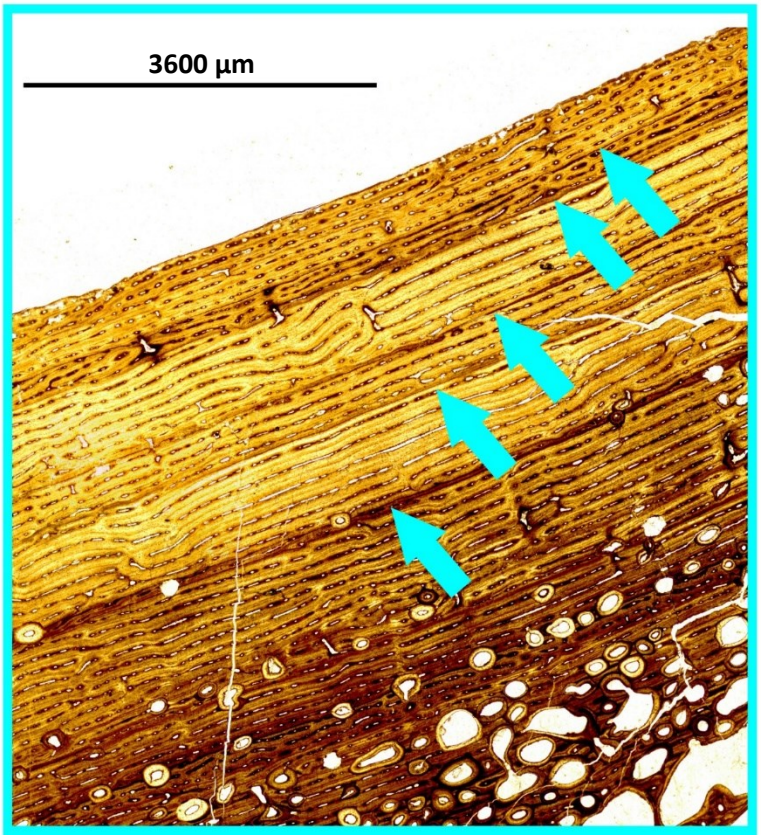

Above: Image of cross section. Blue box shows location of close up image.

Left: Close-up image; arrows show location of 5 LAGs.

FIGURE 3.2.8 OMNH 32250, H8

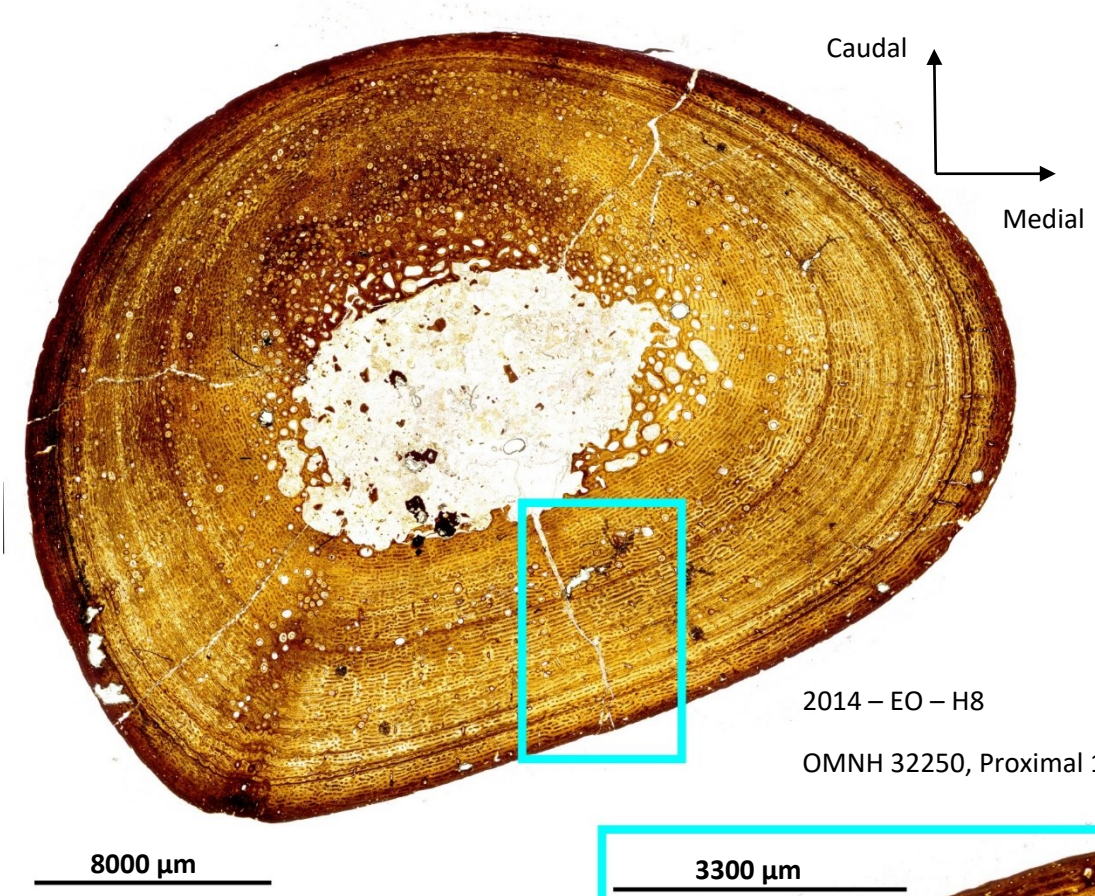

Above: Image of cross section. Blue box shows location of close up image.

Right: Close-up image; arrows show location of 5 LAGs.

FIGURE 3.2.9 FMNH 3848, F0

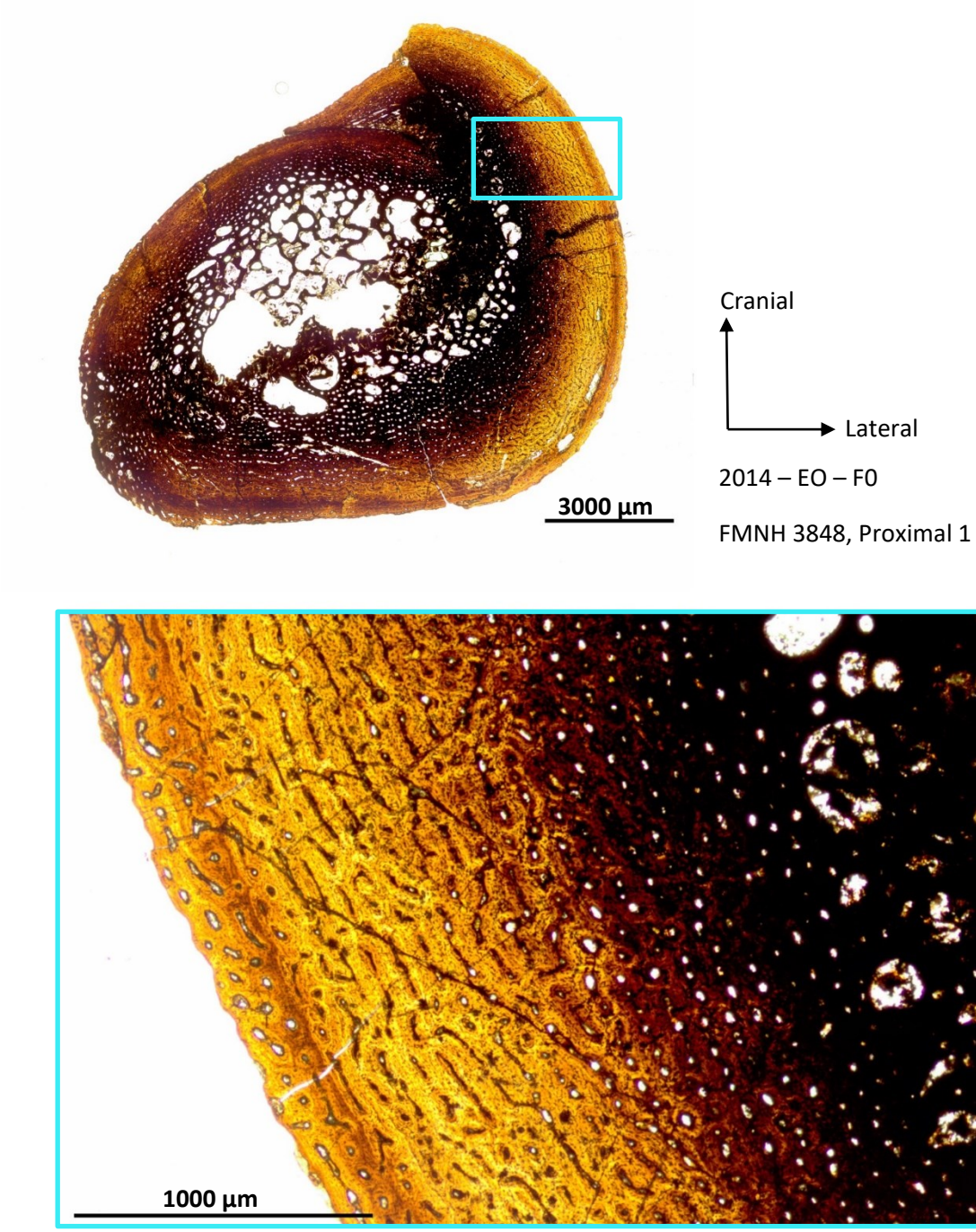

TOP: Image of cross section. Blue box shows location of close up image.

BOTTOM: Close-up image showing no clear distinction between inner and outer cortex.

FIGURE 3.2.10 CEUM 13317, F1

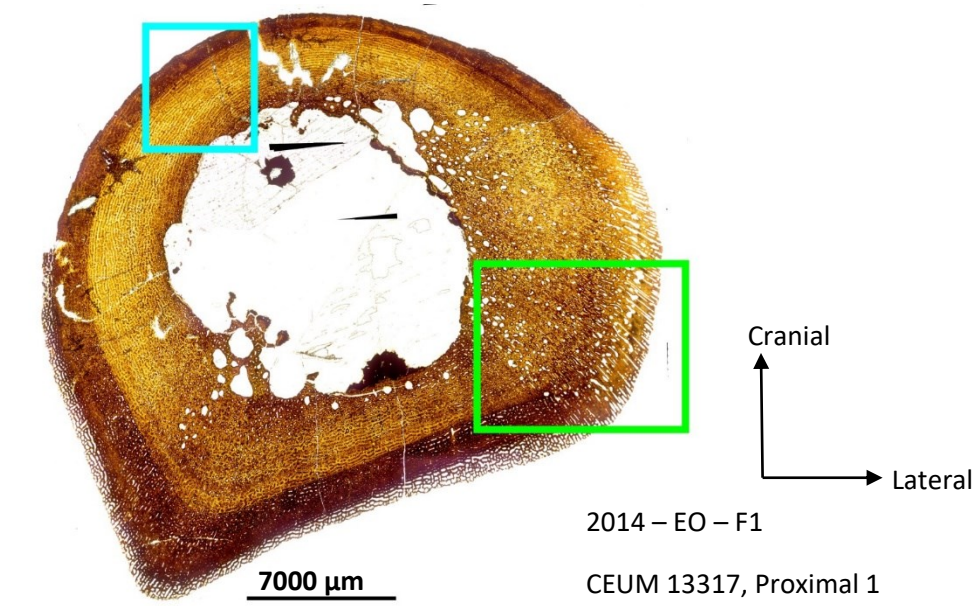

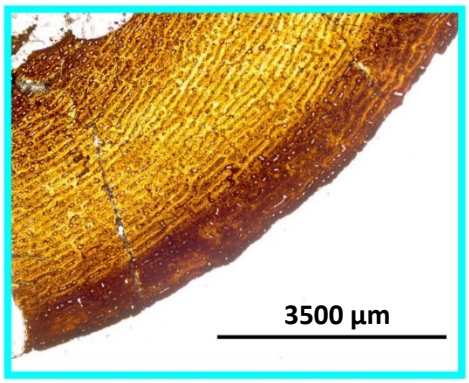

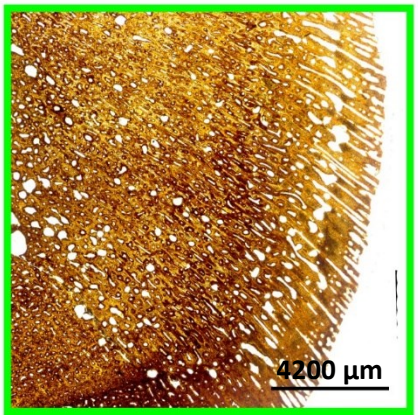

FIGURE 3.2.11 CEUM 34399, F2

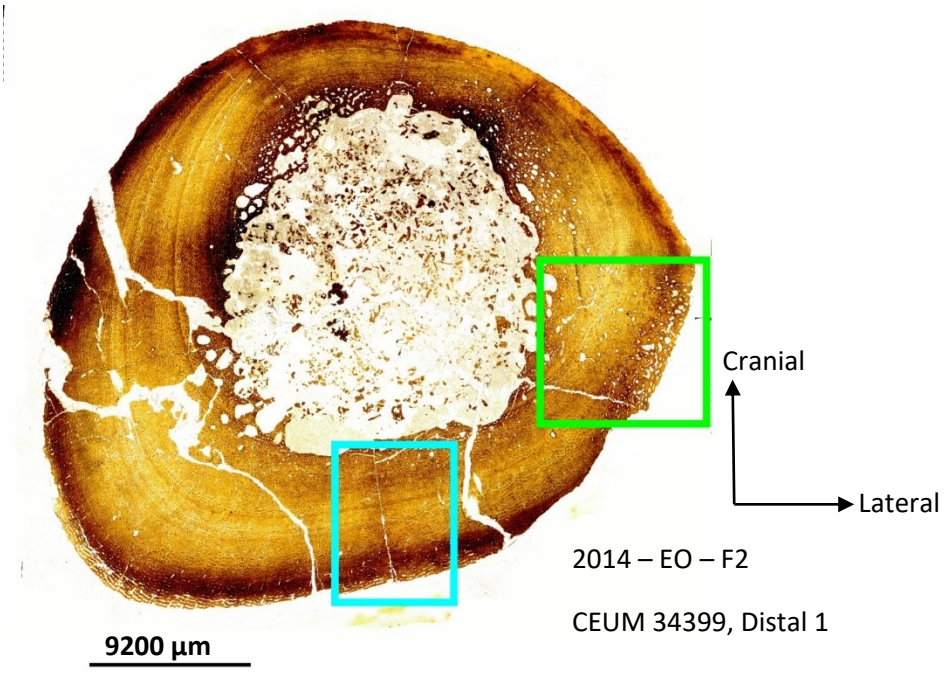

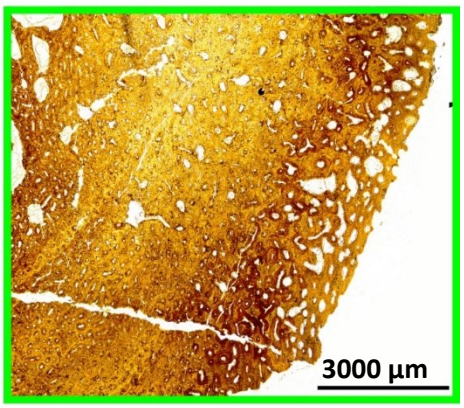

TOP: Image of cross section. Blue and green boxes show locations of close up image.

LEFT: Close-up image showing increasing organization towards the periosteal margin.

Above: Close-up image showing area of disorganization along the posterolateral margin.

FIGURE 3.2.12 CEUM 35444, F3

LEFT: Image of cross section. Blue box shows location of close up image.

BELOW: Close-up image; arrows show locations of 5 LAGs.

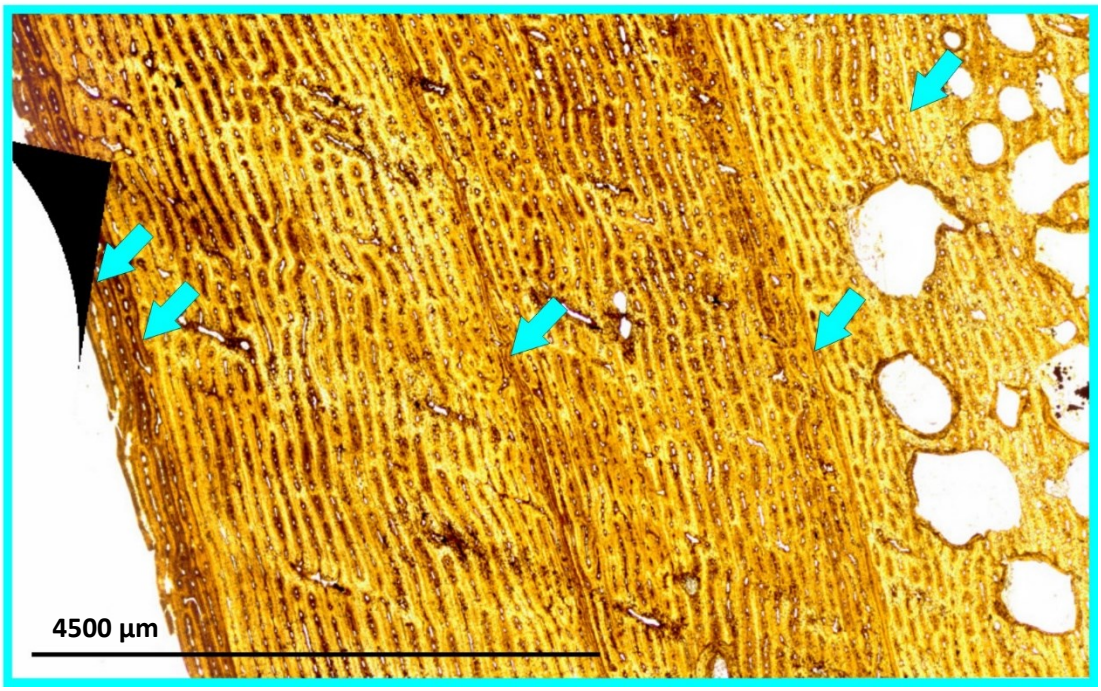

FIGURE 3.2.13 CEUM 14503, F4

2014 – EO – F4

CEUM 14503, Proximal 1

LEFT: Image of cross section. Blue and green boxes shows location of close up image.

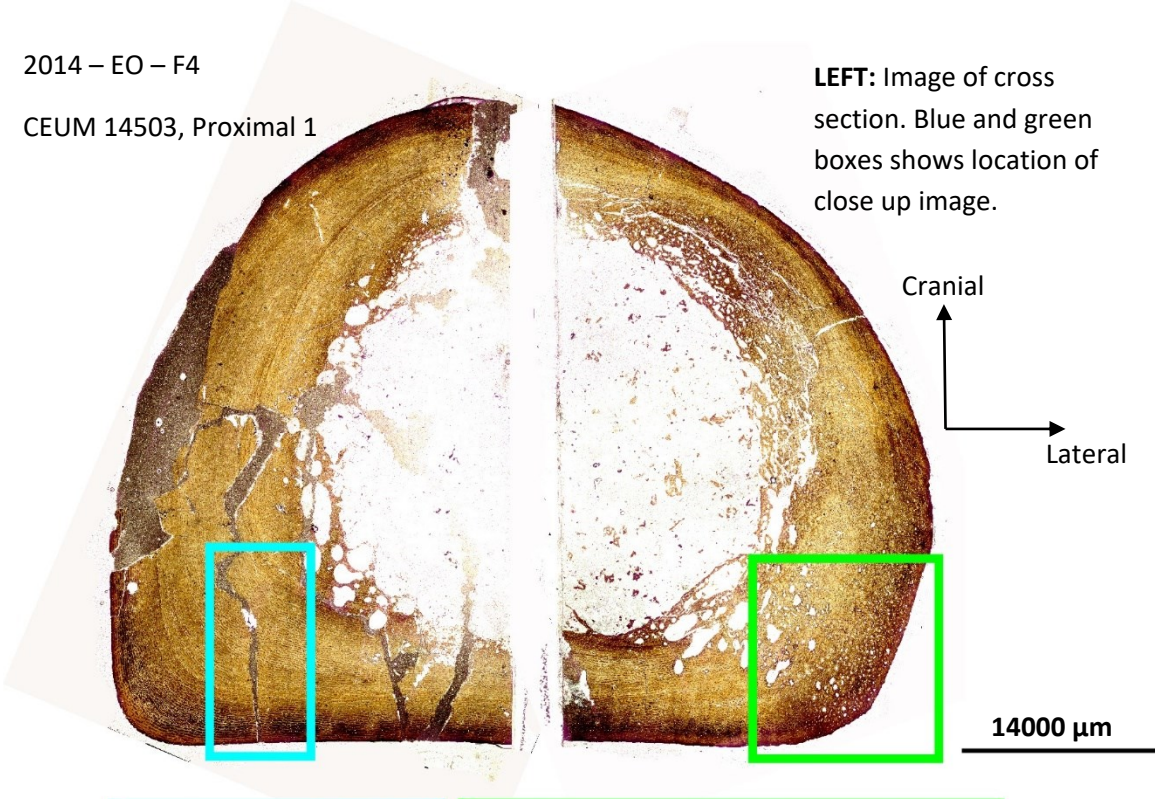

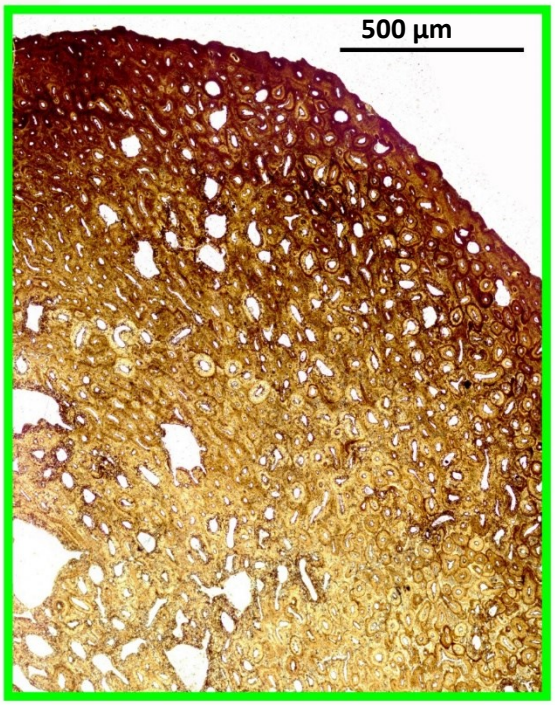

ABOVE: Close-up image showing area of disorganization along the posterolateral margin.

LEFT: Close-up image; arrows show locations of 2 LAGs.

FIGURE 3.2.14 OMNH 62157, F5

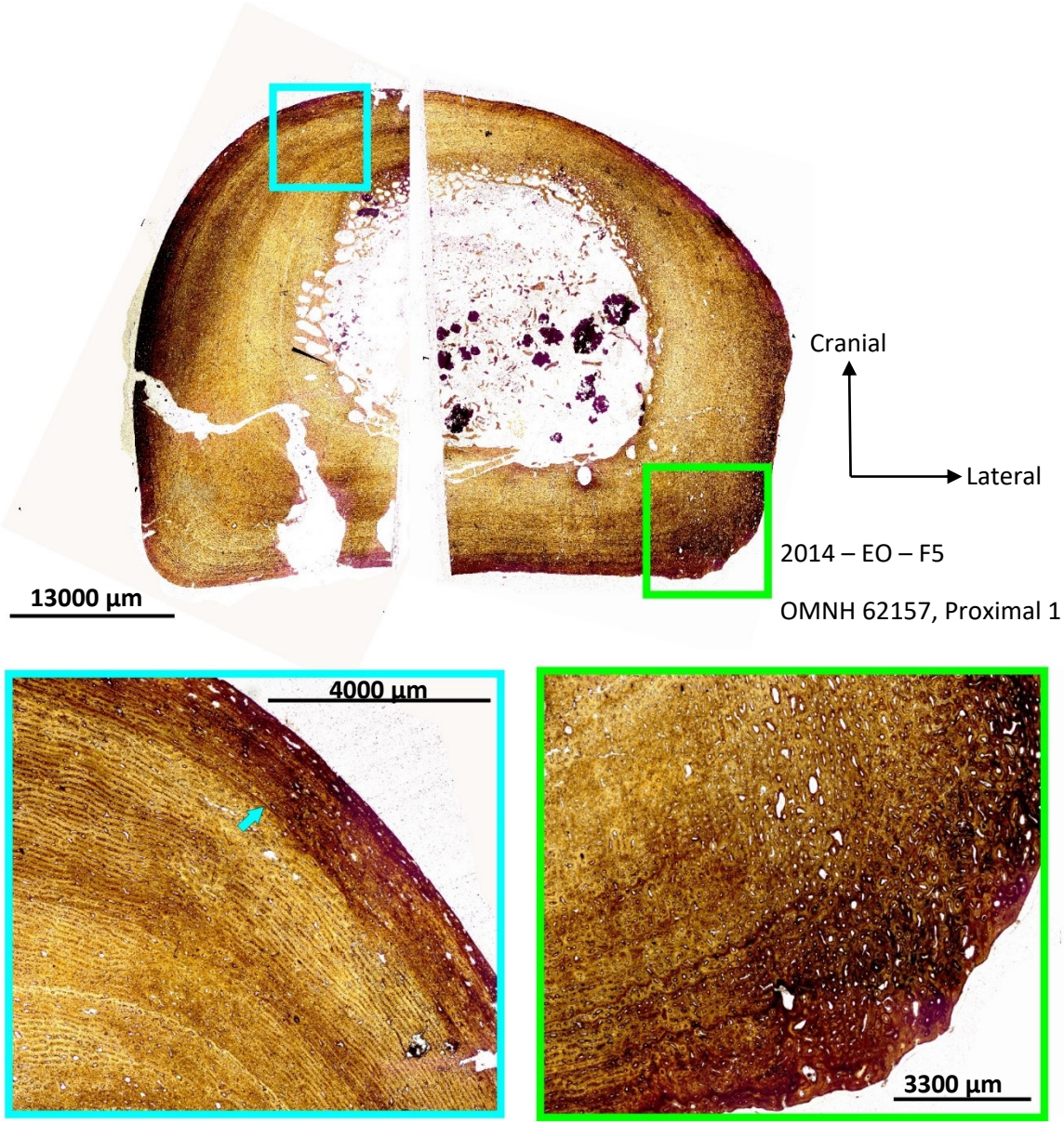

TOP: Image of cross section. Blue and green boxes show locations of close up image.

BOTTOM LEFT: Close-up image; arrow shows location of LAG.

BOTTOM RIGHT: Close-up image showing area of disorganization along the posterolateral margin.

FIGURE 3.2.15 CEUM 34276, T0

ABOVE: Image of cross section. Blue box shows location of close up image.

LEFT: Close-up image showing numerous primary osteons and longitudinal mineral staining (cross-polarized light confirms these are not LAGs).

FIGURE 3.2.16, CEUM 13306, T1

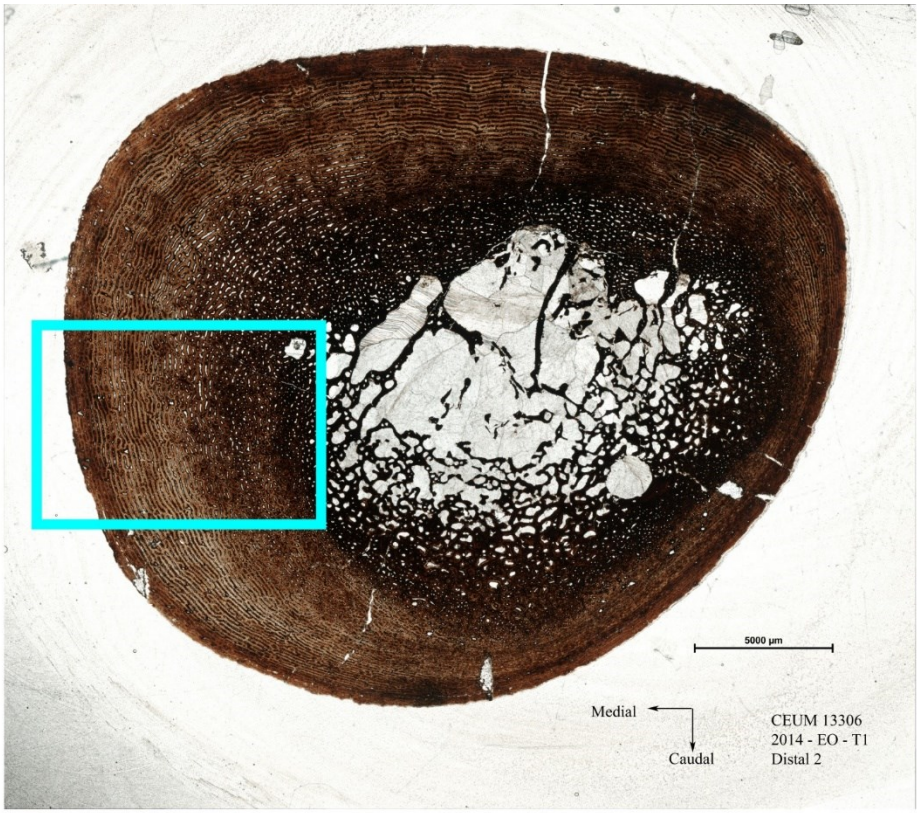

TOP: Image of cross section. Blue box shows location of close up image.

BOTTOM: Close-up image showing progressively more organization from medullary cavity to periosteal margin.

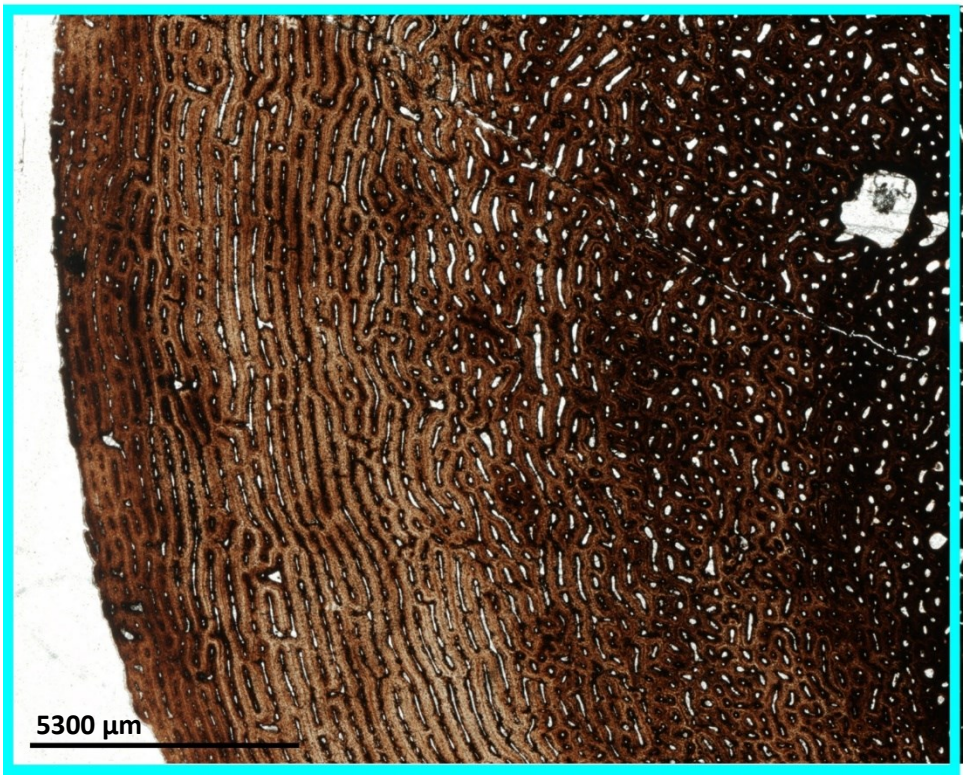

FIGURE 3.2.17 CEUM 35386, T2

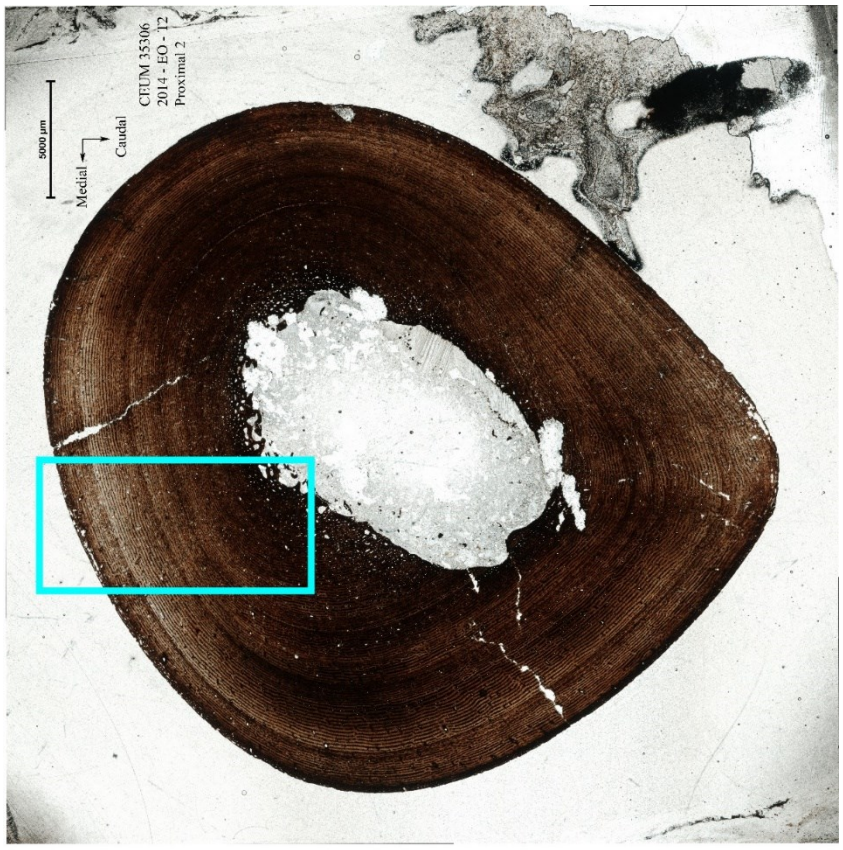

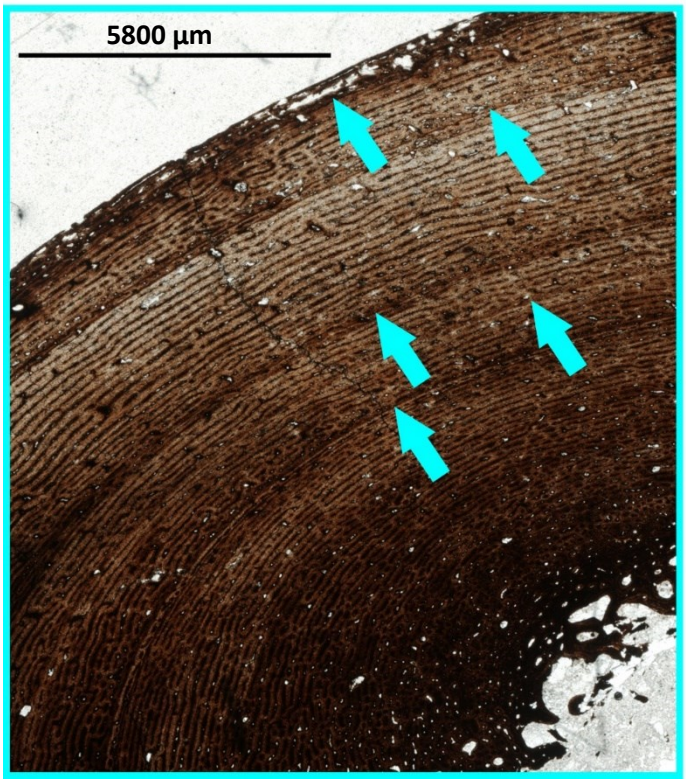

ABOVE: Image of cross section. Blue box shows location of close up image.

LEFT: Close-up image, arrows show locations of 5 LAGs.

FIGURE 3.2.18 CEUM 52874, T3

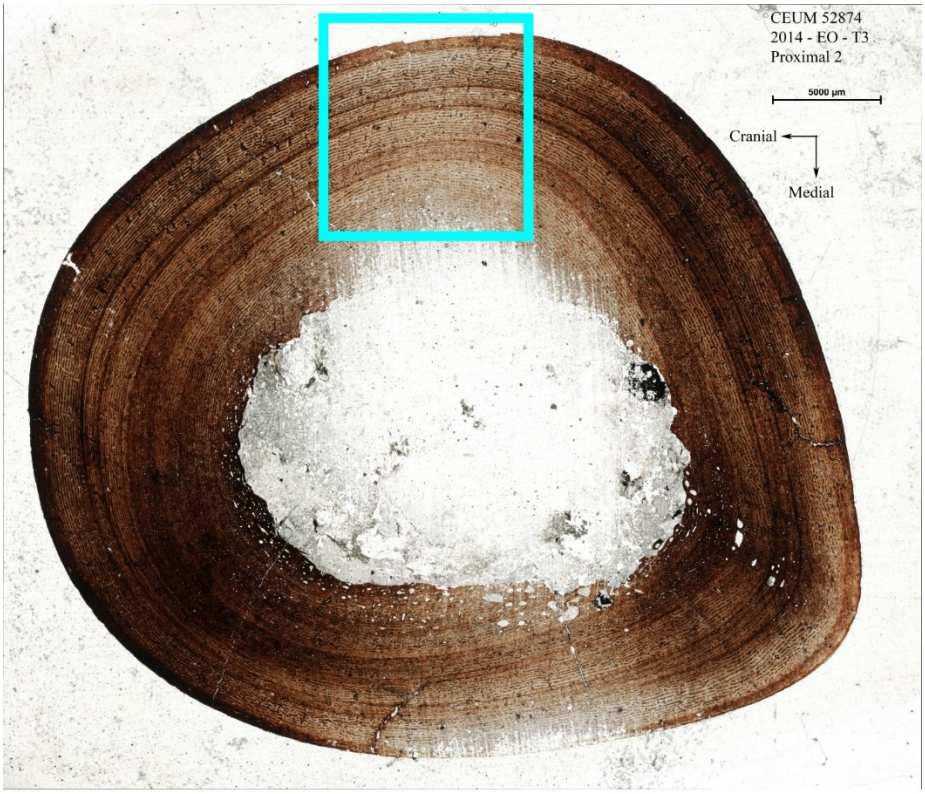

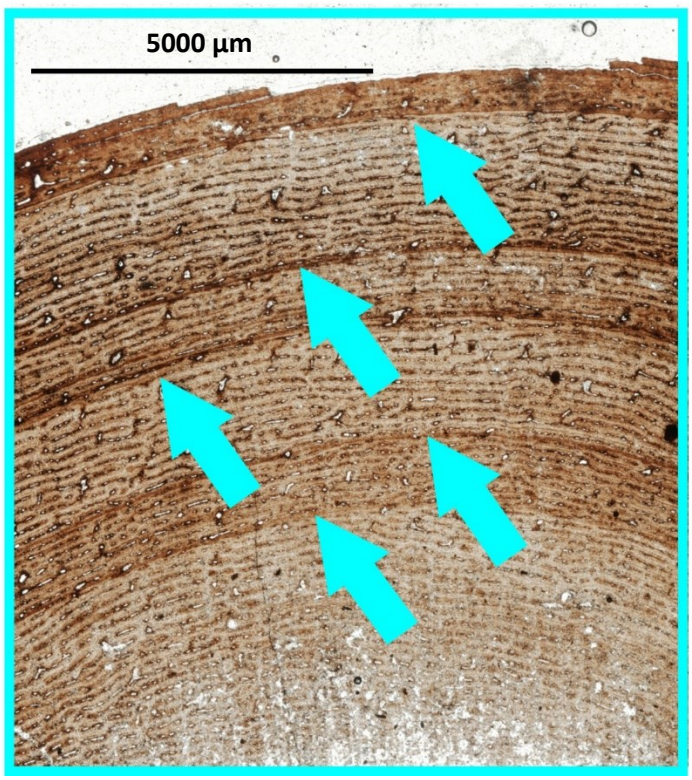

ABOVE: Image of cross section. Blue box shows location of close up image.

LEFT: Close-up image, arrows show locations of 5 LAGs.

FIGURE 3.2.19 CEUM 35704, T4

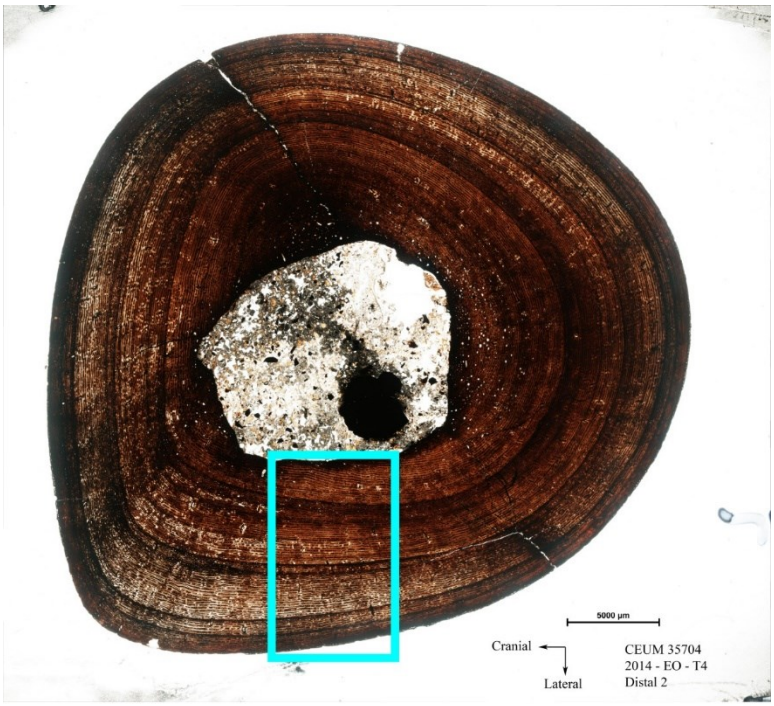

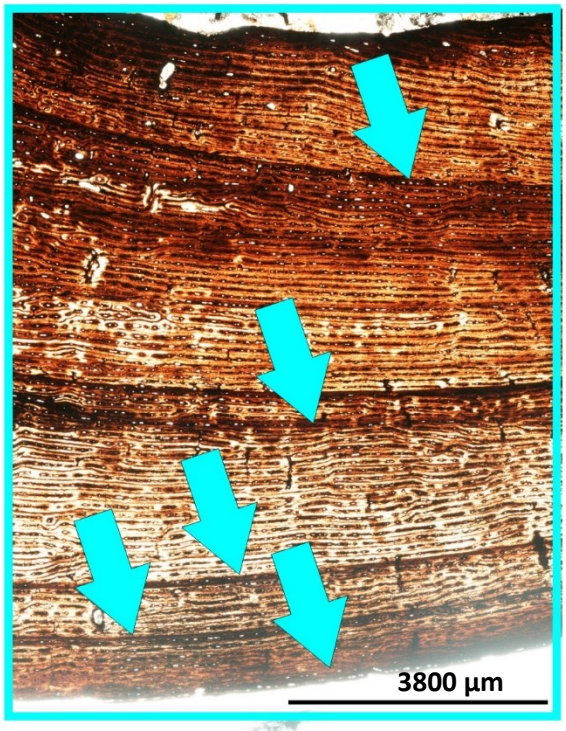

ABOVE: Image of cross section. Blue box shows location of close up image.

LEFT: Close-up image, arrows show locations of 5 LAGs.

FIGURE 3.2.20 CEUM 74590, T5

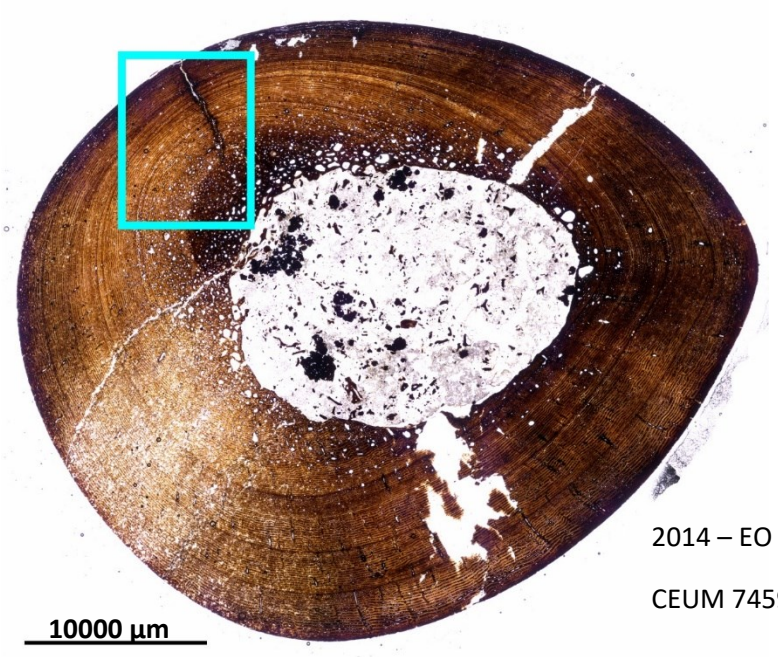

2014 – EO – T5

CEUM 74590, Proximal 1

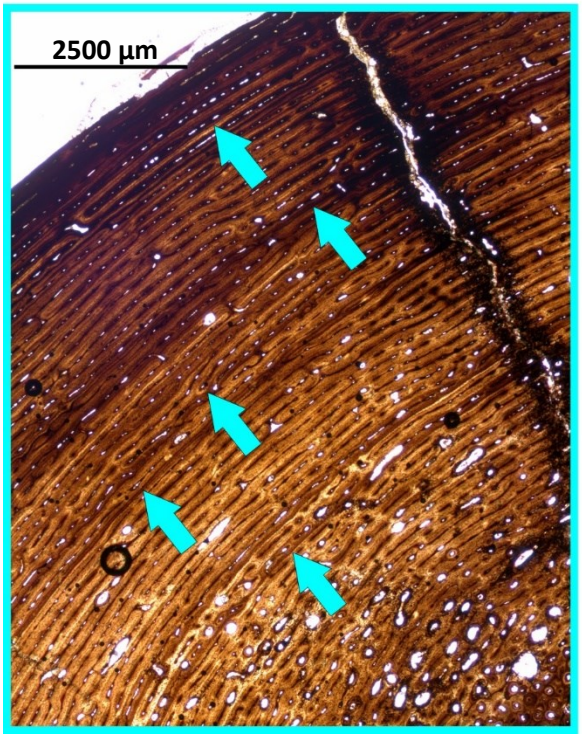

ABOVE: Image of cross section. Blue box shows location of close up image.

LEFT: Close-up image, arrows show locations of 5 LAGs.

FIGURE 3.2.21 CEUM 35471, T6

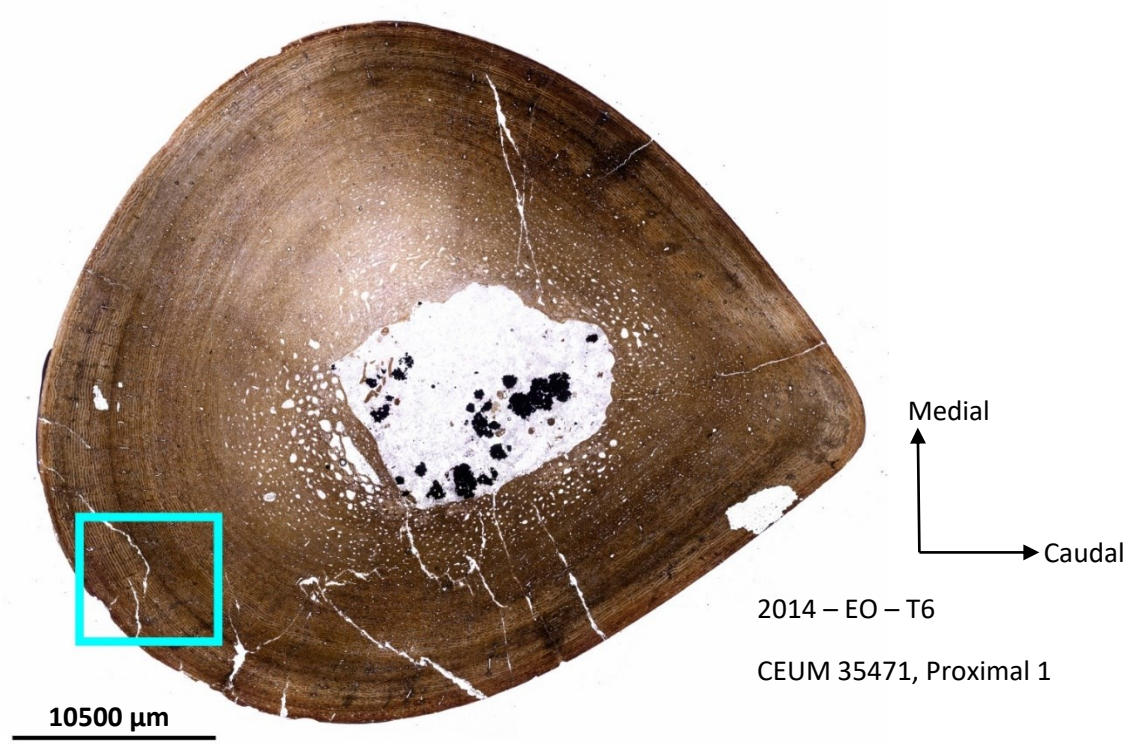

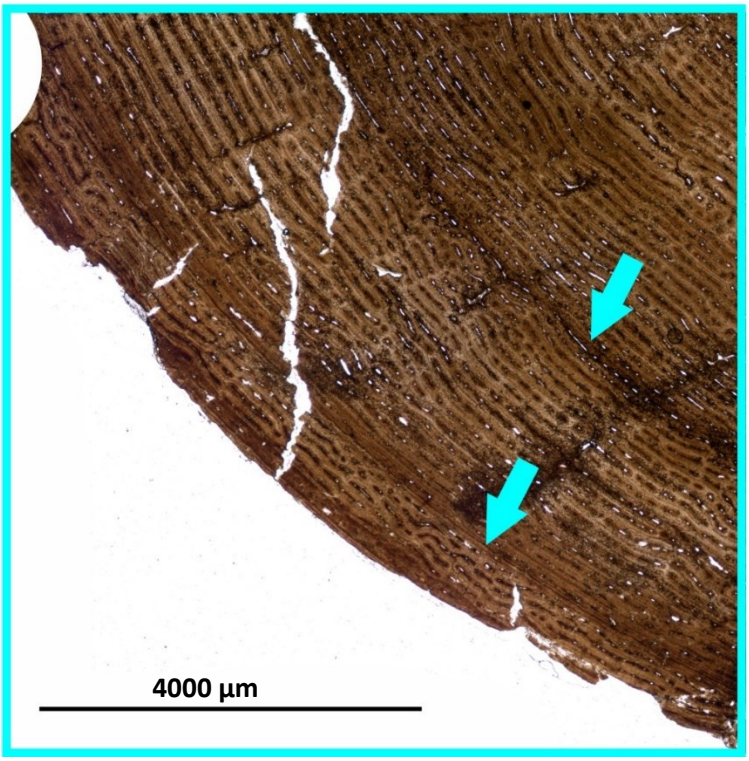

ABOVE: Image of cross section. Blue box shows location of close up image.

LEFT: Close-up image, arrows show locations of 2 LAGs; it is possible that extensive remineralization has obscured other AGMs.

FIGURE 3.2.22 CEUM 14582, T7

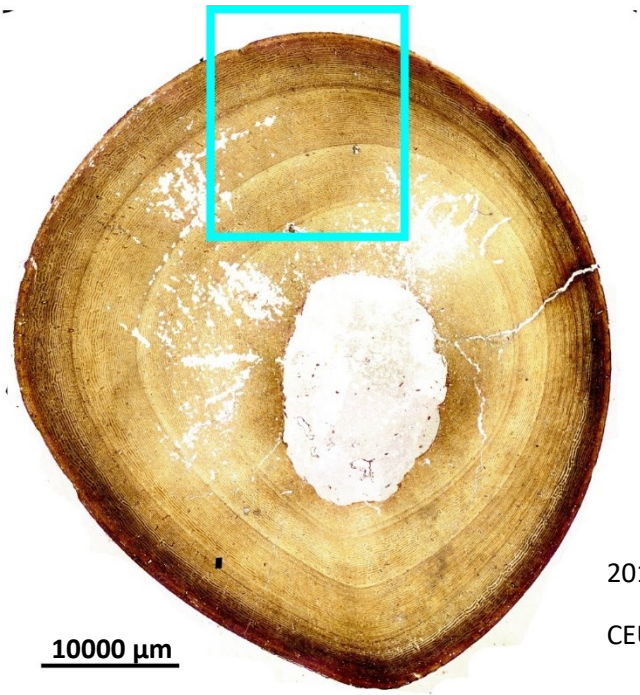

Medial

Caudal

2014 – EO – T7

CEUM 14582, Distal 1

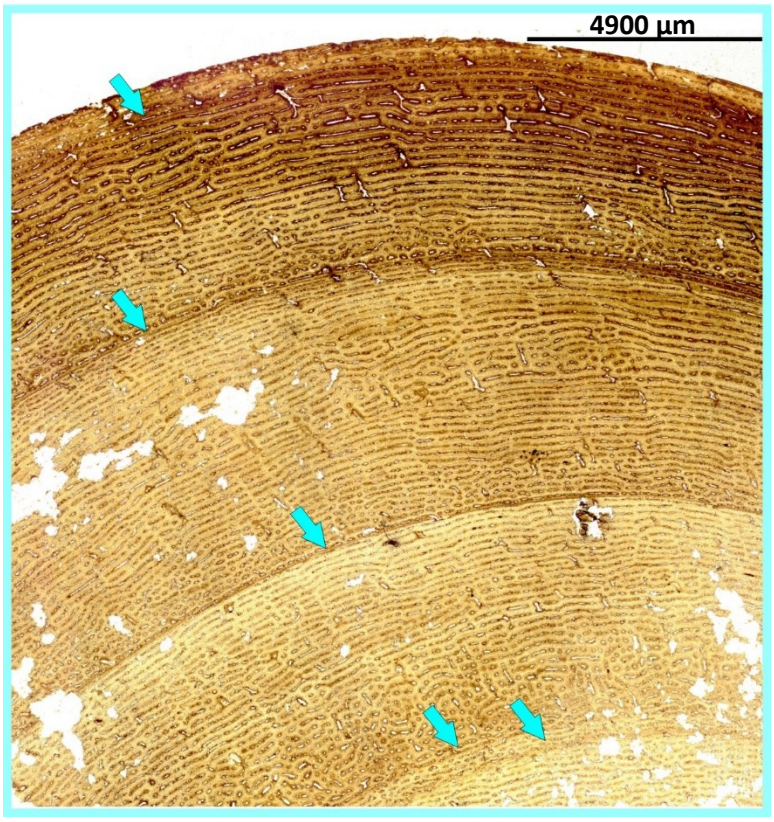

ABOVE: Image of cross section. Blue box shows location of close up image.

LEFT: Close-up image, arrows show locations of 5 LAGs.

FIGURE 3.2.23 CEUM 62213, T8

ABOVE: Image of cross section. Blue box shows location of close up image.

LEFT: Close-up image, arrows show locations of 5 LAGs.

FIGURE 3.2.24 FMNH UT130825-3, F6

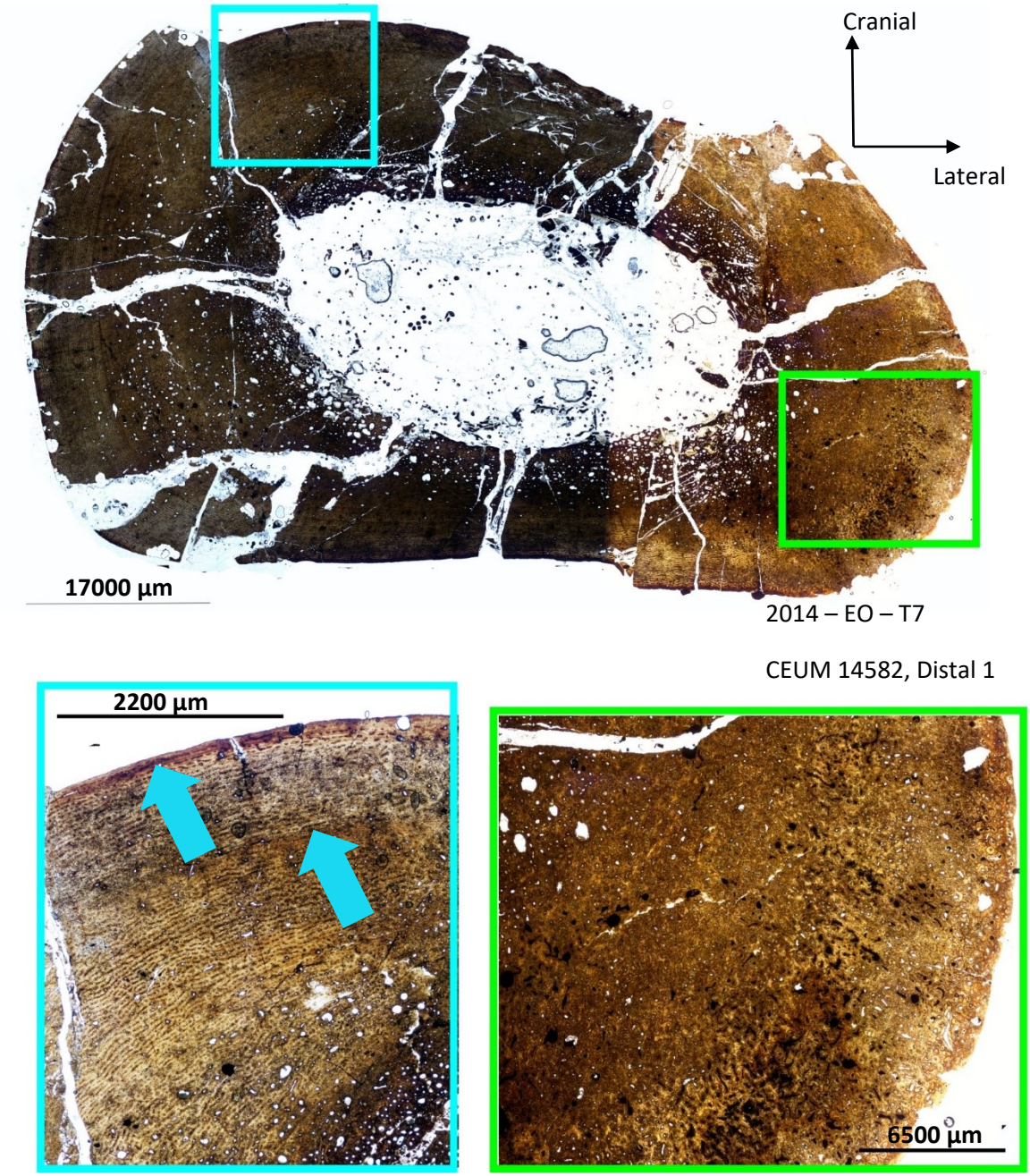

TOP: Image of cross section. Blue and green boxes show locations of close up image.

BOTTOM LEFT: Close-up image, arrows show locations of 2 LAGs.

BOTTOM RIGHT: Close-up image showing area of disorganization along the posteriolateral margin.

FIGURE 3.2.25 Appositional Growth Rate. The graphs below show the appositional growth rate for each element at the time the AGM was deposited. That is, the growth since the previous LAG is plotted for each LAG. Every AGM was either a LAG or an annulus associated with a LAG, so LAGs were plotted. Each specimen has been given a different color. Specimens with no AGMs were not plotted.

A

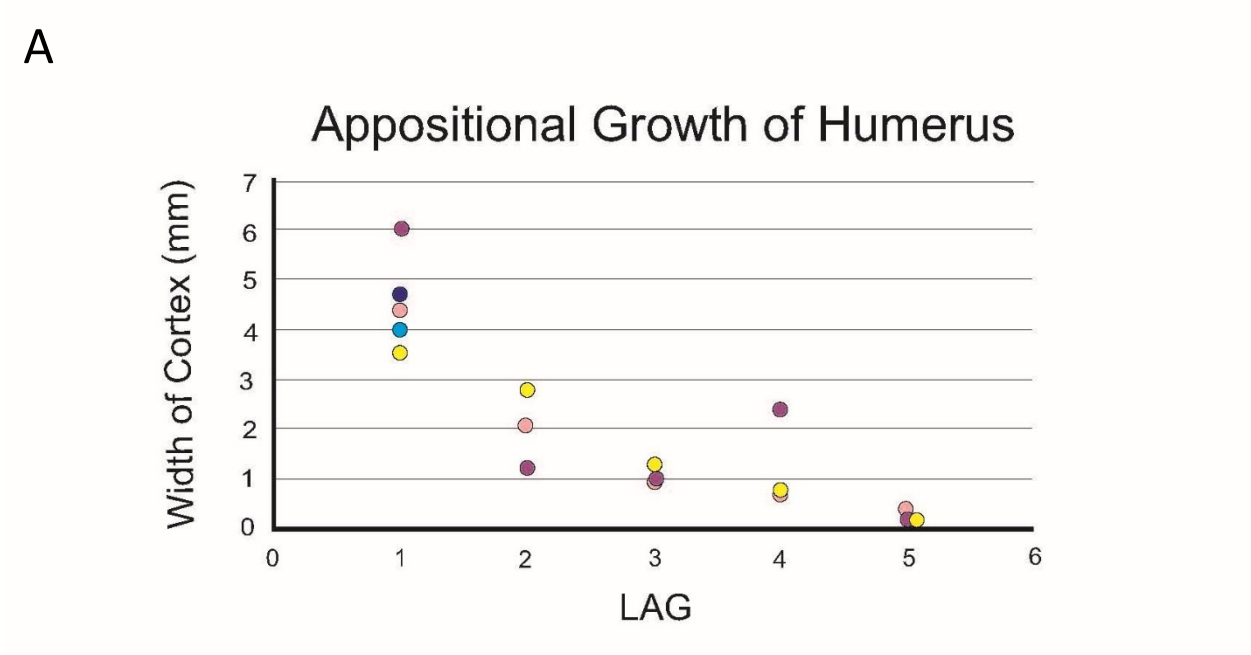

B

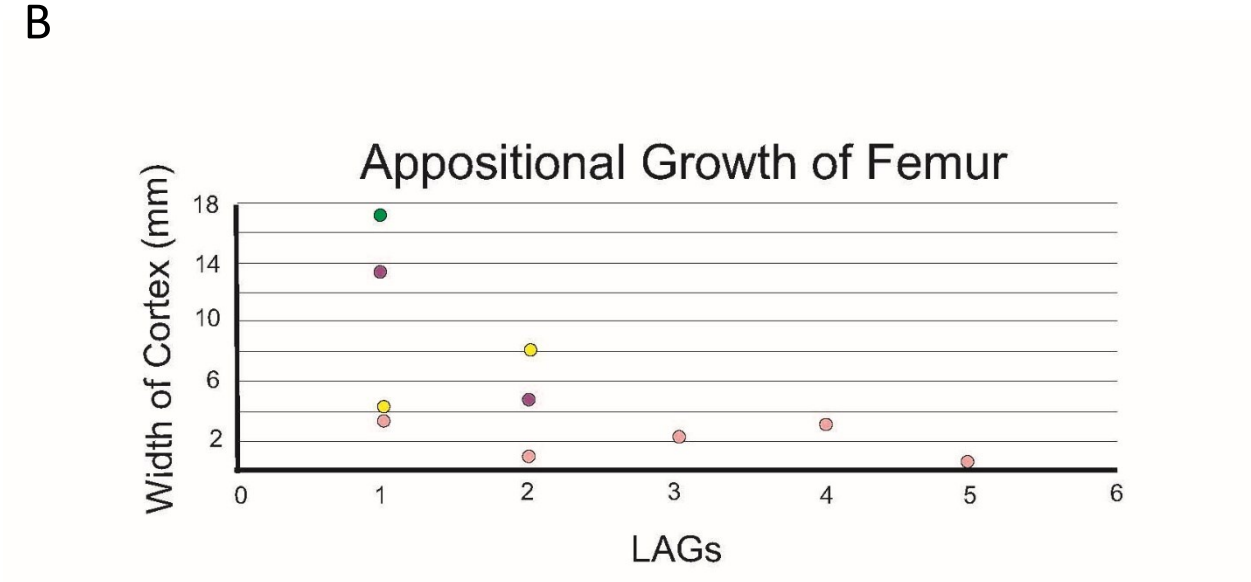

C

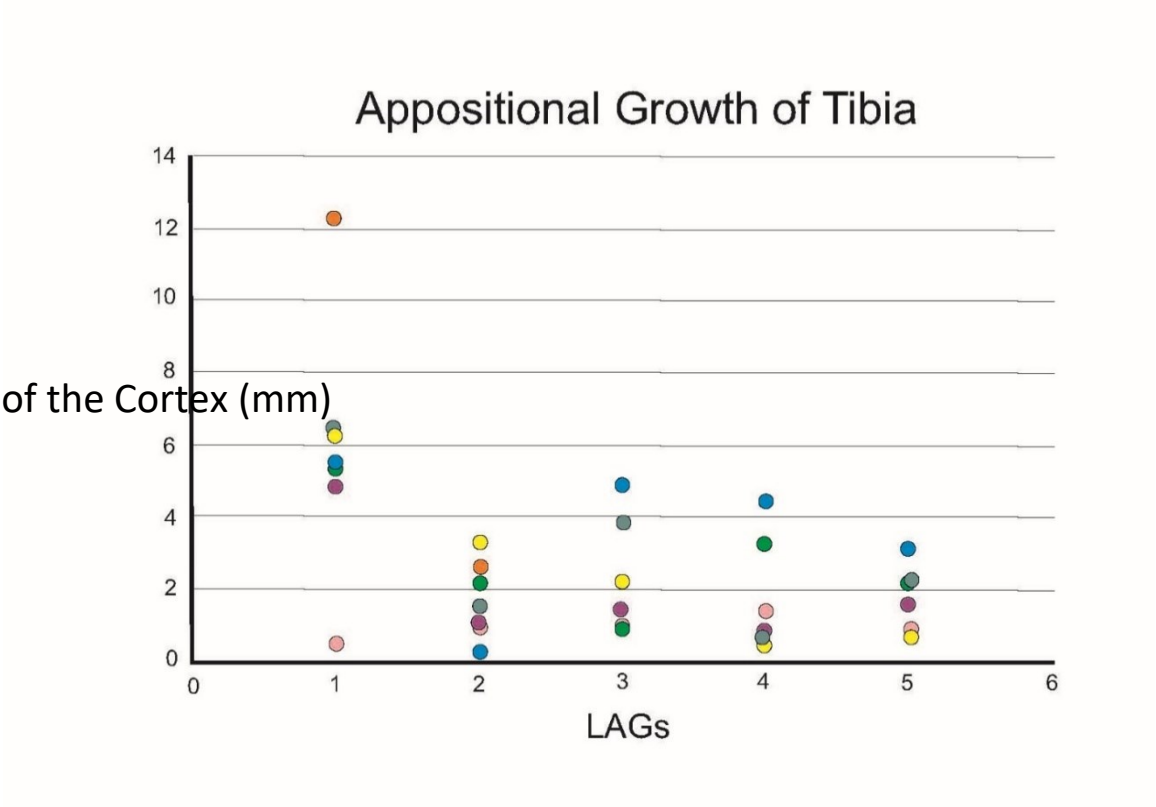
Appositional Growth of Tibia
Width of the Cortex (mm)
14
12
10
8
6
4
2
0
0
1
2
3
4
5
6
LAGs

FIGURE 3.2.26 Linear Growth. The graphs below show the estimated length for each element at the time the AGM was deposited. Each AGM is either a LAG or an annulus in associaction with a LAG. Estimates of length were made using the data from Fig. 3.2.2. Each specimen has been given a different color. Specimens with no AGMs were plotted at 0.5 LAG.

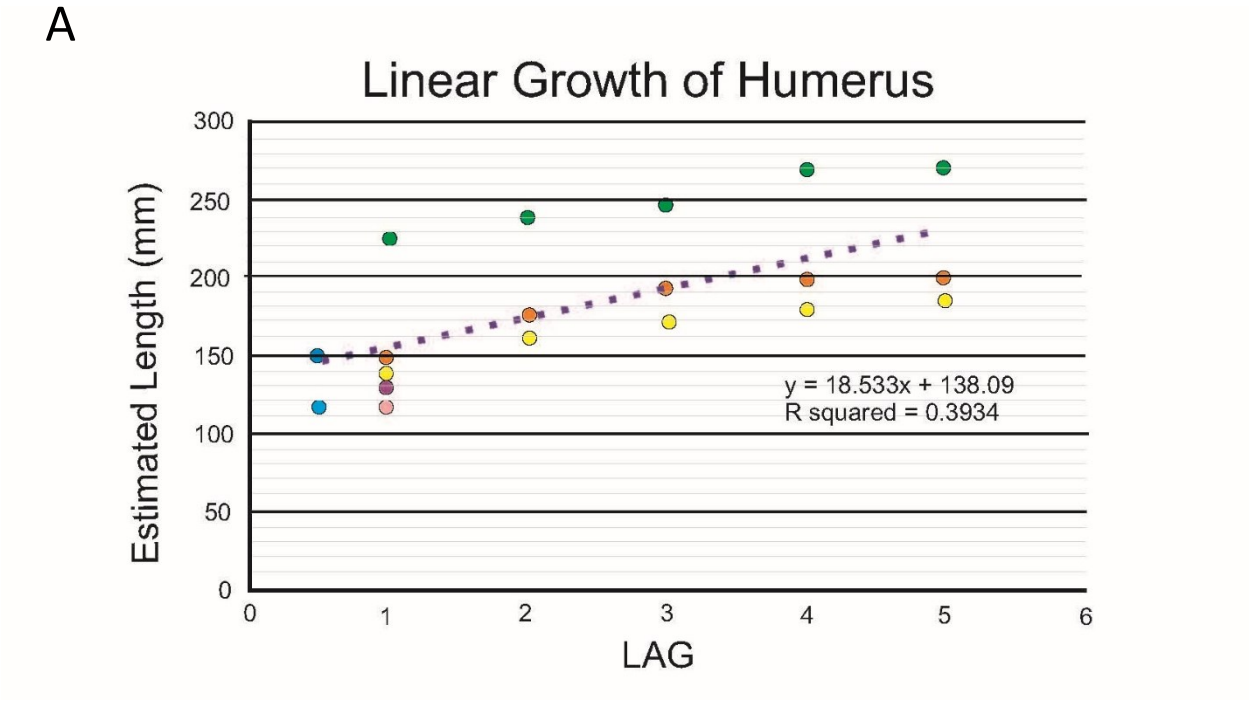

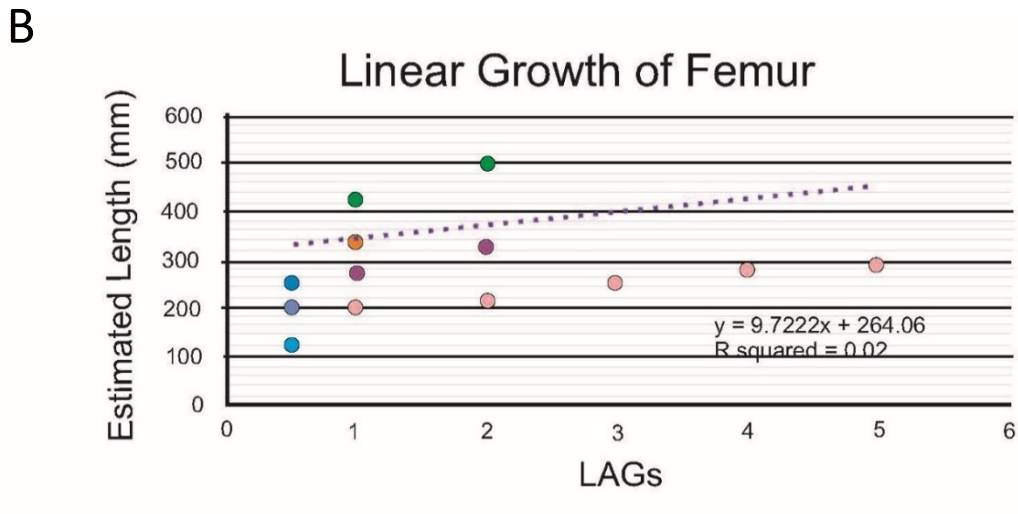

C

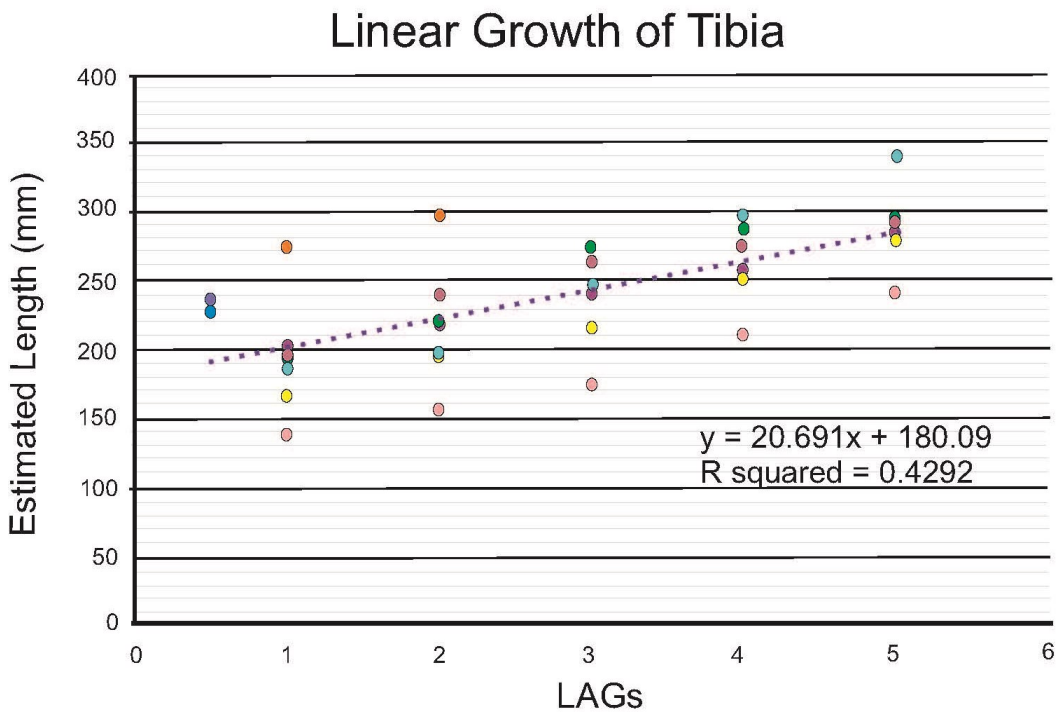
Linear Growth of Tibia
Estimated Length (mm)
400
350
300
250
200
150
100
50
0
0
1
2
3
4
5
6
LAGs
y = 20.691x + 180.09
R squared = 0.4292

Tables

TABLE 3.2.1 Specimen List The table below lists the specimens that were sectioned as a part of this study. The lengths and circumferences taken directly from the specimens are listed, as is the estimated length of each specimen. This estimate is based on the relationship between least circumference and length as determined from complete specimens of the same taxon.

Specimen Number	Study Code	Element	Length (mm)	Estimate Length (mm)	Least Circumference (mm)	Quarry Name
CEUM 35641	H1	Humerus	>80.33	118	48	EC2
CEUM 35369	H2	Humerus	>160.4	152	63	EC2
CEUM 35621	H3	Humerus	>160	156	65	EC2
CEUM 35719	H4	Humerus	>123	167	70	EC2
CEUM 35743	H5	Humerus	>170	192	81	EC2
CEUM 35662	H6	Humerus	>131	205	87	EC2
CEUM 35357	H7	Humerus	>179	280	121	EC2
OMNH 62250	H8	Humerus	235	216	92	EC2
FMNH 3848	F0	Femur	---	126	40	FMNH
CEUM 13317	F1	Femur	>120	207	82	EC2
CEUM 34399	F2	Femur	>221	253	106	EC2
CEUM 35444	F3	Femur	>318	280	120	EC2
CEUM 14503	F4	Femur	>309	373	168	EC2
OMNH 62194	F5	Femur	---	357	160	EC2
FMNH UT130825-3	F6	Femur	---	511	240	FMNH
CEUM 34276	T0	Tibia	259	237	88	EC2
CEUM 13306	T1	Tibia	>156	227	84	EC2
CEUM 35386	T2	Tibia	>216	247	92	EC2
CEUM 52874	T3	Tibia	>185	294	111	EC2
CEUM 35704	T4	Tibia	>194	297	112	EC2
CEUM 74590	T5	Tibia	>220	311	118	EC2
CEUM 35491	T6	Tibia	>193	311	118	EC2
CEUM 14582	T7	Tibia	>301	354	135	EC2
OMNH 62213	T8	Tibia	>283	297	112	EC2

TABLE 3.2.2 Complete Specimen Measurements. The table above shows measurements of total length and least circumference taken of all complete specimens from the EC2 Quarry.

Specimen Number	Element	Length (mm)	Least Circumference (mm)
CEUM 35411	Humerus	216	92
CEUM 34382	Humerus	221	83
CEUM 35384	Humerus	282	117
CEUM 35323	Femur	308	118
CEUM 14571	Femur	336	127
CEUM 35457	Femur	377	166
CEUM 74494	Femur	399	148
CEUM 34252	Femur	405	154
CEUM 12423	Femur	406	152
CEUM 52987	Femur	414	163
CEUM 8786	Femur	809	374
CEUM 35629	Tibia	259	88
CEUM 52918	Tibia	314	113
CEUM 14451	Tibia	315	106
CEUM 14495	Tibia	348	116
CEUM 34379	Tibia	368	118
CEUM 35450	Tibia	380	148
CEUM 34384	Tibia	403	145

TABLE 3.2.3 Cross-Section Measurements. The table below shows the minimum and maximum measurement of the cortex and medullary cavity for each specimen, as well as the average cortical thickness.

Specimen Number	Study Code	Major and Minor Axis (mm)		Average Cortical Thickness (mm)
		Cortex	Medullary Cavity	
CEUM 35641	H1	20 x 19	9 x 8	5
CEUM 35369	H2	21 x 20	9 x 9	5
CEUM 35621	H3	21 x 21	9 x 8	6
CEUM 35719	H4	23 x 21	11 x 9	4
CEUM 35743	H5	28 x 24	17 x 14	5
CEUM 35662	H6	32 x 28	19 x 15	5
CEUM 35357	H7	40 x 32	21 x 15	6
OMNH 62250	H8	34 x 24	27 x 14	9
FMNH 3848	F0	12 x 9	6 x 4	2
CEUM 13317	F1	21 x 20	9 x 9	6
CEUM 34399	F2	23 x 21	10 x 9	6
CEUM 35444	F3	42 x 37	22 x 20	9
CEUM 14503	F4	52 x 44	27 x 25	9
OMNH 62194	F5	50 x 37	25 x 21	9
FMNH UT130825-3	F6	82 x 50	43 x 22	14
CEUM 34276	T0	18 x 15	10 x 5	5
CEUM 13306	T1	26 x 23	11 x 9	6
CEUM 35386	T2	32 x 28	12 x 7	8
CEUM 52874	T3	38 x 33	20 x 14	8
CEUM 35704	T4	37 x 34	14 x 13	10
CEUM 74590	T5	41 x 34	19 x 15	9
CEUM 35491	T6	42 x 35	13 x 12	10
CEUM 14582	T7	45 x 40	16 x 10	16
OMNH 62213	T8	39 x 34	13 x 9	12

TABLE 3.2.4 Quantitative Histology. The table below shows the PVD, OI and HRI values calculated for each specimen in the study. When the distinction between inner and outer cortex could be made, these regions were measured separately.

Specimen Number	AGMs	Percent Vascular Density	Obliquity Index	Haversian Remodelling Index
H1 Outer Cortex	0	24%	13%	---
H1 Inner Cortex	0	23%	20%	---
H2 Outer Cortex	0	22%	38%	---
H2 Inner Cortex	0	24%	21%	---
H3 Outer Cortex	1	15%	22%	---
H3 Inner Cortex	0	21%	20%	< 5%
H4 Outer Cortex	1	15%	46%	---
H4 Inner Cortex	0	19%	20%	< 5%
H5 Outer Cortex	5	13%	65%	---
H5 Inner Cortex	0	20%	20%	< 5%
H7 Outer Cortex	5	12%	65%	< 5%
H7 Inner Cortex	0	21%	25%	40%
H8 Outer Cortex	5	13%	68%	< 5%
H8 Inner Cortex	0	21%	23%	20%
F0 Outer Cortex	0	---	---	---
F0 Inner Cortex	0	---	---	---
F1 Outer Cortex	0	19%	68%	---
F1 Inner Cortex	0	24%	29%	< 5%
F2 Outer Cortex	0	19%	73%	---
F2 Inner Cortex	0	23%	48%	< 5%
F3 Outer Cortex	5	13%	88%	---
F3 Inner Cortex	0	23%	75%	< 5%
F4 Outer Cortex	2	15%	88%	---
F4 Inner Cortex	0	21%	73%	< 5%
F5 Outer Cortex	1	13%	89%	---
F5 Inner Cortex	0	22%	80%	< 5%
F6 Outer Cortex	2	13%	86%	8%
F6 Inner Cortex	0	---	---	48%
T0 Outer Cortex	0	---	---	---
T0 Inner Cortex	0	---	---	---
T1 Outer Cortex	0	19%	48%	---
T1 Inner Cortex	0	23%	13%	---
T2 Outer Cortex	5	15%	78%	---
T2 Inner Cortex	0	23%	34%	---
T3 Outer Cortex	5	13%	81%	---
T3 Inner Cortex	0	23%	48%	---
T4 Outer Cortex	5	13%	83%	---
T4 Inner Cortex	0	22%	48%	---
T5 Outer Cortex	5	14%	83%	---
T5 Inner Cortex	0	21%	52%	---
T6 Outer Cortex	2	13%	86%	---
T6 Inner Cortex	0	19%	56%	---
T7 Outer Cortex	5	12%	88%	---
T7 Inner Cortex	0	18%	63%	---
T8 Outer Cortex	5	11%	88%	---
T8 Inner Cortex	0	19%	68%	---

3.3 Hypacrosaurus

Hypacrosaurus stebingeri is a lambeosaurine hadrosaurid (Fig. 1.2) from the St. Mary River Formation in Montana. In the previous ontogenetic series, *Eolambia*, it was argued that retrocalculations were valid in the example of a large-bodied taxon on the basis of morphologic, taphonomic and histologic evidence. I will examine an ontogenetic series of *Hypacrosaurus,* another large-bodied taxon, and determine if retrocalculations are valid in this taxon as well.

Hypacrosaurus stebingeri is closely related to *Maiasaura* (Fig. 1.2). As discussed in the previously, *Maiasaura* showed no AGMs in specimens of the juvenile size class; the first AGM appeared in subadult-sized individuals. On the weight of this evidence, Woodward et. al (2015) concluded that retrocalculations of AGMs in large specimens were inappropriate. They also called into question the general practice of retrocalculations.

Horner et al (1999) sectioned 12 different elements of the (adult) holotype of *Hypacrosaurus stebingeri*. Horner et al (1999) found between 0 and 8 LAGs in various elements sectioned. For each element, independent counts of LAGs were made by different researchers. The minimum and maximum count was within one LAG for nine of the elements, including the tibia and femur. These elements are commonly sectioned in histologic studies. Horner et al. (1999) found 7 LAGs in the tibia and 6 LAGs in the femur; they also found no signs of resorption along the endosteal margin.

Geologic Setting

Hypacrosaurus stebingeri is known from the Late Cretaceous Two Medicine Formation (Horner et al. 1994) and the St. Mary River Formation of Montana (Sartin et al. in prep.). The specimens examined in this chapter were collected from the the St. Mary River Formation BFD site. The site consists of channel sands and overbank mudstones (Weishampel pers. comm.).

Materials and Methods

Limb elements of the BFD site hypacrosaur were selected based on their completeness and state of preservation (Table 3.3.1). Only elements that could be clearly identified and that had mostly intact shafts (on gross examination) were used; upon histologic analysis, it was found that portions of the outer cortex were missing in some specimes. Care was taken in selecting elements to ensure that all available sizes present were represented. Three femora, four tibiae, three humeri, and three ulnae were included in the sample (Table 3.3.1). For location of the section extracted and methods used to extract it, please refer to "Selection and Extraction of Section ('plug)" in Section 2. Slides were made and imaged according to standard practices as described in Section 2.

Osteohistology of Hypacrosaurus stebingeri.

As part of the histologic description, the minor and major axes of both the outer cortex and medullary cavity, as well as the average cortical thickness were calculated using methods detailed under "Analysis of Slides" in Section 2 (Table 3.3.2). It should be noted that measurements were not always possible due to significant crushing and distortion of certain specimens.

Assessment of age category was made based on histologic features (Table

3.3.1). In addition to this, three measurements of vascularity were taken from each slide (Table 3.3.3). Percent Vascular Density (PVD), Obliquity Index (OI), and Haversian Remodeling Index (HRI) were calculated; a detailed description of these calculations can be found under "Analysis of Slides" in Section 2.

In addition to measurements of vascularity, Annual Growth Marks (AGMs) were identified; when present, the circumference of each AGM was measured and AGMs present in each specimen were counted.

For each section, both a full view and close-up image are included (see Figs. 3.3.1-3.3.13); the images of these sections will also be made available on MorphoBank.

Humerus

Juvenile

Specimens examined: MOR 609-89-82 (H1), MOR 609-89-3 (H2)
(Figs. 3.3.1-3.3.2)

The cross-section and medullary cavity of MOR 609-89-82 (H1) are roughly triangular. The cross-section and medullary cavity MOR 609-89-3 (H2) are oval. In both specimens, the medullary cavities are completely filled in with trabecular bone and calcite crystals.

The distinction between inner and outer cortex of H1 and H2 is not readily apparent. The cortices of H1 and H2 have high Percent Vascularity Densities (PVD); both osteon canals and primary osteons are present. The vascular canals are disorganized, becoming more organized towards the periosteal margin; the Obliquity Index (OI), accordingly becomes higher towards the periosteal margin as well. This portion of the cortex is composed of reticular and plexiform fibrolamellar bone matrix.

H1 and H2 show no signs of secondary remodeling.

No definitive LAGs or annuli are visible in any of these sections; no outer circumferential layer is present in any of these specimens.

Subadult

Specimens examined: MOR 609-89-15 (H3)
(Fig. 3.3.3)

The specimen is roughly lacrimiform in cross section, as is the medullary cavity. There is significant secondary remodeling along the endosteal margin. Where the margins of the cavity remain unremodeled, it shows few or no signs of resorption and the cavity is filled in by trabecular bone, and sparty calcite.

The inner cortex is dominated by secondary osteons. The osteons were visualized under crossed polarized light to verify that they are secondary, and not primary, osteons. The degree of remodeling is significant, and the HRI is accordingly high. Where the original bone matrix is visible, it is plexiform fibrolamellar; however, there is not enough of the original matrix present to calculate the PVD or the OI. There is one LAG visible in this portion of the cortex and, despite being disrupted by secondary osteons at multiple points, it is still possible to trace it circumferencentially.

The outer cortex of the specimen is moderately vascularized and dominated by osteon canals. The canals become increasingly organized and longitudinally oriented closer towards the periosteal margin. The cortex is composed of plexiform fibro-lamellar bone matrix. The PVD of this region is low and OI high, similar to other subadult specimens of other taxa in this study.

Secondary remodeling has begun in this part of the cortex, but a significant portion of the original bone matrix remains; the HRI is moderate. The specimen does not have an outer circumferential layer. It does have a single LAGs in this portion of the cortex, which occurs towards the periosteal margin.

Ulna

Hatchling

Specimens examined: MOR 609-89-191 (U1)
(Fig. 3.3.4)

The cross-section of MOR 609-89-191 (H1) is reniform; the cross-section of the medullary cavity is roughly circular. The margin of the medullary cavity is preserved and shows no signs of resorption. The medullary cavity is filled with trabecular bone tissue and spary calcite. The size of this specimen is commensurate with that of similar bones in *Maiasaura* hatchlings (Horner & Currie, 1994; Horner, et al 2000). There is no clear distinction between the inner and outer cortex. The cortex is highly vascularized and dominated by primary osteons. The osteons are very disorganized and dominate the cortex; when they form canals are radially arranged. Given the scarcity of canals, neither PVD nor OI was calculated. The osteons were visualized under crossed polarized light with a rotating stage to verify that they are primary, not secondary, osteons. The cortex is composed of plexiform fibrolamellar bone matrix. There are no AGMs or outer circumferential layer visible.

Adult

Specimens examined: MOR 609-89-41 (U2), MOR 609-89-111 (U3)
(Fig. 3.3.5-3.3.6)

The cross-sections of MOR 609-89-41 and MOR 609-89-111 are both elliptical, as are the cross-sections of the medullary cavities. The medullary cavities are completely filled with trabecular bone and spary calcite.

There is no distinction between the inner and outer cortex in either specimen; both are completely secondarily remodeled. The remodeling was visualized under cross-polarized light to confirm that there is a predominanace of secondary osteons. Towards the periosteal margin, a number of relatively closely spaced secondary osteons are visible. Four LAGs are visible with primary osteons in-between them. The first and second are moderately spaced, while the others are closely spaced. Moving towards the periosteal margin, there are three to four more LAGs, very closely spaced and with no osteons between. These last LAGs are the beginning of the formation of an outer circumferential layer (OCL).

Femur

Juvenile

Specimens examined: MOR 609-89-173 (F1), MOR 609-89-18 (F2)
(Figs. 3.3.7-3.3.8)

The cross-sections of both specimens (fig. F1-F2) are roughly elliptical. The medullary cavities of F1 has been crushed and distorted; the medullary cavity of F2 is roughly elliptical. The endosteal margin of F1 is not preserved due to the crushing; the endosteal margin of F2 is preserved and shows little to no signs of resorption. The medullary cavity of F2 has primarily been filled in with spary calcite.

The inner cortex is highly vascularized, with highly disorganized osteon canals and primary osteons present. This portion of the cortex composes the majority of the

cortex in both specimens, and is composed of reticular fibrolamellar bone matrix. The inner cortexes have a high PVD and low OI, similar to the inner cortices of juvenile specimens in this study.

The outer cortex is also highly vascularized; it is dominated by osteon canals that are orriented longitudinally. This portion of the cortex is composed of plexiform fibrolamellar bone matrix and has a high PVD, although somewhat lower than the inner cortex. The OI, however, is much higher as the canals are almost exclusively longitudinal.

There are no annuli visible; no outer circumferential layer is visible.

Subadult

Specimens examined: MOR 609-89-43
(Fig. 3.3.9 F3)

The specimen is roughly circular in cross section, although extensive crushing obscures the original outline of the section, as well as the borders of medullary cavity. There is significant secondary remodeling along the endosteal margin; where the margins of this cavity remain unremodeled, it shows few signs of resorption. The cavity is filled in by trabecular bone; calcite fills the medullary space.

The inner cortex is dominated by secondary osteons. The osteons were visualized under crossed polarized light to verify that they are secondary, and not primary, osteons. The degree of remodeling is significant, and the HRI is accordingly high. The original bone matrix is almost completely remodeled; accordingly, neither the PVD nor the OI was calculated for this portion of the cortex.

The outer cortex of the specimen is moderately vascularized; it is dominated by

osteonal canals. The canals become dominanatly longitudinally oriented towards the periosteal margin. The cortex is composed of plexiform fibro-lamellar bone matrix. The PVD of this region is low and OI high, similar to other subadult specimens of other taxa in this study. Secondary remodeling has begun in this part of the cortex, but a significant portion of the original bone matrix remains; the HRI is moderate. The specimen does not have an outer circumferential layer; it does have eight LAGs, which will be discussed below.

Counting from the medullary cavity outwards, the first LAG occurs approximately two- thirds the way through the outer cortex. The first two LAGs are widely spaced from each other. The remaining LAGs are all moderately spaced with respect to each other. The eighth and final LAG is moderately spaces with respect to the periosteal margin. There is no visible outer circumferential layer.

Tibia

Juvenile

Specimens examined: MOR 609-89-145 (T1), MOR 609-89-195, (T2)
MOR 609-89-13 (T3)
(Figs. 3.3.10-3.3.12)

The cross-sections of MOR 609-89-145 and MOR 609-89-13 (fig. T1) are elliptical, as are the medullary cavities. The cross-section of MOR 609-89-195 is roughly triangular; the medullary cavity is circular. The medullary cavity of T1 has been crushed and contains large calcite crystals; the medullary cavities of T2 and T3 are intact and completely filled with trabecular bone and spary calcite. The endosteal margin of T1 is not preserved due to the crushing; the endosteal margins of T2 and T3 are preserved and show little to no signs of resorption.

The inner cortex of all specimens is highly vascularized, with highly disorganized osteon canals and primary osteons present. This portion composes roughly half of the cortex and is composed of reticular fibrolamellar bone matrix. The inner cortices have a high PVD and low OI, similar to the inner cortices of juvenile specimens in this study.

The outer cortices are also highly vascularized; the cortices are dominated by osteonal canals that are oriented longitudinally. This portion of the cortex is composed of plexiform fibrolamellar bone matrix. This portion of the cortex also has a high PVD, although somewhat lower than the inner cortex. The OI, however, is much higher as the canals are almost exclusively longitudinal.

There are no annuli visible; no outer circumferential layer is visible.

Subadult

Specimens examined: MOR 609-89-18 (T4)
(Fig. 3.3.14)

The cross-sections of MOR 609-89-18 and MOR 609-89-13 (fig. T4) are elliptical, s roughly circular, as is the medullary cavity. The medullary cavity is partially intact; the intact portion is filled spary calcite and broken trabecular bone. The endosteal margin of T4 is also partially preserved and shows little to no signs of resorption.

The inner cortex is dominated by secondary osteons. The osteons were visualized under crossed polarized light to verify that they are secondary, and not primary, osteons. The degree of remodeling is significant, and the HRI is accordingly high. The original bone matrix is almost completely remodeled; accordingly, neither the PVD nor the OI was calculated for this portion of the cortex. Where present, the

original bone matrix is highly disorganized reticular to plexiform fibrolamellar bone matrix.

The outer cortex of the specimen is moderately vascularized; it is dominated by osteon canals. The canals become increasingly organized and longitudinally oriented towards the periosteal margin. The cortex is composed of plexiform fibro-lamellar bone matrix. The PVD of this region is low and OI high, similar to other subadult specimens of other taxa in this study. Secondary remodeling has begun in this part of the cortex, but a significant portion of the original bone matrix remains; the HRI is moderate. The specimen does not have an outer circumferential layer; it does have two annuli and three LAGs, which will be discussed below.

Counting from the medullary cavity outwards, the first two AGMs are annuli. The first annulus occurs close to the margin between the inner and outer cortex; the disorganized and organized areas are subequal and wide. The second annulus also has a wide disorganized band, followed by a narrow organized band. The first LAG occurs at the top of this organized band and is approximately 2/3 from the medullary cavity to the periosteal margin. The second LAG is narrowly spaced with respect to the first. The third LAG, however, is moderately spaced with respect to the second; in places, it appears that there is an annulus between second and third LAG. There is no outer circumferential layer visible.

Discussion

Hypacrosaurus stebingeri does not show any AGMs until it reaches subadult size. There are also no signs of resorption along the endosteal margin of any of these specimens. This suggests that in the largest specimens, no AGMs have been obliterated

by remodeling. However, resorption and/or remodeling of AGMs is not the only reason retrocalculations might be reasonable. It could also be the case that AGMs are not laid down annually during the early life of a taxon. As discussed below, I conclude that the retrocalculations are not reasonable in this taxon based on evidence from LAG formation and growth rates of extant taxa, as well as lack of LAGs in juvenile specimens.

While it is the case that the literature supports the view that AGMs are annual marks, the physiological and/or cellular processes that cause them to form are not known (Huttenlocker et al., 2013). However, it is possible to examine the environmental conditions present when AGMs form in modern taxa. By doing this, we gain insight as to the necessary and sufficient conditions for their formation, even if the cause remains unknown.

Köhler et al. (2012) surveyed 115 extant ruminants; this sample included specimens from across the globe, as well as across many different biomes. Kohler et al. found that in each taxon, the timing of growth marks corresponded to the annual unfavorable season for that taxon. During this time, animals decreased their body temperature, metabolic rates, and bone-growth- mediating plasma insulin-like growth factor-1 levels. Buffrenil & Castanet (2000) injected bone-marking dye into wild Nile monitors. The monitors were then recaptured after a year and sacrificed. The formation of one LAG after the marking dye was visible in the specimens. This AGM was formed during the dry season, the annual time of hibernation; during this time animals decreased their body temperature and metabolic rates. Interestingly, Buffrenil & Castanet (2000) found that during years which the unfavorable season was wetter than

usual, the animals would maintain a minimum level of activity and the LAGs produced were weak or poor.

Both of these studies, Kohler et al (2012) and Buffrenil & Castanet (2000), suggest that the annual timing of LAGs is controlled by environmental conditions. Moreover, their results seem to suggest that the cause is related to a scarcity of resources and/or a change in metabolic rates. All three of the taxa in the present study (*Iguanacolossus, Eolambia, Hypacrosaurus*), as well as other ornithopod taxa mentioned in the present study (*Dysalotosaurus, Tenontosaurus, Maiasaura*) lived in environments that were seasonally wet and dry. It is likely that these taxa experienced similar periods of resource scarcity as the modern taxa in the studies above.

In extant taxa, it is possible to examine the extent to which environmental cues affect the formation of LAGs. *Microcebus* is a small lemur from the island of Madagascar. It undergoes torpor every year during the months of May to September; during this time, LAGs are formed. Castanet et al. (2004) experimentally manipulated the photoperiodicity of *Microcebus* such that the animals experienced 365 light/dark cycles compressed into a period of 280 days. The animals were kept under controlled environmental conditions, such that there was no period of resource scarcity. Castanet et al (2004) found that the animals laid down LAGs every 280 days. This suggests that LAGs are laid down annually. Furthermore, it suggests that day/night cycles, not resource scarcity or the relative length of day and night, affect formation of AGMs.

Marangoni et al. (2009) ran a similar experiment with subtropical anurans species from Argentina. The animals were wild caught, then kept in the laboratory under temperature, humidity and photoperiodicity that mimicked their natural

environment for a year. However, they were given a consistent diet, so there was no scarcity of food. Upon examination, all of the toads had a well-defined LAGs for the year prior to sacrifice, when they were kept under experimental conditions. LAGs formed prior to this year, while they were living in the wild, varied in their definition from well-defined to poorly-defined. Poorly defined LAGs were often not visible without staining. LAGs are highly basophilic and react strongly to stains such as Ehrlich's haematoxylin; however, such stains can only be applied to modern bone samples. Similar to Castanet et al (2004), their results suggest that resource scarcity is not the cause of LAG formation. Rather, Marangoni et al. (2009) suggest that LAG formation is the result of intrinsic (genetic) cues. However, given their results, it is also possible that LAG formation is in part caused by the number of light and dark cycles; this would be consistent with the results of Castanet et al (2004).

When taken together, the natural and experimental conditions give us a better understanding of LAG formation. From the animals living in natural conditions, we see that LAGs are formed annually, but that resource availability affects the prominanace of the LAG. From the animals kept in laboratory, we see that LAGs form even when there is no resource scarcity. Furthermore, the results are suggestive that LAG formation is tied to the number of day/night cycles an animal experiences.

As mentioned above, it is the case that the first LAGs in *Hypacrosaurus* appear when the individuals are subadult in size. There are no signs of resorption or remodeling of LAGs. The studies discussed above suggest that LAG formation is the result of day/night cycles, and not environmental conditions. While day and night cycles were of different lengths during the Cretaceous, as compared to today, the cycles presumably

occurred with the same regularity.

Marangoni et al. (2009) did find that resource scarcity can affect the prominanace of the LAG and its ability to be dinstinguished from surrounding tissue without the use of dyes. It could be that the population of *Hypacrosaurus* in this study experienced years of only moderately unfavorable seasons. In response, they laid down poor LAGs that are now either undiscernible in the fossil or account for some of the bands of differential staining observed. A change in the environment for a few years, as opposed to centuries, would not be observable in the sedimentary record. However, the largest specimens have LAGs close to the periosteal margin, meaning that they were laid down relatively close to the time of the individual's death. Given that these individuals were likely living together as a population, if environmental conditions were such that some individuals were able to form LAGs, we would expect this to be true of all the individuals. Therefore, it is not likely that mild unfavorable seasons affected LAG formation *Hypacrosaurus*.

The lack of LAGs in the smallest specimens suggests that within the first year of life, *Hypacrosaurus* reached subadult size. As we saw in the previous chapter, extant birds, in particular ratites, reach adult sizes within the first year of their lives. Emus (*Dromaeuis novaehollandiae*) are approximately 12 cm tall when they hatch, and reach 150-190 cm (adult size) in five to six months (Davies & Bamford, 2002). Adult body mass varies significantly between the sexes and with seasons. On average, during the summer, males weight 40.7 kg, females 45.4; during the winter, males weigh 37 kg, females 39.7 kg (Maloney & Dawson, 1993). Cassowaries (*Casuarius casuarius* and *Casuarius unappendiculatus*) have a similar size to emus

at hatching and as adults; they take approximately nine months to reach adult size. (Davies & Bamford, 2002) As adults, femur length varies between approximately 20-25 cm and the tibiotarsi between 35-38 cm (personal data from USNM and FLMNH; (Fowler, 1991). Body mass varies between the sexes, with, on average, males weighing 40 kg and females 60 kg; however, no seasonal data are available for these taxa.

If we are to examine the size of the individual at the time of the first LAG in *Hypacrosaurus*, we need to know the relationship between the circumference of the element and its total length. In *Eolambia*, there was a sufficient sample size of complete elements that a regression analysis could be undertaken; this is not the case with *Hypacrosaurus*. It is possible, however to compare the major and minor axis of the LAGs with those of the other specimens in the study (Table 3.3.2). We can do this for both the femur and tibia; it should be noted that in ratites, the femora are significantly shorter than the tibiotarsi, whereas in *Hypacrosaurus*, the femur and tibia are more commensurate. It is also possible to estimate the relationship between circumference of the element and its total length by using a closely-related taxon as a proxy. If we take *Maiasaura* to be a good proxy for *Hypacrosaurus*, we can estimate the total length of the tibia for each AGM (Fig 3.3.14). We can also use *Maiasaura* to estimate total length of the femur from the tibia, which are commonly reported values in the literature.

In *Hypacrosaurus,* the smallest tibia to show LAGs (T4) is 75 cm in length (Table 3.3.1); the first AGM is an annuli and appears approximately one third of the way through the cortex, with a major and minor axes of 52 and 40 cm, respectively

(Table 3.3.2). The circumference of this AGM is 16.2 cm (Table 3.3.4); using the linear equations derived from *Maiasaura* data (Figure 3.3.14), the tibia was approximately 45 cm in length when this AGM was laid down. This is close to the size of T3; the major and minor axis of this specimen are 50 and 38 cm, respectively and it has a total length of 37 cm (Tables 5.1 and 5.2). This is interesting given that the juvenile specimen of *Parasaurolophus*, mentioned above, has no LAGs; the tibia of this specimen is 30.7 cm in length, and ~2m total body length (Farke et al., 2013).

The estimated length of the tibia at the deposition of the first AGM is commensurate with the size modern ratites achieve within their first year of life. Adult cassowaries have a tibiotarsal length of 35-38 cm; the tibia of *Hypacrosaurus* at the time of the deposition of the first AGM is here estimated at 45 cm in length. This is suggestive that *Hypacrosaurus* could have reached these sizes within their first year as well.

The smallest femur to show LAGs (F4) is 102 cm in length (Table 3.3.1); the first AGM is a LAG and appears approximately half way through the cortex, with a major and minor axes of 50 and 43 cm, respectively (Table 3.3.2). The circumference of the AGM is 30.0 cm (Table 3.3.4); using the linear and scaling equations derived from *Maiasaura* data (Figure 3.3.14 and Woodward et al., 2015), the femur was approximately 51 cm in length when this AGM was laid down. This is close to the size of F2; the major and minor axis of this specimen are 50 and 40 cm (Table 5.1), and has a total length of 40.6 cm (Table 3.3.2).

Horner et al. (1999) sectioned the type specimen of *Hypacrosaurus stebingeri* (MOR 540). As part of that study, the femur was sectioned; it is 102 cm in total length,

however, neither the least circumference, nor the major and minor axes are reported. Horner et al. (1999) found between 6-8 LAGs (counts by independent researchers), as well as 1 LAG that they attributed to the beginning formation of the EFS. The first LAG occurs near the endosteal margin and is 33.6 cm in circumference (Cooper et al., 2008); the LAGs become more closely spaced as they approach the periosteal margin.

The femur sectioned by Horner et al. (1999) is same total length as the subadult femur sectioned as a part of this study (F3). The LAG counts are also similar between the MOR 540 femur and F3. However, in F6, the first LAG occurs half-way through the cortex, with the remaining LAGs occurring close to the periosteal margin (Fig. 3.3.9). This is markedly different from the even spacing of LAGs seen in MOR 540.

Cooper et al. (2008) also analyzied both the femur and tibia of MOR 540.They measured the circumference of the LAGs in each element, then these measurements were fitted to several different growth curves. Hatchling size for each element was taken from the literature and used in fitting the curves. Cooper et al. (2008) found that MOR 540 was 13 years old at the time of its death. If we take the maximum count, 8 LAGs are present in the specimen; this would mean that 5 LAGs have been resorbed.

The largest femur in this study that lacks AGMs is F2; it has a circumference of 14.5 cm. The first LAG of F6 has a circumference of 30 cm; the least circumference is 37 cm. The first LAG of MOR 540 is 33 cm in circumference; the last, which is close to the periosteal margin, has a circumference of 39.5 cm. However, while MOR 540 shows signs of resorption and the endosteal margin is close to the first LAG, this is not the case for F6. The first LAG of F6 occurs approximately half-way through the cortex. The endosteal margin of F6 has a circumference of 17 cm.

For F6 to also have 5 missing LAGs, they would have to occur between 14.5 and 17 cm of femur circumference; between the circumference of the smallest specimen without LAGs and the endosteal margin. If this was the case, it would mean that for the first five years of life, the individual experienced moderate to slow growth, followed by a significant growth spurt, with the circumference increasing from 17.5 to 30 cm. After this growth spurt, growth rate would have then decreased again. While this is not impossible, it is counter to the growth patterns of known ornithopod, and even non-ornithopod dinosaur taxa.

There does remain the question of why MOR 540 has signs of resorption and F6 does not. There are several possible explanations. For instance, it might be a difference between populations; MOR 540 and F6 do come from different sites. It might also be a difference in sex. We do not have a sufficient sample size to rule out sexual dimorphism in *Hypacrosaurus.* Males and females may employ different growth strategies and/or have different adult body sizes. While there is no evidence of medullary bone in MOR 540, it could also be the case that the increased size of the medullary cavity is related to the egg forming processes.

This highlights the need to section multiple specimens at different ontogentic stages, preferably from a single location. In this way, we can minimize intraspecific variation between specimens. It also gives us a better picture of growth throughout ontogeny.

Conclusion

Based on evidence from LAG formation and growth rates of extant taxa, I conclude that retrocalculations of AGMS are not appropriate for this sample of this taxon. Histologic

analysis of *Hypacrosaurus* suggests that it reached subadult size within its first year of life.

This pattern of growth is similar to what has been found in other large-bodied ornithopods, such as *Maiasaura* and *Iguanacolossus*. By contrast, smaller-bodied ornithopods, such as *Eolambia* and *Tenontosaurus,* have a very different pattern of growth. These taxa grow much more slowly throughout early ontogeny, than the large-bodied taxa.

Figures

FIGURE 3.3.1 MOR 609-89-82, H1

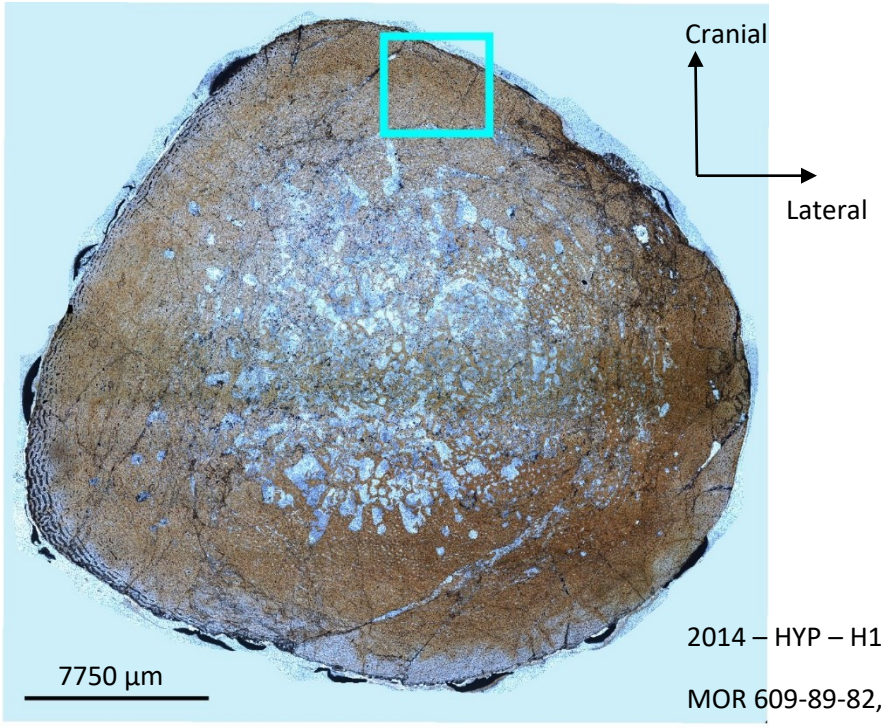

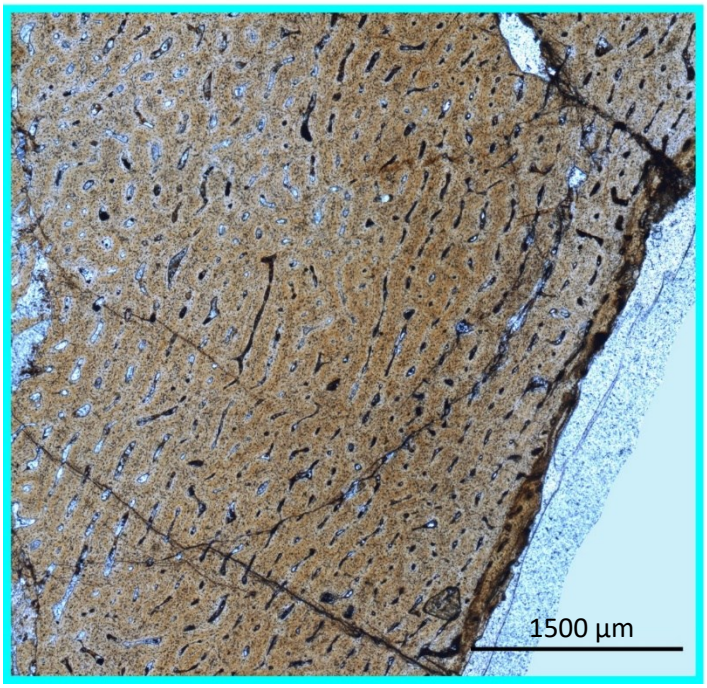

ABOVE: Image of cross section. Blue box shows location of close up image.

LEFT: Close-up image showing highly disorganized cortex, with no clear distinction between inner and outer cortex.

FIGURE 3.3.2 MOR 609-89-3, H2

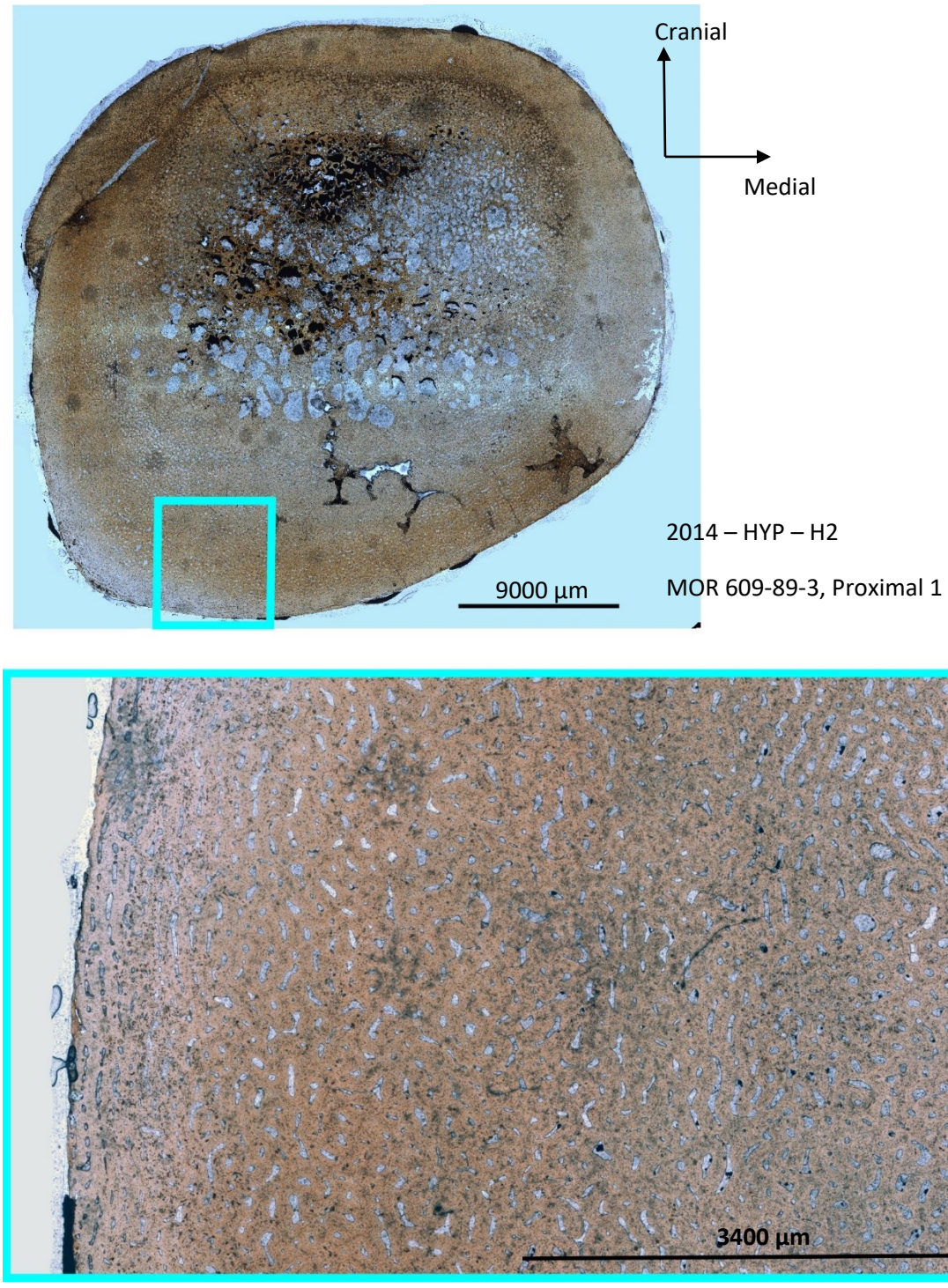

TOP: Image of cross section. Blue box shows location of close up image.

BOTTOM: Close-up image showing highly disorganized cortex, with no clear distinction between inner and outer cortex.

FIGURE 3.3.3 MOR 609-89-15, H3

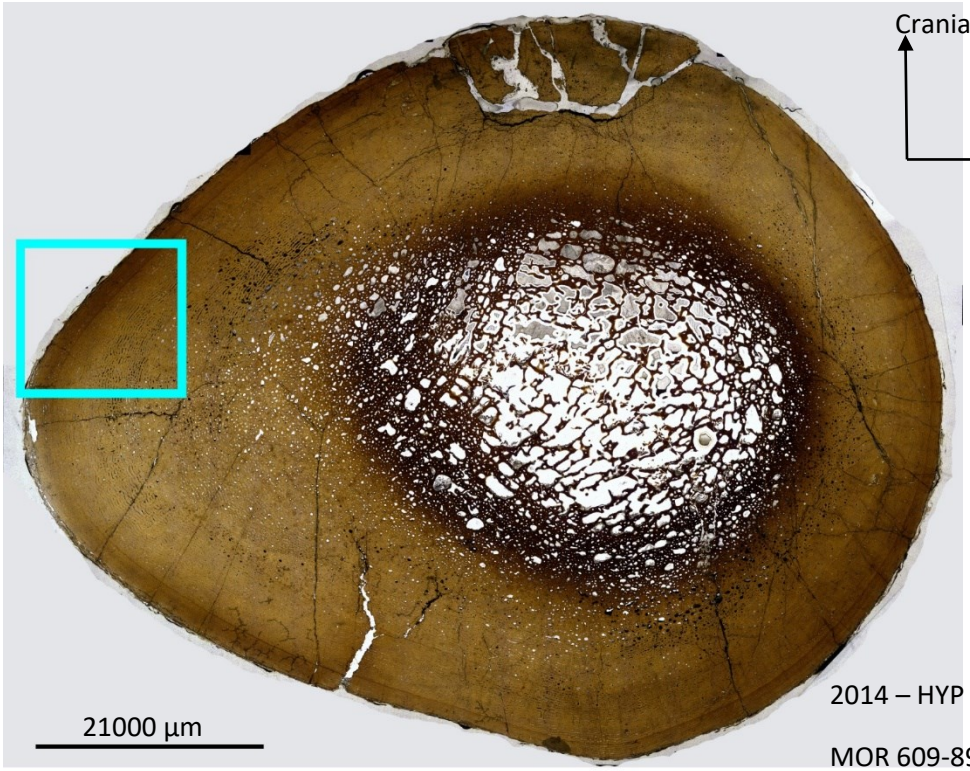

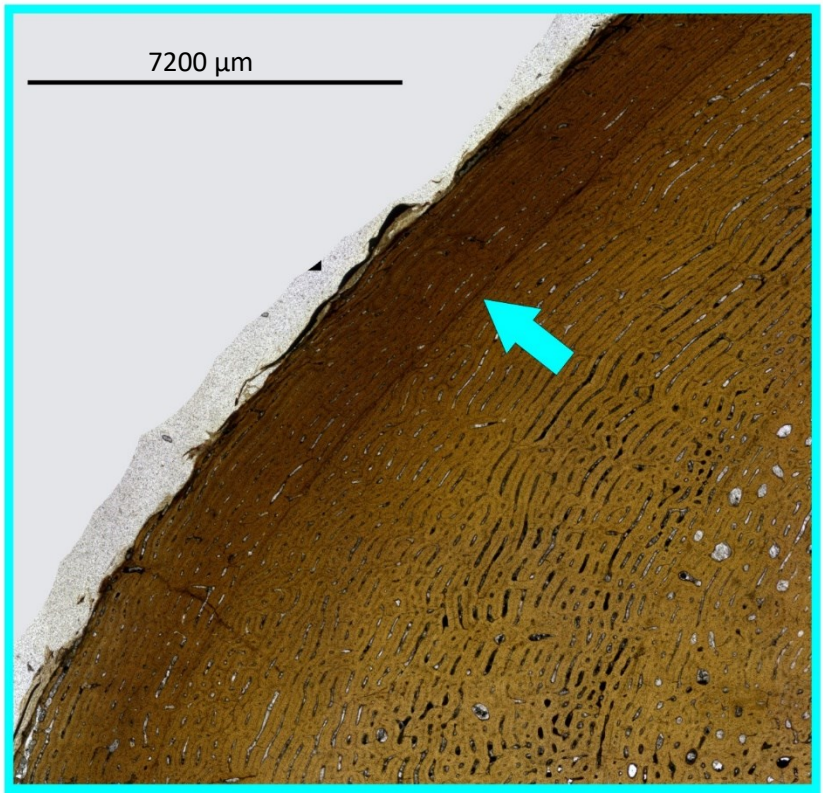

ABOVE: Image of cross section. Blue box shows location of close up image.

LEFT: Close-up image showing organized cortex; arrow indicate location of a LAG.

FIGURE 3.3.4 MOR-609-89-191, U1

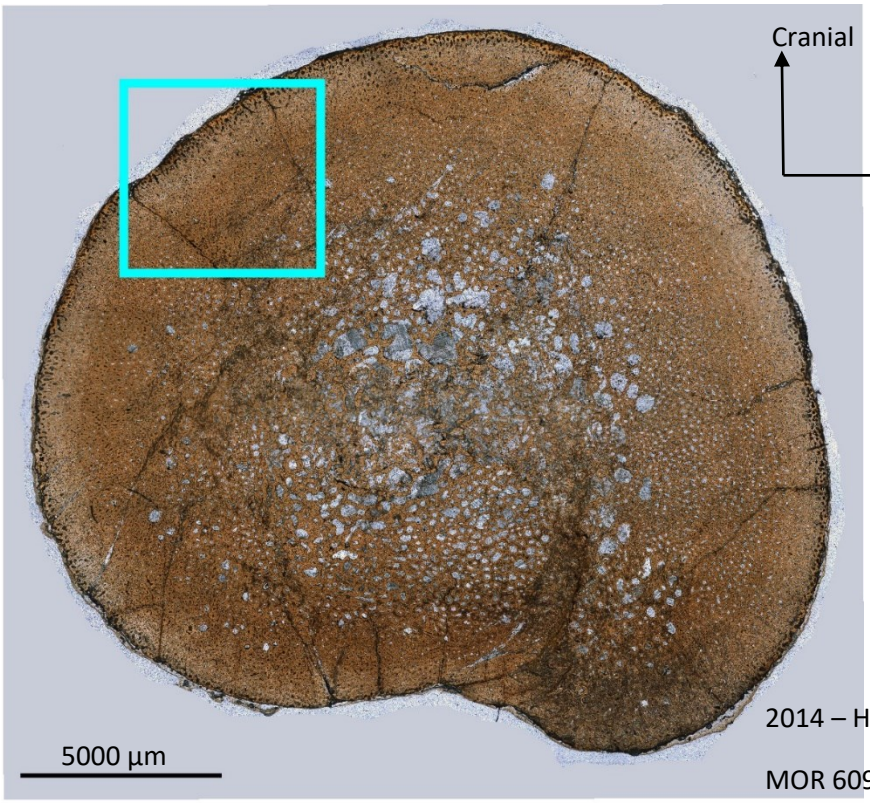

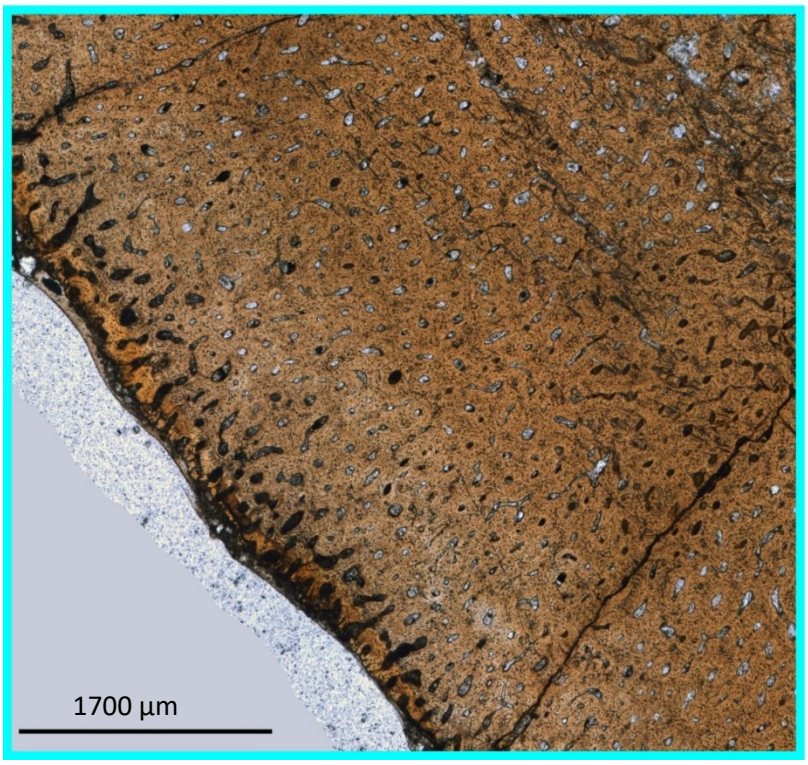

ABOVE: Image of cross section. Blue box shows location of close up image.

LEFT: Close-up image showing a highly diorganized cortex with no clear distinction between inner and outer cortex.

FIGURE 3.3.5 MOR 609-89-41, U2

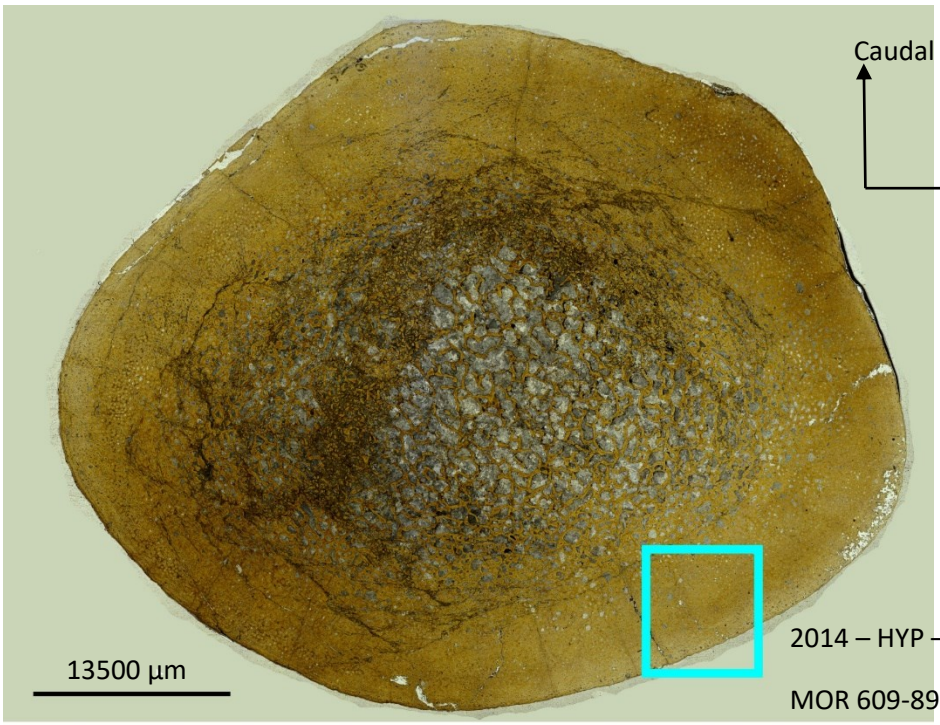

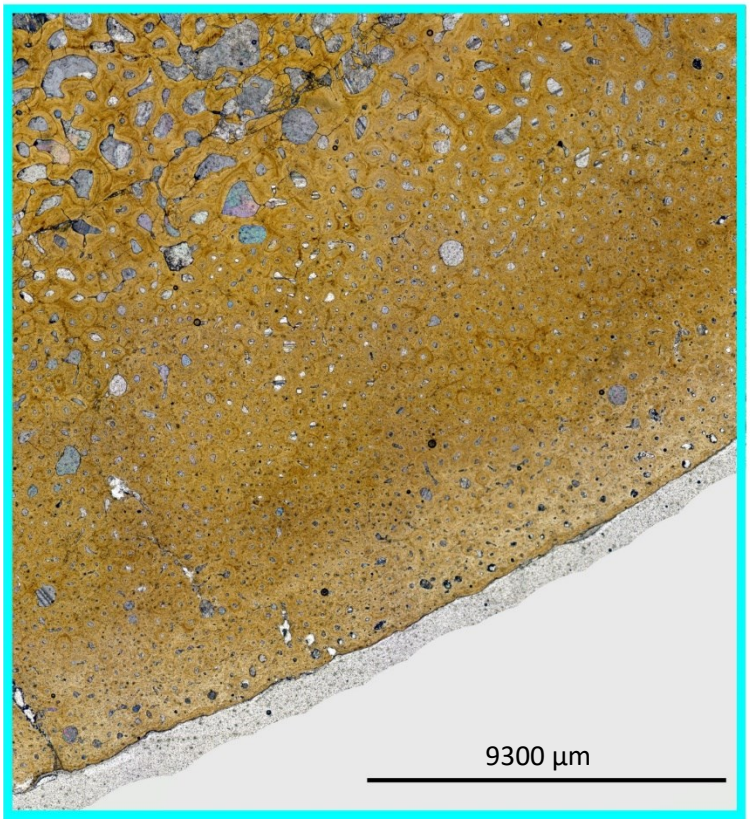

ABOVE: Image of cross section. Blue box shows location of close up image.

LEFT: Close-up image showing extensive secondary remodeling of the cortex.

FIGURE 3.3.6 MOR 609-89-111, U3

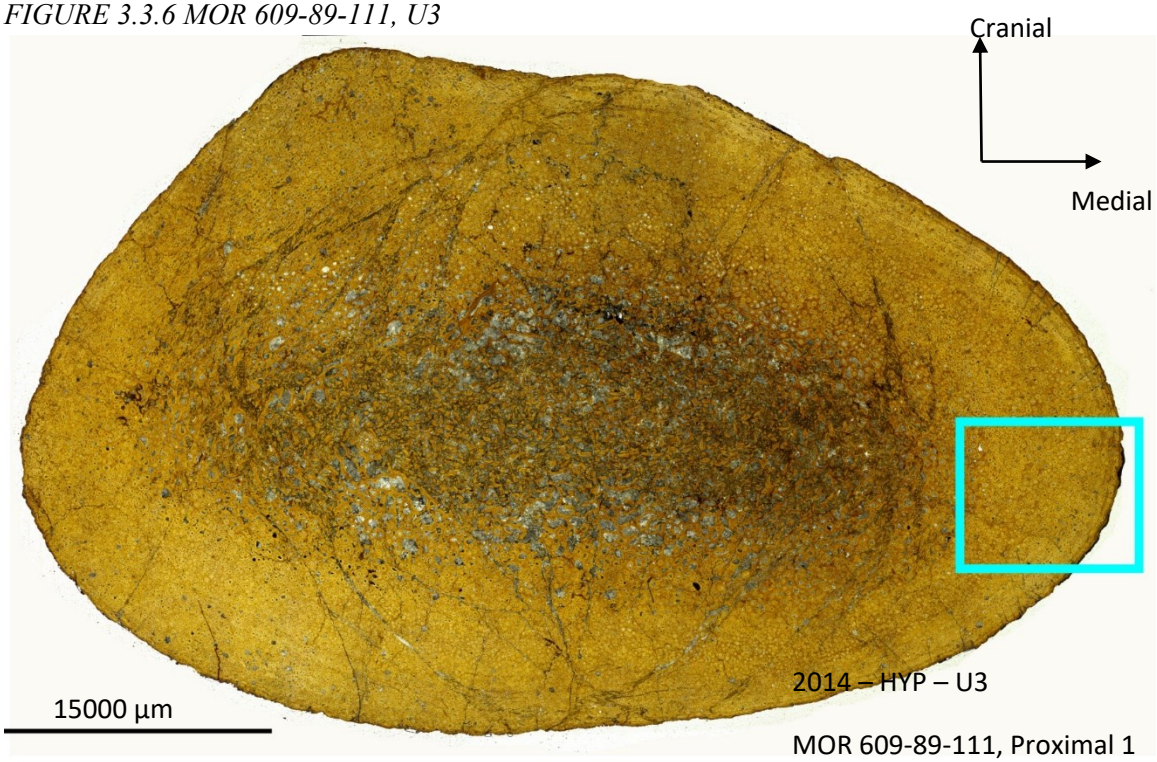

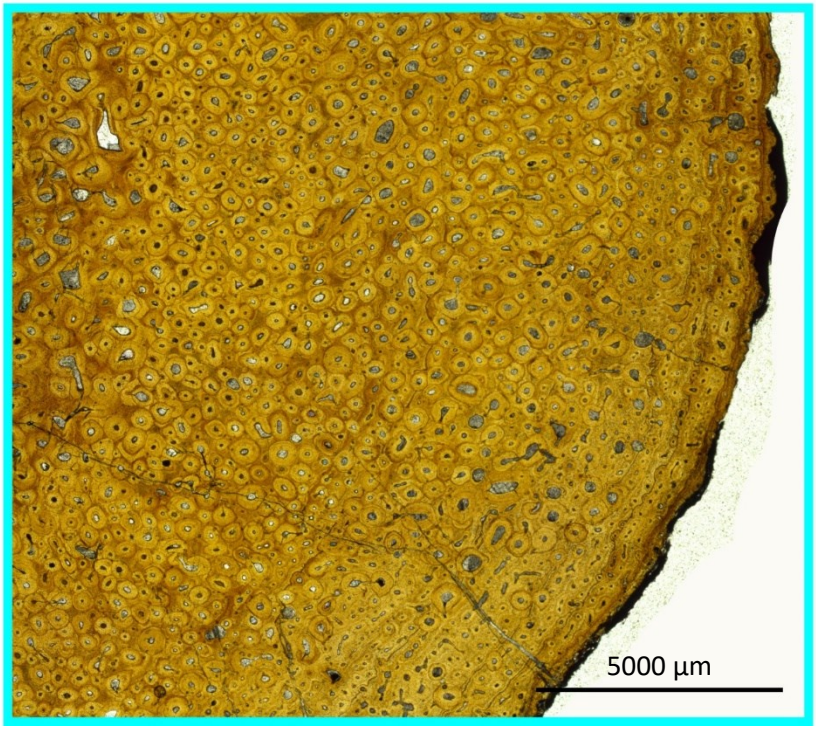

ABOVE: Image of cross section. Blue box shows location of close up image.

LEFT: Close-up image showing extensive secondary remodeling of the cortex.

FIGURE 3.3.7 MOR 609-89-173, F1

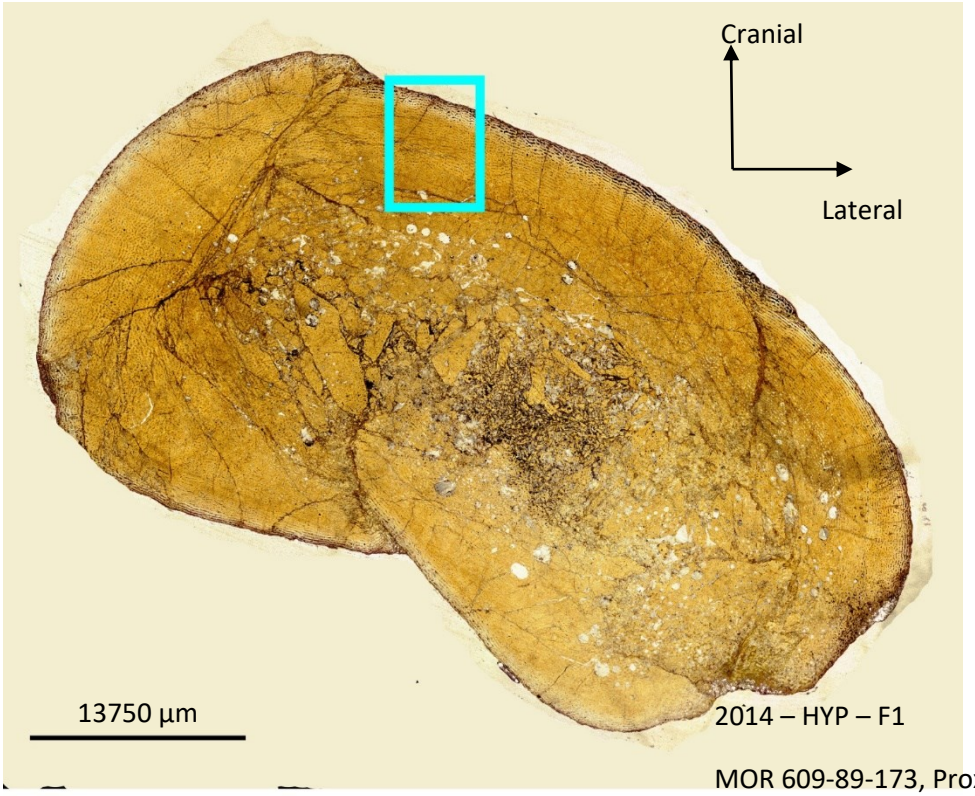

MOR 609-89-173, Proximal 1

ABOVE: Image of cross section. Blue box shows location of close up image.

LEFT: Close-up image showing distinction between the disorganized inner cortex and the organized outer cortex.

FIGURE 3.3.8 MOR 609-89-18, F2

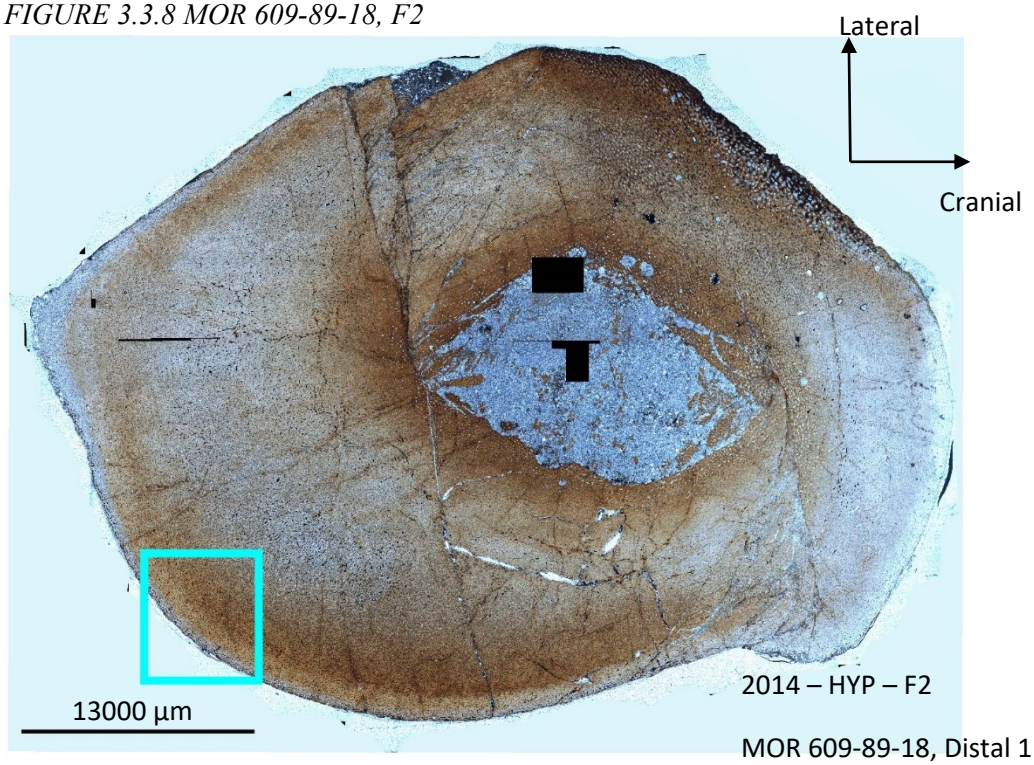

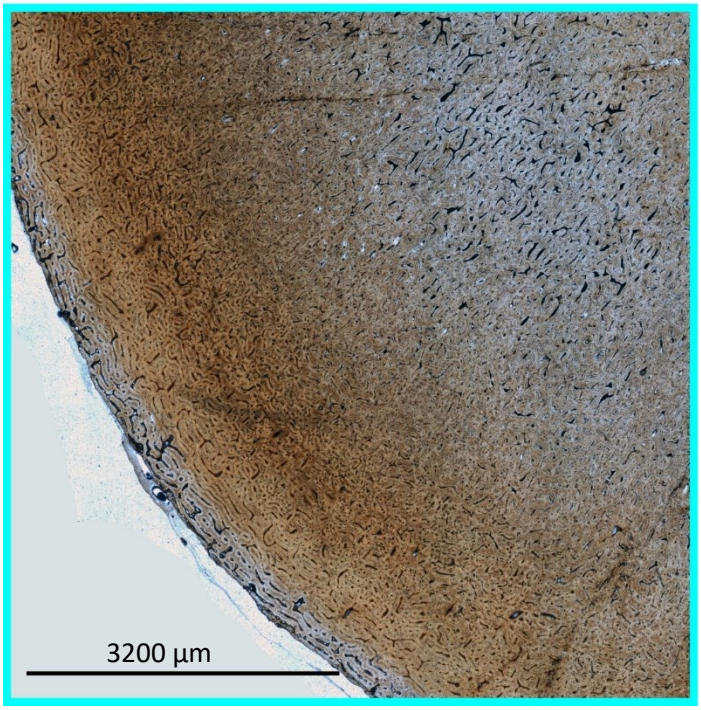

ABOVE: Image of cross section. Blue box shows location of close up image.

LEFT: Close-up image showing distinction between the disorganized inner cortex and the organized outer cortex.

FIGURE 3.3.9 MOR 609-89-43, F3

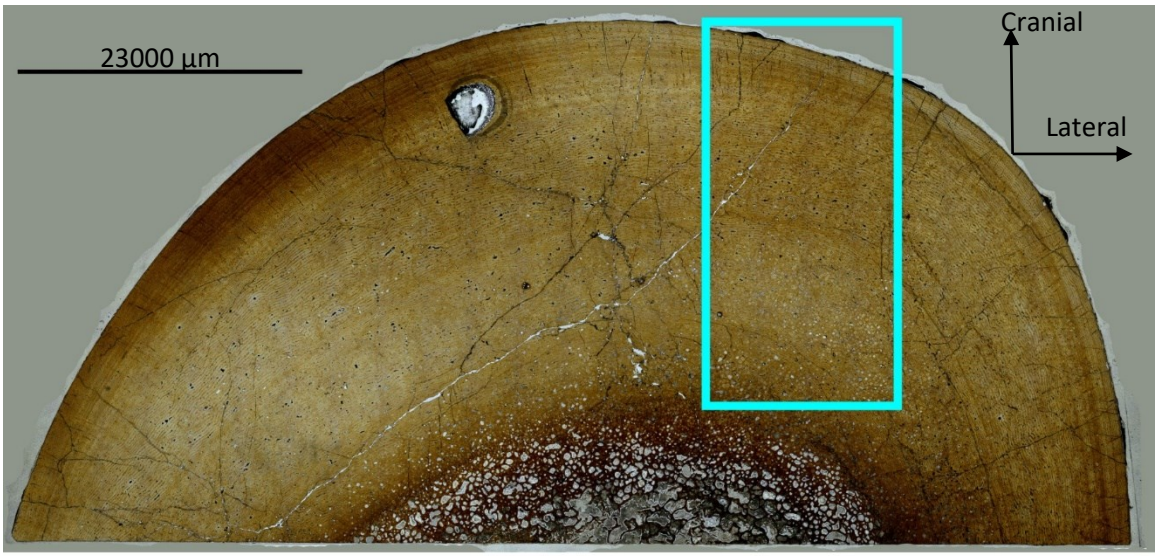

2014 – HYP – F3

MOR 609-89-43, Distal 1

ABOVE: Image of cross section. Blue box shows location of close up image.

LEFT: Close-up image, arrows show locations of 8 LAGs

FIGURE 3.3.10 MOR 609-89-145, T1

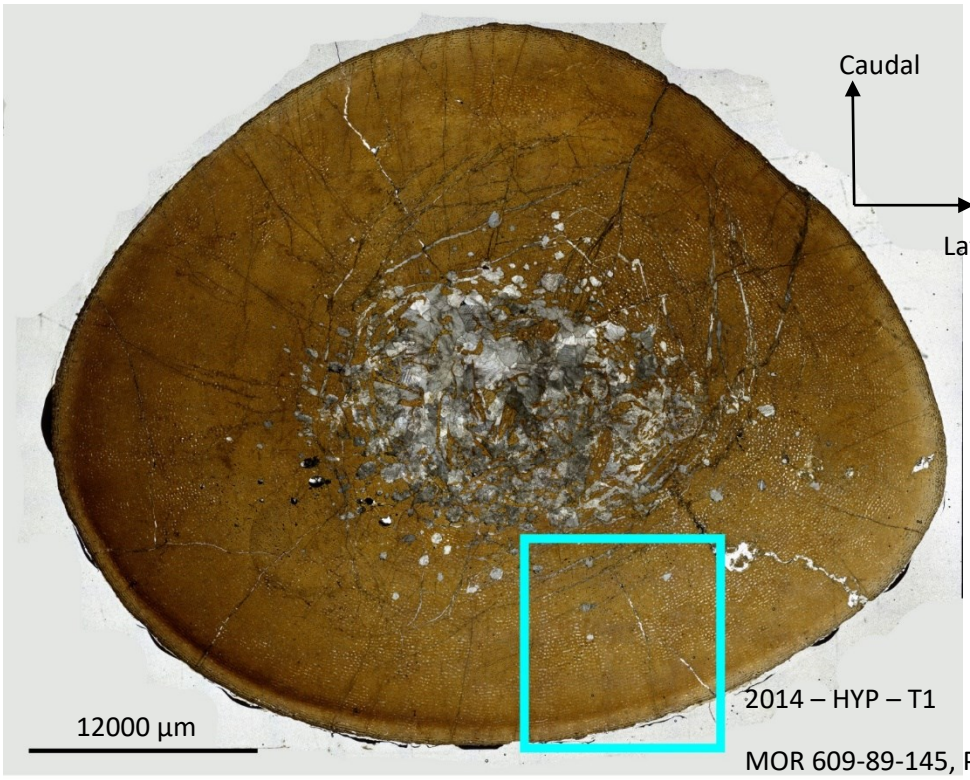

MOR 609-89-145, Proximal 1

ABOVE: Image of cross section. Blue box shows location of close up image.

LEFT: Close-up image showing disorganized inner and outer cortex.

FIGURE 3.3.11 MOR 609-89-195, T2

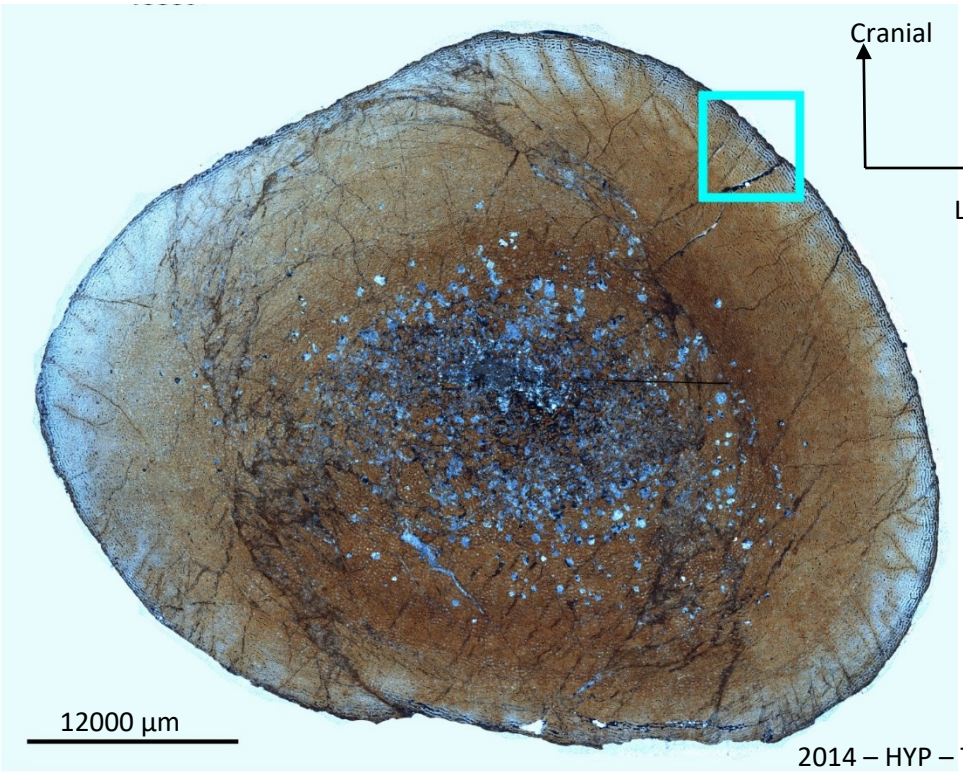

2014 – HYP – T2

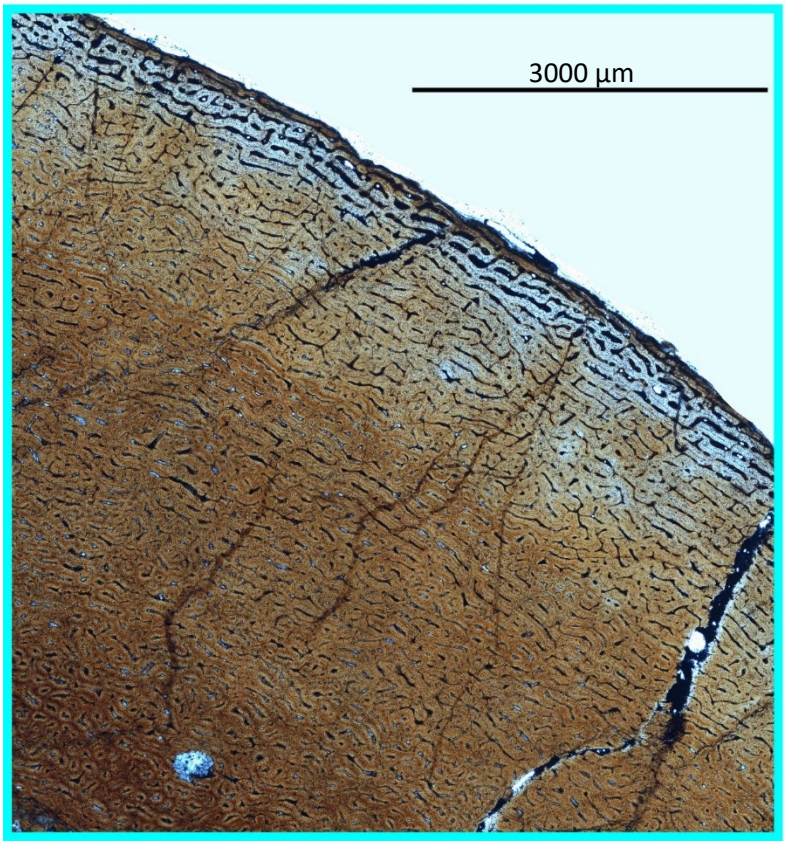

MOR 609-89-195, Distal 1

ABOVE: Image of cross section. Blue box shows location of close up image.

LEFT: Close-up image showing disorganized inner and outer cortex.

FIGURE 3.3.12 MOR 609-89-13, T3

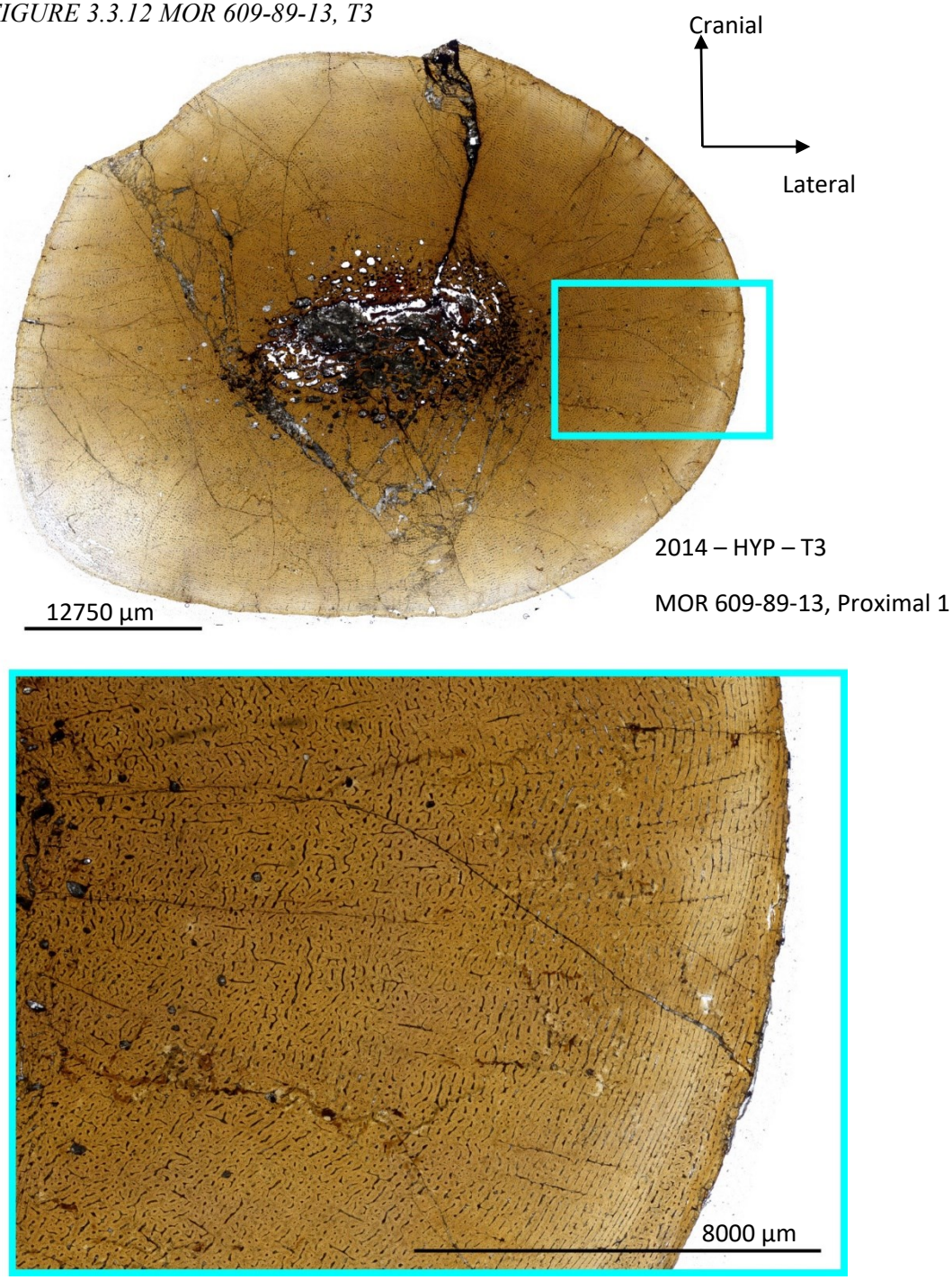

TOP: Image of cross section. Blue box shows location of close up image.

BOTTOM: Close-up image showing disorganized inner and outer cortex.

FIGURE 3.3.13 MOR 609-89-18, T4

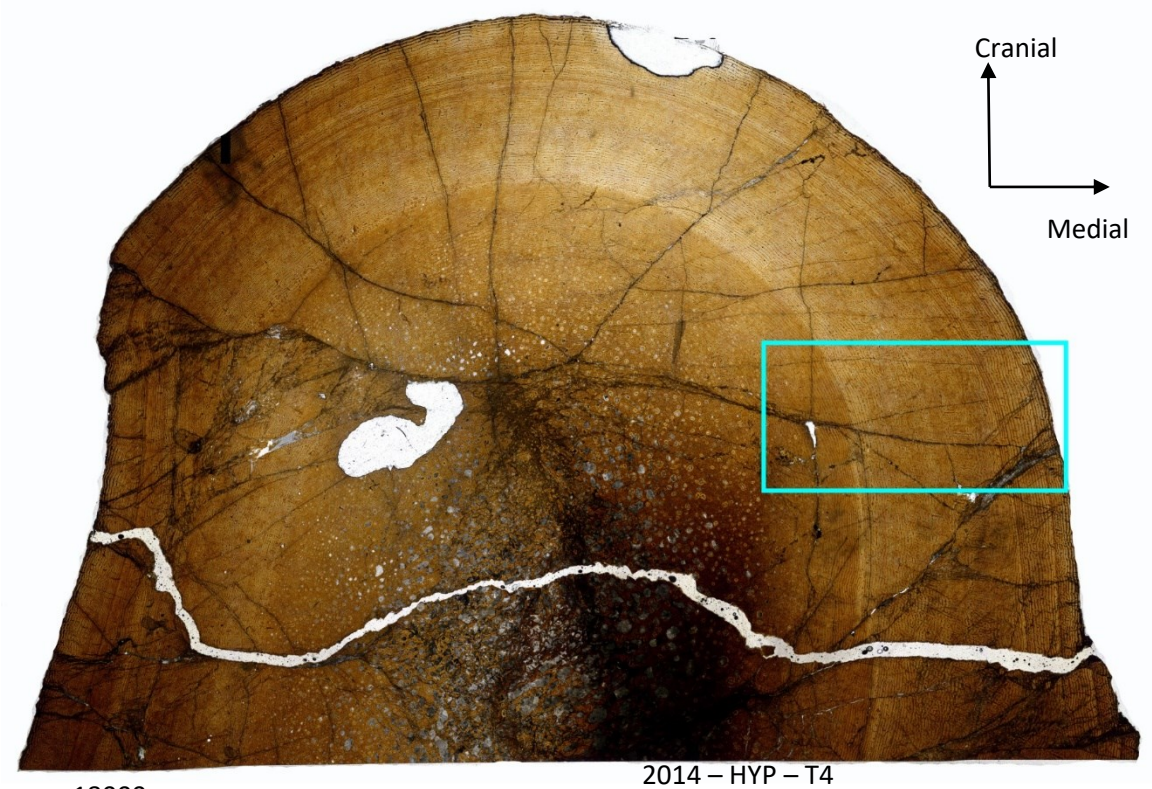

2014 – HYP – T4

MOR 609-89-18, Proximal 1

ABOVE: Image of cross section. Blue box shows location of close up image.

LEFT: Close-up image, arrows show locations of three LAGs.

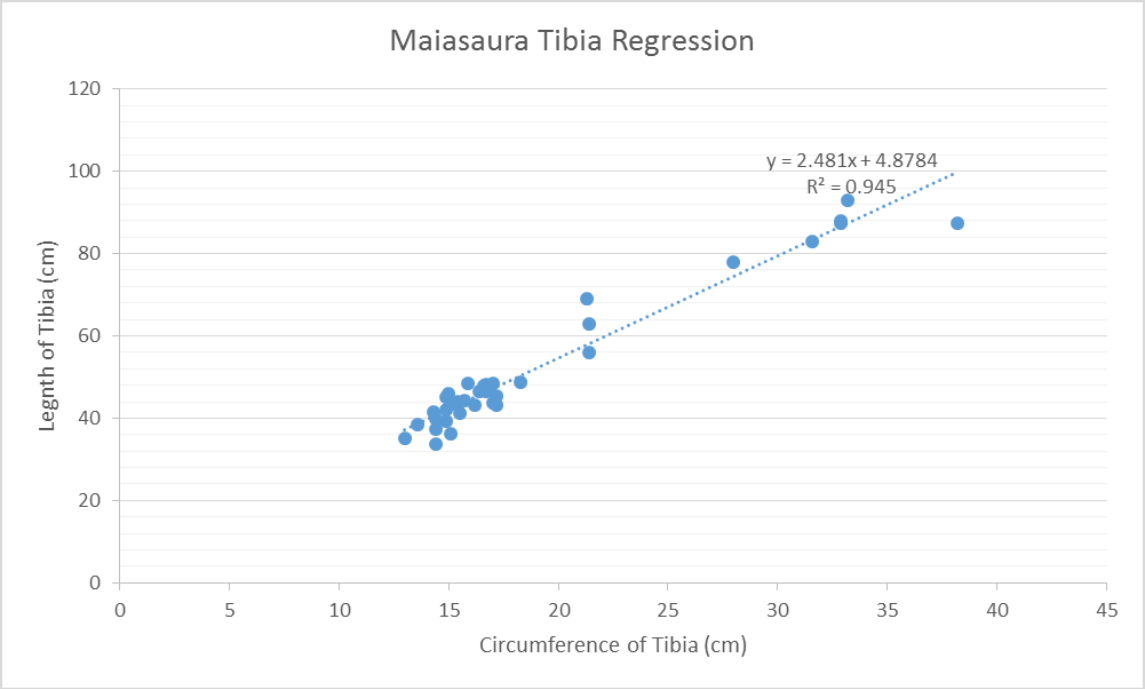

FIGURE 3.3.14 Linear Regression of Maiasaura Tibia Measurements. Data from Woodward et al (2015) was analyzed in the above regression. In total, measurements from 47 specimens were analyzed; 3 specimens were excluded as data for either total length or circumference was missing.This regression allows to estimate the total length of tibia for which only the circumference is available.

Tables

TABLE 3.3.1 Specimen List

Specimen Number	Study Code	Age Assessment	Element	Length (cm)	Least Circumference (cm)
MOR 609-89-82	H1	Juvenile	Humerus	26.4	9.7
MOR 609-89-3	H2	Juvenile	Humerus	22.6	11.8
MOR 609-89-15	H3	Subadult	Humerus	52.5	25.0
MOR 609-89-191	U1	Hatchling	Ulna	23.4	6.5
MOR 609-89-41	U2	Adult	Ulna	65.4	15.0
MOR 609-89-111	U3	Adult	Ulna	---	15.0
MOR 609-89-18	F1	Juvenile	Femur	35.6	14.5
MOR 609-89-173	F2	Juvenile	Femur	40.6	14.5
MOR 609-89-43	F3	Subadult	Femur	102.0	37.0
MOR 609-638-13	T1	Juvenile	Tibia	34.6	14.5
MOR 609-89-195	T2	Juvenile	Tibia	35.6	13.5
MOR 609-89-145	T3	Juvenile	Tibia	37.1	14.5
MOR 609-89-18	T4	Subadult	Tibia	75.0	28.0

TABLE 3.3.2 Cross-Section Measurements. The table above shows the minimum and maximum measurement of the cortex and medullary cavity for each specimen, as well as the average cortical thickness.

			Major and Minor Axis (mm)		Average Cortical
Specimen Number	Project Number	Element	Cortex	Medullary Cavity	Thickness (mm)
MOR 609-89-18	F1	Femur	56 x 30	36 x 15	5
MOR 609-89-173	F2	Femur	50 x 35	11 x 11	12
MOR 609-89-43	F3	Femur	117 x 90	35 x 22	20
MOR 609-638-13	T1	Tibia	51 x 42	14 x 12	6
MOR 609-89-195	T2	Tibia	41 x 35	20 x 14	6
MOR 609-89-145	T3	Tibia	50 x 38	15 x 8	6
MOR 609-89-18	T4	Tibia	82 x 73	22 x 20	23
MOR 609-89-82	H1	Humerus	31 x 27	15 x 15	4
MOR 609-89-3	H2	Humerus	37 x 34	20 x 15	6
MOR 609-89-15	H3	Humerus	80 x 63	42 x 25	10
MOR 609-89-191	U1	Ulna	19 x 17	6 x 6	3
MOR 609-89-41	U2	Ulna	55 x 44	37 x 24	5
MOR 609-89-111	U3	Ulna	58 x 35	35 x 15	5

TABLE 3.3.3 Quantitative Histology Measures The table above shows the PVD, OI and HRI values calculated for each specimen in the study. When the distinction between inner and outer cortex could be made, these regions were measured separately.

Specimen Number	AGMs	Percent Vascular Density	Obliquity Index	Haversian Remodelling Index
H1 Cortex	0	25%	20%	---
H2 Cortex	0	23%	18%	---
H3 Outer Cortex	1	13%	88%	
H3 Inner Cortex	1	---	---	86%
U1 Outer Cortex	0	---	---	---
U2 Outer Cortex	0	---	---	99%
U2 Inner Cortex	0	---	---	99%
U3 Outer Cortex	0	---	---	99%
U3 Inner Cortex	0	---	---	99%
F1 Outer Cortex	0	19%	68%	
F1 Inner Cortex	0	23%	13%	---
F2 Outer Cortex	0	17%	71%	
F2 Inner Cortex	0	22%	16%	---
F3 Outer Cortex		13%	86%	
F3 Inner Cortex	0	---	---	98%
T1 Outer Cortex	0	21%	30%	---
T1 Inner Cortex	0	23%	20%	---
T2 Outer Cortex	0	19%	43%	---
T2 Inner Cortex	0	23%	18%	---
T3 Outer Cortex	0	17%	22%	---
T3 Inner Cortex	0	21%	18%	< 5%
T4 Outer Cortex		9%	88%	< 5%
T4 Inner Cortex	0	---	---	98%

TABLE 3.3.4 AGM Body Size Estimates. The table above shows the estimated tibia and femur length at the time each AGM was laid down.

Specimen Number	Study Code	LAG	Circumference (cm)	Length of Tibia (cm)	Length of Femur (cm)
MOR 609-89-18	T4	1	16.2	45.1	46.5
		2	21.5	58.2	60.0
		3	25.0	66.9	68.9
MOR 609-89-43	F3	1	18.0	49.5	51.0
		2	31.0	81.8	84.2
		3	31.6	83.3	85.8
		4	32.8	86.3	88.8
		5	33.6	88.2	90.9
		6	34.4	90.2	92.9
		7	35.5	93.0	95.7
		8	36.5	95.4	98.3

4. Summary

There are now histologic ontogenetic sequences known for three iguanodontians (see Fig 1.2): *Tenontosaurus* (Werning, 2012), *Iguanacolossus* (considered above) and *Eolambia* (considered below) and two hadrosaurid (see Fig. 1.2): *Maiasaurus* (Woodward et al., 2015) and *Hypacrosaurus* (considered above).

All three iguanodontian taxa are similar in several respects. They are all large-bodied, with estimated adult body lengths of 6.5 to 9 m ((McDonald et al., 2012; McDonald et al., 2010; Werning, 2012). All three occur close together in the geologic record, between the Aptian and Albian, 124 to 100 Ma (Burton et al., 2006). They are found in very similar environments. *Tenontosaurus* is from the Cloverly and Antlers formation of the Western United States (Werning, 2012); these formations are largely composed of silty to sandy mudstones and have been interpreted as floodplain and strandplain environments (Forster, 1984; Hobday, 1981; Meyers et al., 1992; Ostrom, 1970). *Iguanacolossus* is from Lower Yellow Cat Member of the Cedar Mountain Formation (McDonald et al., 2010); this Member is composed of laminated mudstones with interbedded calcrete layers and has been interpreted as an alluvial floodplain environment (Kirkland et al., 1998). *Eolambia* is from the Mussentuchit Member of the Cedar Mountain Formation of Utah (Kirkland et al., 1998); this Member is composed of fining-upwards cycles of muddy sandstones to sandy mudstones and have been interpreted as poorly drained floodplains and/or lacustrine floodplains (Garrison Jr et al., 2007). They also all have similar taphonomies; juveniles and subadults are found in large assemblages, while adults are found as isolated specimens (*Eolambia*, Kirkland, 1998;

pers. comm. P. Makovicky; *Iguanacolossus*, pers. comm. J. Kirkland; *Tenontosaurus,* Forster, 1984).

Given all of these similarities, it would be reasonable to expect that all three taxa would also have similar growth patterns. In all three taxa, we find that AGMs do not occur until subadulthood. This is not surprising, given that when a specimen reaches subadult in these studies is determined, at least in part, by histologic features. However, the size at which subadulthood is reached and the first LAG (or annulus) is laid down in each taxon is different (Table 3.1.5).

With respect to *Tenontosaurus*, the smallest tibia to be diagnosed as subadult is OMNH 2926. This specimen is 14.5 cm in circumference and has five LAGs, two of which compose a double LAG. This is also the smallest specimen to have LAGs. The smallest femur to be diagnosed as a subadult is MOR 682. This is a partial specimen; the section is roughly half of the full circumference, and measures 7.4 cm (which would indicate that the full circumference would be approximately 15 cm). This specimen has three LAGs; the outermost LAG is close to the periosteal margin and is a double LAG. This is also the smallest specimen to have a LAG.

With respect to *Eolambia*, the smallest tibia to be diagnosed as subadult is CEUM 35386. This specimen is incomplete; its partial length is 20.1 cm and it has a least circumference of 9.2 cm. There are five LAGs, two of which compose a double LAG, in this specimen. This is also the smallest specimen to have LAGs. The smallest femur to be diagnosed as a subadult is CEUM 35443. This specimen is incomplete and distorted by post depositional crushing; it has a least circumference of 5.1 cm and a length of 31.8 cm. There are three LAGs, two of which compose a double LAG, in this

specimen. This is also the smallest specimen to have LAGs.

With respect to *Iguanacolossus*, none of the tibiae have LAGs. The two largest tibiae (T2, T3) are both subadults. T2 is 42.4 cm in length and has a least circumference of 15.6 cm; T3 is 48 cm in length and has a least circumference of 16.6 cm. A tibia from a similarly sized animal as that of the largest femur, would be 59.9 to 63.9 cm in length. The two largest femora (F3, F4) are both subadults. F3 is 48.3 cm in length and has a least circumference of 21.6 cm; F4 is 63.9 cm in length and has a least circumference of 30.0 cm. F4 is the only specimen to have LAGs; it has a single LAG near the periosteal margin.

Iguanacolossus is clearly reaching subadulthood and laying down the first LAG at a much larger body size than either *Eolambia* or *Tenontosaurus*. As seen above, this is more similar to the growth strategy of *Maiasaura*. However, *Eolambia* is more closely related to *Maiasaura* than either *Iguanacolossus* or *Tenontosaurus* (see Fig. 1.2). *Maiasaura* does have some life history traits in common with these iguanodontians. It is usually found either as assemblages of subadults and younger individuals, or as isolated adult specimens. *Maiasaura* does occur considerably later, during the late Campanian (~76 Ma). It is found in the middle Member of the Two Medicine Formation of Montana (Horner, 1983). This formation is composed of bentonitic siltstones and mudstones, with occasional sandstone lenses. It has been interpreted to be a coastal plain, although it several kilometers inland from the shoreline and much closer to the sediment source (Horner, 1983; Trexler, 2001). This is a very different environment than the environment in which any of the iguanodontians (discussed here) are found.

Hypacrosaurus, the other hadrosaurid for which an ontogenetic series is available, shares a similar growth strategy to *Maiasaura*, laying down the first LAG at a large body size and is usually found either as assemblages of subadults and younger individuals, or as isolated adult specimens. *Hypacrasaurus* also occurs during the late Cretaceous, during the early Maastrichtian (~66 Ma), in the St. Mary River Formation of Montana. This formation is dominated by channel sands and mudstones (Weishampel, pers. comm.). This is more similar to the inland environment of *Maiasaura*, than the near shore environments of the iguanodontians.

Museum Abbreviations

BYU: Brigham Young University Museum of Paleontology; Provo, Utah, USA

CEUM: Utah State University Eastern College Prehistoric Museum; Price, Utah, USA

CM: Carnegie Museum; Pittsburgh, Pennsylvania, USA

DMNS: Denver Museum of Nature and Science; Denver, Colorado, USA

FMNH: Field Museum of Natural History; Chicago, Illinois, USA

JHU: Johns Hopkins University; Baltimore, Maryland, USA

MOR: Museum of the Rockies; Bozeman, Montana, USA

MWC: Museum of Western Colorado; Fruita, Colorado, USA

RAM: Raymond M. Alf Museum of Paleontology; Claremont, California, USA

SMA: Sauriermuseum Aathal near Zurich, Switzerland; UC

OMNH: Sam Noble Oklahoma Museum of Natural History; Norman, Oklahoma, USA

UMNH: Natural History Museum of Utah; Salt Lake City, Utah, USA

Bibliography

Aguirre, J. I., L. I. Plotkin, S. A. Stewart, R. S. Weinstein, A. M. Parfitt, S. C. Manolagas, and T. Bellido. 2006. Osteocyte Apoptosis Is Induced by Weightlessness in Mice and Precedes Osteoclast Recruitment and Bone Loss. Journal of Bone and Mineral Research 21(4): 605-615. doi:10.1359/jbmr.060107

Anderson, John F., A. Hall-Martin, and D. A. Russell. 1985. Long-bone circumference and weight in mammals, birds and dinosaurs. Journal of Zoology 207(1):53-61.

Andrade, J. M., and M. G. Estévez-Pérez. 2014. Statistical comparison of the slopes of two regression lines: a tutorial. Analytica chimica acta 838:1-12.

Angilletta, J. M. J., T. D. Steury, and M. W. Sears. 2004. Temperature, Growth Rate, and Body Size in Ectotherms: Fitting Pieces of a Life-History Puzzle. Integrative and Comparative Biology 44(6):498-509.

Ashley, L. M. 1975. Comparative fish histology. Paper presented at the The Pathology of Fishes: Proceedings of a Symposium.

Averbeck, C., A. Apio, M. Plath, and T. Wronski. 2010. Hunting differentially affects mixed-sex and bachelor-herds in a gregarious ungulate, the impala (Aepyceros melampus: Bovidae). African Journal of Ecology 48(1):255-264.

Bakker, R. T., and M. Williams. 1988. Nanotyrannus, a new genus of pygmy tyrannosaur, from the latest Cretaceous of Montana. Hunteria 1(5):1.

Baron, M. G., D. B. Norman, and P. M. Barrett. 2017. A new hypothesis of dinosaur relationships and early dinosaur evolution. Nature 543(7646):501-506.

Barrett, P. M., R. J. Butler, and F. Knoll. 2005. Small-bodied ornithischian dinosaurs from the Middle Jurassic of Sichuan, China. Journal of Vertebrate Paleontology 25(4):823-834.

Becerra, Marcos G., D. Pol, O. W. M. Rauhut, and I. A. Cerda. 2016. New heterodontosaurid remains from the Cañadón Asfalto Formation: cursoriality and the functional importance of the pes in small heterodontosaurids. Journal of Paleontology 90(3):555-577.

Bell, P. R. 2011. Cranial osteology and ontogeny of Saurolophus angustirostris from the Late Cretaceous of Mongolia with comments on Saurolophus osborni from Canada. Acta Palaeontologica Polonica 56(4):703-722.

Bety, J., G. Gauthier, and J. F. Giroux. 2003. Body Condition, Migration, and Timing of Reproduction in Snow Geese: A Test of the Condition-Dependent Model of Optimal Clutch Size. The American Naturalist 162(1):110-121. doi:10.1086/375680

Botha, J., and A. Chinsamy. 2001. Growth patterns deduced from the bone histology of the cynodonts Diademodon and Cynognathus. Journal of Vertebrate Paleontology 20(4):705-711.

Bourdon, E., J. Castanet, A. De Ricqlès, P. Scofield, A. Tennyson, H. Lamrous, and J. Cubo. 2009. Bone growth marks reveal protracted growth in New Zealand kiwi (Aves, Apterygidae). Biology Letters 5(5):639-642.

Boyd, C. A. 2015. The systematic relationships and biogeographic history of ornithischian dinosaurs. PeerJ, 3, e1523.

Brink, K. S., D. K. Zelenitsky, D. C. Evans, F. Therrien, and J.R. Horner. 2011. A sub-adult skull of *Hypacrosaurus stebingeri* (Ornithischia: Lambeosaurinae): anatomy and comparison. Historical Biology 23(1):63-72. doi:10.1080/08912963.2010.499169

Brinkman, D. B., D. A. Eberth, P. J. Currie, R. Rogers, D. Eberth, and A. Fiorillo. 2007. From bonebeds to paleobiology: applications of bonebed data. In R. R. Rogers, D. A. Eberth, and A. R. Fiorillo (Ed), Bonebeds: genesis, analysis, and paleobiological significance. University of Chicago Press, Chicago and London, pp. 221-264.

Brown, C. M., D. C. Evans, M. J. Ryan, and A. P. Russell. 2013. New data on the diversity and abundance of small-bodied ornithopods (Dinosauria, Ornithischia) from the Belly River Group (Campanian) of Alberta. Journal of Vertebrate Paleontology 33(3):495-520. doi:10.1080/02724634.2013.746229

Brochu, C. A. 1996. Closure of neurocentral sutures during crocodilian ontogeny: implications for maturity assessment in fossil archosaurs. Journal of Vertebrate Paleontology 16(1):49-62.

Brusatte, S. L., T.D. Carr, T. E. Williamson, T. R. Holtz, D. W. Hone, and S. A. Williams. 2016. Dentary groove morphology does not distinguish 'Nanotyrannus' as a valid taxon of tyrannosauroid dinosaur. Comment on "Distribution of the dentary groove of theropod dinosaurs: Implications for theropod phylogeny and the validity of the genus Nanotyrannus Bakker et al., 1988". Cretaceous Research 65:232-237.

Burton, D., B. W. Greenhalgh, B. B. Britt, B. J. Kowallis, and W. Elliot. 2006. New radiometric ages from the Cedar Mountain Formation, Utah and the Cloverly Formation, Wyoming: implications for contained dinosaur faunas. Paper presented at the Geological Society of America Annual Meeting: Philadelphia.

Butler, R. J., P. M. Galton, L. B. Porro, L. M. Chiappe, D. M. Henderson, and G. M. Erickson. 2010. Lower limits of ornithischian dinosaur body size inferred from a new Upper Jurassic heterodontosaurid from North America. Proceedings of the Royal Society of London B: Biological Sciences 277(1680):375-381.

Butler, R. J., P. Upchurch, and D. B. Norman. 2008. The phylogeny of the ornithischian dinosaurs. Journal of Systematic Palaeontology 6(01):1-40.

Bybee, P. J., A. H. Lee, and E. T. Lamm. 2006. Sizing the Jurassic theropod dinosaur Allosaurus: assessing growth strategy and evolution of ontogenetic scaling of limbs. Journal of Morphology 267(3):347-359.

Callison, G., and M. Q. Helen. 1984. Tiny Dinosaurs: Are They Fully Grown? Journal of Vertebrate Paleontology 3(4):200-209.

Campione, N., K. Brink, E. Freedman, C. McGarrity, and D. Evans. 2013. 'Glishades ericksoni', an indeterminate juvenile hadrosaurid from the Two Medicine Formation of Montana: implications for hadrosauroid diversity in the latest Cretaceous (Campanian-Maastrichtian) of western North America. Palaeobiodiversity and Palaeoenvironments 93(1):65-75. doi:10.1007/s12549-012-0097-1

Campione, N. E., and D. C. Evans. 2011. Cranial growth and variation in edmontosaurs (Dinosauria: Hadrosauridae): implications for latest Cretaceous megaherbivore diversity in North America. PLoS ONE 6(9):e25186.

Carpenter, Kenneth. 1999 Eggs, nests, and baby dinosaurs: a look at dinosaur reproduction. Indiana University Press, Bloomington and Indianapolis, Indiana, 341 pp.

Case, J. A., J. E. Martin, D. S. Chaney, M. Reguero, S. A. Marenssi, S. M. Santillana, and M. O. Woodburne. 2000. The first duck-billed dinosaur (Family Hadrosauridae) from Antarctica. Journal of Vertebrate Paleontology 20(3):612-614.

Case, T. J. 1978. Speculations on the Growth Rate and Reproduction of Some Dinosaurs. Paleobiology 4(3):320-328. doi:10.2307/2400208

Castanet, J. 1994. Age estimation and longevity in reptiles. Gerontology 40(2-4):174-192.

Castanet, J., H. Francillon-Vieillot, and F. J. Meunier. 1993. Bone and Individual Aging. In B. K. Hall (Ed.), Bone (Vol. 7, pp. 245-283). CRC Press, Boca Raton, FL.

Castanet, J., K. C. Rogers, J. Cubo, and J. Jacques-Boisard. 2000. Periosteal bone growth rates in extant ratites (ostriche and emu). Implications for assessing growth in dinosaurs. Comptes Rendus de l'Académie des sciences-Series III-Sciences de la Vie 323(6):543-550.

Castanet, J., S. Croci, F. Aujard, M. Perret, J. Cubo, and E. D. Margerie. 2004. Lines of arrested growth in bone and age estimation in a small primate: Microcebus murinus. Journal of Zoology, 263(1):31-39.

Chapman, R. E., D. Weishampel, G. Hunt, and D. Rasskin-Gutman. 1997. Sexual dimorphism in dinosaurs. Paper presented at the Dinofest international, proceedings of a symposium sponsored by Arizona State University.

Chinnery, B. J. 2001. Morphometric Analysis of Evolution and Growth in the Ceratopsian Postcranial Skeleton. Journal of Vertebrate Paleontology 24(3):591-609.

Chinsamy-Turan, A. 2005. The microstructure of dinosaur bone: deciphering biology with fine-scale techniques: Johns Hopkins University Press, Baltimore, Maryland, 216 pp.

Chinsamy, A. 1990. Physiological implications of the bone histology of Syntarsus rhodesiensis (Saurischia: Theropoda). Paleontologia Africana 27:77-82.

Chinsamy, A. 1993. Bone histology and growth trajectory of the prosauropod dinosaur Massospondylus carinatus Owen. Modern Geology 18(3):319-329.

Chinsamy, A. 1995. Ontogenetic Changes in the Bone Histology of the Late Jurassic Ornithopod Dryosaurus lettowvorbecki. Journal of Vertebrate Paleontology 15(1):96-104. doi:10.2307/4523608

Chinsamy, A. 1997. Assessing the biology of fossil vertebrates through bone histology. Paleontolgia Africanan 33:29-35.

Chinsamy, A., and A. Elzanowski. 2001. Bone histology: evolution of growth pattern in birds. Nature 412(6845):402-403.

Church, L. E., and L. C. Johnson. 1964. Growth of long bones in the chicken. Rates of growth in length anddi ameter of the humerus, tibia, and metatarsus. American Journal of Anatomy 114(3):521-538.

Cifelli, R. L., J. I. Kirkland, A. Weil, A. L. Deino, and B. J. Kowallis. 1997. High-precision 40Ar/39Ar geochronology and the advent of North America's Late Cretaceous terrestrial fauna. Proceedings of the National Academy of Sciences 94(21):11163-11167.

Cifelli, R. L., R. L. Nydam, J. D. Gardner, A. Weil, J. G. Eaton, J. I. Kirkland, S. K. Madsen. 1999 Medial Cretaceous vertebrates from the Cedar Mountain Formation, Emery County, Utah: the Mussentuchit local fauna. Vertebrate Paleontology in Utah 99(1):219-242.

Coombs, W. P., Jr. 1978. Theoretical aspects of cursorial adaptations in dinosaurs. Q. Rev. Biol. 53:393-418.

Cooper, L. N., A. H. Lee, M. L. Taper, J. R. Horner. 2008. Relative growth rates of predator and prey dinosaurs reflect effects of predation. Proceedings of the Royal Society of London B: Biological Sciences 275(1651):2609-2615.

Coria, R. A., and L. Salgado. 1996. A basal iguanodontian (Ornithischia: Ornithopoda) from the Late Cretaceous of South America. Journal of Vertebrate Paleontology 16(3):445-457.

Cox, R. M., M. A. Butler, H. B. John-Alder. 2007. The evolution of sexual size dimorphism in reptiles. In D. J. Fairbairn, W. U. Blackenhorn, and T. Szekely (Ed), Sex, size and gender roles: evolutionary studies of sexual size dimorphism (pp. 38-49), Oxford University Press, Oxford.

Cruzado-Caballero, P., and J. I. Canudo. 2015. Presence of diminutive hadrosaurids (Dinosauria: Ornithopoda) in the Maastrichtian of the south-central Pyrenees (Spain). Journal of Iberian Geology 41(1):71.

Cubo, J., F. Ponton, M. Laurin, E. De Margerie, and J. Castanet. 2005. Phylogenetic signal in bone microstructure of sauropsids. Systematic Biology 54(4):562-574.

Currey, J. 2003. The many adaptations of bone. Journal of biomechanics 36(10):1487-1495.

Currie, P. J., J. H. Hurum, and K. Sabath. 2003. Skull structure and evolution in tyrannosaurid dinosaurs. Acta Palaeontologica Polonica 48(2).

Dalla Vecchia, F. M. 2009. Tethyshadros insularis, a new hadrosauroid dinosaur (Ornithischia) from the Upper Cretaceous of Italy. Journal of Vertebrate Paleontology 29(4):1100-1116.

Davies, S. J., and M. Bamford. 2002. Ratites and Tinamous: Tinamidae, Rheidae, Dromaiidae, Casuariidae, Apterygidae, Struthionidae. Oxford University Press, New York, 310 pp.

De Boef, M., and H. Larsson. 2007. Bone microstructure: quantifying bone vascular orientation. Canadian Journal of Zoology 85(1):63-70.

De Buffrénil, V., and J. Castanet. 2000. Age estimation by skeletochronology in the Nile monitor (*Varanus niloticus*), a highly exploited species. Journal of Herpetology 34(3):414-424. doi:10.2307/1565365

De Ricqlès, A. 1976. On bone histology of fossil and living reptiles, with comments on its functional and evolutionary significance. Morphology and biology of reptiles 3:123-149.

De Ricqlès, A. D. 1980. Tissue structures of dinosaur bone: functional significance and possible relation to dinosaur physiology. Paper presented at the A cold look at the warm-blooded dinosaurs. AAAS Selected Symposium.

De Ricqlès, A. J., K. Padian, and J. R. Horner. 2003. On the bone histology of some Triassic pseudosuchian archosaurs and related taxa. Annales de Paléontologie 89(2).

De Ricqlès, A., K. Padian, F. Knoll, and J. R. Horner. 2008. On the origin of high growth rates in archosaurs and their ancient relatives: Complementary histological studies on Triassic archosauriforms and the problem of a "phylogenetic signal" in bone histology. Paper presented at the Annales de Paléontologie.

Dean, D. R. 1999. Gideon Mantell and the discovery of dinosaurs. Cambridge University Press, 312 pp.

Dodson, P. 1975. Taxonomic Implications of Relative Growth in Lambeosaurine Hadrosaurs. Systematic Zoology, 24(1):37-54. doi:10.2307/2412696

Dodson, P. 1976. Quantitative aspects of relative growth and sexual dimorphism in Protoceratops. Journal of Paleontology 50(5):929-940.

Dodson, P. 1980. Comparative osteology of the American ornithopods *Camptosaurus* and *Tenontosaurus*. Mémoires de la Société géologique de France 139:81-85.

Erickson, G. 1996. Incremental lines of von Ebner in dinosaurs and the assessment of tooth replacement rates using growth line counts. Proceedings of the National Academy of Sciences 93(25):14623-14627.

Erickson, G. M. 2005. Assessing dinosaur growth patterns: a microscopic revolution. Trends in Ecology & Evolution 20(12):677-684.

Erickson, G. M., P. J. Makovicky, P. J. Currie, M. A. Norell, S. A. Yerby, and C. A. Brochu. 2004. Gigantism and comparative life-history parameters of tyrannosaurid dinosaurs. Nature 430:772-775. doi:10.1038/nature02699

Erickson, G. M., K C. Rogers, D. J. Varricchio, M. A. Norell, X. Xu. 2007. Growth patterns in brooding dinosaurs reveals the timing of sexual maturity in non-avian dinosaurs and genesis of the avian condition. Biology Letters 3(5): 558-561.

Erickson, G. M., and T. A. Tumanova. 2000. Growth curve of *Psittacosaurus mongoliensis* Osborn (Ceratopsia: Psittacosauridae) inferred from long bone histology. Zoological Journal of the Linnean Society 130(4):551-566.

Evans, D. C. 2007. Ontogeny and evolution of lambeosaurine dinosaurs (Ornithischia: Hadrosauridae. PhD Thesis, Universtiy of Toronto.

Evans, D. C. 2010. Cranial anatomy and systematics of Hypacrosaurus altispinus, and a comparative analysis of skull growth in lambeosaurine hadrosaurids (Dinosauria: Ornithischia). Zoological Journal of the Linnean Society 159(2):398-434. doi:10.1111/j.1096-3642.2009.00611.x

Evans, D. C., D. A. Eberth, M. J. Ryan, and F. Therrien. 2015. Hadrosaurid (*Edmontosaurus*) bonebeds from the Horseshoe Canyon Formation (Horsethief Member) at Drumheller, Alberta, Canada: geology, preliminary taphonomy, and significance. Canadian Journal of Earth Sciences 52(8):642-654.

Evans, D. C., and R. R. Reisz. 2007. Anatomy and Relationships of *Lambeosaurus magnicristatus*, a Crested Hadrosaurid Dinosaur (Ornithischia) from the Dinosaur Park Formation, Alberta. Journal of Vertebrate Paleontology 27(2):373-393. doi:10.2307/30126306

Evans, D. C., R. Ridgely, and L. M. Witmer. 2009. Endocranial anatomy of lambeosaurine hadrosaurids (Dinosauria: Ornithischia): a sensorineural perspective on cranial crest function. The Anatomical Record 292(9):1315-1337.

Farke, A. A. 2014. Evaluating combat in ornithischian dinosaurs. Journal of Zoology 292(4):242-249.

Farke, A. A., D. J. Chok, A. Herrero, B. Scolieri, and S. Werning. 2013. Ontogeny in the tube-crested dinosaur *Parasaurolophus* (Hadrosauridae) and heterochrony in hadrosaurids. PeerJ 1:e182.

Fitzhugh, H. 1976. Analysis of growth curves and strategies for altering their shape. Journal of Animal Science 42(4):1036-1051.

Forster, C. A. 1984. The paleoecology of the ornithopod dinosaur *Tenontosaurus tilletti* from the Cloverly Formation, Big Horn Basin of Wyoming and Montana. The Mosasaur 2:151-163.

Forster, C. A. 1990. Evidence for juvenile groups in the ornithopod dinosaur *Tenontosaurus tilletti* Ostrom. Journal of Paleontology 64(01):164-165.

Forster, C. A. 1990. The Postcranial Skeleton of the Ornithopod Dinosaur *Tenontosaurus tilletti*. Journal of Vertebrate Paleontology 10(3):273-294. doi:10.2307/4523326

Foster, J. 1966. The giraffe of Nairobi National Park: home range, sex ratios, the herd, and food. African Journal of Ecology 4(1):139-148.

Fowler, E. A. F., and J. R. Horner. 2015. A New Brachylophosaurin Hadrosaur (Dinosauria: Ornithischia) with an Intermediate Nasal Crest from the Campanian Judith River Formation of Northcentral Montana. PLoS ONE, 10(11):e0141304.

Fowler, M. E. 1991. Comparative Clinical Anatomy of Ratites. Journal of Zoo and Wildlife Medicine 22(2):204-227. doi:10.2307/20095143

Francillon-Vieillot, H., et al. "Microstructure and mineralization of vertebrate skeletal tissues." *Skeletal biomineralization: patterns, processes and evolutionary trends* (1990): 175-234.

Galton, P. and J. Jensen. 1979. Remains of ornithopod dinosaurs from the Lower Cretaceous of North America. Brigham Young University Geology Studies 25(1):1-10.

Galton, P. 1983. The cranial anatomy of Dryosaurus, a hypsilophodontid dinosaur from the Upper Jurassic of North America and East Africa, with a review of hypsilophodontids from the Upper Jurassic of North America. Geologica et Palaeontologica 17:207-243.

Garrison Jr, J. R., D. Brinkman, D. J. Nichols, P. Layer, D. Burge, and D. Thayn. 2007. A multidisciplinary study of the Lower Cretaceous Cedar Mountain Formation, Mussentuchit Wash, Utah: a determination of the paleoenvironment and paleoecology of the Eolambia caroljonesa dinosaur quarry. Cretaceous Research 28(3):461-494.

Gibson, R. and F. Guinness. 1980. Behavioural factors affecting male reproductive success in red deer (*Cervus elaphus*). Animal Behaviour 28(4):1163-1174.

Gilmore, C. W. 1909. Osteology of the Jurassic reptile Camptosaurus: with a revision of the species of the genus, and description of two new species (Vol. 332): Govt. pr. off.

Goshe, L. R., L. Avens, J. Bybee, and A. A. Hohn. 2009. An evaluation of histological techniques used in skeletochronological age estimation of sea turtles. Chelonian Conservation and Biology 8(2):217-222.

Grigorescu, D. 2010. The “Tustea Puzzle”: hadrosaurid (Dinosauria, Ornithopoda) hatchlings associated with Megaloolithidae eggs in the Maastrichtian of the Hateg Basin (Romania). Ameghiniana 47(1): 89-97.

Grigorescu, D., G. Garcia, Z. Csiki, V. Codrea, and A. Bojar. 2010. Uppermost Cretaceous megaloolithid eggs from the Haţeg Basin, Romania, associated with hadrosaur hatchlings: Search for explanation. Palaeogeography, Palaeoclimatology, Palaeoecology 293(3): 360-374.

Guarino, F. M., F. Andreone, and F. Angelini. 1998. Growth and longevity by skeletochronological analysis in *Mantidactylus microtympanum*, a rain-forest anuran from southern Madagascar. Copeia 1:194-198.

Guenther, M. F. 2007. Morphology and ontogeny of the postcranial skeleton of the Hadrosauridae. Ph.D. Thesis, University of Pennsylvania.

Guenther, M. F. 2009. Influence of Sequence Heterochrony on Hadrosaurid Dinosaur Postcranial Development. The Anatomical Record: Advances in Integrative Anatomy and Evolutionary Biology 292(9):1427-1441. doi:10.1002/ar.20988

Hailu, Y. and P. Dodson. 2004. Basal ceratopsia. In D.Weishampel, P. Dodson, H. Osmolska (Ed). The Dinosauria. University of California Press, Berkeley, pp. 478-493.

Halliday, T. R., and P. Verrell. 1988. Body size and age in amphibians and reptiles. Journal of Herpetology 3:253-265.

Hass, C. C. and D. A. Jenni. 1991. Structure and ontogeny of dominance relationships among bighorn rams. Canadian Journal of Zoology 69(2):471-476.

Hayashi, S., K. Carpenter, D. Suzuki. 2009. Different growth patterns between the skeleton and osteoderms of *Stegosaurus* (Ornithischia: Thyreophora). Journal of Vertebrate Paleontology 29(1):123-131.

Head, J. 1998 A new species of basal hadrosaurid (Dinosauria, Ornithischia) from the Cenomanian of Texas. Journal of Vertebrate Paleontology 18(4): 718-738.

Head, J. 2001. A Reanalysis of the Phylogenetic Position of *Eolambia Caroljonesa* (Dinosauria, Iguanodontia). Journal of Vertebrate Paleontology 21(2):392-396.

Hedgecock, N. L., T. Hadi, A. A. Chen, S. B. Curtiss, R. B. Martin, and S. J. Hazelwood. 2007. Quantitative regional associations between remodeling, modeling, and osteocyte apoptosis and density in rabbit tibial midshafts. Bone 40(3):627-637.

Heinrich, R. E., C. B. Ruff, D. B. Weishampel. 1993. Femoral ontogeny and locomotor biomechanics of *Dryosaurus lettowvorbecki* (Dinosauria, Iguanodontia). Zoological Journal of the Linnean Society 108(2):179-196.

Hendrix, B. 2015. A new approach to date paleosols in terrestiral strata: a case study using U- Pb zircon ages for the Yellow Cat Member of the Cedar Mountain Formation of Eastern Utah. Geological Society of America, Abstracts with Programs 47(7).

Hibiya, T., M. Yokote, M. Oguri, H. Sato, F. Takashima, and K. Aida. 1982. An atlas of fish histology. Normal and pathological features. Gustav Fischer, Verlag, 195 pp.

Hobday, D. K. 1981. Paleotopographic and structural controls on non-marine sedimentation of the Lower Cretaceous Antlers Formation and correlatives, north Texas and southeastern Oklahoma. The Society of Economic Paleontologists and Mineralogists Special Publication 31:71-87.

Hone, D., and D. Naish. 2013. The 'species recognition hypothesis' does not explain the presence and evolution of exaggerated structures in non-avialan dinosaurs. Journal of Zoology 290(3):172-180.

Hone, D. W., C. Sullivan, Q. Zhao, K. Wang, and X. Xu. 2014. Body size distribution in a death assemblage of a colossal hadrosaurid from the Upper Cretaceous of Zhucheng, Shandong Province, China. In D. Eberth and D. Evans (Ed). Hadrosaurs. Indiana University Press, Bloomington, pp. 524-531.

Hooker, J., A. Milner, S. Sequeira. 1991. An ornithopod dinosaur from the Late Cretaceous of West Antarctica. Antarctic Science 3(03):331-332.

Hopson, J. A. 1975. The evolution of cranial display structures in hadrosaurian dinosaurs. Paleobiology 1(01):21-43.

Horner, J. R. 1983. Cranial osteology and morphology of the type specimen of *Maiasaura peeblesorum* (Ornithischia: Hadrosauridae), with a discussion of its phylogenetic position. Journal of Vertebrate Paleontology 3(1):29-38.

Horner, J. R., A. de Ricqlès, and K. Padian. 1999. Variation in Dinosaur Skeletochronology Indicators: Implications for Age Assessment and Physiology. Paleobiology 25(3):295-304. doi:10.2307/2666000

Horner, J. R., A. de Ricqlès, and K. Padian. 2000. Long Bone Histology of the Hadrosaurid Dinosaur *Maiasaura peeblesorum*: Growth Dynamics and Physiology Based on an Ontogenetic Series of Skeletal Elements. Journal of Vertebrate Paleontology 20(1):115-129. doi:10.2307/4524067

Horner, J. R., A de Ricqlès, K. Padian, and R. D. Scheetz. 2009. Comparative Long Bone Histology and Growth of the "Hypsilophodontid" Dinosaurs *Orodromeus makelai*, *Dryosaurus altus*, and *Tenontosaurus tillettii* (Ornithischia: Euornithopoda). Journal of Vertebrate Paleontology 29(3):734-747. doi:10.2307/20627086

Horner, J. R. and P. J. Currie. 1994. Embryonic and neonatal morphology and ontogeny of a new species of *Hypacrosaurus* (Ornithischia, Lambeosauridae) from Montana and Alberta. In K. Carpenter, K. F. Hirsch, J. R. Horner (Ed). Dinosaur eggs and babies. Cambridge University Press, Cambridge, pp. 312-336.

Horner, J. R., and M. B. Goodwin. 2006. Major cranial changes during *Triceratops* ontogeny. Proceedings of the Royal Society of London B: Biological Sciences 273(1602):2757-2761.

Horner, J. R., and M.B. Goodwin. 2009. Extreme cranial ontogeny in the Upper Cretaceous dinosaur *Pachycephalosaurus*. PLoS ONE 4(10):e7626.

Horner, J. R., K. Padian, and A. de Ricqlès. 2001. Comparative Osteohistology of Some Embryonic and Perinatal Archosaurs: Developmental and Behavioral Implications for Dinosaurs. Paleobiology 27(1):39-58. doi:10.2307/2666028

Horner, J. R. and K. Padian. 2004. Age and growth dynamics of *Tyrannosaurus rex*. Proceedings of the Royal Society of London B: Biological Sciences 271(1551):1875-1880.

Horner, J. R. and R. Makela. 1979. Nest of juveniles provides evidence of family structure among dinosaurs. Nature 282(5736):296-298.

Horner, J. R., and D. B. Weishampel. 1988. A comparative embryological study of two ornithischian dinosaurs. Nature 332(6161):256-257.

Horner, J. R., D. B. Weishampel, D. B., and C. A. Forster. 2004. Hadrosauridae. In D.Weishampel, P. Dodson, H. Osmolska (Ed). The Dinosauria. University of California Press, Berkeley, pp. 438-463.

Hübner, T. R. 2012. Bone Histology in *Dysalotosaurus lettowvorbecki* (Ornithischia: Iguanodontia) - Variation, Growth, and Implications. PLoS ONE 7(1):1-29. doi:10.1371/journal.pone.0029958

Hübner, T. R., and O. W. M. Rauhut. 2010. A juvenile skull of *Dysalotosaurus lettowvorbecki* (Ornithischia: Iguanodontia), and implications for cranial ontogeny, phylogeny, and taxonomy in ornithopod dinosaurs. Zoological Journal of the Linnean Society 160(2):366-396. doi:10.1111/j.1096-3642.2010.00620.x

Hurvich, C. M. and C. L. Tsai. 1989. Regression and time series model selection in small samples. Biometrika 76:297–307. doi:10.1093/biomet/76.2.297

Huttenlocker, A. K., H. N. Woodward, and B. K. Hall. 2013. The biology of bone. In K. Padian and E-T. Lamm (Ed). Bone histology of fossil tetrapods, University of California Press, Berkeley, California, pp. 13-34.

Hutton, J. M. 1986. Age Determination of Living Nile Crocodiles from the Cortical Stratification of Bone. Copeia 1986(2):332-341. doi:10.2307/1444994

Huxley, T. H. 1869. On Hypsilophodon, a new genus of Dinosauria. Proceedings of the Geological Society of London 204(3).

Huxley, T. H. 1870. On Hypsilophodon foxii, a new dinosaurian from the Wealden of the Isle of Wight. Quarterly Journal of the Geological Society 26(1-2):3-12.

Irmis, R. B. 2007. Axial skeleton ontogeny in the Parasuchia (Archosauria: Pseudosuchia) and its implications for ontogenetic determination in archosaurs. Journal of Vertebrate Paleontology 27(2):350-361.

Juárez Valieri, R. D., J. A. Haro, L. E. Fiorelli, and J. O. Calvo. 2010. A new hadrosauroid (Dinosauria: Ornithopoda) from the Allen Formation (Late Cretaceous) of Patagonia, Argentina. Revista del Museo Argentino de Ciencias Naturales 12(2):217-231.

Kirkland, J. I. 1998. A New Hadrosaurid from the Upper Cedar Mountain Formation (Albian- Cenomanian: Cretaceous) of Eastern Utah - The Oldest Known Hadrosaurid (Lambeosaurine?). New Mexico Museum of Natural History and Science Bulletin 14:283-296.

Kirkland, J. I., B. B. Britt, D. L. Burge, K. Carpenter, R. Cifelli, F. DeCourten, J. Eaton, S. Hasiotis, and T. Lawton. 1997. Lower to middle Cretaceous dinosaur faunas of the central Colorado Plateau: a key to understanding 35 million years of tectonics, sedimentology, evolution, and biogeography. Brigham Young University Geology Studies 42: 69-104.

Kirkland, J. I., B. B. Britt, and C. H. Whittle. 1998. Cedar Mountain Formation (Lower Cretaceous, Barremian) of Eastern Utah. Lower and Middle Cretaceous Terrestrial Ecosystems: Bulletin 14(14):239.

Klein, N., and P. M. Sander. 2007. Bone histology and growth of the prosauropod dinosaur *Plateosaurus engelhardti* von Meyer, 1837 from the Norian bonebeds of Trossingen (Germany) and Frick (Switzerland). Special Papers in Palaeontology 77:169.

Klein, N., and P. M. Sander. 2008. Ontogenetic stages in the long bone histology of sauropod dinosaurs. Paleobiology 34(2):247-263.

Klein, N., T. Scheyer, and T. Tütken. 2009. Skeletochronology and isotopic analysis of a captive individual of *Alligator mississippiensis* Daudin, 1802. Fossil Record 12(2):121-131.

Köhler, M., N. M. Moratalla, X. Jordana, and R. Aanes. 2012. Seasonal bone growth and physiology in endotherms shed light on dinosaur physiology. Nature 487(7407):358-361. doi:10.1038/nature11264

Latimer, H. B. 1927. Postnatal growth of the chicken skeleton. Developmental Dynamics 40(1):1-57.

Lauters, P., Y. L. Bolotsky, J. Van Itterbeeck, and P. Godefroit. 2008. Taphonomy and age profile of a latest Cretaceous dinosaur bone bed in Far Eastern Russia. Palaios 23(3):153-162.

Lee, A. H., A. K. Huttenlocker, K. Padian, & H. N. Woodward. 2013. Analysis of growth rates. In K. Padian and E-T. Lamm (Ed). Bone histology of fossil tetrapods, University of California Press, Berkeley, California, pp. 217-251.

Lee, A. H. and P. M. O'Connor. 2013. Bone histology confirms determinate growth and small body size in the noasaurid theropod *Masiakasaurus knopfleri*." Journal of Vertebrate Paleontology 33(4):865-876.

Lee, A. H., and S. Werning. 2008. Sexual maturity in growing dinosaurs does not fit reptilian growth models. Proceedings of the National Academy of Sciences 105(2):582-587.

Lepage, D., et al. (1998). Seasonal variation in growth of greater snow goose goslings: the role of food supply. *Oecologia*, *114*(2): 226-235.

Lei, Y. C. & S. Y. Zhang. 2004. Features and partial derivatives of Bertalanffy–Richards growth model in forestry. Nonlin. Anal. Modell. Control 9:65–73.

Lull, R. S., and N. E. Wright. 1942. Hadrosaurian dinosaurs of North America. Geological Society of America Special Papers 40:1-272.

Main, R. P., A. De Ricqlès., J. R. Horner, and K. Padian. 2005. The evolution and function of thyreophoran dinosaur scutes: implications for plate function in stegosaurs. Paleobiology 31(02):291-314.

Maisano, J. A. 2002. Terminal fusions of skeletal elements as indicators of maturity in squamates. Journal of Vertebrate Paleontology 22(2):268-275.

Mallon, J. C. 2017. Recognizing sexual dimorphism in the fossil record: lessons from nonavian dinosaurs. Paleobiology 43(3):1-13.

Maloney, S., and T. Dawson. 1993. Sexual dimorphism in basal metabolism and body temperature of a large bird, the emu. The Condor 95(4):1034-1037.

Marangoni, F., E. Schaefer, R. Cajade, and M. Tejedo. 2009. Growth-mark formation and chronology of two neotropical anuran species. Journal of Herpetology 43(3):546-550.

Marsh, O. C. 1879. Principal characters of American Jurassic dinosaurs. American Journal of Science 97:86-92.

Marsh, O. C. 1894. The typical ornithopoda of the American Jurassic. American Journal of Science 283:85-90.

McCarthy, S., and M. Gilbert. 1994. The Crystal Palace dinosaurs: The story of the world's first prehistoric sculptures. Crystal Palace Foundation.

Maryanska, T., R. E. Chapman, D. B. Weishampel. 2004. Pachycephalosauria. In D.Weishampel, P. Dodson, H. Osmolska (Ed). The Dinosauria. University of California Press, Berkeley, pp. 464-477.

McDonald, A. T. 2012. Phylogeny of Basal Iguanodonts (Dinosauria: Ornithischia): An Update. PLoS ONE 7(5):1-5. doi:10.1371/journal.pone.0036745

McDonald, A. T., J. I. Kirkland, D. D. DeBlieux, S. K. Madsen, J. Cavin, A. R. C. Milner, and L. Panzarin. 2010. New Basal Iguanodonts from the Cedar Mountain Formation of Utah and the Evolution of Thumb-Spiked Dinosaurs. PLoS ONE 5(11):1-35. doi:10.1371/journal.pone.0014075

McDonald, A. T., J. Bird, J. I. Kirkland, and P. Dodson. 2012. Osteology of the Basal Hadrosauroid *Eolambia caroljonesa* (Dinosauria: Ornithopoda) from the Cedar Mountain Formation of Utah. PLoS ONE 7(10):e45712. doi:10.1371/journal.pone.0045712

McFarlin, S. C., C. Terranova, A. L. Zihlman, D. H. Enlow, and T. G. Bromage, T. G. 2008. Regional variability in secondary remodeling within long bone cortices of catarrhine primates: the influence of bone growth history. Journal of Anatomy 213(3):308-324.

Measey, G. J., and M. Wilkinson. 1998. Lines of arrested growth in the caecilian, *Typhlonectes natans* (Amphibia: Gymnophiona). Amphibia-Reptilia 19(1):91-95.

Meyers, J., L. Suttner, L. Furer, M. May, and M. Soreghan. 1992. lntrabasinal tectonic control on fluvial sandstone bodies in the Cloverly Formation (Early Cretaceous), west-central Wyoming, USA. Basin Research 4(3-4):315-333.

Mitchell, J., and P. M. Sander. 2014. The three-front model: a developmental explanation of long bone diaphyseal histology of Sauropoda. Biological Journal of the Linnean Society 112(4):765-781. doi:10.1111/bij.12324

Mori, S., and D. B. Burr. 1993. Increased intracortical remodeling following fatigue damage. Bone 14(2):103-109. doi:http://dx.doi.org/10.1016/8756-3282(93)90235-3

Myhrvold, N. P. 2013. Revisiting the Estimation of Dinosaur Growth Rates. PLoS ONE 8(12):e81917. doi:10.1371/journal.pone.0081917

Nicholson, K. L., S. M. Arthur, J. S. Horne, E. O. Garton, and P. A. Del Vecchio. 2016. Modeling Caribou Movements: Seasonal Ranges and Migration Routes of the Central Arctic Herd. PLoS ONE 11(4):e0150333. doi:10.1371/journal.pone.0150333

Norman, D. B. 2004. Basal iguanodontia. In D.Weishampel, P. Dodson, H. Osmolska (Ed). The Dinosauria. University of California Press, Berkeley, pp. 413-437.

Norman, D. B. 2015. On the history, osteology, and systematic position of the Wealden (Hastings group) dinosaur *Hypselospinus fittoni* (Iguanodontia: Styracosterna). Zoological Journal of the Linnean Society 173(1):92-189.

Norman, D. B., A. W. Crompton, R. J. Butler, L. B. Porro, and A. J. Charig. 2011. The Lower Jurassic ornithischian dinosaur *Heterodontosaurus tucki* Crompton & Charig, 1962: cranial anatomy, functional morphology, taxonomy, and relationships. Zoological Journal of the Linnean Society 163(1):182-276.

Ősi, A., E. Prondvai, R. Butler, D. B. Weishampel, and A. R. Evans. 2012. Phylogeny, Histology and Inferred Body Size Evolution in a New Rhabdodontid Dinosaur from the Late Cretaceous of Hungary. PLoS ONE 7(9):1-25. doi:10.1371/journal.pone.0044318

Ostrom, J. H. 1970. Stratigraphy and paleontology of the Cloverly Formation (Lower Cretaceous) of the Bighorn Basin area: Wyoming and Montana. Peabody Museum of Natural History, Yale University.

Owens, I. P. and I. R. Hartley. 1998. Sexual dimorphism in birds: why are there so many different forms of dimorphism? Proceedings of the Royal Society of London B: Biological Sciences 265(1394):97-407.

Padian, K., and J. R. Horner. 2011. The evolution of 'bizarre structures' in dinosaurs: biomechanics, sexual selection, social selection or species recognition? Journal of Zoology 283(1):3-17.

Padian, K., E.-T. Lamm, S. Werning, K. Padian. 2013. Selection of specimens In K. Padian and E-T. Lamm (Ed). Bone histology of fossil tetrapods, University of California Press, Berkeley, California, pp. 35-54.

Paternoster R, R. Brame, P. Mazerolle, and A. Piquero. 1998. Using the correct statistical test for the equality of regression coefficients. Criminology 36(4):859-866.

Paul, G. S. 2016. The Princeton field guide to dinosaurs. Princeton University Press, Princeton, NJ and Oxford, 359 pp.

Peabody, F. E. 1961. Annual growth zones in living and fossil vertebrates. Journal of Morphology 108(1):11-62.

Peczkis, J. 1995. Implications of body-mass estimates for dinosaurs. Journal of Vertebrate Paleontology 14(4):520-533.

Petermann, H. and J. A. Gauthier. 2017. Osteohistology and sequence of suture fusion reveal complex environmentally influenced growth in the teiid lizard *Aspidoscelis tigris*—Implications for fossil squamates. Palaeogeography, Palaeoclimatology, Palaeoecology 475:12-22.

Price, G. J. and K. J. Piper. 2009. Gigantism of the Australian Diprotodon Owen 1838 (Marsupialia, Diprotodontoidea) through the Pleistocene. Journal of Quaternary Science 24(8):1029-1038.

Prieto-Márquez, A. 2010. Global phylogeny of Hadrosauridae (Dinosauria: Ornithopoda) using parsimony and Bayesian methods. Zoological Journal of the Linnean Society 159(2):435-502.

Prieto-Márquez, A. 2011. Cranial and appendicular ontogeny of *Bactrosaurus johnsoni*, a hadrosauroid dinosaur from the Late Cretaceous of northern China. Palaeontology 54(4):773-792.

Prieto-Márquez, A., G. M. Erickson, and J. A. Ebersole. 2016. Anatomy and osteohistology of the basal hadrosaurid dinosaur *Eotrachodon* from the uppermost Santonian (Cretaceous) of southern Appalachia. PeerJ 4: e1872.

Rao, C. R. 1958. Some statistical methods for comparison of growth curves. Biometrics 14(1):1-17.

Ray, S., J. Botha, and A. Chinsamy. 2004. Bone histology and growth patterns of some nonmammalian therapsids. Journal of Vertebrate Paleontology 24(3):634-648.

Rayfield, E. J. 2007. Finite element analysis and understanding the biomechanics and evolution of living and fossil organisms. Annu. Rev. Earth Planet. Sci. 35:541-576.

Rich, T., P. Rich, B. Wagstaff, J. McEwen-Mason, C. Douthitt, and R. Gregory. 1989. Early Cretaceous biota from the northern side of the Australo-Antarctic rift valley. Geological Society, London, Special Publications 47(1):121-130.

Rogers, R. R., S.M. Kidwell, R. Rogers, D. Eberth, and A. Fiorillo. 2007. A conceptual framework for the genesis and analysis of vertebrate skeletal concentrations In R. R. Rogers, D. A. Eberth, and A. R. Fiorillo (Ed), Bonebeds: genesis, analysis, and paleobiological significance. University of Chicago Press, Chicago and London, pp. 1-63.

Ruiz-Omeñaca, J., X. Pereda Suberbiola, P. Galton, and K. Carpenter. 2007. Callovosaurus leedsi, the earliest dryosaurid dinosaur (Ornithischia: Euornithopoda) from the Middle Jurassic of England. In K. Carpenter (Ed). Horns and Beaks: Ceratopsian and Ornithopod Dinosaurs. Indiana University Press, Bloomington, 3-16 pp.

Sander, D. P. M. 2006. Lines of arrested growth and long bone histology in Pleistocene large mammals from Germany: What do they tell us about dinosaur physiology? Palaeontographica Abteilung A 277:143-159.

Sander, P. M. 2000. Longbone histology of the Tendaguru sauropods: implications for growth and biology. Paleobiology 26(3):466-488.

Sander, P. M., N, Klein, K. Stein, O. Wings. 2011. Sauropod bone histology and its implications for sauropod biology. In N. Klein, K. Remes, C. Gee, and P. M. Sander (Ed), Biology of the sauropod dinosaurs: Understanding the life of giants, Indiana University Press, Bloomington and Indianapolis, Indiana, pp. 276-302.

Sander, P. M., and C. Tückmantel. 2003. Bone lamina thickness, bone apposition rates, and age estimates in sauropod humeri and femora. Paläontologische Zeitschrift 77(1):161-172.

Scannella, J. B., and J. R. Horner. 2010. *Torosaurus* Marsh, 1891, is *Triceratops* Marsh, 1889 (Ceratopsidae: Chasmosaurinae): synonymy through ontogeny. Journal of Vertebrate Paleontology 30(4):1157-1168.

Scheetz, R. D. Osteology of *Orodromeus makelai* and the phylogeny of basal ornithopod dinosaurs. PhD Thesis, Montana State University-Bozeman, College of Letters & Science, 1999.

Schott, R. K., D. C. Evans, M. B. Goodwin, J. R. Horner, C. M. Brown, and N. Longrich. 2011. Cranial ontogeny in *Stegoceras validum* (Dinosauria: Pachycephalosauria): a quantitative model of pachycephalosaur dome growth and variation. PLoS ONE 6(6):e21092.

Schwarz, G. 1978. Estimating the dimension of a model. Ann. Statist. 6:461–464. doi:10.1214/aos/1176344136

Seebacher, F. 2001. A new method to calculate allometric length-mass relationships of dinosaurs. Journal of Vertebrate Paleontology 21(1):51-60.

Senter, P., J. I. Kirkland, D.D. DeBlieux, S. Madsen, and N. Toth. 2012. New Dromaeosaurids (Dinosauria: Theropoda) from the Lower Cretaceous of Utah, and the Evolution of the Dromaeosaurid Tail. PLoS ONE 7(5):e36790. doi:10.1371/journal.pone.0036790

Smuts, G. 1975. Reproduction and population characteristics of elephants in the Kruger National Park. South African Journal of Wildlife Research-24-month delayed open access 5(1):1-10.

Snover, M. L., A. A. Hohn. 2004. Validation and interpretation of annual skeletal marks in loggerhead (*Caretta caretta*) and Kemp's ridley (*Lepidochelys kempii*) sea turtles. Fishery Bulletin 102(4):682-692.

Stokes, W. L. 1944. Morrison Formation and related deposits in and adjacent to the Colorado Plateau. Geological Society of America Bulletin 55(8):951-992.

Stokes, W. L. 1952. Lower Cretaceous in Colorado Plateau. AAPG Bulletin 36(9):1766-1776.

Straehl, F. R., T. M. Scheyer, A. M. Forasiepi, R. D. MacPhee, and M. R. Sánchez-Villagra. 2013. Evolutionary Patterns of Bone Histology and Bone Compactness in Xenarthran Mammal Long Bones. PLoS ONE 8(7):e69275. doi:10.1371/journal.pone.0069275

Sues, H.-D. 1997. European dinosaur hunters The Complete Dinosaur. Indiana University Press, Bloomington, pp. 12-23.

Szekely, T., et al. (2007). Sexual size dimorphism in birds. In T. Szekely, T. Lislevand, and J. Figuerola (Ed). Sex, size and gender roles: evolutionary studies of sexual size dimorphism. Oxford University Press, New York, pp. 27-37.

Therrien, F. and D. M. Henderson. 2007. My theropod is bigger than yours… or not: estimating body size from skull length in theropods. Journal of Vertebrate Paleontology 27(1):108-115.

Tjørve, E. and K. M. C. Tjørve. 2010. A unified approach to the Richards-model family for use in growth analyses: Why we need only two model forms. Journal of Theoretical Biology 267(3):417-425.

Tjørve, K. M. C. and E. Tjørve. 2010. Shapes and functions of bird-growth models: how to characterise chick postnatal growth. Zoology 113(6):326-333.

Trexler, D. 2001. Two Medicine Formation, Montana: geology and fauna. In D. Tanke, K. Carpenter (Ed), Mesozoic Vertebrate Life, Indiana University Press, Bloomington and Indianapolis, Indiana, pp. 298-309.

Tsoularis, A. and J. Wallace. 2002. Analysis of logistic growth models. Mathematical biosciences 179(1):21-55.

Tucker, J. K. 2000. Body Size and Migration of Hatchling Turtles: Inter- and Intraspecific Comparisons. Journal of Herpetology 34(4):541-546. doi:10.2307/1565269

Tumarkin-Deratzian, A. R. 2003. Bone surface textures as ontogenetic indicators in extant and fossil archosaurs: Macroscopic and histological evaluations. PhD Thesis, Universtiy of Pennsylvania, Philadephia.

Tumarkin-Deratzian, A. R., D. R. Vann, and P. Dodson. 2006. Bone surface texture as an ontogenetic indicator in long bones of the Canada goose *Branta canadensis* (Anseriformes: Anatidae). Zoological Journal of the Linnean Society 148(2):133-168.

Tumarkin-Deratzian, A. R., D. R. Vann, P. Dodson. 2007. Growth and textural ageing in long bones of the American alligator *Alligator mississippiensis* (Crocodylia: Alligatoridae). Zoological Journal of the Linnean Society 150(1):1-39.

Turvey, S. T., O. R. Green, and R. N. Holdaway. 2005. Cortical growth marks reveal extended juvenile development in New Zealand moa. Nature 435(7044):940-943.

Van Oers, R. F. M., R. Ruimerman, E. Tanck, P. A. Hilbers, & R. Huiskes. 2008. A unified theory for osteonal and hemi-osteonal remodeling. Bone 42(2):250-259. doi:http://dx.doi.org/10.1016/j.bone.2007.10.009

Varricchio, D. J., and J. R. Horner. 1993. Hadrosaurid and lambeosaurid bone beds from the Upper Cretaceous Two Medicine Formation of Montana: taphonomic and biologic implications. Canadian Journal of Earth Sciences 30(5):997-1006.

Varricchio, D. J., and F. D. Jackson. 2004. A phylogenetic assessment of prismatic dinosaur eggs from the Cretaceous Two Medicine Formation of Montana. Journal of Vertebrate Paleontology 24(4):931-937.

Virchow, H. 1919. Atlas und Epistropheus bei den Schildkröten. Sitzungsberichte der Gesellschaft Naturforschender Freunde zu Berlin pp. 303-332.

Von den Driesch, A. 1976. A guide to the measurement of animal bones from archaeological sites: as developed by the Institut für Palaeoanatomie, Domestikationsforschung und Geschichte der Tiermedizin of the University of Munich. Vol. 1. Peabody Museum Press.

Weishampel, D., D. Norman, and D. Grigorescu. 1993. *Telmatosaurus transsylvanicus* from the late Cretaceous of Romania: the most basal hadrosaurid dinosaur. Palaeontology 36:361-361.

Weishampel, D. B. 1981. The Nasal Cavity of Lambeosaurine Hadrosaurids (Reptilia: Ornithischia): Comparative Anatomy and Homologies. Journal of Paleontology 55(5):1046-1057.

Weishampel, D. B., J. R. Horner, D. Weishampel, P. Dodson, and H. Osmólska. 1990. Hadrosauridae. In D.Weishampel, P. Dodson, H. Osmolska (Ed). The Dinosauria. University of California Press, Berkeley, pp. 534-561.

Werning, S. 2012. The Ontogenetic Osteohistology of Tenontosaurus tilletti. PLoS ONE 7(3):1-25. doi:10.1371/journal.pone.0033539

Wilson, D. S., C. R. Tracy, & C. R. Tracy. 2003. Estimating age of turtles from growth rings: a critical evaluation of the technique. Herpetologica 59(2):178-194.

Wirtz, P. 1981. Territorial defence and territory take-over by satellite males in the waterbuck *Kobus ellipsiprymnus* (Bovidae). Behavioral Ecology and Sociobiology 8(2):161-162.

Woodward, H., K. Padian, and A. Lee. 2013. Skeletochronology Bone histology of fossil tetrapods: advancing methods, analysis, and interpretation. In K. Padian and E-T. Lamm (Ed). Bone histology of fossil tetrapods, University of California Press, Berkeley, California, pp. 187-207.

Woodward, H. N., E. A. F. Fowler, J. O. Farlow, and J. R. Horner. 2015. *Maiasaura*, a model organism for extinct vertebrate population biology: a large sample statistical assessment of growth dynamics and survivorship. Paleobiology 41(4):1-25.

Woodward, H. N., J. R. Horner, and J. O. Farlow. 2011. Osteohistological Evidence for Determinate Growth in the American Alligator. Journal of Herpetology 45(3):339-342. doi:10.1670/10-274.1

Woodward, H. N., T. H. Rich, A. Chinsamy, and P. Vickers-Rich. 2011. Growth Dynamics of Australia's Polar Dinosaurs. PLoS ONE 6(8):1-5. doi:10.1371/journal.pone.0023339

Xing, H., X. Zhao, K. Wang, D. LI, S. CHEN, J. C. Mallon, X. XU. 2014. Comparative Osteology and Phylogenetic Relationship of *Edmontosaurus* and *Shantungosaurus* (Dinosauria: Hadrosauridae) from the Upper Cretaceous of North America and East Asia. Acta Geologica Sinica (English Edition) 88(6):1623-1652.

Yoccoz, N. G., and S. Mesnager. 1998. Are alpine bank voles larger and more sexually dimorphic because adults survive better? Oikos 82(1):85-98.

Young, R. G. 1960. Dakota Group of Colorado Plateau. AAPG Bulletin 44(2):156-194.

Zar, J. H. 1996. Biostatistical Analysis 3rd ed. Prentic Hall, Upper Saddle River, NJ, 662 pp.

Zenzal Jr, T. J. and F. R. Moore. 2016. Stopover biology of Ruby-throated Hummingbirds (*Archilochus colubris*) during autumn migration. The Auk 133(2):237-250.

Curriculum Vitae

Catherine E. Sartin **July 2017**

Educational History

M.S. expected	2017	Program in Functional Anatomy & Evolution Mentors: Dave Weishampel and Chris Ruff	Johns Hopkins School of Medicine
M.A.	2008	Philosophy (Bioethics)	University of Florida
B.A.	2004	Philosophy	University of Colorado

Other Profesional Experience

2015	Associated Researcher, Denver Museum of Nature and Science expedition to Grand Staircase Escalante National Monument, Utah to collect Kaiparowits and Wahweap flora and fauna
2014	Associated Researcher, Denver Museum of Nature and Science expedition to Grand Staircase Escalante National Monument, Utah to collect Kaiparowits flora and fauna
2014	Associated Researcher, Denver Museum of Nature and Science expedition to New Mexico to collect Cretaceous fauna
2013	Associated Researcher, Denver Museum of Nature and Science expedition to Grand Staircase Escalante National Monument, Utah to collect Kaiparowits flora and fauna
2013	Member, University of Toronto expedition to Alberta, Canada to collect Milk River fauna
2012	Member, University of Utah quarry at Ghost Ranch, New Mexico to collect Triassic vertebrates
2012	Member, University of Utah expedition to Dinosaur National Monument to prospect for Triassic trackways and collect Jurassic ichthyosaur
2011	Member, University of Pennsylvania expedition to Buffalo, South Dakota to collect Hell Creek flora and fauna
2011	Member, University of Pennsylvania expedition to Gansu Province, China to correlate strata across basins
2010	Member, Johns Hopkins School of Medicine expedition to the Big Horn Basin, Wyoming to collect Eocene mammals
2010	Member, University of Utah quarry at Ghost Ranch, New Mexico to collect Triassic vertebrates
2010	Member, University of Florida quarry at Thomas Farms, Florida to collect Miocene mammals

2013 Member, University of Southern California expedition to Farmington, New Mexico to collect Cretaceous fauna

Research Grants

2014 "Ontogeny in Ornithopoda" American Association of Anatomists Visiting Scholar Grant; $1000

2014 "Ontogeny in Ornithopoda" Mid-American Paleontological Society Outstanding Student Research Award; $800

Popular Publications

Sartin, C. 2009. If the End Doesn't Justify the Means, then What Does? In: House and Philosophy: Everybody Lies, Jacoby, Henry (ed). Hoboken, NJ: John Wiley & Sons, Inc., pp. 164-173.

Abstracts

Sartin, C. (2015) Ontogeny in Igunaodontia. American Association of Anatomists Annual Meeting, Boston, MA, April 2015.

Sartin, C. (2014) Estimating Body Mass in Terrestiral Bipeds. Society of Vertebrate Paleontology Annual Meeting, Dallax, TX, October 2014.

Sartin, C. (2013) Assymmetry and Vestigial Structures in Extant Birds. Society of Vertebrate Paleontology Annual Meeting, Berlin, Germany, November 2013.

Sartin, C. (2012) Intraspecific Variation in the Stylar Cusps of *Didelphis Virginiana*. Socienty of Verebrate Paleontology Annual Meeting, Raliegh, NC, 2012.